



The
University
Of
Sheffield.

**“ANALYSIS OF THE GATING
STRUCTURES AT THE CILIA BASE”**

by

Khodor S. HAZIME

**A thesis submitted in partial fulfilment of the
requirements for the degree of Doctor of Philosophy
(Biomedical Science) in the University of Sheffield**

December 2017

Committee

Professor Colin Johnson

Dr. Anne-Gaelle Borycki

Acknowledgments

I am very grateful to my supervisor Jarema Malicki for his sincere supervision and valuable discussions throughout my PhD. I would like to thank my PhD advisors Andrew Furley, Nicolas Olivier, and Anton Nikolaev for their support and scientific advices.

Special thanks are to Natalia Bulgakova, Darren Robinson, Christa Walther, and aquarium staff for their cooperation. I would also like to appreciate the educational support I received from the Department of Biomedical Science.

Part of this work was performed at the Nencki Institute in Warsaw. Many thanks are to Dorota Wloga and Ewa Joachimiak for their contribution to this work and for being friendly and helpful whenever I visited their institute.

My special thanks are to my wife Marzieh Radi for her great support, patience, love, and encouragement throughout my PhD. Special thanks are to all my family and family-in-laws members for their care, support, and prayers.

Finally, I would like to dedicate this work to my beloved mother. I wish you were with me today.

Preface

- **Chapters II and III – Co-authors: Natalia Bulgakova, Ewa Joachimiak, Dorota Wloga, and Jarema Malicki.** Natalia Bulgakova kindly worked on writing the MATLAB codes to estimate the radial and axial positions of the proteins investigated in this study. Ewa Joachimiak from the Laboratory of Cytoskeleton and Cilia Biology, The Nencki Institute of Experimental Biology, Polish Academy of Sciences in Warsaw, performed most of the transformation experiments and western blots in *Tetrahymena thermophila*. Dorota Wloga, the principal investigator at the Laboratory of Cytoskeleton and Cilia Biology, The Nencki Institute of Experimental Biology, Polish Academy of Sciences, performed the majority of the cloning experiments, prepared the constructs before transforming into *Tetrahymena thermophila*, and supervised *Tetrahymena* work. Jarema Malicki is the principal investigator and the leading author of the work. These two chapters will be submitted as a single manuscript very soon.
- **Chapter IV** is published as: HAZIME, K. & MALICKI, J. J., 2017. GENETICS. Apico-basal Polarity Determinants Encoded by crumbs Genes Affect Ciliary Shaft Protein Composition, IFT Movement Dynamics, and Cilia Length. Vol. 207 (3) – 1041-1051; <http://doi.org/10.1534/genetics.117.300260>.
- Some of the methods in chapter V are published as following:
LEVENTEA, E.*, HAZIME, K.*, ZHAO, C. & MALICKI, J. 2016. Analysis of cilia structure and function in zebrafish. *Methods Cell Biol*, 133, 179-227.
* These first authors contributed equally to this work.

Table of Contents

Abstract	x
Chapter I. Introduction.....	1
I.1. What are cilia?	2
I.2. Ciliogenesis.....	4
I.3 The Ciliary Transition zone (TZ).....	4
I.3.1. Modules of the TZ.....	7
I.3.2. Functions of the TZ.....	8
I.4. The Transition Fibres	9
I.5. Ciliopathies	10
I.6. Intraflagellar Transport (IFT).....	11
I.6.1. IFT complexes and functions.....	13
I.6.2. Protein Interactions within the IFT Particle	15
I.6.3. BBSome.	16
I.7. Regulation of Protein Transport at the Cilia Base.....	17
I.8. An overview of nucleoporins in cilia	18
I.8.1. Where do nucleoporins localise in the ciliary compartment?.	18
I.8.2. Possible functions of nucleoporins in cilia	20
I.9. Cilia and Polarity.....	20
I.10. Coventional versus Super-resolution microscopy.....	23
I.11. Stochastic Optical Reconstruction Microscopy (STORM).....	24
I.12. Applications of Super-resolution Imaging in Cilia Biology	26
I.13. Models used in this thesis	28
I.13.1. <i>Tetrahymena thermophila</i>	28
I.13.2. <i>Danio rerio</i> (Zebrafish)	32
I.14. Aims of the PhD project(s) and main findings.....	33
Chapter II – MATERIALS AND METHODS	36
II.1. <i>Tetrahymena thermophila</i> culture.....	37
II.2. Genomic DNA extraction from <i>T.thermophila</i>	37
II.3. Protein tagging	38
II.4. Alignments.....	39

II.5. Preparing constructs for transformation into <i>Tetrahymena thermophila</i>	39
II.6. Plasmid DNA extraction.....	40
II.7. Biolistic Transformation and selection of transgenic (Knock-in) lines	42
II.8. Protein extraction in <i>T.thermophila</i>	44
II.9. SDS-PAGE and Western Blot	44
II.10. Deciliation (pH shock method).....	45
II.11. Immunostaining for confocal microscopy	46
II.12. Immunostaining for STORM imaging	47
II.13. Settings used to process STORM images.....	48
II.14. Reconstruction and analysis of STORM images.....	49
II.15. Estimation of average radial position (MATLAB).....	50
II.16. Estimation of axial positions (MATLAB)	52
II.17. Degree of labelling (dol)	53
II.18. Zebrafish strains and maintenance	53
II.19. Photograpy of adult zebrafish.....	54
II.20. Immunostaining, mounting, and microscopy (zebrafish).....	54
II.21. IMCD3 cell culture and siRNA experiments	55
II.22. Immunostaining of IMCD3 cells for confocal imaging	56
II.23. TIRF imaging of IFT in IMCD3-IFT88 cells.....	56
II.24. Cilia length measurements and statistical analysis	53

Chapter III. STORM Super-Resolution Imaging of the Ciliary Transition Zone

III.1. Introduction	63
III.2. Results	68
II.2.1. TZ proteins localise to the cilia base in <i>Tetrahymena thermophila</i>	68
III.2.2. STORM imaging of the TZ components.....	69
III.2.3. TZ proteins form discrete clusters arranged in rings at cilia base	71
III.2.4. TZ proteins form rings of different radii at the cilia base	76
III.2.5. TZ proteins form rings in NHBE cells	77
III.2.6. Nucleoporins may localise to the cilia base in <i>Tetrahymena thermophila</i>	79
III.2.7. Axial positions of TZ proteins	82

III.3 Discussion.....	86
Chapter IV. STORM Imaging Unveils the Architecture of the IFT particle in its Docking Site	94
IV.1. Introduction	95
IV.2. Results	98
IV.2.1. IFT proteins localise to the cilia base in <i>Tetrahymena thermophila</i>	98
IV.2.2. STORM imaging of IFT proteins in ciliated and de-ciliated <i>T. thermophila</i>	99
IV.2.3. IFT-B complex proteins form 9-fold symmetrical rings with different radii at the cilia base.....	102
IV.2.4. IFT-A complex localises outside IFT-B complex.....	106
IV.2.5. IFT88 forms "ring-like structures" in mTECs and IMCD3 cells.....	108
IV.2.6. IFT proteins dock between the transition zone and the basal body.....	109
IV.2.7. STORM imaging of the IFT motor Kif3a.....	113
IV.2.8. STORM imaging of other ciliary proteins at the cilia base	116
IV.3. Discussion	118
Chapter V. Apico-basal Polarity Determinants Encoded by <i>crumbs</i> Genes Affect Ciliary Shaft Protein Composition, IFT Movement Dynamics, and Cilia Length.....	125
V.1 Introduction	126
V.2. Results	129
V.2.1. <i>crb3a</i> affects cilia length in vestibular system cristae	129
V.2.2. <i>oko meduzy (ome)</i> mutations affect ciliogenesis	131
V.2.3. Crumbs proteins accumulate in cilia of <i>oko meduzy</i> mutants.....	132
V.2.4. IFT proteins are highly enriched in cilia of <i>ome;crb3a</i> double mutants .	135
V.2.5. CRB3 affects IFT train dynamics in IMCD3 cells	137
V.2.6. <i>crb2b</i> mutation increases cilia length in a subset of tissues	139
V.3. Discussion	142
Chapter VI. Conclusions and Future Directions	150
VI.1. Conclusions	150

VI.1.1. STORM imaging reveals the docking sites of IFT at the cilia base and the architecture of TZ proteins.....	150
VI.1.2. <i>crumbs</i> genes affect ciliogenesis and maybe part of the ciliary gating strcutures at the cilia base.....	152
VI.2. Future Directions	157
VI.2.1. Nanobodies and photoactivatable fluorescent proteins	157
VI.2.2. Analysis of double transgenic lines and mutants	158
VI.2.3. STORM imaging of other proteins.....	159
VI.2.4. Immuno-electron microscopy and correlation of STORM with EM	160
VI.2.5. Analysis of Crumbs proteins in knock-in lines followed by STORM imaging.....	161
References	162
Appendix	177

List of Figures

CHAPTER - I

Figure I.1. Overview of Cilia	3
Figure I.2. The process of cilia formation or ciliogenesis.....	5
Figure I.3. Ciliary transition zone is marked by Y-links.....	6
Figure I.4. Ciliopathies.....	12
Figure I.5. Intraflagellar transport and BBSome	14
Figure I.6. Nucleoporins and Cilia	19
Figure I.7. The relationship between apico-basal polarity determinants, <i>crumbs</i> , and ciliogenesis	23
Figure I.8. Applications of super-resolution microscopy in cilia biology.....	27
Figure I.9. Models used in this thesis	32

CHAPTER – II

Figure II.1. Estimation of the radial positions of the proteins using MATLAB.....	51
---	----

CHAPTER - III

Figure III.1. Transition zone proteins localise to the cilia base in <i>Tetrahymena thermophila</i>	70
Figure III.2. STORM imaging of TZ proteins	72
Figure III.3. TZ proteins form rings at the cilia base.....	73
Figure III.4. NPHP4 forms 9-fold symmetrical rings in top views and shows 2 layers in side views	74
Figure III.5. TZ components form rings of different radii at the cilia base	75
Figure III.6. TZ proteins form rings in NHBE cells	78

Figure III.7. Nucleoporins may localise to the cilia base in <i>Tetrahymena thermophila</i>	81
Figure III.8. Axial positions of TZ proteins.....	83
Figure III.9. Axial positions of NPHP4	84
Figure III.10. Model of the TZ.....	94

CHAPTER - IV

Figure IV.1. IFT proteins localise to the cilia base in <i>Tetrahymena thermophila</i>	99
Figure IV.2. IFT proteins are arranged in 9-fold symmetrical rings at the cilia base and move rapidly into cilia following deciliation	101
Figure IV.3. IFT-B proteins form 9-fold symmetrical rings with different radii at the cilia base.....	103
Figure IV.4. IFT-A complex proteins are arranged in 9-fold symmetrical rings at the cilia base.....	105
Figure IV.5. STORM images of IFT88 show ring-like structures at the cilia base in mTECs and IMCD3 cells.....	107
Figure IV.6. Axial positions of IFT-B proteins	110
Figure IV.7. Axial positions of IFT-A proteins	112
Figure IV.8. STORM analysis of other ciliary proteins.....	115
Figure IV.9. Model of the radial and axial distribution of IFT proteins.....	123

CHAPTER - V

Figure V.1. <i>crb3a</i> mutant phenotype	130
Figure V.2. <i>oko meduzy</i> and <i>crb3a</i> genes modulate cilia length.....	132
Figure V.3. Crumbs expression in <i>crb3a</i> mutants at early stages of development.....	133

Figure V.4. Crumbs proteins accumulate in cilia of <i>ome</i> mutants at 5 days postfertilisation (dpf)	135
Figure V.5. Intraflagellar transport (IFT) particle components accumulate in the ciliary compartment of <i>crumbs</i> mutants	136
Figure V.6. CRB3 knockdown in mammalian cells affects intraflagellar transport (IFT) dynamics	138
Figure V.7. <i>crb2b</i> affects cilia length.....	141

CHAPTER - VI

Figure VI.1. Radial and Axial Positions of the proteins characterised in this study.....	151
Figure VI.2. The orientation of proteins examined in this study	154
Figure VI.3. 3D model of the cilia base.....	155
Figure VI.4. Crumbs proteins affect ciliogenesis and contribute to gating mechanisms at the cilia base	156

List of TABLES

Table I.1. Ciliary proteins in <i>Tetrahymena thermophila</i> are well conserved with higher vertebrates, including humans	31
Table II.1. List of transgenic lines (Knock-in) used in this study	58
Table II.2. List of primers sequences	59
Table II.3. List of antibodies used in this thesis.....	61
Table IV.1. The IFT particle	124
Table V.1. Summary of mutant and morphant crumbs phenotypes in cilia	148
Table VI.1. Ciliary proteins analyzed for the STORM study	162

Abstract

Cilia are microscopic microtubule-based projections that emanate from basal bodies and protrude from the cell membrane of most eukaryotic cells. The base of the cilium is an evolutionary conserved sub-domain that acts as a gate to regulate and modulate trafficking of proteins to and from cilia. All proteins destined for the cilium cross the gating barriers at the base of the cilium in a tightly regulated manner preventing small polypeptides from entering while permitting the entrance of large protein complexes, such as the intraflagellar transport (IFT). Where exactly these gating structures are positioned, where IFT assembly takes place, and how this process is regulated is still ambiguous.

Based on STORM imaging, I present the first detailed 3D-model that shows the position of over 30 epitope tags in the IFT, transition zone (TZ), and basal body. We established *Tetrahymena thermophila* transgenic lines with C- and/or N- termini epitope tags of over 18 different proteins. I show that IFT, TZ, and other ciliary proteins form 9-fold symmetrical rings at the cilia base. I reveal for the first time the architecture of IFT particles in their docking sites. By using particle averaging of the radial and axial locations at the N- and C- termini of the proteins, I was able to determine the orientation of these proteins. I show that in the radial dimension, IFT-A complex lies outside IFT-B complex. I also reveal the localisation of the binding sites of cargoes, such as tubulin and outer dynein arms, at the cilia base. These studies made it possible to generate a 3D model of the cilia base encompassing crucial components in unprecedented details.

Moreover, I examined the relationship between the apico-basal polarity determinants, *crumbs* genes, and the gating mechanisms at the cilia base. I investigated mutant phenotypes of zebrafish *crumbs* genes. These mutations affect cilia length in a subset of tissues, and in some mutants, this is accompanied by accumulation of other Crumbs proteins and IFT particle components in the ciliary shaft. These findings reveal *crumbs*-dependent mechanisms that regulate the localisation of ciliary proteins at the cilia base, including Crumbs proteins themselves, and show that *crumbs* genes modulate intraflagellar transport and cilia elongation possibly acting as a component of a gating mechanism.

Chapter I

“INTRODUCTION”

I.1. What are cilia?

Cilia are microscopic finger-like protrusions on the plasma membrane of most eukaryotic cells. Motile cilia (Fig. I.1A-A') propel sperms, regulate embryonic left–right patterning, clear airway mucus, and participate in cerebrospinal fluid movement (Goetz and Anderson, 2010, Garcia-Gonzalo and Reiter, 2012). Motile cilia in the lungs beat to perform airway mucociliary clearance that is necessary for defence against microorganisms inhaled with breathing (Wanner et al., 1996). Non-motile or primary cilia (Fig. I.1B) are antennae-like projections that house a variety of signalling pathways, such as hedgehog pathway (Shh) and Wnt signalling, which are necessary for embryonic development, kidney function, vision, and smell (Goetz and Anderson, 2010, Garcia-Gonzalo and Reiter, 2012, Malicki, 2017 #4955).

Several groups of proteins are involved in maintaining the structure and the function of the cilium. These proteins contribute to several structures such as the transition fibres (TF), or distal appendages (DAP), transition zone (TZ), ciliary membrane (CM), ciliary pocket, and ciliary tip (Fig. I.1C). The transition zone and transition fibres are thought to form gating structures at the cilia base, which control the composition of the cilia (Garcia-Gonzalo et al., 2011, Garcia-Gonzalo and Reiter, 2012, Shi et al., 2017). The cilium contains an axoneme, which in turn is composed of 9 microtubule doublets surrounding a central pair (9+2 arrangement) in almost all motile cilia (Fig. I.1D, left). This central pair is missing in primary cilia and so have the “9+0” arrangement (Fig. I.1D, right) (Garcia-Gonzalo and Reiter, 2012, Fisch and Dupuis-Williams, 2011, Malicki and Johnson, 2017). Moreover, motile cilia contain proteins that are involved in the motility machinery. Dynein arms, radial spokes, and nexins are found in

motile cilia (Lindemann and Lesich, 2010, Fisch and Dupuis-Williams, 2011). The diameter of the ciliary axoneme ranges between 200 and 300nm and their lengths vary between 1 and 30µm. For example, very long cilia have been reported in the cristae of the zebrafish inner ear (Pooranachandran and Malicki, 2015, Hazime and Malicki, 2017). For a cilium to be formed, a set of several well-organised events take place in a process known as ciliogenesis.

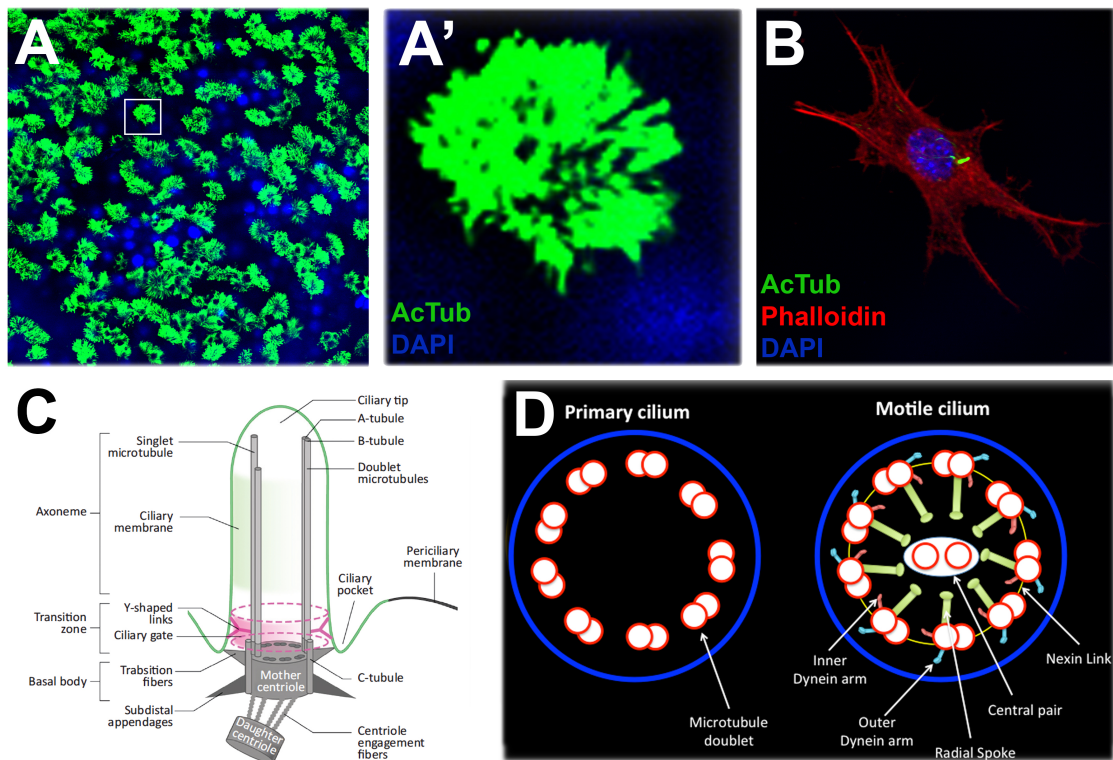


Figure I.1. Overview of Cilia. **(A)** A confocal image of primary culture of mouse tracheal epithelial cells (mTEC) showing hundreds of motile cilia (green) marked with anti-acetylated tubulin and counterstained with DAPI (blue) to detect nuclei. **(A')** Inset in **(A)**. **(B)** A confocal image of a 3T3 cell stained with anti-acetylated tubulin (green) to mark the primary cilium, phalloidin to mark actin (red) and DAPI (blue) to mark nuclei. **(C)** A schematic of a primary cilium showing different regions of the cilium (Adapted from (Malicki and Johnson, 2017)). **(D)** An illustration showing a cross-section of a primary cilium (left) with “9+0” arrangement of microtubules versus a motile cilium (right) with an additional microtubule pair in the middle showing “9+2” arrangement. Motile cilia contain other structures such as outer dynein arms, inner dynein arms, and radial spokes as indicated.

I.2. Ciliogenesis

Ciliogenesis, or cilia formation, is initiated by the extension of the axoneme from the mother centriole, the older of the two centrioles inherited during mitosis (Fig. I.2). In one scenario, the basal body migrates and docks directly to the plasma membrane followed by the extension of the ciliary axoneme (Dawe et al., 2007). In another scenario, the basal body of the cilium attaches by its distal appendages to a ciliary vesicle. This is followed by the migration and docking of the “basal body-ciliary vesicle” to the cell membrane. The docking creates a bud that starts to emerge by bending the membrane. The bud continues to elongate to form the axoneme that is built and maintained by the intraflagellar transport (IFT) system. After docking to the cell membrane, transition fibres (TF) will link the basal body to the ciliary membrane (Sorokin, 1962). The TZ controls what comes in and out of the cilium and the axoneme extends through IFT dependent manner (Fig. I.2) (Pedersen and Rosenbaum, 2008, Garcia-Gonzalo and Reiter, 2012).

I.3. The Ciliary Transition Zone

During ciliogenesis, two distinct regions appear at the base of the cilium to make membrane connections, the transition zone and the transition fibres (Fig. I.1C) (Reiter et al., 2012, Garcia-Gonzalo and Reiter, 2012, Williams et al., 2011). The transition zone is an evolutionary conserved sub-domain of the cilium (Garcia-Gonzalo and Reiter, 2012). In electron microscopy, the transition zone is marked by the presence of 9-symmetrical Y-shaped fibres, called Y-links, that connect the microtubule doublets to the overlying membrane (Garcia-

Gonzalo et al., 2011, Garcia-Gonzalo and Reiter, 2017) (Fig. I.3A). Moreover, the transition zone ensures that the cilium is isolated from the neighbouring membrane and the rest of the cell. Freeze fracture microscopy of the transition zone revealed little bumps on the ciliary membrane, called the ciliary necklace, which may correspond to the tips of the Y-links (Fig. I.3B) (Gilula and Satir, 1972). The length of the necklace may correspond to the length of transition zone in different cilia of different organisms. For example, there are 2 necklaces in the transition zone of *Tetrahymena* (Gilula and Satir, 1972), while 40 were reported in the connecting cilium of retinal rod cells (Fisch and Dupuis-Williams, 2011, Besharse and Horst, 1990).

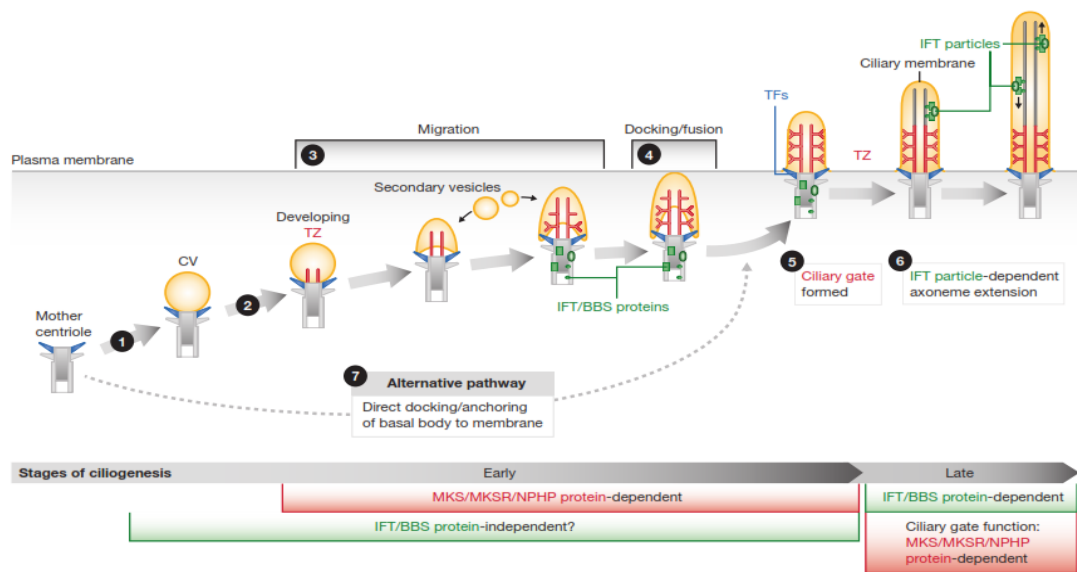


Figure I.2. The process of cilia formation or ciliogenesis. The mother centriole (1) attaches to the ciliary vesicle. The mother centriole-ciliary vesicle migrates to the cell membrane and the transition zone starts to develop (2-3). This is followed by the docking and fusion of the mother centriole to the cell membrane. The transition fibres connect the cilium to the cell membrane (4). Ciliary gate forms and IFT particles build and maintain the axoneme of the cilium (5-6). In another scenario, the basal body directly docks to the plasma membrane followed by the extension of the ciliary axoneme. Adapted from (Reiter et al., 2012).

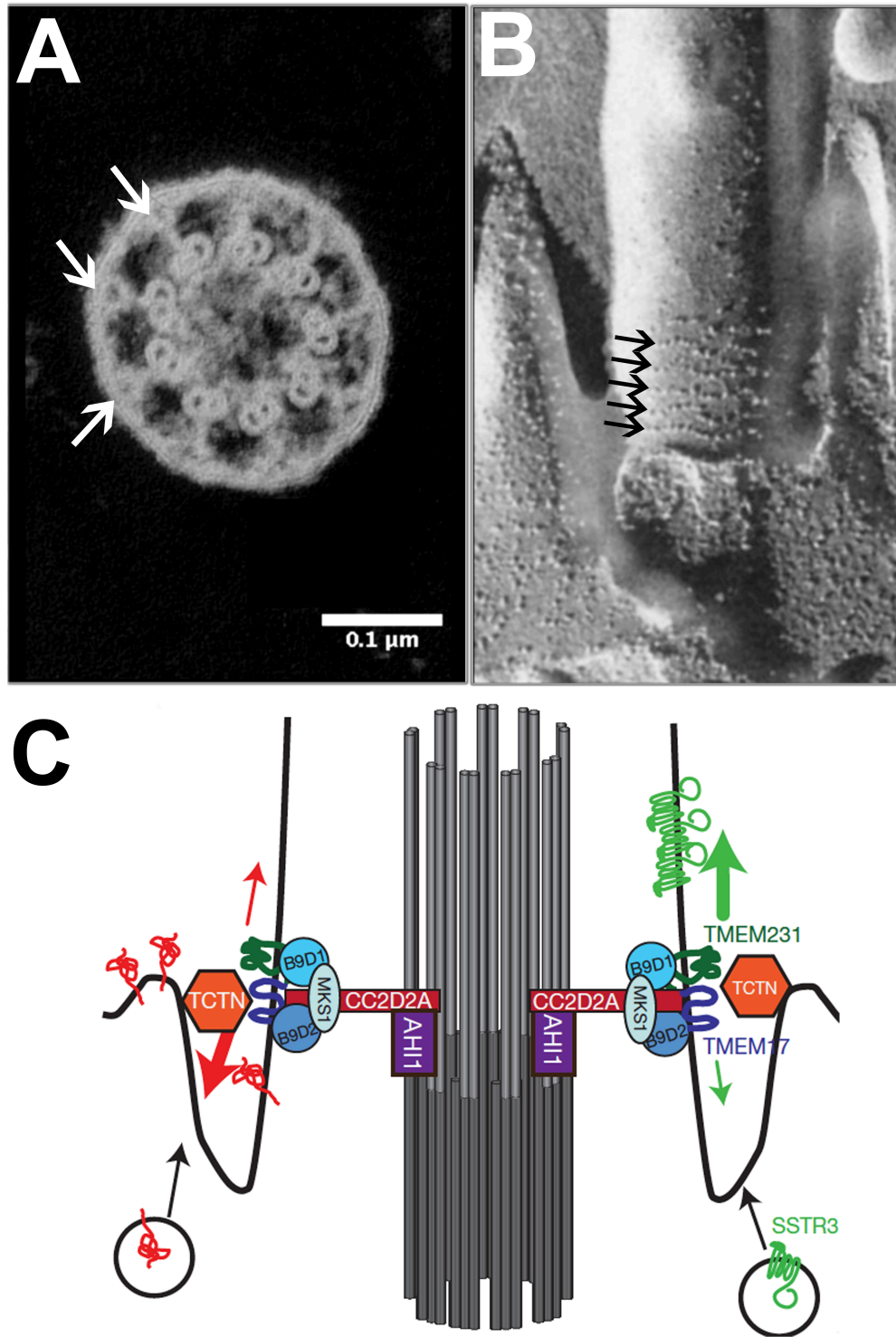


Figure I.3. Ciliary transition zone is marked by Y-links. (A) An EM micrograph showing the Y-links of a photoreceptor connecting cilium. Arrows point to the Y-Links (Adapted from (Besharse and Horst, 1990)). **(B)** Freeze-fracture SEM of a rat tracheal cell showing the ciliary necklace with little bumps (arrows) that may correspond to the tips of Y-links (adapted from (Gilula and Satir, 1972)). **(C)** A model of the cilia base showing transition zone proteins of the MKS module, B9d complex, and transmembrane proteins (adapted from (Chih et al., 2011)).

I.3.1. Modules of the TZ

Numerous biochemical and genetic analyses of the transition zone revealed a network of interactions between TZ proteins (Garcia-Gonzalo et al., 2011, Sang et al., 2011, Chih et al., 2011, Pazour et al., 2005). For instance, genetic analysis in *C.elegans* lead to the classification of the TZ proteins into two main modules: “MKS/MKSR” module which includes MKS1, B9d1, B9d2, TMEM67 (MKS3), and CC2D2A (MKS6) and “NPHP” module which comprises NPHP1 and NPHP4 (Williams et al., 2011). These two modules act redundantly and were found to be necessary for the early steps in ciliogenesis (Williams et al., 2011). The two modules are functionally linked to each other by another transition zone component, RPGRIP1L (MKS5), which controls the localisation of the proteins in both complexes (Williams et al., 2011). Mutations in NPHP and MKS modules alone did not affect the architecture of the transition zone, however, mutating components of both complexes had severe effects on the formation of the Y-links and thus affected ciliogenesis (Williams et al., 2008, Williams et al., 2011, Huang et al., 2011, Jensen et al., 2015, Yee et al., 2015). These genetic analyses reveal the importance of the transition zone components and their involvement in the structure and function of cilia. Moreover, proteomic analysis of TZ proteins revealed a network of interactions between proteins belonging to MKS and NPHP complexes. This network was divided into NPHP1-4-8, NPHP5-6, and MKS (Sang, et al. 2011).

I.3.2. Functions of the TZ

The transition zone is involved in controlling what is transported in and out of the cilium, and thus is widely involved in ciliogenesis. Some of the TZ components are thought to be necessary for the formation of the Y-links (Shi et al., 2017), others have roles in the vesicular transport machinery and the fusion of the ciliary vesicle with the plasma membrane to initiate the formation of the axoneme (Fig. I.3C) (Williams et al., 2011, Reiter et al., 2012, Awata et al., 2014, Garcia-Gonzalo et al., 2011). Due to its role in regulating the entry and exit of ciliary proteins, the transition zone is also thought to act as a ciliary gate or a diffusion barrier that coordinates and prevents non-specific movements of proteins into and out of the cilium. It also hypothesized that the TZ modulates the intraflagellar transport (IFT) proteins to carry cargoes into and out of the cilium (Nachury et al., 2010, Sang et al., 2011, Czarnecki and Shah, 2012, Garcia-Gonzalo and Reiter, 2012).

Although plenty of efforts have been devoted to characterizing the gating mechanism and localising individual transition zone proteins at the cilia base entity, it is still mysterious how some proteins are restricted from entering the cilium, while others, even large complexes, such as intraflagellar transport proteins (IFT), still gain access through this barrier. The architecture and arrangement of the TZ protein has been a very hot topic recently, especially with the emergence of several super-resolution imaging tools that are suitable to pinpoint slight differences in the arrangement and distribution of different proteins at the cilia base. It is very important to reveal the architecture and orientation of the TZ proteins to elucidate how these proteins are involved in controlling what comes in and out of the cilium and their relation to diseases.

I.4. The Transition Fibres

The transition fibres constitute a region that is distinct from the transition zone. They come nine in number spaced by about 60 nm from each other, extend from the C-tubule of the basal body, and attach to the ciliary membrane at the proximal end of the cilia base (Ringo, 1967, Nachury et al., 2010) (Fig. I.1C). These fibres do not only serve as the first point of attachment of the basal body to the cell membrane, but also serve as a physical barrier to the transport of proteins, as their inter-spaces are too small to allow the passage of vesicles (Buisson et al., 2012, Garcia-Gonzalo and Reiter, 2012, Klionsky et al., 2012, Reiter et al., 2012, Nachury et al., 2010).

There are at least 5 different proteins that form or regulate the formation of the transition fibres. These proteins include Cep83, Cep89, Sclt1, FBF1, and Cep164 (Tanos et al., 2013). The localization of these proteins requires other proteins, such as OFD1 and c2cd3, where the disruption of OFD1 prevented the formation of the distal appendages and thus blocked cilia formation (Singla et al., 2010, Thauvin-Robinet et al., 2014, Ye et al., 2014). Transition fibres have also been shown to be important recruitment sites for the IFT and transition zone components at the early stages of ciliogenesis (Deane et al., 2001, Schmidt et al., 2012). This has been confirmed by the failure of recruitment of the IFT protein IFT88 to the basal body in the absence of Cep164, one of the transition fibre components (Wei et al., 2013, Deane et al., 2001). Overall, this shows that the transition fibres contribute to ciliogenesis by recruiting necessary proteins to initiate cilia formation.

I.5. Ciliopathies

Defects in the assembly or function of cilia can cause several cilia-related diseases, collectively known as ciliopathies. Ciliopathies are a group of cilia-related diseases that affect many organs in the human body including the brain, lungs, kidney, and limbs (Fig. I.4) (Pedersen and Rosenbaum, 2008, Chih et al., 2011, Mitchison and Valente, 2017). Ciliopathies are caused by defects in the assembly, structure or function of primary or motile cilia. Defects in motile cilia usually affect cilia function in tissues and organs that contain them, such as the lungs and brain. Motile cilia diseases arise from mutations in the assembly of motile ciliary proteins or due to defects in the motility machinery. Proteins affected in motile cilia disease include dynein arms and radial spokes (Lucas et al., 2014) (Fig. I.1D). Dysfunctional motile cilia in the lungs manifest abnormal clearance of mucus in the respiratory airway, which leads to chronic diseases such as “primary ciliary dyskinesia” or “PCD” (Lucas et al., 2014, Mitchison and Valente, 2017). Because of the impaired ciliary clearance, patients with PCD suffer from recurrent chronic chest infections, sinusitis, and hearing impairment. Some PCD patients manifest *situs inversus*, or organ laterality, and are frequently infertile (Lucas et al., 2014).

On the other hand, defects in primary cilia cause cystic kidney diseases, Joubert syndrome (JBTS), Bardet-Biedel syndrome (BBS), Meckel-Gruber syndrome (MKS), and nephronophthisis (NPHP), where MKS is the most lethal among these ciliopathies (Fisch and Dupuis-Williams, 2011, Klionsky et al., Ishikawa and Marshall, 2011, Chih et al., 2011, Garcia-Gonzalo and Reiter, 2012). Many of the proteins causing ciliopathies localise to the transition zone and/or to the transition fibres of the cilium. For example, mutations in *Cep164*

and Cep83 (transition fibre components) cause nephronophthisis (Slaats et al., 2014, Failler et al., 2014). On the other hand, mutations in transition zone components, such as Tmem216, Tmem67, CEP290, RPGRIP1L, CC2D2A, TCTN2, TCTN3, and Tmem231 cause either Joubert syndrome, a ciliopathy characterized by cerebellar abnormalities and polydactyly (Valente et al., 2014, Huppke et al., 2015), or MKS, which is characterised by occipital encephalocele, polycystic kidneys, and polydactyly (Shaheen et al., 2013, Filges et al., 2014, Valente et al., 2014, Roberson et al., 2015, Shaheen et al., 2015).

While the genetic disruption of the NPHP complex components Nphp1 and Nphp4 usually cause mild defects that affect certain types of cilia, such as nephric and photoreceptor connecting cilia (Jiang et al., 2008, Jiang et al., 2009, Won et al., 2011), mutations in the MKS complex components, cause severe defects, and mostly are embryonic lethal (Weatherbee et al., 2009, Chih et al., 2011, Dowdle et al., 2011, Garcia-Gonzalo et al., 2011, Sang et al., 2011).

I.6. Intraflagellar Transport (IFT)

Intraflagellar transport or IFT is the bidirectional movement of multi-subunit protein complexes, known as the IFT particles, along the axonemal microtubules beneath the ciliary membrane. IFT is a highly conserved system that is required for the maintenance and assembly of cilia in several eukaryotic organisms. Since no protein synthesis takes place within the cilium, the extension of the ciliary axoneme is mediated by the intraflagellar transport

system, which supplies the building blocks of the axoneme (Scholey and Anderson, 2006, Pedersen and Rosenbaum, 2008, Goetz and Anderson, 2010, Sang et al., 2011). This transport system is powered by kinesin-II motor and cytoplasmic dynein-1b/2 molecules that aid IFT particle to walk along the microtubules within the ciliary shaft. IFT particles are moved from the base of the cilium to the tip of the cilium by kinesin-II proteins on the B-microtubules in a process known as anterograde transport; whereas, cytoplasmic dynein-1b, using the A-microtubules, powers IFT particle to exit the cilium in the retrograde transport (Stepanek and Pigino, 2016)(Fig. 1.5A).

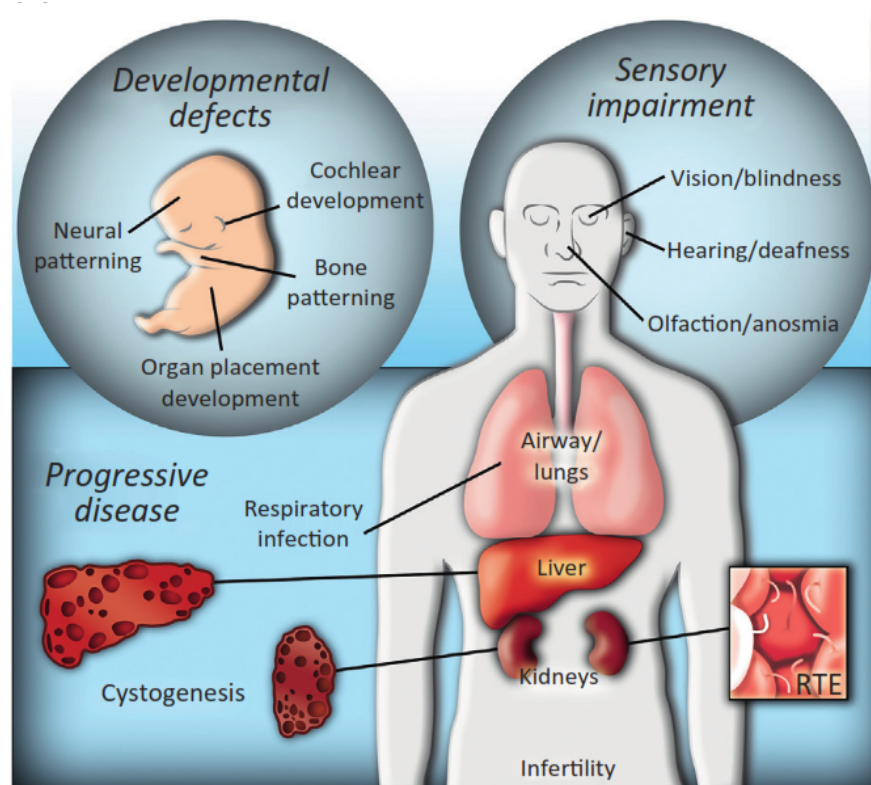


Figure 1.4. Ciliopathies. An illustration showing the organs affected by mutations in ciliary proteins causing several ciliopathies. Mutations in many ciliary proteins can cause defects in organs such as the lungs, kidneys, and brain. These cilia-related diseases are collectively known as “ciliopathies” (Adapted from (McIntyre et al., 2013)).

I.6.1 IFT complexes and functions

The IFT particle is composed of 22 unique proteins organised in two complexes called IFT-A (6 proteins) and IFT-B (16 proteins) (Fig. I.5B) (Pedersen and Rosenbaum, 2008, Silverman and Leroux, 2009) (Table IV.1 in chapter IV). IFT-B complex appears to be critically important for anterograde transport and ciliary assembly as mutations in most IFT-B proteins block cilia assembly (Tsujikawa and Malicki, 2004, Krock and Perkins, 2008). IFT-A mutations typically cause less severe defects in ciliary assembly and often result in accumulation of materials in the cilium, mainly at the ciliary tip, suggesting that it is important for the retrograde transport (Cole, 2003, Scholey, 2003, Taschner et al., 2011). This does not exclude roles of IFT-A complex in early steps of ciliogenesis as it was reported that the IFT-A component WDR35 (IFT121) is important for the fusion with Rab8 vesicles and the selectivity of ciliary membrane cargoes, such as Arl13b (ADP Ribosylation Factor Like GTPase 13b), INPP5E (Inositol Polyphosphate-5-Phosphatase E), and SSTR3 (Somatostatin receptor 3) (Fu et al., 2016). In addition to that, IFT-B proteins were shown to be required for the transport of ciliary cargoes (Keady et al., 2012, Eguether et al., 2014, Huet et al., 2014).

Moreover, another functional subdivision of IFT-B and IFT-A complex proteins has been recently proposed. IFT-B complex is subdivided into IFT-B1 and IFT-B2 subcomplexes, or core and peripheral, respectively. The core complex contains 10 IFT-B proteins and the remaining 6 IFT-B proteins belong to IFT-B2 subcomplex, or the peripheral complex (Fan et al., 2010, Lechtreck et al., 2009, Wang et al., 2009, Ishikawa et al., 2014). IFT88/IFT52 from IFT-B1 subcomplex bridges with IFT38/57 from IFT-B2 (Taschner et al., 2016). Similar

functional subdivision is used for the IFT-A complex that is also divided into 2 subcomplexes termed “core” and “non-core” proteins (Mukhopadhyay et al., 2010) (Fig. I.5B).

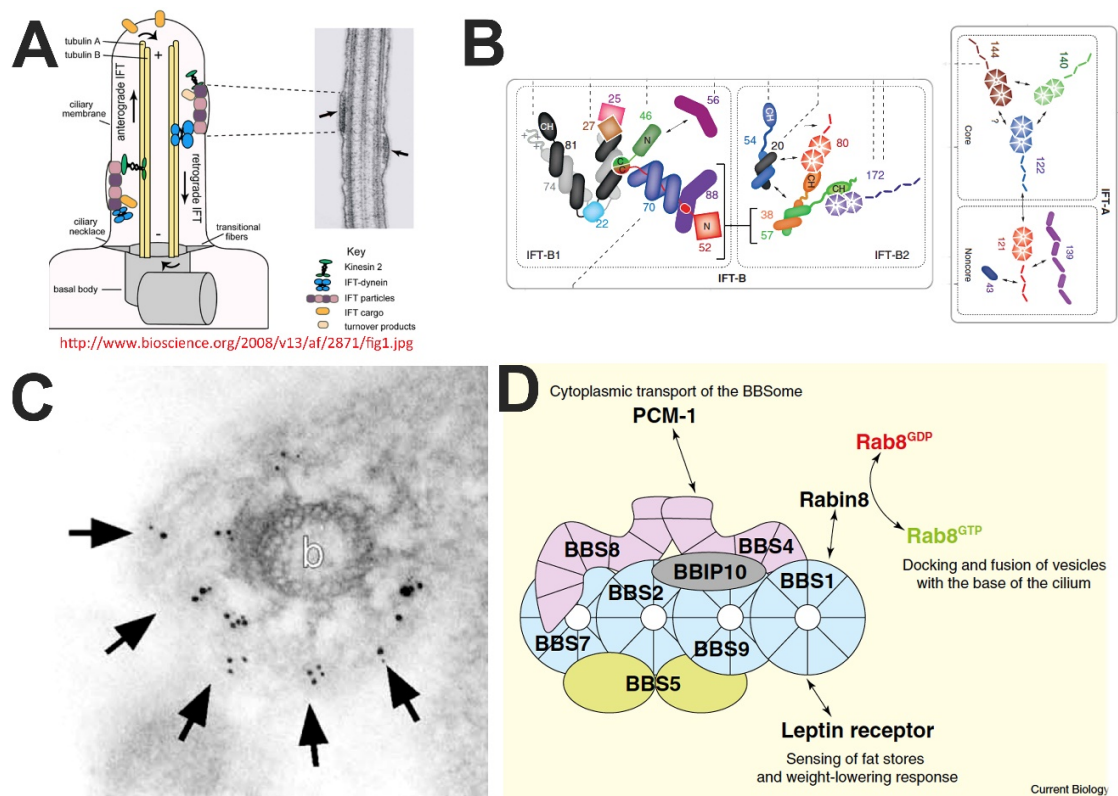


Figure I.5. Intraflagellar transport and BBsome. (A) A schematic depicting intraflagellar transport (IFT) showing the bidirectional movement of IFT particle into the cilium (anterograde) and out of the cilium (retrograde) (adapted from (Blacque et al., 2008)). (B) IFT-B complex (left) is subdivided into IFT-B1 (core) or IFT-B2 (peripheral) subcomplexes. IFT-A (right) is also divided into core and non-core complexes (adapted from (Taschner et al., 2016)). (C) Immunoelectron micrograph showing the distribution of IFT52 protein near the basal bodies (adapted from Deane, et al 2001). (D) An illustration of the BBsome octameric complex showing its components (Jin and Nachury, 2009).

Numerous immunofluorescence studies revealed that many IFT proteins accumulate at or near the base of the cilium (Zhao and Malicki, 2011, Krock and Perkins, 2008, Brown et al., 2015). Using immunoelectron microscopy,

Chlamydomonas IFT52 seemed to assemble at the distal ends of the basal body, or the transition fibres (Deane et al., 2001) (Fig. I.5C). Other IFT proteins, such as IFT57, IFT88, and IFT140, were shown to concentrate at that region too (Sedmak and Wolfrum, 2010, Williams et al., 2011). This shows that the transition fibres may also be essential for the docking and assembly for many proteins, mainly the IFT proteins, which in turn are important for cilia formation and maintenance. The determination of the roles of individual IFT proteins is quite complex, as in most cases the loss of one IFT protein leads to the destabilization of the whole complex. It is still unclear where exactly the IFT proteins dock and assemble to form particles before they gain access to the cilium. Super-resolution imaging of single IFT proteins may reveal the docking sites of the IFT proteins at the cilia base.

I.6.2. Protein interactions within the IFT Particle

Many interactions have been reported between the individual subunits of the B complex and include direct interactions between: “IFT88, IFT52 and IFT46”; “IFT81 and IFT74”; “IFT70 and IFT46”; and “IFT25 and 27”. IFT25/IFT27 is required for sonic hedgehog (Shh) signalling (Brazelton et al., 2001, Deane et al., 2001, Davis and Katsanis, 2012, Liew et al., 2014, Eguether et al., 2014). In addition to that, studies on interaction of IFT proteins with their cargoes have been widely investigated. For instance, IFT46 is important in the transport of outer dynein arms (ODAs) (Qin et al., 2004, Ahmed et al., 2008). IFT81/74 were reported to be necessary for the transport of tubulin to build the cilium (Bhogaraju et al., 2013).

On the other hand, IFT-A components were shown to indirectly transport membrane proteins (Mukhopadhyay et al., 2010, Fu et al., 2016) and most likely interact directly with BBS1, a protein that belongs to the BBSome protein complex (please see below) (Wei et al., 2012). Finally, no direct interactions between IFT-A and IFT-B complexes have been reported, with an exception of the possibility of IFT-B protein IFT74 to link the interaction between IFT-B and IFT-A complexes (Brown et al., 2015). However, a study suggested a physical link between IFT-A and IFT-B complexes through the BBSome and that the BBSome is involved in the assembly of IFT-A and IFT-B at the base of the cilium before anterograde transport and at the tip during the turnover to initiate the retrograde transport (Wei et al., 2012).

I.6.3. BBSome

The BBSome is an octameric protein complex composed of BBS1, BBS2, BBS4, BBS5, BBS6, BBS7, BBS9, and BBIP10 (Nachury et al., 2007, Loktev et al., 2008) (Fig. I.5D). The BBSome is required for trafficking membrane proteins and signaling receptors, such as SSTR3 and rhodopsin (Jin et al., 2010, Nachury et al., 2010, Berbari et al., 2008, Loktev et al., 2008, Wei et al., 2012, Liew et al., 2014). Mutations in these proteins cause Bardet Biedel Syndrome or BBS, which is a ciliopathy characterised by obesity, polydactyly, and mental retardation (Fliegauf et al., 2007, Zaghoul and Katsanis, 2009). The BBSome is thought to mediate the turnover of IFT particles at the ciliary tip (Wei et al., 2012). IFT27, a GTPase that belongs to the IFT-B complex is thought to detach from the IFT particle inside cilia to mediate the exit of BBSome from cilia

(Liew et al., 2014).

I.7. Regulation of Protein Transport at the Cilia Base

Numerous proteins are recruited to the cilium to maintain its structure and function (Awata et al., 2014, Breslow et al., 2013, Najafi and Calvert, 2012, Kee et al., 2012). The transport of membrane proteins is thought to be regulated at the base of the cilium by a diffusion barrier. Proteins move from the cytosol in vesicles, if these vesicles carry a ciliary membrane protein, they dock at the base of the cilium to be transported into the cilium. It is not clear how the interaction of different proteins at the ciliary base occurs to regulate the gating function.

For soluble proteins, the molecular mass barrier at the transition zone varies from one type of cell to another. For example, in *Xenopus* rods, the monomeric form (27kD), dimeric (54kD), and the trimeric GFP (81kD) could cross in a similar fashion the photoreceptor connecting cilium (Najafi and Calvert, 2012). However, dextrans, which have a molecular mass of 40kD, could not cross the barriers at the cilia base, but smaller dextrans of 10kD mass or less could enter these cilia (Fig. I.6A) (Kee et al., 2012, Kee and Verhey, 2013, Najafi and Calvert, 2012). Some studies also showed that the transition zone acts a size-exclusion filter, where proteins of stoke radii of 8nm or less could enter the cilium (Lin et al., 2013). So, for soluble cytoplasmic proteins, transition zone gating might not involve a diffusion barrier such as that proposed for membrane-associated proteins. For a soluble protein to enter the cilium, features including the molecular weight and the structural conformation of the

transport proteins are important to cross the gates at the cilia base (Reiter et al., 2012, Kee and Verhey, 2013).

I.8. An overview of nucleoporins in cilia

Recent studies suggested similarities between ciliary and nuclear transport entry (Kee et al., 2012, Diener et al., 2015, Takao and Verhey, 2016). The nuclear pore excludes proteins greater than 30kD in mass, but allows the passage of larger proteins if they contain nuclear localisation signals such as these in importins (Kee et al., 2012). Nucleoporins (Nups) are the main components of the nuclear pore; they form the structure of the pore and regulate the entry of cytosolic proteins into the nucleus. The nuclear pore complex is a large proteinaceous structure composed of more than 30 different nucleoporins that assemble into complexes (reviewed in (Lim and Fahrenkrog, 2006)). Similar to nuclei, cilia restrict the entry of proteins based on size, but utilize active transport to allow the entry of large proteins (Kee et al., 2012, Kee and Verhey, 2013). It was shown that the active transport into the cilium involves nuclear trafficking components including importins, a Ran-guanosine triphosphate concentration gradient (Ran-GTP), and nucleoporins (Dishinger et al., 2010b, Kee et al., 2012). This could indicate that nuclei and cilia share similar molecular components that regulate import into their compartments.

I.8.1. Where do nucleoporins localise in the ciliary compartment?

Using GFP-fusions to nucleoporins, it was shown that some nucleoporins, such as Nup37, Nup35, Nup93, and Nup62 localized to the cilia

base in Odora and hTERT-RPE-1 cells (Fig. I.6B). Other Nups, such as POM121, GP210, and NDC1, did not localise to the cilia base (Kee et al., 2012, Najafi and Calvert, 2012). In addition to that, using mAb414 antibody that recognizes several FG-containing (phenylalanine-glycine motif) nucleoporins, including Nup358, Nup214, Nup62, and Nup53, also localized to the cilia base.

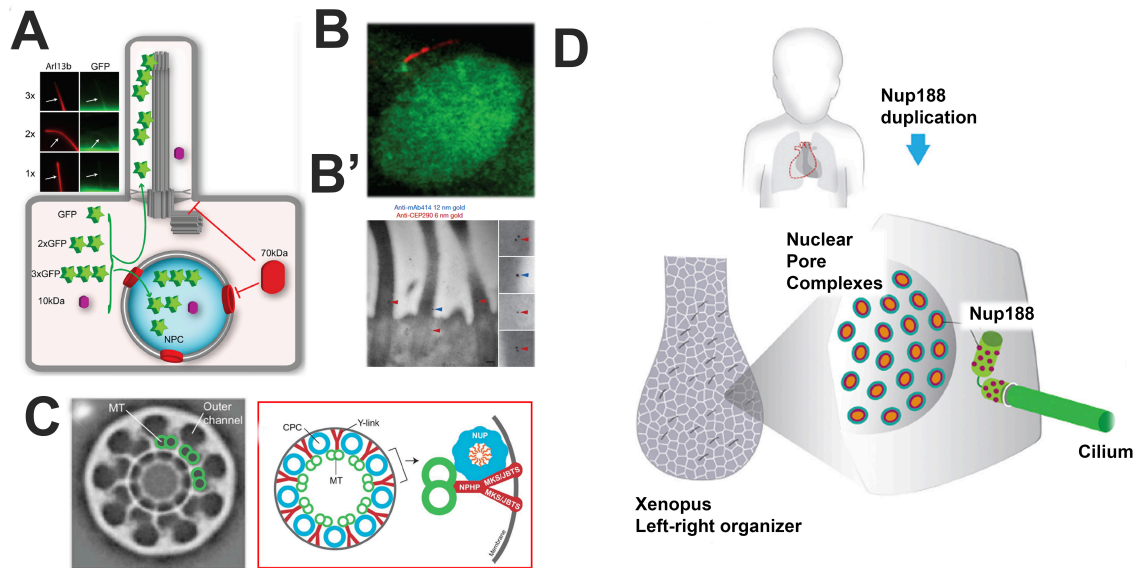


Figure I.6. Nucleoporins and cilia. (A) Monomeric GFP (27kD), dimeric GFP (54kD), and trimeric GFP (81kD) can cross both the ciliary gate and nuclear pores. Dextrans of 70kD could not cross both gates, but 10kDa dextran crossed both gates easily (adapted from (Kee et al., 2012)). (B) Nucleoporin Nup62 (green) localise to the base of cilium in odora cells (Adapted from (Kee et al., 2012)). (C) An illustration proposing that nucleoporins form ciliary pore complex between the Y-Links at the cilia base (adapted from (Takao and Verhey, 2016)). (D) An illustration showing that Nup188 and Nup93 localize in barrel-like structures around the centrioles of the basal bodies in Xenopus left-right organizer (Adapted from (Del Viso et al., 2016)).

Using immunoelectron microscopy on rat tracheal cells with mAb414 and CEP290 antibodies showed that nucleoporins localise at the transition zone and basal bodies of motile cilia (Fig. I.6B') (Kee et al., 2012). However, recent studies in xenopus embryos using super-resolution imaging, showed that

nucleoporins form barrel-like structures near basal bodies (Del Viso et al., 2016)(Fig. I.6D); this contradicts the idea that nucleoporins form rings/pores at the cilia base as was proposed earlier (Fig. I.6C) (Kee and Verhey, 2013, Takao and Verhey, 2016). Thus, nucleoporins could hypothetically assemble in different architectures at the cilia base in different model systems. This, however, requires much more investigation of the localisation and function of nucleoporins in cilia of different organisms.

I.8.2. Possible functions of nucleoporins in cilia

The presence of nucleoporins at the base of the cilium is interesting and suggests an important role of these proteins in ciliogenesis. The disruption of nucleoporins in NIH3T3 cells affected the entry of the kinesin motor protein KIF17 (Kee et al., 2012, Dishinger et al., 2010b). In addition to that, the depletion of Nup188 and Nup93 affected ciliogenesis in the left-right organizer in xenopus larvae (Del Viso et al., 2016). This reveals that the nucleoporins might contribute to the gating structures at the cilia base, and thus might be involved in regulating ciliary protein composition. Therefore, disrupting some nucleoporins could affect the transport of some ciliary proteins.

I.9. Cilia and Polarity

Cilia emerge from the apical surfaces of most epithelial cells and thus proteins important for determining the polarity of epithelial tissues may also have roles in ciliogenesis. The highly conserved apico-basal polarity determinants, Crumbs proteins, are necessary for the determination of the

apico-basal polarity in epithelia (Bilder et al., 2003, Tanentzapf and Tepass, 2003, Bachmann et al., 2001). *crumbs* genes were first discovered in *Drosophila melanogaster* where a loss of function of *crumbs* produced “crumby” epithelia (Tepass and Knust, 1990). In humans, there are three isoforms of crumbs, *CRB1*, *CRB2*, and *CRB3*. Loss-of-function of *CRB1* causes ciliopathies known as retinitis pigmentosa (RP) and Leber congenital amaurosis (den Hollander et al., 2001, den Hollander et al., 1999). In zebrafish there are 5 crumbs orthologues, named *crb1*, *crb2a (ome)*, *crb2b*, *crb3a*, and *crb3b* (Omori and Malicki, 2006) (Fig. I.7A).

Zebrafish crumbs genes display distinct expression patterns. *crb2b*, for example, is highly enriched in the pronephros and in photoreceptor cells (Hsu et al., 2006, Omori and Malicki, 2006, Zou et al., 2012). *crb3a*, on the other hand, is expressed predominantly in the otic vesicle at stages that were investigated thus far (Omori and Malicki), (Gosens et al., 2008, Omori and Malicki, 2006, van den Hurk et al., 2005) (Fig. I.7A). Crumbs proteins contain a transmembrane region (TM), a well-conserved intracellular region (cytoplasmic tail), and an extracellular domain of varying size (Tepass and Knust, 1990, van den Hurk et al., 2005, Omori and Malicki, 2006). For example, zebrafish *Crb3a* and *Crb3b* contain a very short extracellular domain compared to *Crb1* and *Crb2* that contain very large ones (Fig. I.7A).

Crumbs extracellular domains, such as EGF-like repeats and Laminin-G domains, mediate cell adhesion (Zou et al., 2012). On the other hand, the very-well conserved C-terminal intracellular tail of Crumbs proteins contains two domains known as FERM (F for 4.1 proteins, E for Ezrin, R for Radixin, and M for Moesin (Chishti et al., 1998)), and PDZ (P for postsynaptic density

protein (PSD95), D for Drosophila disc large tumor suppressor (Dlg1), and Z for Zonula Occludens-1 protein (ZO-1) (Kennedy, 1995) binding domains (PDB) (Fig. 1.7A). Both FERM and PDB domains mediate the apico-basal polarity function of the Crumbs protein (Wodarz et al., 1995).

Crumbs proteins have been also shown to be involved in ciliogenesis. They localize to cilia in mammalian cells (Fig. 1.7B) (Whiteman et al., 2014, Szymaniak et al., 2015, Hurd et al., 2003), and the loss of CRB3 activity blocks cilia formation (Fan et al., 2004). *In vivo* studies using morpholino knockdown experiments showed that zebrafish *crb3* is essential for the elongation of kinocilia in the ear (Omori and Malicki, 2006). An indirect interaction between CRB3 and Kif3a, a component of the kinesin-II family important for powering the anterograde transport into cilia, has been postulated (Sfakianos et al., 2007, Huang et al., 2008) (Fig. 1.7C). However, it has not been investigated whether crumbs zebrafish mutants would show similar phenotypes to those shown in *in vitro* and morpholino knockdown studies. In addition, the role of crumbs in ciliogenesis *in vivo* is poorly understood.

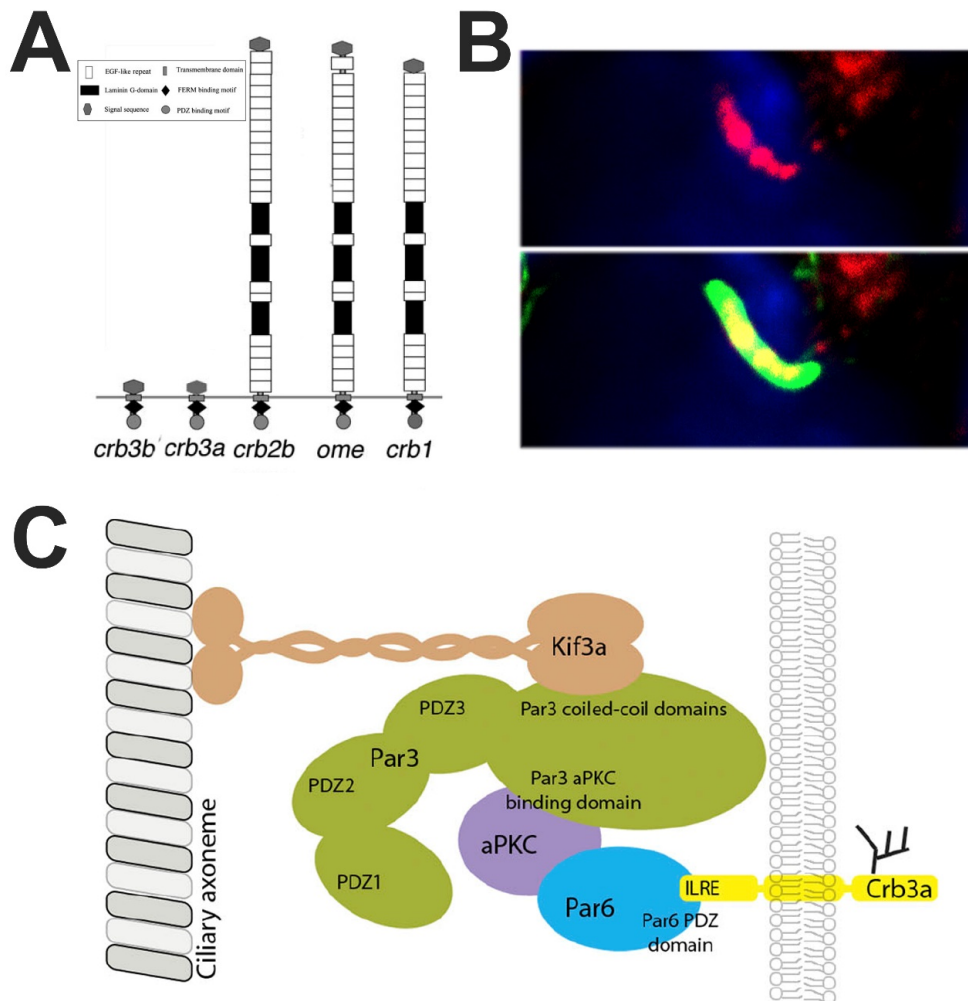


Figure I.7. The relationship between apico-basal polarity determinants, *crumbs* genes, and ciliogenesis. (A) An illustration showing the 5 orthologues of *crumbs* in zebrafish, *crb1*, *crb2a* (*ome*), *crb2b*, *crb3a*, and *crb3b*. Note that *crb3a* and *crb3b* have very short extracellular domains compared to *crb2a*, *crb2b*, and *crb1* proteins (adapted from (Omori and Malicki, 2006)). **(B)** A confocal image of an IMCD3 cell stained with anti-acetylated tubulin to mark cilia (green) and anti-CRB antibody that recognizes the conserved C-terminus of Crumbs proteins (red). The cell is counterstained with DAPI (blue) to mark the nucleus. **(C)** An illustration depicting an indirect interaction between Crb3a and Kif3a, the motor that powers the movement of IFT particle into the cilium (Adapted from (Sfakianos et al., 2007)).

I.10. Conventional versus Super-resolution microscopy

Light microscopy is a very powerful and versatile tool in biological and medical research. Light microscopy is widely used to image biological

specimens, but the nature of light limits the resolution to about 200-300nm. This does not make it possible to image complexes, interactions, architectures, and subcellular structures, which mostly occur at a scale of few tens of nanometres (Huang et al., 2008, Huang et al., 2010, Schermelleh et al., 2010). Super-resolution microscopes, such as stimulated emission depletion (STED), structured illumination microscopy (SIM), and single molecule localization based microscopy (SMLM): including stochastic optical reconstruction microscopy (STORM) and photoactivated localization microscopy (PALM), have emerged as very powerful light microscopy tools that can surpass the diffraction limit of light and achieve resolutions of about 100nm for SIM (Gustafsson et al., 2008), 50nm for STED (Sieber et al., 2007), and 20nm for STORM (Huang et al., 2010). Using such advanced imaging techniques, one can improve the resolution up to 10 times compared to that of conventional light microscopy (Huang et al., 2010). This allows imaging of protein complexes in unprecedented details (Huang et al., 2010, Huang et al., 2008), and thus can be very suitable to image structures and complexes within the ciliary compartment (Del Viso et al., 2016, Shi et al., 2017).

I.11. Stochastic Optical Reconstruction Microscopy (STORM)

STORM imaging is a form of super-resolution microscopy that relies on the photoswitching characteristic of the fluorescent dyes used, such as Alexa Fluor 647 (Rust et al., 2006). Photoswitchable fluorophores rotate between fluorescent (ON) and dark (OFF) states for several times before they irreversibly photobleach. These switching events between fluorescent and dark states

enable bypassing the subdiffraction limit, therefore improving the resolution ((Chozinski et al., 2014)). In order to photoswitch these fluorophores, a continuous illumination with a red laser (such as 637 laser) is required. This activates a subset of these fluorophores, excite them (or switch them on), and keep the remaining fluorophores “off” (Dempsey et al., 2009, Huang et al., 2010, Dempsey et al., 2011). For this to be achieved, the buffer conditions must be optimal so that the fluorophores keep switching between fluorescent “on” and dark “off” states (Olivier et al., 2013) before they become irreversibly photobleached. These buffers usually contain thiol reagents, such as mercaptoethylamine, and oxygen scavenging reagents, such as catalase and glucose oxidase. Several buffer conditions have been tested and optimised for different fluorophores and fluorescent proteins (Olivier et al., 2013, Nahidiazar et al., 2016).

For a STORM image to be produced, the following steps must take place: a small subset of fluorophores is switched “on” (excited state), while most of the remaining fluorophores are still “off” (dark state) (Dempsey et al., 2011), this is known as “blinking events. This is followed by another subset of fluorophores switching on stochastically while most fluorophores are off. The process of switching “on” and “off” is repeated many times and recorded over thousands of frames, so that most or all the fluorophores will be localized. Finally, computational analysis with software (such as NIS Elements from NIKON), or “ThunderSTORM” plug-in available in the FIJI (ImageJ) package, can be used to process and reconstruct STORM fluorophore localisation data. Positions of proteins are reconstructed based on the positions of all the activated fluorophores to produce the super-resolution image (Fig. I.8A).

I.12. Applications of Super-Resolution Imaging in Cilia Biology

SIM, STED, STORM, and PALM, have emerged as great microscopy tools to image different ciliary structures including those at the basal body (Mennella et al., 2012, Lau et al., 2012), the distal appendages (Yang et al., 2015), and the transition zone (Shi et al., 2017, Lambacher et al., 2016).

For instance, by using 3D-STORM combined with quantitative imaging analysis, *Shi et al.*, could elucidate some components of the ciliary gating structures at the cilia base. By analysing different components of the ciliary transition zone in murine tracheal cells, they showed that RPGRIP1L, B9d1, and NPHP1 form rings outside the microtubule doublets and are close or at the ciliary membrane. They proposed that these proteins might be the building blocks of the arms of the Y-links (Fig. I.8B) (Shi et al., 2017). Moreover, using STED and STORM imaging in *C.elegans* and mammalian cells, it was shown that some transition zone components are periodically distributed along the axial plane and either form multiple stacked rings or form spiral orientations along the ciliary axoneme (Fig. I.8C). Using STORM, TZ components RPGRIP1L and Tmem67 formed rings at the cilia base. Tmem67 had a diameter that positions it to the ciliary membrane, whereas, RPGRIP1L seemed to be away from the ciliary membrane (Fig. I.8C) (Lambacher et al., 2016).

SIM and STORM imaging combined with quantitative analysis were also utilised to define the PCM (peri-centriolar material) structure by showing that peri-centrin like protein (PLP) is positioned at the centriolar wall, and organised in clusters of nine-fold symmetry (Mennella et al., 2012). The orientation, architecture, and the relative position of many transition fibre proteins have been

extensively analysed using STED and STORM imaging. Just recently, it was shown that the distal appendages show a cone-shaped architecture rather than a pinwheel shape as was previously proposed (Yang, et al., 2017). Using STORM imaging, it was shown that cep83, cep89, and cep164, form the backbone of the distal appendages, while FBF1, is found at the distal regions of the appendages near the ciliary membrane (Yang, et al., 2017) (Fig. 1.8D). Cep164 was also shown to form 9-fold symmetric rings using STED imaging in mouse tracheal cells (Lau et al., 2012). STED microscopy was also used to map proteins at the cilia base, including those of the transition zone, transition fibre, IFT proteins, and basal body proteins (Yang et al., 2015).

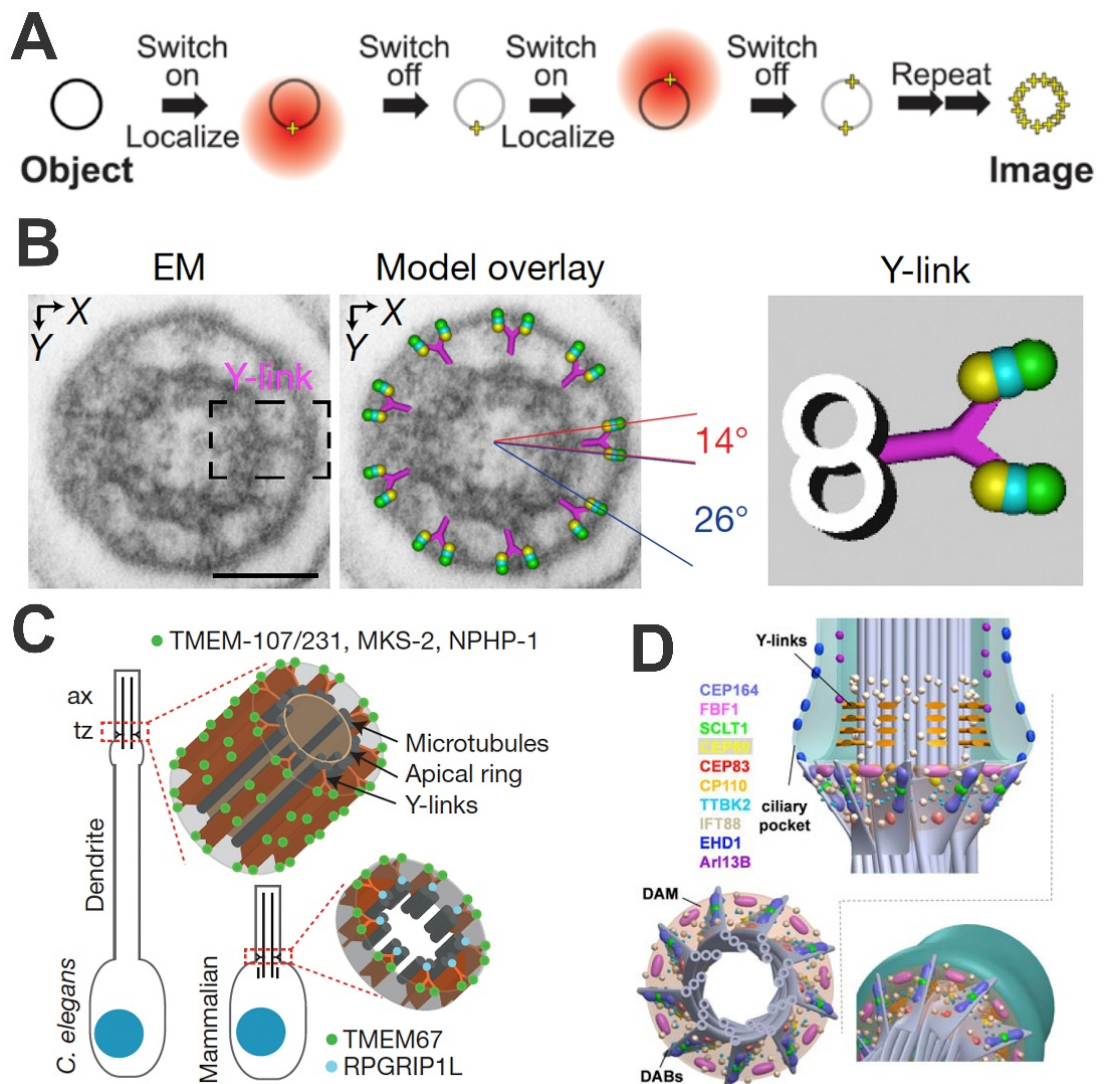


Figure I.8. Applications of super-resolution imaging in cilia biology. (A) An illustration showing the principle of fluorophore photoswitching during STORM imaging and the reconstruction process to form a STORM image (adapted from Huang, et al., 2011). (B) A model proposing the radial distribution of transition zone proteins: Tmem231 (green), Nphp1 (blue), and RPGRIP1L (yellow) on the arms of Y-links (Shi et al., 2017). (C) Using STED and STORM microscopy in *C.elegans* and mammalian cells, transition zone proteins seem to form clusters arranged in rings at the cilia base (Lambacher et al., 2016). (D) A model depicting the arrangement of several transition fibre proteins as indicated at the cilia base using STORM imaging (Adapted from Yang et al., 2017).

I.13. Models used in this thesis

In addition to mammalian cell cultures (mainly IMCD3) and primary cell cultures (normal human bronchial epithelial cells: NHBE and mouse tracheal epithelial cells: mTECs), *Tetrahymena thermophila* was the main model used to generate a super-resolved model of the cilia base using STORM microscopy. On the other hand, zebrafish was the main model used to analyse the role of *crumbs* genes in ciliogenesis and gating mechanisms at the cilia base.

I.13.1. *Tetrahymena thermophila*

Tetrahymena thermophila are 30 by 50µm unicellular eukaryotes that belong to the kingdom Protista (Orias et al., 2011, Gaertig et al., 2013) (Fig. I.9A). Each cell differentiates about 500 cilia arranged in about 20 longitudinal rows. Cilia in *Tetrahymena* are required for movement, feeding (by phagocytosis at the oral apparatus), and for mating (Orias et al., 2011, Collins and Gorovsky, 2005). A *Tetrahymena* cell contains two nuclei, the germ-line micronucleus (Mic), which is diploid, transcriptionally inactive and contains 5 pairs of chromosomes, and the somatic macronucleus (Mac), which is polyploid, transcriptionally active (Collins and Gorovsky, 2005, Gaertig et al.,

2013) and estimated to contain about 45 copies of each protein coding gene. They grow relatively fast and divide once each 2-3hr under optimal conditions. During the vegetative life cycle, *Tetrahymena* cells divide by binary fission, during which the micronucleus divides by mitosis, while the macronucleus divides amitotically (Dave et al., 2009). Therefore, when *Tetrahymena* cells undergo vegetative life cycle, it is not possible to deliver the same number of copies of modified alleles to both macronuclei in daughter cells. This random allelic distribution in the macronucleus produces cells with slight different allelic content between each other. By the process of “phenotypic assortment”, it is possible to select a population of *Tetrahymena* cells that contains a high copy number of a particular allele (Merriam and Bruns, 1988).

Tetrahymena thermophila (Fig. 1.9A) has been widely used in the biological research to answer several scientific questions (Collins and Gorovsky, 2005), such as the function of catalytic RNA (Herschlag and Cech, 1990), telomeric repeats (Allshire et al., 1988), telomerase (Bryan et al., 1998), and histone acetylation (Pfeffer et al., 1989). It grows rapidly in axenic media and share many important biological processes with higher vertebrates, including humans (Cassidy-Hanley, 2012). There are several reasons that make *Tetrahymena thermophila* a very good model to study cilia and ciliogenesis. Each cell has about 500 cilia, this provides a plenty of cilia to be examined all at once. The ability to deciliate (remove) cilia and regenerate cilia facilitates the study of cilia assembly in these organisms (Rosenbaum and Carlson, 1969). One can also stop cilia assembly by starving cells, which allows examining cilia after being assembled (Vonderfecht et al., 2011). Moreover, the genome of *Tetrahymena* contains many conserved ciliary

proteins (Eisen et al., 2006) (Table I.1) and is very suitable for reverse genetics (Dave et al., 2009).

Many *Tetrahymena* ciliary proteins are very well conserved with higher vertebrates, including humans (Table I.1). However some transition fibre proteins, such as Cep83 and Sclt1 are not found in the *Tetrahymena* genome. In addition to that, the transition zone protein RPGRIP1L has at least 6 homologues in *Tetrahymena thermophila*, and therefore was difficult to investigate in this current study.

Finally, through homologous recombination, any region of the *Tetrahymena* genome can be targeted (Chalker, 2012). This makes it possible to tag genes at their native locus by transforming *Tetrahymena* cells with expression vectors containing the tagged genes of interests. The tagged gene will replace all the wild-type copies of the target gene under antibiotic selection. In this thesis, we also show that *Tetrahymena thermophila* is an excellent model for super-resolution imaging of several protein complexes at the cilia base. We present here novel approaches on how to image these proteins using STORM.

Protein Name	Size of protein in humans (aa)	Name of Tetrahymena protein/size in aa	% Positives (% Identities)
TZ			
MKS6/CC2D2A	1620	TTHERM_00348780/ /1599	38 (21)
MKS3/Tmem67	995	TTHERM_01016240 /946	43 (24)
MKS1	559	TTHERM_00630490 /492	46 (25)
B9D1	204	TTHERM_00219110 /215	62 (39)
Ahi-1	1196	TTHERM_00460620 /820	45 (24)
Tmem231	316	TTHERM_000441849 /295	36 (23)
Tmem216	145	TTHERM_00842510 /149	46 (33)
NPHP4	1426	TTHERM_00653970 /1714	48 (25)
IFT			
IFT54	691	TTHERM_01070330 /451	56 (35)
IFT52	437	TTHERM_00648910 /434	59 (42)
IFT46	304	TTHERM_00193580 /342	74 (50)
IFT81	676	TTHERM_01013160 /716	52 (27)
IFT27/Rabl4	186	TTHERM_00298510 /148	55 (35)
IFT122	1241	TTHERM_00694540 /1251	52 (32)
IFT144/WDR19	1342	TTHERM_01093530 /1387	55 (34)
IFT140	1462	TTHERM_00220810 /1407	53 (29)
Kinesin-II			
Kif3a	699	TTHERM_00481220 /736	57 (41)
IFT adaptor			
ODA16	DAW1/415	TTHERM_00762930 /426	75 (60)
BB			
OFD-1	1012	TTHERM_00214750 /976	(23)

Table I.1. Ciliary proteins in *Tetrahymena thermophila* are well conserved with higher vertebrates, including humans. A summary of *T.thermophila* proteins investigated in this study showing their similarities/identities with human ciliary proteins.

I.13.2. *Danio rerio* (Zebrafish)

Zebrafish has emerged an excellent model in the biological and biomedical research in the past few decades (Fig. I.9D). It has been widely used as a model for many ciliary genes (Zhao and Malicki, 2011, Pooranachandran and Malicki, 2016, Tsujikawa and Malicki, 2004) (Fig. I.9D). It has been a very productive model for imaging, and this is because the zebrafish embryos are transparent and relatively easy to immunostain, they produce tens to hundreds of fish in one cross. Moreover, the advances in generation of zebrafish mutants using TALEN nucleases and CRISPRs made it easy to generate very effective mutants. Here, we used zebrafish mutants to analyse the role of crumbs proteins in ciliogenesis in several ciliated tissues in the zebrafish, such as the mechanosensory kinocilia in the ear, nasal cilia, lateral line cilia, and pronephric cilia.

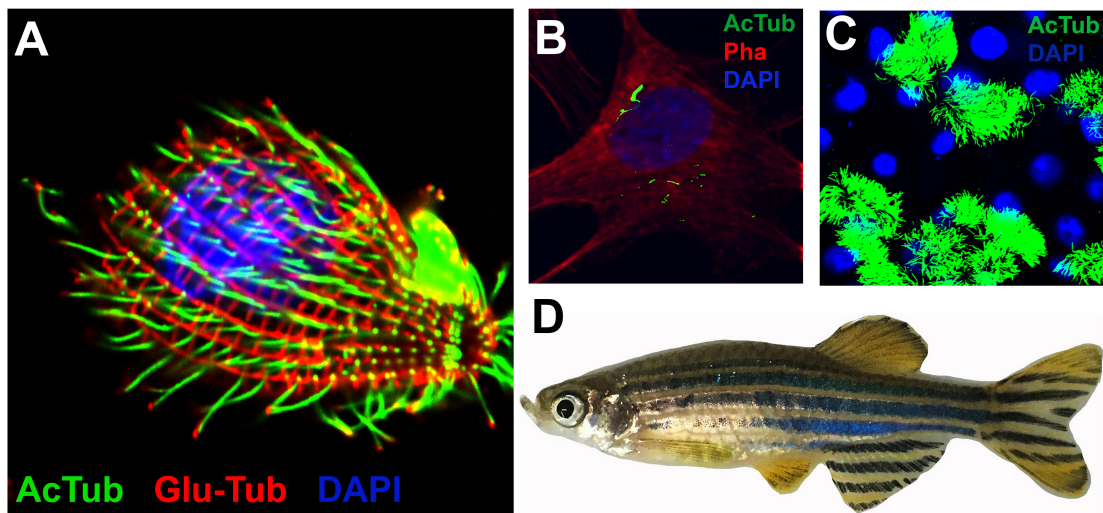


Figure. I.9. Model systems used in this thesis. (A) A confocal image of *Tetrahymena* cell stained with anti-acetylated tubulin (green) and anti-glutamylated tubulin (red) to mark cilia. **(B)** A confocal image of a 3T3 cell stained with anti-acetylated tubulin (green) to mark cilia and phalloidin (red) to detect actin. **(C)** Primary culture of nasal epithelial cells stained with anti-acetylated tubulin to mark cilia (green). All cells in **(A)**, **(B)**, and **(C)** are counterstained with DAPI to mark the nuclei. **(D)** A photograph of an adult zebrafish.

I.14. Aims of the PhD project(s) and main findings

To reveal the architecture of different protein complexes at the cilia base, we mainly utilised *Tetrahymena thermophila* to generate a super-resolved model of the cilia base. We have characterised the localisation, distribution, and orientation of at least 18 different ciliary proteins, most of which reside at the cilia base. These proteins included those that belong to the transition zone (7 proteins), basal body (1 protein), cargo adaptor (1 protein), IFT particle (8 proteins: 5 IFT-B proteins, and 3 IFT-A proteins), and kinesin (1 protein). To reveal the architecture of these ciliary proteins, radially and axially, we analysed their localisation using tags at the N- and C- termini. To do so, we generated transgenic lines (knock-ins) in *Tetrahymena thermophila*, where we added tags (HA, V5, or GFP) at either the C- or N- termini at the native locus of the gene (Gaertig et al., 2013). This enabled us to localise the exact position of the proteins using antibody staining against the tag. For this purpose, we employed a combination of different imaging techniques, including confocal microscopy, TIRF imaging, and mainly STORM imaging. This was followed by computational quantitative analysis of STORM data using codes written in MATLAB. These analyses enabled us to determine the radial and axial positions of the C- and N-termini of the proteins.

Moreover, to confirm our results in other model system, we examined some of these proteins in either primary cultures derived from human bronchial epithelial cells or mouse tracheal cells, and mammalian cells, such as IMCD3. In combination with quantitative and imaging analysis using codes written in MATLAB, we present here the super-resolved model of the cilia base revealing the architecture of at least 18 different ciliary protein. Most importantly, this

model shows the docking sites of the IFT particle and the binding sites of tubulin and outer dynein complex at the cilia base. It also reveals the position of IFT proteins with respect to TZ proteins.

Furthermore, we investigated the relationship of Crumbs proteins to ciliogenesis and their possible roles in the gating mechanisms at the cilia base. For this purpose, we examined the role of Crumbs proteins in cilia of zebrafish mutants and mammalian cells. Using TALEN nucleases, we generated several zebrafish crumbs mutants and analysed them using confocal microscopy and image analysis. We also used TIRF imaging in IMCD3 cells to elucidate the effect of the absence of Crumbs proteins on the dynamics of the intraflagellar transport proteins and ciliogenesis. Our findings show that Crumbs proteins mediate IFT proteins, and therefore contribute to gating mechanisms at the cilia base.

Main findings

1. Using STORM combined with image analysis, I show that the ciliary transition zone proteins display 9-fold radial symmetry and localize to distinct radial and axial positions. The characterization of the position of the N- and C-termini of some TZ proteins enabled me to determine their orientation at the cilia base and eventually generate a super-resolved model of 10 epitopes in 7 different TZ proteins → CHAPTER III
2. Using STORM imaging combined with image analysis, I show for the first time the arrangement of IFT proteins in their docking sites at the cilia base. In *Tetrahymena thermophila*, I characterized the distribution, radial and

axial positions of 3 IFT-A proteins, 5 IFT-B proteins, one IFT motor protein, and one cargo adaptor protein. I determined the N- and C- termini distribution of these proteins at the cilia base. I show that IFT proteins dock between the transition zone and the basal body and that IFT-A complex lies to the outside of IFT-B complex in the radial dimension. I show that all IFT proteins examined are organised in clear 9-fold symmetrical rings at the cilia base. I reveal the localization of the binding sites of cargoes such as tubulin and outer dynein arm complex (ODA) at the cilia base. I also show the arrangement and localization of IFT88 in IMCD3 cells and primary cultures of mouse tracheal epithelial cells (mTECs). I present the first super-resolved model that reveals the architecture of IFT particles in their docking sites and shows the orientation of IFT proteins at the cilia base → CHAPTER IV

3. The analysis of *crumbs* genes function in zebrafish mutants revealed that the absence of some *crumbs* genes affects cilia length in a subset of ciliated tissues in the zebrafish, such the cristae in the ear and nasal cilia. In the absence of one *crumbs* gene, other crumbs proteins accumulated massively inside the ciliary compartment accompanied by accumulation of the IFT particle inside the ciliary shaft of these mutants. On the other hand, the absence of Crb3 in IMCD3 cells produced relatively shorter cilia with reduced IFT track lengths, but surprisingly, IFT trains were somewhat faster in the cilia of knocked-down cells. Since Crumbs proteins affect the ciliary composition, this implies that *crumbs* genes may contribute to gating mechanisms at the cilia base → Chapter V

Chapter II

“MATERIALS AND METHODS”

II.1. *Tetrahymena thermophila* culture

Tetrahymena thermophila were grown, handled and maintained as previously described (Gaertig et al., 2013). Wild-type cells (Cu428.1) were grown in SPP medium, containing 1% proteose peptone (Bacto, 211684), 0.2% glucose (VWR, 101174Y), 0.1% yeast extract (Bacto, 288620), and 0.003% Fe-EDTA (Sigma, E6760), supplemented with 1% antibiotic-antimycotic mix (Lonza, 17-745E) at final concentrations of 100U/mL of penicillin, 100µg/mL of streptomycin, and 0.25µg/mL of amphotericin B. Cells were grown at 30°C with moderate shaking at 80 rounds per minute (rpm).

To select the transgenic lines examined in this study and promote the phenotypic assortment, the following antibiotics were used: paromomycin sulphate (Sigma, P9297), puromycin (LKT labs, P8168), or cycloheximide (Sigma, C7698). For long-term storage, cells were maintained at RT in 15mL falcon tubes (Corning, 352097). Cells were checked every other day on a light microscope, such as Zeiss Axio Lab1, to ensure cells are healthy and have good morphology. Before experiments, cells were inoculated in SPP medium for about 24hr before proceeding with experiments. All transgenic lines used in this study are listed in “Table II.1”.

II.2. Genomic DNA extraction from *Tetrahymena thermophila*

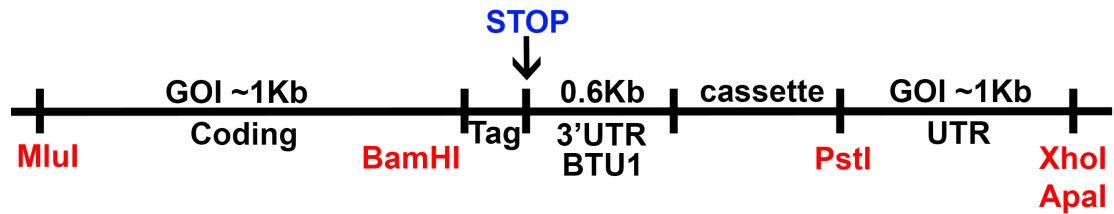
Tetrahymena cells were grown in SPP medium at a final density of 3-5 x 10⁵ cells/mL. 25mL of cells were starved in 10mM Tris-HCl (pH 7.4) for 18-24hr. Cells were then spun at 3000rpm for 5min. The supernatant was removed, and cells were resuspended in about 0.5mL of Tris-HCl buffer and transferred to a 15 mL Falcon tube. 3.5mL of Urea lysis buffer (42% urea, 0.35M NaCl, 0.01M

Tris pH 7.5, 0.01M EDTA, and 1% SDS) were added to the cells and gently mixed for 4min. Next, the lysate was extracted with an equal volume of phenol:chloroform:isoamyl alcohol (25:24:1) and spun at 3500rpm for 15min. The water phase containing genomic DNA was collected and extracted again with equal volume of phenol:chloroform:isoamyl alcohol (25:24:1). After centrifugation (as before), the collected water phase was extracted with equal volume of chloroform:isoamyl alcohol (24:1) and spun again for 15min at 3500rpm. To precipitate the DNA, 1mL of 5M NaCl was added to approximately 3mL of the collected water phase and next DNA was precipitated by the addition of an equal volume of isopropyl alcohol. The DNA was then spooled using a glass pipette and transferred to an eppendorf tube, washed with 70% ethanol and dried out. The pellet was resuspended with 600 μ L of TE buffer with 6 μ L of RNase A (10mg/mL, ThermoFischer, EO0381). To solubilize the genomic DNA, the sample was heated at 55 $^{\circ}$ C O/N. Carbohydrates were removed by spinning the sample at 31,000g for 45min at 20 $^{\circ}$ C. The yield of the DNA obtained varied between 100-300 μ g/mL.

II.3. Protein tagging

Epitope tagging at the native locus of the gene is expected to produce the natural pattern of expression of all the proteins examined in this study (Gaertig et al., 2013). The tags used (3HA, 3V5, or GFP) were inserted either at the C-terminus or the N-terminus of the coding region of the gene of interest in the macronuclear genome by homologous recombination with the linearized construct as depicted in the figure below. Note that the map of the construct

shown in the figure below was used for the epitope tagging at the C-terminus only.



Construct used that allows epitope tagging of the C-terminus at the native locus of the gene. “GOI”: gene of interest; “3’UTR BTU1”: terminator of beta tubulin 1; cassette: *Neomycin*, *cycloheximide*, or *pruromycin*; Tag: 3HA, 3V5, or GFP were used in this study. Antibiotic selection will promote the growth of the transformed *Tetrahymena* cells and assortment of the transgene.

II.4. Alignments

The sequences of the proteins of interest were obtained from www.uniprot.org of either human, mouse, *Chlamydomonas*, or *C.elegans* proteins. The sequences were then blasted against *Tetrahymena thermophila* database (ciliate.org). Examples of alignments for some proteins are shown in the appendix. Primers for 3’UTR, 5’UTR and coding regions of the genes of interest were designed and used to amplify the genes of interests. The lists of primer sequences used for the amplification of the genes of interest in this study are summarised in “Table II.1”.

III.5. Preparing constructs for transformation into *Tetrahymena thermophila*

The coding and untranslated (UTR) regions of the genes of interest were amplified using standard PCR protocols. To clone the UTR regions, the PCR products and the construct to be used for cloning were digested using the following restriction enzymes: *MluI* and *BamHI* for the coding region, *SacI* and

PstI for 5'UTR (N-terminal tagging), and *PstI* and *XhoI* for 3'UTR (C-terminal tagging). The constructs were incubated for 3hr at RT followed by incubation at -20°C over night (O/N).

The digests were then run on 1% agarose gels and the DNA was extracted from the gel using the DNA extraction kit (QIAquick Gel Extraction Kit, 28704) as recommended by the manufacturer. The extracted insert and construct were then ligated at RT for 3hr using T4 DNA ligase (NEB, M0202S) following the manufacturer's instructions. Plasmids were then transformed into XL gold *E.coli* and plated onto LB plates supplemented with ampicillin and incubated at 37°C O/N. At least 8 colonies from each strain were picked and inoculated in 2.7mL of LB medium containing ampicillin (Sigma, 108035242001) for about 16hr shaking at 200rpm to be used for plasmid DNA extraction.

II.6. Plasmid DNA extraction

DNA from the bacterial clones was extracted using the "Dirty Prep Protocol": 2mL of the 2.7mL grown cultures were transferred to 2mL round-bottomed eppendorf tubes (the remaining 0.7ml were used later for mini-preps). Cell cultures were spun at maximum speed for 1min, the supernatant was discarded, and the pellet was resuspended in 100µl of "Solution I: 25mM Tris pH 8 + 10mM EDTA, pH 8 + 50mM glucose + RNaseA". Resuspended cells were lysed by adding 200µl of solution containing: 1% SDS + 0.2M NaOH. Cells were lysed for 4min at RT. Next, 150µl of "Solution III: 60% 5M KAc + 11.5% glacial acetic acid + 28.5% water" were added and mixed, kept on ice for 5min and then the tubes were spun at maximum speed for 5min at 10°C. The supernatant was transferred to the new sterile tubes and plasmid DNA was

precipitated with 550µl of 100% isopropanol. After centrifugation, plasmid DNA was washed with 500µl of 70% ethanol for 5min at RT. All the ethanol was removed, and the pellets were kept at RT on the bench to dry out. 40µl of distilled water were added to each pellet and kept at the bench for 5min. Finally, the pellet was resuspended in distilled water by pipetting up and down to get the DNA sample. The correct plasmids were selected based on the analysis with the restriction enzymes. Plasmid DNA was digested for 2hr at 37°C. The digestion product was then run on 1% agarose gel to check the correct band size

Bacteria containing the correct plasmid were inoculated (remaining 0.7mL) into 20mL of LB containing ampicillin and grown O/N at 37°C to be used for extracting DNA using the mini-prep kit (Biolabs, T1010S) following the manufacturer's recommendations. After extracting the DNA using mini-preps, (this DNA now contains the cloned UTR region of the genes of interest), 7µg of the DNA were digested with the appropriate restriction enzymes to clone the coding region of the genes of interest. The product of digestion was run on 1% agarose gel and the DNA was extracted from the gel. The same procedure was applied to clone the coding region of the genes of interest into the same vector, as done for the UTR regions.

After ensuring that both the UTR and coding regions were inserted correctly into the vector by restriction digests and running on gels, the DNA was sent for sequencing to confirm the correct sequences were obtained. Final plasmids were digested with *SacII* and *BamHI* (N-terminal tagging) or *MluI* and *XhoI* (C-terminal tagging) to separate transgene from the plasmid backbone and used to transform into *Tetrahymena* cells by biolistic transformation.

II.7. Biolistic Transformation and selection of transgenic (knock-in) lines

The biolistic transformation was carried out as described previously (Dave et al., 2009). *Tetrahymena* cells were grown in SPP medium to a density of 2×10^5 cells/mL. Cells were then starved in 10mM Tris-HCl, pH 7.4 O/N (about 16-20hr) before transformation. To prepare the DNA for shooting, about 10 μ g of final plasmids was digested with the appropriate restriction enzymes to separate the targeting fragment from the plasmid, precipitated onto DNAdel Gold Carrier Particles (Seashell Technology, La Jolla, CA) according to the manufacturer's instruction. After digestion, 2-3 μ l of the digest was run on 1% agarose gel to ensure that the digestion was successful. If so, the digestion product was cleaned using QIAquick PCR purification kit (QIAGEN, 28104) and biolistically transformed into CU428.2 cells (WT cells). For shooting, a circular Whatmann paper was placed in a 100mm petri dish and made moist with some 10mM Tris-HCl (pH 7.4). Starved cells were then centrifuged at 3000rpm for 3min, and placed on the moist Whatmann paper. Shooting was performed using the BioRad Gun (PDS-1000) following the manufacturer's recommendation. After shooting, cells were transferred to 50 mL SPP medium supplied with antibiotic and kept at 30 $^{\circ}$ C for at least 2hr without shaking. Transformants were selected for 3-4 days at 30 $^{\circ}$ C on SPP with 2.5 μ g/ml of Cadmium chloride (CdCl₂) and either 100 μ g/ml paromomycin (BioShop Canada Inc) or 200 μ g/ml puromycin (BioShop Canada Inc). The positive clones were grown in media with decreasing concentrations of CdCl₂ (to 0.05 – 0.1 μ g/ml) and increasing concentration of the drug to promote phenotypic assortment.

For lines tagged at the C-terminus using *neo4* cassette, 120 μ g/mL (final concentration) of the antibiotic paromomycin and 1 μ g/mL of CdCl₂ were added

to the 50mL cell culture. After 2hr, cells were transferred to 96-well plates (Costar, 3590), 100µl per well using a multi-channel pipette. Plates were placed in a humidified container at 30°C without shaking for 48-72hr. For lines tagged at the N-terminus using *neo2* cassette, 100µg of paromomycin was added to the cells before spreading on 96-well plates. For lines tagged at the C-terminus using the *cycloheximide* cassette, cells were kept in SPP without shaking at 30°C for 6hr before cycloheximide antibiotic was added to the cells at a final concentration of 7.5µg/mL. And for the lines tagged at the C-terminus using *puromycin* cassette, the final concentration of antibiotic added was 200µg/mL. In all lines, the wells that showed good growth were used for further selection using increased concentrations of the antibiotics depending on the cassette of selection that was used.

The cells were checked every day for growth and the antibiotic concentrations for selection were increased gradually. The maximum concentration of paromomycin sulfate used was 2mg/mL, 8µg/mL for cycloheximide, and 200µg/mL for puromycin dihydrochloride. When this was achieved, the cells were then grown in SPP medium for 24hr; the protein was then extracted for further analysis.

II.8. Protein extraction in *Tetrahymena thermophila*

3×10^7 cells/mL were used for protein extraction. Cells were spun at 3000rpm for 3min, washed with 10mM Tris-HCl, pH 7.4 and spun again at 3000rpm. 2x lysis buffer (1.4M sucrose, 4mM EGTA (Alfa Aesar 67-425), 4mM EDTA (Sigma Aldrich, 27285) in 20mM Tris buffer, pH 8) was added on the cells and kept on ice for 1-2min. Cells were then centrifuged at 16000g for 10min at 4°C. The supernatant was discarded, and the cells were washed with 10mM Tris-HCl, pH 7.4 and centrifuged again at full speed for 10min to get the protein pellet. The pellet was resuspended in about 300µl of 10mM Tris-HCl, pH 7.4 and used for further analysis, or stored at -20°C for later use. The protein concentration was assessed using the BCA assay (ThermoFischer, 23225).

II.9. SDS-PAGE and Western Blot

50µg of protein were heated at 95°C for 5min in 2x lamelli buffer containing 4% SDS (Fischer, UN1325) and 20% glycerol (VWR, 444485B), and 0.2M TRIS pH 6.8, bromophenol blue, DTT or β-mercaptoethanol. The samples were loaded on SDS-PAGE gel (concentration of the gel varied between 8 and 12% depending on the size of the protein of interest). The gel was run at 90V for 10min followed by 120V for at least 1hr. Western blots were performed using standard protocols. The transfer was done into nitrocellulose membranes (GE, 10600002) at 160mA for 1hr. The blot was blocked in 5% skimmed milk (Oxoid, LP0031) in TBSTw (TBS with Tween, Sigma, T7949) for 1hr shaking at RT, and then incubated with the appropriate primary antibody diluted in milk O/N at 4°C shaking. Primary antibodies used included: mouse monoclonal anti-HA (1:2000; Covance, MMS-101R); rabbit monoclonal anti-V5 (1:1000; Cell Signalling,

D3H8Q); mouse anti-GFP antibody (1:5000; Life Technologies, A11122). The blot was then washed 3x with TBSTw, 10min each, and incubated in the secondary antibody (1:10,000; goat polyclonal, HRP, Abcam, ab97051) diluted in 5% milk for 1hr at RT. The blot was washed 3x in TBSTw, 10min each, the ECL substrate (ThermoFisher, 32106) was added and images of the blots were collected using the G-box. Lines with successful WBs were then immunostained for confocal and STORM imaging.

II.10. Deciliation (pH shock method)

Cilia of *Tetrahymena thermophila* were deciliated as previously described (Gaertig et al., 2013). Cells were grown in SPP at 30°C with moderate shaking (80rpm) until they reached a density of 2×10^5 cells/mL. Cells were then centrifuged for 3min at 1680g in a swinging rotor centrifuge (Sigma, 3-16 KL). Cells were then washed with 10mM Tris-HCl, pH 7.4, centrifuged again at 1680g for 3min then resuspended in 20mL of deciliation buffer containing 10mM Tris-HCl, pH 7.4, 50mM sucrose (Amresco, M117), 10mM Calcium Chloride (Alfa Aesar, L13191), and protease inhibitors (Complete Roche, 04693159001) in an Erlenmeyer flask.

To force cells shed their cilia off, 420µl of 0.5M acetic acid (BDH, 200-580-7) were added to cells drop-wise and the flask was gently swirled for approximately 45sec. This will drop the pH to 4.3 and cause the cells to shed their cilia off. Then 360µl of 0.6M KOH (Merck, 1.05033.0500) were added to the same flask to neutralize the pH again. Cells were gently mixed and checked under light microscope (Zeiss Axio Lab1) to ensure they stopped moving, but still have good morphology. The cells tend to shake in their place as they shed

their cilia off. Deciliated cells were either fixed and immunostained directly, or left for 30-60min in Tris-HCl (pH 7.4) to allow them to regenerate cilia before fixing the cells and immunostaining them as explained below.

II.11. Immunostaining for confocal microscopy

Tetrahymena cells were resuspended in fresh SPP medium at 30°C for 16-24hr. 15µl of *Tetrahymena* cells were added as one drop on coverslips (VWR, ECN 631-1570), followed by adding 15µl of 0.5-2% Triton X-100 (Sigma, T8787) prepared in PHEM buffer (60mM PIPES (Fischer Bioreagents, BP2924-50) + 25mM HEPES (Gibco, 15630-056) + 10mM EGTA (Alfa Aesar, A16086 + 2mM MgCl₂ (Chemcruz, sc-2031267) pH 6.9). After 45-60 seconds, 15µl of 4% PFA prepared in PHEM buffer were added on the permeabilised cells.

The whole cell mixture (now ~45µl) was then spread gently all over the coverslip using a yellow tip. The coverslips were kept at RT or at 30°C to dry out completely. Cells were then rehydrated and blocked by adding 150-200µl of the blocking solution (3% BSA + 0.02% Tween in 1x PBS) for 10min at RT. Cells were then incubated in the primary antibody diluted in the blocking solution for 1hr at RT or O/N at 4°C. Primary antibodies used in this study are listed in Table II.3. Cells were washed with PBS (1X) for 3x, 10min for each wash, and then incubated in the secondary antibodies diluted in the blocking solution for 1hr at RT or 4°C O/N in the dark. Secondary antibodies included goat anti-mouse 488, goat anti-rabbit 488, goat anti-mouse 568, goat anti-mouse 647, and goat anti-rabbit 647. Cells were washed again with PBS (1X) for 3x, 10min each and counterstained with DAPI (1µg/mL) to mark nuclei. Coverslips containing the stained cells were mounted on glass slides (VWR,

ECN 631-1550) by adding 5µl of ProLong Gold (Life Technologies, P36930) mounting media and sealed with nail polish. Samples were then imaged on the Olympus FV1000 confocal system using the 60x/1.42 oil lens.

For IMCD3-IFT88 cells and primary cultures of mouse tracheal cells (mTEC) or human bronchial epithelial cells (NHBE), the cells were fixed with 4%PFA for 30min at RT and then washed at least 3 x with 1x PBS solution, 10min each. The cells were then permeabilised using 0.5% Triton X-100 in PBS (1x) for 10min at RT followed by blocking with 3%BSA in PBS for 1hr at RT. Cells were then incubated in the primary antibody for 90min followed by 5x washes with PBSTr (0.1%Triton X-100 in 1x PBS). Cells were then incubated with the secondary antibody for 1hr at RT in the dark. Finally, cells were washed with PBSTr for at least 3x, counterstained with DAPI to mark nuclei. For primary cultures, the membranes of the transwells where the cells were growing were cut using a blade and the stained cells were mounted on glass slides and covered with coverslips to be imaged on the Olympus FV1000 confocal microscope using the 60x/1.42 oil lens.

II.12. Immunostaining for STORM imaging

The preparation of the sample for STORM imaging was done the same as that for confocal imaging, except that the coverslips used here were of high precision 22 x 22 coverslips (Marienfeld, 0107052) and the secondary antibody used here was specifically Alexa Flour 647 (1:500; goat anti-mouse, ThermoFischer, A21235 or goat anti-rabbit, A27040). We also stained most of *Tetrahymena* transgenic lines using anti-HA directly conjugated to A647, such as 1:100; Cell Signalling, 3444 or 1:150, Invitrogen, 26183A647).

To determine the axial position of the proteins of interest with respect to Nup50, the samples were incubated with two primary antibodies at once, one to recognise the protein of interest and another to mark the reference point (Nup50). Samples were incubated in the primary antibody solution at 4°C O/N. The samples were washed and incubated in goat anti-rabbit or mouse A647 secondary antibody to detect both primary antibodies. After the incubation with the secondary antibody, the samples were washed once with PBS (1x) for 10min and in most cases, the samples were postfixed with 4%PFA or 4% PFA with 0.1% glutaraldehyde (VWR, UN2927) for 10min at RT. Samples were then washed at least 5x in PBS (1x), 10min each. Finally, the samples were mounted on depression slides (Marienfeld, 1320002) with 90-100µl of GLOX buffer containing 100mM glucose + 40µg Catalase from bovine liver (Sigma; C9322) + 100µg glucose oxidase from *Aspergillus niger* (Sigma; 49180) supplied with 100mM of Cysteamine (MEA, Sigma; M9768). The coverslip was sealed with nail polish and imaged on the Nikon STORM system using the 100x/1.49 oil lens. The samples were used in STORM imaging for a maximum of 3hr after sealing, as the intensity of the signal fades after that, and therefore the switching process becomes weaker.

II.13. Settings used to process STORM images

Stochastic Optical Reconstruction Microscopy (STORM) imaging was performed on the NIKON Eclipse Ti inverted Microscope using the Apo TIRF 100x/1.49 NA oil lens equipped with “30mW 405 laser” and “300mW 638 laser”. Images were acquired at 4.8ms (128 x 128 pixels) or 9.2ms (256 x 256 pixels, pixel size: 0.157646µm) for 20,000-50,000 frames using the ixOn Ultra EMCCD

camera (Andor Technology) in the TIRF mode with no binning. EM gain was set at 17 MHz – 16-bit, EM gain multiplier at 300, and conversion gain multiplier at 3. The cells were first detected at a very low laser power (0.5-1% of the 638 laser) and then illuminated with 100% 638nm laser to force fluorophores to photoswitch. Blinking events could be detected within a few seconds in most of the cases. When photoswitching reduced, the 405nm laser was used to activate the remaining A647 fluorophores; this was either controlled manually or by using the “Auto LP” option provided by the NIS-Elements software.

II.14. Reconstruction and analysis of STORM images

The STORM images were reconstructed using the NIS Elements Imaging Software, version 4.51.01, provided by Nikon. The acquired raw data (nd2 files) were run on NIS Elements with following settings: “Auto ROI”, minimum height 2500-3000 and maximum height 65535; Andor Baseline was set to 100, minimum width 200nm, maximum width 400nm, initial fit width 300nm, maximum axial ratio 1.3, and maximum displacement of 1 pixel. At the end of the run, a “molecule list” file in a binary format (.bin) was generated and contained many parameters including the coordinates, intensity, and lateral localisation accuracy of each frame. The lateral localisation accuracy was calculated using NIS Elements software (Thompson et al., 2002). The minimal localisation accuracy was about 2 nm in most of our experiments of all the lines investigated in this study. The lateral drift in the images was corrected during the analysis using the automatic drift correction option that is provided in the NIS Elements software. Using autocorrelation, the entire set of molecules is

used to track the drift. The coordinates of the molecules after drift correction were also automatically stored in the molecules list at the end of the analysis.

While all image analysis was carried out using the molecules lists (raw data), images of the rings in all the figures were displayed as normalised Gaussians to make them appear as spots or blobs. A normalised Gaussian is a display method provided by NIS Elements to visualise a molecule's location, intensity, and width. The size of the width is scaled to correspond to the theoretical localisation uncertainty based on the number of photons collected during imaging (Thompson et al., 2002). The appearance of the images was also adjusted using the "Advanced Gaussian Rendering" option in the NIS Elements software. An example of how images look before and after Gaussian smoothing is depicted in Fig. II.

II.15. Estimation of average radial position (MATLAB)

Identifying the centre of the ring: Coordinates of individual fluorophore blinking events were clustered using "k-means" method with k from 6 to 15. The optimal number of clusters was evaluated using silhouette criterion (Kaufman & Rousseeuw, 1990). The clustering was then interactively validated for being adequate. Two clusters with lowest summarized intensity of fluorophore blinking events were removed (Fig. II.1B), to exclude signal coming from the background noise. The centres of remaining clusters were fit with a circle, and the centre of this circle was used as a centre of the ring for further analysis. Only rings with the circular fit of cluster centres with goodness-of-fit R^2 greater than 0.9 were used.

Quantification of radius of individual rings: The radial distances of

individual fluorophore blinking events from identified ring centres were calculated. Intensities of blinking events were summed at 2nm intervals from the centre, producing a histogram with radial distribution of signal for each ring. This histogram was then fitted with either Gaussian distribution. Means of the best-fit distributions corresponded to radii of individual rings, and standard deviations to their width. Only the rings where the goodness-of-fit of Gaussian distribution of 0.7-0.8 or more were used for statistical analysis and generation of an averaged ring (Fig. II.1A). To generate an averaged ring, radial distribution of individual rings was summed and normalized to the number of rings. The resulting distribution was fitted with either Gaussian distribution or circularly convolved Gaussian distribution to obtain the radius and width of the averaged ring. Finally, the summed distribution of signal and the profiles of best-fit distribution were plotted radially from a centre of empty images to create a visual representation of averaged rings (Fig. II.1A).

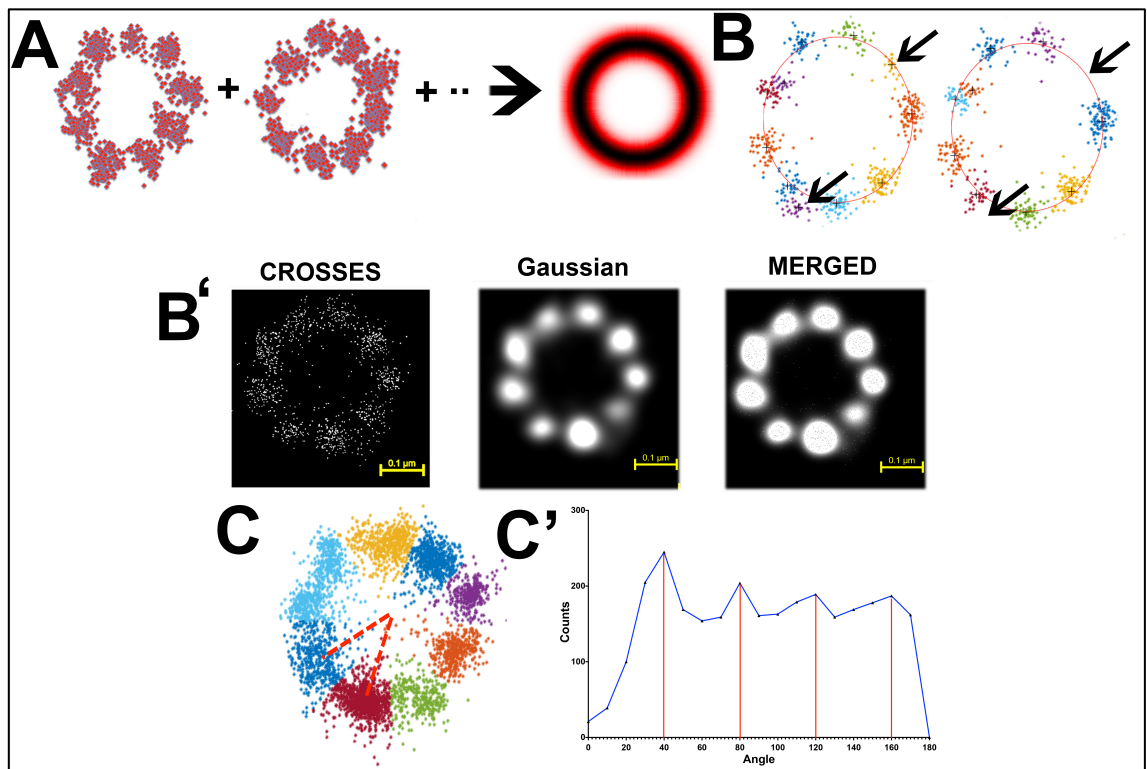


Figure. II.1. Graphical representation and estimation of the radial positions of the proteins using MATLAB. (A) The coordinates of the molecules collected for each ring are averaged and summed using codes written in MATLAB to produce a summarised fit ring (shown in red). Examples shown in (A) are from NPHP4-N terminus lines. (B) To exclude signal coming from background, the code eliminates the 2 clusters with the lowest summarised intensities (shown with black arrows). Data shown in (B) are obtained from NPHP4-C terminus lines. (B') A representation of how Gaussian smoothing is applied to data using NIS Elements software. Crosses represent the centroids of each molecule and blobs/spots show data after Gaussian smoothing. Data are for NPHP4-C terminus line. (C) A representation of how the code measures the angle between adjacent clusters. (C') Angular distribution of adjacent clusters. The example shown here represents the angular distribution of NPHP4-C terminus which clearly shows peaks every 40° , thus confirming the 9-fold symmetry.

II.16. Estimation of axial positions (MATLAB)

To determine the distance between two parallel rings the individual fluorophore blinking events were split into two clusters. As in this case clusters are not spherical, individual fluorophore blinking events were fit with a Gaussian mixture model. Then the clustering was interactively validated for being adequate. The brighter of two clusters was fit with an ellipse with individual blinking events being weighted proportionally to their intensity. The centre of each dataset was calculated as a mean of cluster centres. Then each dataset was shifted and rotated. Namely, the coordinates of individual blinking events were shifted so that the new centre of each dataset corresponded to coordinates of origin, and rotated so that the major axis of the brighter cluster was aligned with X-axis. Intensities of blinking events were summed at 2nm intervals along X- and Y-axis, producing histograms of signal distributions along each axis. Y-axis histogram was used to fit the signal with a sum of two Gaussian distributions. The distance between means of two distributions corresponded to the distance between two rings. Only the datasets with the

goodness-of-fit being 0.6-0.7 or more were used for statistics and to generate a summarized image. The Y- and X-axes distributions of individual rings were summed and normalized to the number of datasets. The outer product of summarized distributions was plotted to produce an image of an averaged dataset. The summarized Y-axis distribution was fit with a sum of two Gaussian distributions. The distance between mean of distributions corresponded to the distance in averaged dataset between two parallel rings (Fig. II.1A).

II.17. Degree of labelling (dol)

For indirect labelling (primary antibodies followed by secondary antibodies), all the secondary antibodies used in this study were IgG Fc whole antibodies against the heavy and light chains of the immunogen, with a degree of labelling that ranged between 3 and 6 fluorophores per a molecule of IgG. For the direct labelling (primary antibody directly conjugated to the fluorophore), the HA tag mouse monoclonal antibody conjugated to A647 was used (Table II.3). This antibody recognizes the HA tag fused to either the C- or N-termini. The degree of labelling of these antibodies ranged between 2-6 fluorophores per an IgG molecule.

II.18. Zebrafish strains and maintenance

crb3a mutant alleles *crb3a^{sh410}* and *crb3a^{sh346}* were generated using transcription activator-like effector nucleases (TALENs) as described previously (Zu et al., 2013, Pooranachandran and Malicki, 2016). The *crb2a^{m98}* mutant allele was described previously in detail (Omori and Malicki, 2006, Malicki et al.,

1996a, Malicki and Driever, 1999) and the *crb2b*^{sa18042} allele was obtained from the Sanger Institute TILLING project. Zebrafish were maintained in accordance with UK Home Office regulations and the UK Animals (Scientific Procedures) Act 1986. Fish genotypes were determined by fin-clipping adults at 3 months of age or later followed by DNA isolation, PCR amplification of mutant sites, and Sanger sequencing. The following primers were used: 5'-TTCTACACTTCTGGCTTCCG-39 and 5'-ATTGTGGCCATCGTTGTA-3' for *crb3a*^{sh410} and *crb3a*^{sh346}, and 5'-AAACTTCCGACTCCTCTCCG-3' and 5'AAAGATGTCCTACCCAGCTT-3' for *crb2b*^{sa18042}. During phenotypic analysis, mutants were compared to phenotypically wild-type siblings or to phenotypically wild-type animals derived from common ancestral generation. Mutations that do not cause lethality (*crb3a*^{sh410}; *crb3a*^{sh346}; and *crb2b*^{sa18042}) were maintained as homozygous strains. Consequently, analysis of cilia phenotype was performed on maternal/ zygotic mutants.

II.19. Photography of adult zebrafish

To record adult phenotypes, zebrafish 6 months old or older more were placed in weighing boats (7mL, 611–9179; VWR) containing E3 medium with tricaine (E10521, 0.2mg/ml; Sigma). Photographs were obtained using an iPad Pro digital camera, 12MP, F/2.2, 29mm, phase detection autofocus.

II.20. Immunostaining, mounting, and microscopy (zebrafish)

Staining of whole zebrafish at 36 hours postfertilization (hpf), 72hpf, and 5 days postfertilization (dpf) was performed as previously described (Leventea

et al., 2016). The following primary antibodies and dilutions were used: anti-acetylated tubulin, 1:500–1:1000 (T6793; Sigma [Sigma Chemical], St. Louis, MO); anti-CRB (Omori and Malicki), 1:250; anti-Kif17(ab11261; Abcam), 1:500; anti-IFT88, 1:500; and anti-IFT52, 1:500. Anti-IFT antibodies were kindly provided by Brian Perkins. Embryos were then counterstained with DAPI to visualize nuclei. Stained embryos were placed in imprinted wells created by placing molds onto a liquid 1% agarose layer in 35-mm petri dishes (Leventea et al., 2016). To examine the cilia of the ear, the nasal pit, the pronephros, and the lateral line, embryos were positioned on their sides in the imprinted wells and immobilized by overlaying with 1.5% low-melting point agarose. Images of whole embryos were collected using an Olympus FV1000 confocal microscope with either a 40x/0.8 or 60x/0.9 water-dipping lens.

II.21. IMCD3 cell culture and siRNA experiments

Mouse inner medullary collecting duct cells stably expressing IFT88 (IMCD3-IFT88-GFP cells, a gift from Hiroaki Ishikawa) were grown in full medium containing Dulbecco's modified Eagle's medium (DMEM) and Ham's F12 nutrient mixture (Invitrogen, Carlsbad, CA) supplemented with 10% fetal bovine serum (FBS) and 1% Pen/Strep Amphotericin B (1003) (Lonza) at 37°C in a tissue culture incubator (Sanyo inCu Safe). Cells were seeded in cell culture flasks (cat no. 156472; Nunc). Medium was changed daily.

ON-TARGET plus SMART pool siRNAs (Dharmacon, GE Healthcare) against mouse *Crb3* were used to transfect IMCD3-IFT88 cells using Lipofectamine RNAiMAX transfection reagent (Life Technologies) following the

manufacturer's recommendations. The following siRNA target sequences were used: 5'-GCACCGGACCCUUUCCAA-3', 5'-AGGCAAGCAGGAUGGGACU-3', 5'-CAACACCCUCUUUGGGCAA-3', and 5'-GAUAGGGACAAUAAAGGUU-3'. As a negative control, we used nontargeting pool directed to the following sequences: 5'-UGGUUUACAUGUCGACUAA-3', 5'-UGGUUUACAUGUUGUGUGA-3', and 5'-UGGUUU ACAUGUUUUCUGA-3', 5'-UGGUUUACAUGUUUCCUA-3'.

II.22. Immunostaining of IMCD3 cells for confocal imaging

For staining with anti-acetylated tubulin and anti-Crumbs (CRB) antibodies, cells were rinsed with PBS, fixed with 4% PFA for 10 min at room temperature (RT), permeabilized with 0.1% Triton X-100 in PBS for 10 min, and blocked with 3% BSA in PBS (13) for 30 min at RT. Cells were then incubated with appropriate primary and secondary antibodies using standard protocols. Cells were counterstained with DAPI and mounted on glass slides using ProLong Gold anti-fade reagent (Life Technologies). Imaging was performed on an Olympus FV1000 confocal microscope using a 603/1.42 Plan Apo N oil lens.

II.23. TIRF imaging of IFT in IMCD3-IFT88 cells

IMCD3 cells were seeded on transwell cups (Costar, Cambridge, MA; 6.5 mm–0.5 mm pore size) at a density of $2-3 \times 10^5$ cells/ml as previously described (Ott and Lippincott-Schwartz, Ishikawa and Marshall). Upon reaching 60 - 70% confluency, cells were transfected with siRNAs as above. 48 hr after transfection, cells were serum-starved for an additional 48 hr to

induce ciliogenesis. The transwell cups were then placed in glass-bottom dishes (cat. no. 81153; ibidi) and imaged on an Eclipse Ti Microscope (Nikon, Shinagawa, Tokyo, Japan) supplied with a heating chamber (Okol Touch) using the Apo TIRF 1003, 1.49 NA 100x oil lens. Images were acquired at 100 msec intervals using the ixOn Ultra EMCCD camera (Andor Technology) and analyzed using the “KymoResliceWide” Fiji plug-in as previously described (Ishikawa and Marshall). The lengths of tracks were measured using the “segmented line tool” in Fiji and expressed as the percentage of cilia length.

II.24. Cilia length measurements and statistical analysis

Zebrafish cilia were measured on TIFF files of Z-stack projections of cristae and the nasal pit confocal images using the “segmented line tool” in ImageJ software. At least 10 animals (mutants and wild-types each) from two to three independent experiments were used. Measurements from each crista were averaged before performing comparisons. Cilia of IMCD3 cells were measured on TIFF images of cells stained with anti-acetylated tubulin antibody by tracing their length using ImageJ/FIJI software as above. Statistical analysis was carried out using the *Student’s t-test*, and the *Mann–Whitney* test included in GraphPad Prism 7.0 software (<http://www.graphpad.com/>). Data are presented as mean \pm 95% C.I (confidence interval), standard deviation (SD), or standard error of the mean (SEM) as indicated. Statistical significance is indicated as follows: * for P , 0.05, ** P , 0.01, *** P , 0.001, and **** P , 0.0001.

Table II.1. List of transgenic (Knock-in) lines used in this study

Strain name	Cassette used	Terminus tagged
Cu428.1 (WT)		
Transition Zone (TZ)		
MKS6-HA	Neomycin	C
HA-MKS6	Neomycin	N
MKS1-HA	Neomycin	C
Tmem216-HA	Neomycin	C
Tmem231-HA	Neomycin	C
NPHP4-HA	Neomycin	C
HA-NPHP4	Neomycin	C
B9d1-HA	Neomycin	C
Ahi1-HA	Neomycin	C
HA-Ahi1	Neomycin	N
MKS3-HA	Neomycin	C
Motor – Kinesin		
Kif3a-HA	Neomycin	C
HA-Kif3a	Neomycin	N
Cargo Adaptor		
ODA16-HA	Neomycin	C
IFT Particle – IFT-B		
IFT52-HA	Neomycin	C
HA-IFT52	Neomycin	N
IFT54-HA	Neomycin	C
HA-IFT54	Neomycin	N
IFT81-HA	Neomycin	C
HA-IFT81	Neomycin	N
HA-IFT46	Neomycin	N
IFT46-HA	Neomycin	C
IFT27-HA	Neomycin	C
IFT Particle – IFT- A		

IFT122-HA	Neomycin	C
HA-IFT122	Neomycin	N
IFT140-GFP	Puromycin	C
HA-IFT140	Neomycin	N
IFT144-GFP	Puromycin	C
HA-IFT144	Neomycin	N
Basal body		
HA-OFD1	Neomycin	N
OFD1-V5	Cycloheximide	C

Table II.2. List of Primer sequences

LINE (TERMINUS)	PRIMER SEQUENCE
TRANSITION ZONE	
CC2D2A (MKS6) CODING (C)	5' AATT ACGCGTGGTCATGCTATACCTGAAGG 3' 5' AATT GGATCCATCTTCGTATATTACACCTACAAATACC 3'
CC2D2A (MKS6) 3'UTR (C)	5' TTAA CTGCAGAAAAGCTTAGATATGAAACAATTTAATTATCA 3' 5' TTAA CTCGAGAATATAACTCTCATTAGCAGCCA 3'
B9d-1 CODING (C)	5' AAAT ACGCGT CTA GCA TGC ATG ATC AGT CAA T 3' 5' AATT GGATCC TGAGTAACCTTCTCTTTTAAAATTTCTC 3'
B9d-1 3'UTR (C)	5' AAAT CTGCAG GCA AAC AAT CGC TTT AGT CTT TTA G 3' 5' AATT CTC GAG AAGCTT TGAGCAAATAAAGGTGG 3'
TMEM231 CODING (C)	5' AAAT ACGCGT GGA AGG ATA AGA AAA TAG GGT AGC 3' 5' AATT GGATCC ATCTTATTTATATTTTCCGAACTATCTAAATGC 3'
TMEM231 3'UTR (C)	5' AAAT CTGCAG GTGGTATGCATTCAATCAATTAATCAG 3' 5' AATT CTCGAG ATTGAACTACTCTCCCTCAATTTAG 3'
TMEM216 CODING (C)	5' AAAT ACGCGT T ATG TCA AGC TCA TAG AAA ATTAGAGATAG 3' 5' AATT GGATCC GTATTATTGCTTTTCAAAGTTTTTAAAAC 3'
TMEM216 3'UTR (C)	5' AAAT CTGCAG TTCTTGTGCTGGTTAAACTTAGAATA 3' 5' AATT CTCGAG TCCTCTTCTACTTCTTCCTACA 3'
NPHP4 CODING (C)	5' AAAT ACGCGT CCT CAT AGA TAG GTT GTT GAT CAC 3' 5' AATT GGATCC TTTATTGACTGTAAAATGCAATTTAAATAGAA 3'
NPHP4 3'UTR (C)	5' AAAT CTGCAG ATG AAG AGG GAG TTT GTT GG 3' 5' AATT CTCGAG GAGGTGAAAGCTTCTGTTTGCATTAG 3'
MKS1 CODING (C)	5' AAAT ACGCGT CTCATAACTAACTTCTGCTTCCC 3' 5' AATT GGATCC ATTTAATTTCTACGTAGTATATCTTAGTGAAG 3'
MKS1 3'UTR (C)	5' AAAT CTGCAG CAACTAATTAACTAACTAACTAACTTATTCTAT 3' 5' AATT CTCGAG TTGATATCTGCTATTTTCCAACAGTT 3'
AH1 CODING (C)	5' AAAT ACGCGT AAGTTAAGGAGGAGAATTCGAATAA 3' 5' AATTGGATCCATACGTAGTGTAATAGTTATTTTAGTATTATCTATTG 3'
AH1 3'UTR (C)	5' AAAT CTGCAG GGTCTAAATCATTTCCTAGCGTT 3' 5' AATT CTCGAG TCTATGGGAGTAGTAGAGATTGC 3'
AH1 CODING (N)	5' AATT ACGCGT T ATG AAT AGC AGA GAT CGT CTT AA 3' 5' AATT GGATCC GAATTC CTCTAATTAAGCAATCGCGATC 3'

AH11	5' TTAA CCGCGG TAAGGAAAGTTTGTTTTAGTGATGA 3'
5'UTR (N)	5' TTAT CTGCAG AATATTGATGGATAAAGATATAGATAGC 3'
IFT PARTICLE	
IFT52	5' AAAT ACGCGT GGAAAGGATGATGAAGAAGATGAAT 3'
CODING (C)	5' AATT GGATCC GTTATTGAGCTTCTTGAAATTTATCTGT 3'
IFT52	5' AAAT CTGCAG AACAAATCATGCTTCCATTCAA 3'
3'UTR (C)	5' AATT CTC GAG AAGCTT CTAATCCTACATGTTATGTCT 3'
IFT52	5' AATT ACGCGT T ATG TCT GGT GAG TAA AAG ATA ATT GTC TTC AAC GCT TCA AAG AAGG 3'
CODING (N)	5' AATT GGATCC GTACGAGGCGTTGCTTAAAATA 3'
IFT52	5' TTAA CCGCGG GATATC ATGCAATTCTATATTTGAGGTGAG 3'
5'UTR (N)	5' TTAA TCGGCTAAATGA CTGCAGT 3'
IFT54	5' AAAT ACGCGT GCT ACA ACT CCT GAA TTA TGC T 3'
CODING (C)	5' AATT GGATCC TTTGGTTGAAACAACAGAGTAGAGC 3'
IFT54	5' AAAT CTGCAG CATTGTCTATCTAGCTAATTACAAACGT 3'
3'UTR (C)	5' AATT CTCGAG GCACCTTAGAAAGCTTAATTATGC 3'
IFT54	5' AATT ACGCGT T ATGGCTGATGATAAATTTGGGA 3'
CODING (N)	5' AATT GGATCC GTGGTTCATGCTTTTCGATATC 3'
IFT54	5' TTAA CCGCGG GAATTC CAATCAAGAAGGAGTTGCACTT 3'
5'UTR (N)	5' TTAA CTGCAG CGCTTAAACGTCTCTTTTGC 3'
IFT81	5' AAAT ACGCGT TCT TGC TTT CAC GTA CTG AAG 3'
CODING (C)	5' AATT GGATCCATTAATAGTTAATATATTATAGTCTCCACCAG 3'
IFT81	5' AAAT CTGCAG AATCATAGAATTTGCATATTTGTTAAAAGC3'
3'UTR (C)	5' AATT CTCGAGCCAATCATTCTTTTCAGACGTG 3'
IFT81	5' TTAA CCGCGG CGATCTCACTACTATTCTTGAGTGT 3'
CODING (N)	5' TTAA CTGCAG GTATTTGACTATGTTAGCGATTATGC 3'
IFT81	5' AATT ACGCGT T ATG AATTATAATAGCTACGGAAATCCG 3'
5'UTR (N)	5' CTG CTT TGC GCG AAT CTT A GGATCC AATT 3'
IFT46	5' AATA ACGCGT AGG TGC TTA TAA TCC AGC TG 3'
CODING (C)	5' AATTGGATCCATTAATTTGGAGCTGCATCTAATC 3'
IFT46	5' AAAT CTGCAG CACTGTATCAGCTATAATCAGAAAG 3'
3'UTR (C)	5' AATTCTCGAGCATCATCTTCTTCTTCACTTTC 3'
IFT46	5' AATT ACGCGT T ATG TCA GAT TCA GAC GAT AGG G 3'
CODING (N)	5' AATTGGATCCGGCTTAAGCTTGGCATCTAG 3'
IFT46	5' TTAA CCGCGG TC ACA CTA TTA AGC TTA TTA ATG TTT AG 3'
5'UTR (N)	5' TTAAGTGCAGATTTTGATTTTGGCAACTATTTAGTTTATC 3'
IFT122	5' AAAT ACGCGT ACTTACACTGACAATTCAAAATTAATT 3'
CODING (C)	5' AATT GGATCC GAAATCAAAAACATCTTTCTAAGGTCCT 3'
IFT122	5' AAAT CTGCAG TTCTACTTAAAGACTACCCATAAACT 3'
3'UTR (C)	5' AATT CTCGAG GGATTAATTCTGGTGATAGGTAAG 3'
IFT122	5' AATT ACGCGT C ATGAAGTGTTTCAGAACTATGGAC 3'
CODING (N)	5' AATT GGATCC TATTCGAGAGCTCTGTTTCTTATT 3'
IFT122	5' TTTT CCGCGGGATATCATAATGCAAATAATGGTGGTTGATAC 3'
5'UTR (N)	5' TTAA CTGCAG CCTAAAATTTGCTTCTATTCTGC 3'
IFT140	5' AATA ACGCGT GTATTGAGTAATTAGAAACTAAGCTCAA 3'
CODING (C)	5' AATT GGATCCTTCTGGGACATCTTCTTCAATG 3'
IFT140	5' AAAT CTGCAG CTTCATAGTAACTGACTACATTTAAAA 3'
3'UTR (C)	5' AATT CTCGAGACAAGCCATGCGAAAATG 3'
IFT140	5' AATT ACGCGT T ATG AGC TTG TTT TCA GAA CTT CC 3'
CODING (N)	5' AATT GGATCC TGCTTGGGCCTGTCTTA 3'
IFT140	5' TTAA CCGCGG GATTTAACTATAAATGATTGTTCTCAAC 3'
5'UTR (N)	5' TTAA CTGCAG TGCTTGAAGTCTCTCTTTCTCT 3'
IFT144	5' AAAT ACGCGT CAG ACC ACT AGC TTA CAA GTG 3'
CODING (C)	5' AATTGGATCC CTTCTTCTTTTACTCAGAACTTTATCTTGTGCTC 3'
IFT144	5' AAAT CTGCAG GTTAGATTCATGCATTAATTATTAGTTCAA AG 3'

3'UTR (C)	5' AATT CTCGAGCTTGAAGACTCAGATCTGGAAATAG 3'
IFT144 CODING (N)	5' AATT ACGCGT T ATG GCA TCA AGC AAG AAA GTA ATA C 3'
	5' AATT GGATCC TTAACAATCCTTCATCGTTCCAAT 3'
IFT144 5'UTR (N)	5' TTAA CCGCGG ATGTGTAAGCTTGTGTAATGAAC 3'
	5' TTAA CTGCAG GCAGGATATTCAGAAATCAATTATATTTTTT 3'
ODA16 CODING (C)	5' AAAT ACGCGT GAT AAG GTA GTA ACA GGT TCA TTT G 3'
	5' AATT GGATCC ATTTGTAGGAGGTTTATGTAATAACTC 3'
ODA16 3'UTR (C)	5' AAAT CTGCAG GCG ATA TCT AAA CAA AGA CCT AAA TAG 3'
	5' AATT CTCGAG AAGCTTAACATTGAATTGTTGGTTGCT 3'
OFD1 CODING (C)	5' AAAT ACGCGT CTCTAGGCTAAGAGTTATGAGTGAAG 3'
	5' AATT GGATCCGAAATATTCTAGATCTTCAACGATTTCC 5'
OFD1 3'UTR (C)	5' AAAT CTGCAG AAATCTAAATATAATTAATCAGTCTACTAT 3'
	5' AATTCTCGAGAAGCTTGAATAACTTGCTCAGAAATGCC 3'
OFD1 CODING (N)	5' AATT ACGCGT T ATG GAA TAA GGA GAA GAT AAT AAT GAT T 3'
	5' AATT GGATCC AACCTTCACTTGCTTTATCTTG 3'
OFD1 5'UTR (N)	5' TTAA CCGCGG AATT CCCTTTATATTTAACAAGATATTCACC 3'
	5' TTAA CTGCAG CCTACATTCATTAACCTCATTTCATATAGC 3'
NUCLEOPORINS	
NUP93 CODING (C)	5' AATT ACGCGT TGAATCTGGAAATTCATCCTATGG 3'
	5' AATT GGATCC AACTTAATCTGTAACCTTAGGCATTGT 3'
NUP93 3'UTR (C)	5' TTAA CTGCAG AAGAGGAGAAATAACTTTTAATTTAGGAA 3'
	5' TTAA CTCGAG GCATCTTCATCTTCATCTTCTACT 3'
NUP96 CODING (C)	5' AATT ACGCGT CAGACTTGATAAACGTCTAAGTTG 3'
	5' AATTGGATCCCATATATTAATTTTATTTTAAAGTTGATAGGATGAG 3'
NUP96 3'UTR (C)	5' TTAA CTGCAG CAAACACTTCATCCTCTCTATGC 3'
	5' TTAA CTCGAG GTCTCACATTAGCAGGTCTTG 3'

Table II.3. List of antibodies used in this thesis

Antibody	Detection	Dilution	Source
Mouse Monoclonal anti-Acetylated tubulin	Cilia marker	1:500	Sigma; T6793
Rabbit Monoclonal anti-acetylated tubulin	Cilia marker	1:500	Cell signalling; 5335S
Mouse Monoclonal anti-HA	HA tag	1:1000 / 1:2000	Covance; MMS-101R
Rabbit Monoclonal anti-HA	HA tag	1:1600	Cell signalling; C29F4
Rabbit monoclonal Anti-Nup50	Mammalian cells: Nucleus	1:250	Abcam; ab137092
	<i>Tetrahymena</i> : basal body?		
Rabbit monoclonal Nup153	Mammalian cells: Nucleus	1:250	Abcam; 171074
	<i>Tetrahymena</i> : Nucleus & basal		

	body?		
Mouse monoclonal Anti-Nup98	Mammalian cells: Nucleus	1:250	Santa Cruz Biotechnology; Sc-74553
	<i>Tetrahymena</i> : cilia?		
Mouse monoclonal Anti-Nup88	Mammalian cells: Nucleus	1:250	Santa Cruz Biotechnology; Sc-365868
	<i>Tetrahymena</i> : basal body?		
Mouse monoclonal Anti-Nup93	Mammalian cells: Nucleus	1:250	Santa Cruz Biotechnology; Sc-374339
	<i>Tetrahymena</i> : Nucleus		
Mouse anti-HA conjugated to A647	HA tag	1:100	Cell signalling; 3444
Mouse anti-HA conjugated to A647	HA tag	1:150	Invitrogen; 26183-A647
Rabbit polyclonal Anti-RPGRIP1L	RPGRIP1L	1:250	Proteintech; 55160-1-AP
Rabbit polyclonal Anti-IFT88	IFT88	1:250	Proteintech; 13967-1-AP
Rabbit polyclonal Anti-GFP	GFP tag	1:500	Life Technologies; A-11122
Mouse monoclonal Anti-V5	V5 tag	1:1000	Sigma-Aldrich; V8012
Rabbit Anti-CRB3	Crumbs	1:250	(Makarova et al., 2003)
Rabbit Anti-IFT88 (Fish)	IFT88	1:500	Perkins Lab
Rabbit Anti-IFT52 (Fish)	IFT52	1:500	Perkins lab
Rabbit polyclonal Anti-Kif17	Kif17	1:250	Abcam; ab11261
Mouse Monoclonal Anti-Centrin	Basal body	1:500	Millipore; 04-1624
Mouse monoclonal MAb414	FG-rich nucleoporins	1:500	Biologend; MMS-120P
Mouse monoclonal Anti-Polyglutamylated Tubulin (B3)	Cilia and basal bodies	1:500	Sigma-Aldrich; T9822

Chapter III

“STORM Super-Resolution Imaging of the Ciliary Transition Zone”

III.1. Introduction

The transition zone is an evolutionary conserved sub-domain of the cilium that acts as a ciliary gate to control the entrance and exit of proteins to form the cilium and maintain its function (reviewed in (Czarnecki and Shah, 2012) and (Szymanska and Johnson, 2012)). All proteins destined for the cilium cross these gating barriers at the base of the cilium in a regulated manner that excludes some small polypeptides while permitting the entry of selected large molecular complexes (Breslow et al., 2013, Kee et al., 2012). The function of these barriers at the base of the cilium is fascinating and puzzling, and is influenced, to some extent, by factors such as protein size and shape (Najafi and Calvert, 2012).

Two main modules comprise the transition zone proteins: the “NPHP module”, and “MKS module”. NPHP module includes the proteins Nphp1 and Nphp4, and the MKS module is comprised of the proteins TCTNs, B9 domain proteins (B9d-1, B9d-2, and MKS1), coiled-coil domain proteins (MKS6), Ahi1, and several transmembrane proteins, such Tmem216, Tmem67 (MKS3), and Tmem231 (Garcia-Gonzalo et al., 2011, Chih et al., 2011, Dowdle et al., 2011, Mollet et al., 2005, Arts et al., 2007, Sang et al., 2011, Williams et al., 2011). RPGRIP1L is upstream the proteins in both modules and seems to have a crucial role in the assembly of both MKS and NPHP protein complexes (Jensen et al., 2015, Lambacher et al., 2016, Shi et al., 2017). It also interacts with Nphp4 (Arts et al., 2007). Mutations in RPGRIP1L in *C. elegans* affect the localisation of Nphp1 and Nphp4, and thus RPGRIP1L was shown to be on the top of the hierarchy of the assembly of TZ proteins at the cilia base (Williams et al., 2011). Moreover, mutations of human RPGRIP1L were also shown to

disrupt the localisation of some ciliary membrane proteins, such as smoothed (Smo) and Arl13b (Shi et al., 2017).

Many studies have reported interactions between transition zone proteins at the cilia base, which in turns are necessary for the proper function of the transition zone as a barrier at the cilia base. For instance, immunoprecipitation experiments have shown that the transmembrane proteins Tmem216 and Tmem67 (MKS3) interact with each other at the cilia base (Valente et al., 2010). Moreover, the B9d domain proteins, B9d1 and MKS1, are known to bind with each other, localise to the same area, and bind membrane lipids (Chih et al., 2011, Dowdle et al., 2011). Defects in the assembly or function of many of the transition zone proteins have been linked with several cilia-related diseases; collectively known as ciliopathies (reviewed in (Novarino et al., 2011) (Mitchison and Valente, 2017)).

The transition zone occupies a small part of the ciliary compartment ranging between 300-1000nm in length (Serwas et al., 2017) and 250-350nm in diameter (Yang et al., 2015). In EM images, it is marked by the presence of Y-links (Besharse et al., 1985, Gilula and Satir, 1972). It functions as a ciliary gate or a diffusion barrier to regulate the entry and exit of required proteins to build the cilium (Nachury et al., 2010, Sang et al., 2011, Czarnecki and Shah, 2012, Garcia-Gonzalo and Reiter, 2012). While plenty of efforts have been dedicated to reveal the exact localization of individual transition zone proteins at the cilia base, it is still unclear how some small proteins are restricted from entering the cilium, while others, even large complexes, such as intraflagellar transport proteins (IFT), still gain access through this barrier.

Conventional optical microscopy is limited by about 200-300nm resolution, which hinders the ability to detect differences in the arrangement of proteins at the transition zone (Huang et al., 2010). This necessitates the use of advanced imaging technique that can resolve proteins at the nanometre level. Super-resolution microscopy, such as stimulated emission depletion microscopy (STED), structured illumination microscopy (SIM) and stochastic optical reconstruction microscopy (STORM) overcome the diffraction limit and can detect subtle differences in position of proteins and protein complexes, and thus would be very suitable for the analysis of the architecture of proteins at the transition zone (Mennella et al., 2012, Lambacher et al., 2016, Shi et al., 2017). Previous immuno-EM studies have localised several proteins at the transition zone of the cilium, but the sample preparation for EM is challenging, time consuming, and the outcomes are inaccurate (Craigie et al., 2010).

The study of architectural organisation of the ciliary base beyond the diffraction limit was carried out using STED imaging (Yang et al., 2015). The best achievable resolution using STED microscopy is about 50nm (Sieber et al., 2007). However, STORM microscopy can reach up to 20nm of lateral resolution, so that it is possible to resolve much more details of the protein complexes at the base of the cilium (Schermelleh et al., 2010, Szyborska et al., 2013, Shi et al., 2017). Recently, it was shown that the TZ proteins Tmem231, B9d1, NPHP1, and RPGRIP1L form rings of different diameters at the cilia base in mouse tracheal cells. The rings were composed of 9 doublets that could correspond to the arms of the Y-Links. This may suggest that some TZ proteins could be the structural units involved in building the Y-Link at the cilia base (Shi et al., 2017). Moreover, the TZ proteins RPGRIP1L and Tmem67

(MKS3) were shown to be distributed periodically along the axis of the cilium in *C. elegans* (Lambacher et al., 2016). Using STORM imaging, RPGRIP1L and Tmem67 revealed rings of 7, 8, or 9 clusters arranged around rings at the cilia base (Lambacher et al., 2016).

Based on STORM imaging in the ciliate *Tetrahymena thermophila*, combined with computational particle averaging using codes written in MATLAB, we present a very detailed model of the transition zone at the cilia base. We established knock-in lines with C- and N- terminal epitope tags of 7 transition zone proteins. These include the transmembrane proteins Tmem216 (MKS2) and Tmem231, two B9 domain proteins MKS1 and B9d1, one coiled-coil protein CC2D2A (MKS6), a WD-repeat protein Ahi1, and NPHP4. All these 7 TZ proteins were tagged with HA at the C-terminus. Moreover, Ahi1, MKS6, and NPHP4 were also tagged at the N-terminus. Using antibody staining against the tags, we show that TZ proteins form rings with varying radii relative to the centre of the ciliary axoneme. In addition to that, our analysis of nucleoporins showed that some anti-Nup antibodies produced signals at the cilia base in *Tetrahymena thermophila*. For example, anti-Nup50 antibody seems to form 9-fold symmetrical rings near the basal bodies of *Tetrahymena* cilia. We took the advantage of the oval shape of *Tetrahymena* cells that could show top views, oblique views, and side views of cilia and used Nup50 as a reference protein to axially map the 7 transition zone proteins. Computational averaging of the radial and axial locations at the N- and C- termini of proteins enabled us to determine their orientation. Our analysis of the examined TZ proteins shows that the transition zone in *Tetrahymena thermophila* spans a region of about 25nm in the radial dimension and a region of 20-30nm along the

ciliary axis. Our STORM super-resolution analysis of the TZ reveals the orientation of crucial components at the cilia base in unprecedented detail.

III.2. Results

III.2.1 TZ proteins localise to the cilia base in *Tetrahymena thermophila*

Epitope tagging of the open reading frame (ORF) at the native locus of the gene produces accurate localisations of the protein (Gaertig et al., 2013). We tagged the genes of interest at either N- or C- termini with 3-HA tags (as detailed in the methods part in Ch. III). MKS6 (CC2D2A), NPHP4 and Ahi1 were tagged at both termini, whereas, Tmem231, Tmem216, MKS1, and B9d1 were only tagged at the C-terminus. To initially evaluate the localisation of these proteins in *Tetrahymena*, we used anti-HA antibody to detect the protein of interest and imaged on the FV-1000 Olympus confocal microscope. We also detected the proteins using western blots to confirm that proteins of the correct size are tagged. We tested at least 2 clones of each TZ line to ensure the localisation is correct and that the western blot shows correct size of the protein in both clones.

Immunostaining analysis revealed that all the transition zone proteins successfully localised to the base of the cilia (Fig. III.1). MKS6-C terminus localised to the base of cilia in *Tetrahymena thermophila* (Fig. III.1A-A' and C). To confirm that MKS6 is at the transition zone, we immunostained MKS6-line with anti-centrin antibody that marks the basal bodies, this shows that MKS6 is located distal to the basal body, i.e. the transition zone (Fig. III.1B-B'). We also

show that using antibody against the tag at the N-terminus of MKS6 also localise it to the cilia base (Fig. III.1C'). Moreover, Tmem216-C terminus (Fig. III.1D), B9d1-C (Fig. III.1E), MKS3-C (Fig. III.1F), Tmem231-C (Fig. III.1G), MKS1-C (Fig. III.1H), NPHP4-C terminus (Fig. III.1I) and N- terminus (Fig1. III.1I'), and Ahi1-C terminus (Fig. III.1J) and N-terminus (Fig. III.1J') all localised to the base of cilia in *Tetrahymena thermophila*. Using WB analysis, we detected the expected correct size of the proteins in at least 2 different clones. For example, WBs of Tmem216 show the expected size of approximately 16kDa, NPHP4: about 190kDa, and Ahi1: about 90kDa (Fig. III.1K). Thus, we show by using epitope tagging at both termini of the transition zone proteins that the proteins localise correctly to the cilia base.

III.2.2. STORM imaging of the TZ components

The resolution achieved by confocal microscopy is limited to about 200-300nm (Huang et al., 2010); this will restrict the ability to resolve subcellular structures, as those positioned at the cilia base. For that reason, we sought to improve the resolution of imaging and reveal the architecture of the proteins at the cilia base by using stochastic optical reconstruction microscopy (STORM), a super-resolution imaging technique that can increase the resolution limit for up to 10 times compared to that of conventional microscopy (20nm) (Huang et al., 2010, Shi et al., 2017). We used the "NIKON Eclipse Ti microscope" to perform 2D-STORM imaging of the transition zone proteins in *Tetrahymena thermophila*. We show that transition zone proteins examined form 9-fold symmetrical rings at the cilia base (Fig. III.2B-B'). An overlay of the images produced by the two

imaging techniques, conventional versus STORM (Fig. III.2C-C'), illustrates the level of detail one can achieve using STORM microscopy. Such detail could not be seen using conventional fluorescence microscopy.

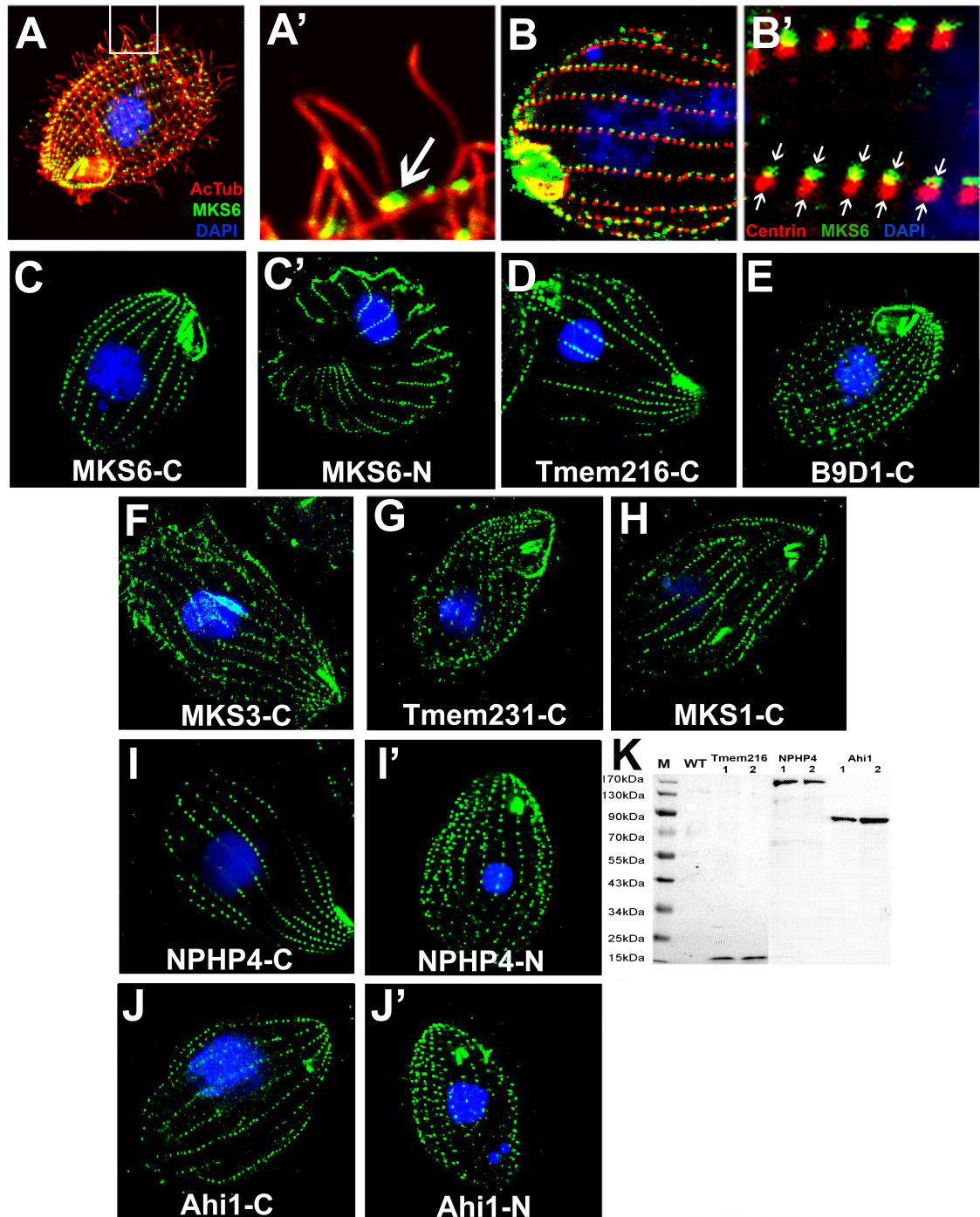


Figure. III.1. Transition zone proteins localise to the cilia base in *Tetrahymena thermophila*. (A-A') Confocal images showing the localisation of MKS6 (CC2D2A) at the cilia base using anti-HA antibody to detect the tagged protein (TZ, green) and anti-acetylated tubulin

to mark cilia (red). **(B-B')** MKS6 (green) localises just above the basal bodies, detected by centrin (red) at the cilia base. **(C-J')** Confocal images showing localisation of transition zone proteins tagged at the C- and N-termini: MKS6-C terminus **(C)**, MKS6-N terminus **(C')**, Tmem216-C terminus **(D)**, B9d1-C terminus **(E)**, MKS3-C terminus (Tmem67) **(F)**, Tmem231-C terminus **(G)**, MKS1-C terminus **(H)**, NPHP4-C terminus **(I)**, NPHP4-N terminus **(I')**, Ahi1-C terminus **(J)**, and Ahi1-N terminus **(J')**. All cells were counterstained with DAPI to mark nuclei. **(K)** Western blots showing the expected sizes of Tmem216 (~16kDa), NPHP4 (~190kDa), and Ahi1 (~90kDa). WBs shown are duplicates from two different clones. Protein extracted from WT *Tetrahymena* cells was utilised as control. WB from WT cells does not show any band (1st lane).

III.2.3. TZ proteins form discrete clusters arranged in rings at the cilia base

The transition zone architecture has been under investigation in the past few years, especially after the emergence of several super-resolution techniques that could resolve subcellular structures at the nanometre level (Shi et al., 2017, Huang et al., 2010, Lambacher et al., 2016). Genetic analyses have shown that mutations in transition zone proteins disrupt the formation of the Y-links at the cilia base (Williams et al., 2008, Williams et al., 2011, Huang et al., 2011, Jensen et al., 2015, Yee et al., 2015), but how these proteins arrange relative to each other and to other protein complexes at the cilia base, remained a mystery. Recently, using 3D-STORM imaging combined with quantitative analysis in mouse tracheal cells, Shi. *et al.* could show that 4 transition zone proteins: RPGRIP1L, B9d1, Tmem231, and NPHP1 form rings of doublets with different diameters that could correspond to the arms of Y-links (Shi et al., 2017). Moreover, RPGRIP1L also formed rings at the cilia base of hTERT-RPE1 cells (Lambacher et al., 2016).

To further determine the organisation and architecture of transition zone proteins at the cilia base, we used STORM imaging in *Tetrahymena thermophila* and primary cultures of human bronchial epithelial cells (NHBE).

Tetrahymena cells are covered with more than 500 cilia (Orias et al., 2011, Gaertig et al., 2013). As *Tetrahymena* cells are oval, one can examine transition zones that are straight up towards the optical axis of the lens (top views), while also examining nearby transition zones that are either at an angle or perpendicular to the optical axis of the lens: oblique views and side views respectively. Using STORM imaging, we show that the transition zone proteins form rings at the cilia base.

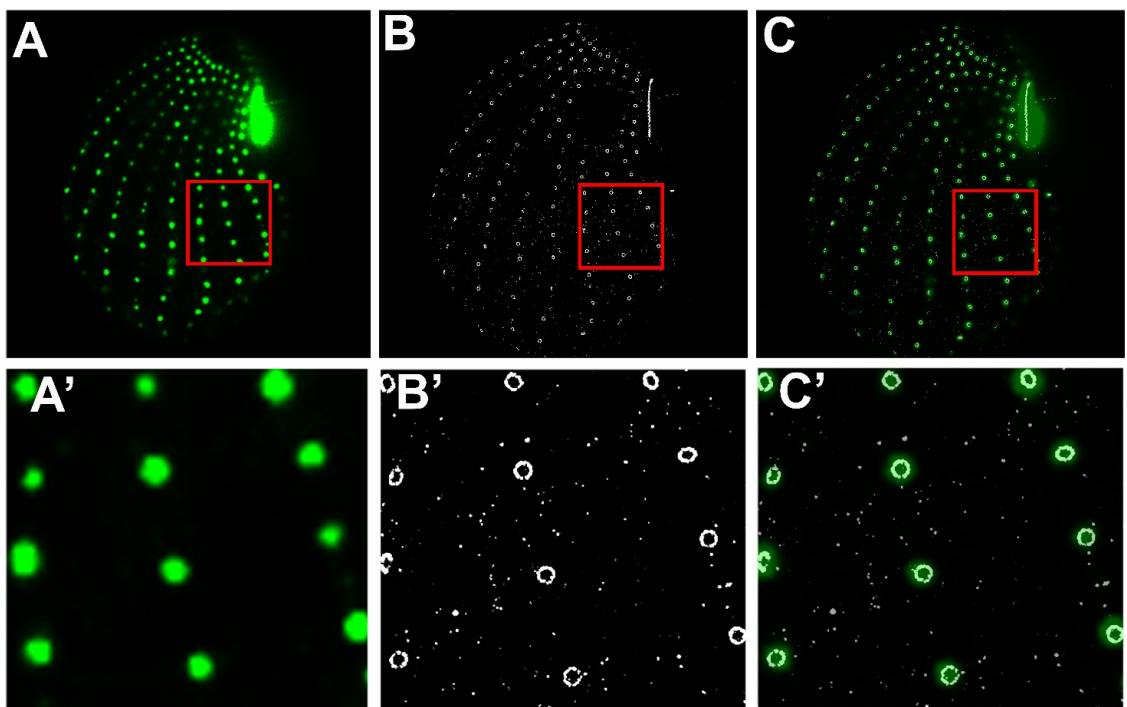


Figure. III.2. STORM imaging of TZ proteins. (A-A') Widefield images of Tmem216-C terminus showing rows of transition zones (A', inset in A). (B-B') STORM images of Tmem216-C terminus showing that TZ components form rings at the cilia base (B', inset in B). (C-C') An overlay of fluorescence and STORM images showing the details that can be achieved using STORM imaging (C', inset in C).

Using indirect labelling (primary antibody followed by secondary antibody), MKS6 tagged at the C-terminus, shows 9-fold symmetrical rings at the cilia base of *Tetrahymena* (Fig. III.3A-A'). The N-terminal tagging of the same

protein also revealed similar clusters distributed in 9-fold symmetrical rings (Fig. III.3B-B'). MKS1-C terminus (Fig. III.3C-C'), B9d1-C terminus (Fig. III.3D-D'), Ahi1-C terminus (Fig. III.3E-E'), Ahi1-N terminus (Fig. III.3F-F'), and Tmem231-C terminus (Fig. III.3H-H') show rings with 9-fold symmetry at the cilia base. Tmem216-C terminus seems to form more than 9 clusters arranged in thinner rings (Fig. III.3G-G''). Using direct labelling (primary antibody directly conjugated to the fluorophore), all transition zone proteins examined showed rings with doublets observed in some cases (Fig. III.3A''-H''; arrows). NPHP4 is also arranged in 9-fold symmetrical rings at the cilia base in almost all the rings examined. These 9-fold symmetrical rings are observed at the C- and N- termini of this protein (Fig. III.4A-B').

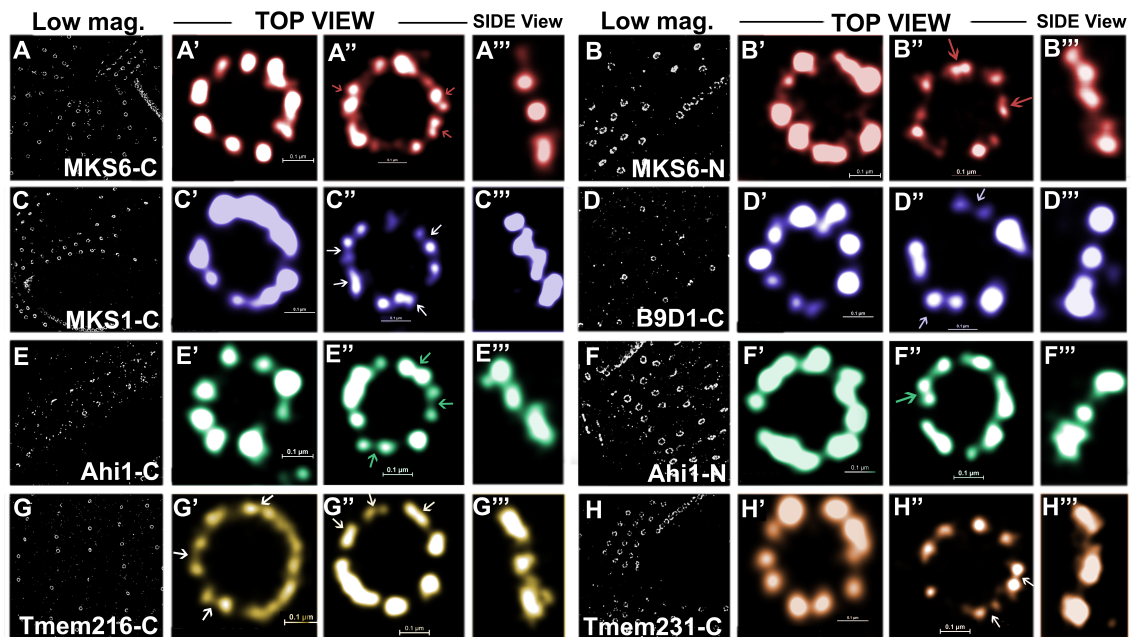


Figure. III.3. TZ proteins form rings at the cilia base. STORM images showing the top views of the arrangement of MKS6-C terminus (A-A'), MKS6-N terminus (B-B'), MKS1-C terminus (C-C'), B9d1-C terminus (D-D'), Ahi1-C terminus (E-E'), Ahi1-N terminus (F-F'), Tmem216-C terminus (G-G'), and Tmem231-C terminus (H-H') at the transition zone using indirect labelling (1Ab + 2Ab). Images in A''- H'' show the arrangement of the TZ proteins using direct labelling (1Ab-A647). Arrows in A''- H'' show possible doublets. (A'''- H''') STORM images showing the side views of the TZ proteins at the cilia base. These images were obtained from cilia that are perpendicular to the optical axis of the lens.

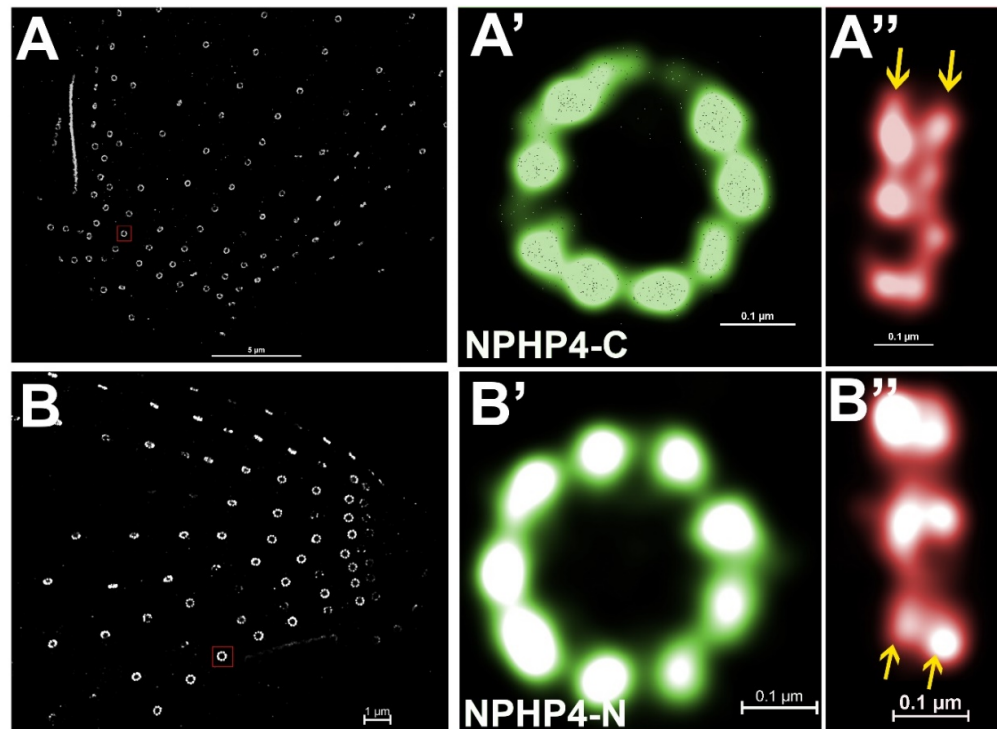


Figure. III.4. NPHP4 forms 9-fold symmetrical rings in the top view and shows 2 layers in side views. (A-A') STORM images of the top views of NPHP4 tagged at the C-terminus showing 9-fold symmetrical rings. **(A'')** In side views, NPHP4-C terminus seems to be arranged in two layers at the TZ of *Tetrahymena thermophila*. **(B-B')** NPHP4 tagged at the N-terminus top views also shows 9-fold symmetrical rings. **(B'')** Side views also show 2 layers.

To assess the side views of the TZ proteins, we looked at cilia that are perpendicular to the optical axis and thus observing the side views of the transition zone proteins. All TZ proteins examined, except NPHP4, are arranged in one-layer of clusters at the cilia base (Fig. III.3A'''-H'''). NPHP4 protein, however, is arranged in clusters with 2 layers. This arrangement was prominent at both termini of the protein (Fig. III.4A'' and B''). Therefore, STORM imaging of transition zone proteins shows that these proteins form discrete clusters arranged in rings in top views. The side views of cilia show that TZ proteins form one layer at the cilia base except for NPHP4 with 2 layers observed.

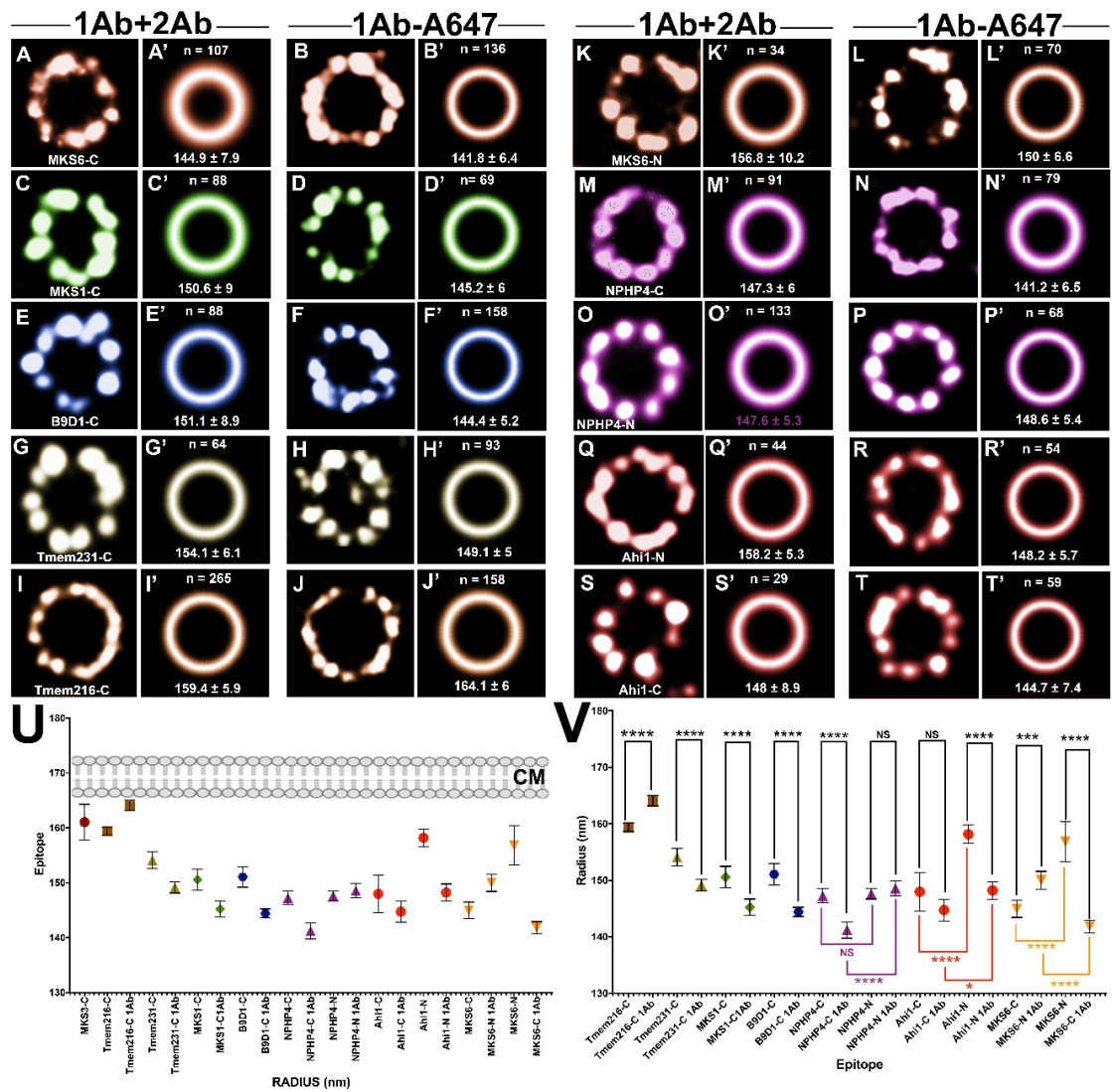


Figure. III.5. TZ components form rings of different radii at the cilia base. (A-T') Indirect labelling (primary antibody followed by secondary antibody-A647) versus direct labelling (primary antibody directly conjugated to Alexa Fluor 647) shows differences in the measurements of the radii of TZ components. **MKS6-C terminus:** 144.9 ± 7.9 nm, n = 107 rings (A-A') versus 141.8 ± 6.4 nm, n = 136 rings (B-B'). **MKS1-C terminus:** 150.6 ± 9 nm, n = 88 rings (C-C') versus 145.2 ± 6 nm, n = 69 rings (D-D'). **B9d1-C terminus:** 151.1 ± 8.9 nm, n = 88 rings (E-E') versus 144.4 ± 5.2 nm, n = 158 rings (F-F'). **Tmem231-C terminus:** 154.1 ± 6.1, n = 64 (G-G') versus 149.1 ± 5 nm, n = 93 (H-H'). **Tmem216-C terminus:** 159 ± 5.9 nm, n = 265 (I-I') versus 164.1 ± 6 nm, n = 158 (J-J'). **MKS6-N terminus:** 156.8 ± 10.2 nm, n = 34 rings (K-K') versus 150 ± 6.6 nm, n = 70 rings (L-L'). **NPHP4-C terminus:** 147.3 ± 6 nm, n = 91 rings (M-M') versus 141.2 ± 6.5 nm, n = 79 rings (N-N'). **NPHP4-N terminus:** 147.6 ± 5.3 nm, n = 133 (O-O') versus 148.6 ± 5.4 nm, n = 68 rings (P-P'). **Ahi1-N terminus:** 158.2 ± 5.3 nm, n = 44 (Q-Q') versus 148.2 ± 5.7 nm, n = 54 rings (R-R'). **Ahi1-C terminus:** 148 ± 8.9 nm, n = 29 rings (S-S') versus 144.7 ± 7.4 nm, n = 59 rings (T-T'). Data are means ± SD. **(U)** The distribution of the epitopes of all the TZ proteins examined and their relative position in the radial direction with respect to the likely position of the ciliary membrane (CM). Data are means

\pm 95% CI (confidence interval). **(V)** Average radii of all the TZ components using indirect versus direct labelling. Data are means \pm 95% CI. Based on Student's *t*-tests; * **P**, 0.05, ** **P**, 0.01, *** **P**, 0.001, and **** **P**, 0.0001; not significant, ns. All differences were also significant based on Mann–Whitney test.

III.2.4. TZ proteins form rings of different radii at the cilia base

Using quantitative image analysis and codes written in MATLAB (please refer to methods in Ch. III), we measured the radii of at least 10 epitopes in 7 different transition zone proteins. We calculated the radii using both direct and indirect labelling. Using indirect labelling, out of the 7 transition zone proteins investigated, Tmem216-C terminus has the largest radius (159 ± 5.9 nm, Fig. III.5I-I', U), followed by MKS6-N terminus (156.8 ± 10.2 nm, Fig. III.5K-K', U), Ahi1-N terminus (158.2 ± 5.3 nm, Fig. III.5Q-Q', U), Tmem231-C terminus (154.1 ± 6.1 nm, Fig. III.5G-G', U), B9d1-C terminus (151.1 ± 8.9 nm, Fig. III.5E-E', U), MKS1-C terminus (150.6 ± 9 nm, Fig. III.5C-C', U), Ahi1-C terminus (148 ± 8.9 nm, Fig. III.5S-S, U), NPHP4-N terminus (147.6 ± 5.3 nm, Fig. III.5O-O', U), and NPHP4-C terminus (147.3 ± 6 nm, Fig. III.5M-M', U). The smallest radius is for MKS6-C terminus (144.9 ± 7.9 nm, Fig. III.5A-A', U).

However, when using direct labelling, 7 out of 10 epitopes examined show significant differences in radii between indirect and direct labelling procedures (Fig. III.5V). For example, the radii of the following proteins are reduced by: Tmem231-C terminus: 5nm (Fig. III.5H-H', compare to G-G'), MKS1-C: 5.4nm (Fig. III.5D-D', compare to C-C'), B9d1-C: 6.7 nm (Fig. III.5F-F'. compare to E-E'), Ahi1-N: 10nm (Fig. III.5R-R', compare to Q-Q'), MKS6-N: 6.8nm (Fig. III.5L-L', compare to K-K'), and NPHP4-C: 6.1nm (Fig. III.5N-N', compare to M-M'). Only the radius of Tmem216-C terminus increased by 4.7nm

(Fig. III.5J-J', compare to I-I'). On the other hand, only NPHP4-N terminus and Ahi1-C terminus did not show a significant difference when using the two immunostaining approaches (indirect versus direct) (Fig. III.5V). NPHP4-N terminus has a shift of only 1nm (Fig. III.5P-P', compare to O-O') and Ahi1-C terminus has a shift of only 0.3nm (Fig. III.5T-T', compare to S-S').

In conclusion, using antibodies directly conjugated to Alexa Fluor 647 in STORM imaging produces more accurate measurements of the radii of the TZ at the cilia base. 9 out of 10 epitopes examined, revealed smaller radii most likely because the antibody is closer to the epitope. Direct labelling seems to produce smaller error. We show that localising the two termini of the same protein produced different radii for some TZ proteins (Fig. III.5A' compare to K', Fig. III.5Q' to S'). Using direct labelling, the N- and C- termini of MKS6, Ahi1, and NPHP4 produced different radii that were statistically significant (Fig. III.5V). The position of each TZ protein using direct or indirect labelling with respect to the likely location of the ciliary membrane (CM) is shown in Fig. III.5U.

III.2.5. TZ proteins form rings in NHBE cells

To ensure that the transition zone components also form rings at the base of cilia in other model systems, we stained primary cultures of normal human bronchial epithelial cells (NHBE) and nasal cells (Cells were kindly provided by Robert Hirst at the PCD diagnostic centre in Leicester Royal Infirmary, UK) with antibodies against RPGRIP1L and IFT88. These primary cultures are composed of cells that contain hundreds of motile cilia important for clearing mucus and debris from the respiratory epithelium. Confocal images

show that IFT88 localises to the ciliary shaft (Fig. III.6A-A''). RPGRIP1L localises to the base of cilia in these cells (Fig. III.6B-B''). We then used STORM imaging to assess the arrangement of RPGRIP1L at the cilia base. RPGRIP1L is arranged in rings of separate clusters (Fig. III.6C-C'). The average diameter of 15 rings is $236.8 \pm 6.39\text{nm}$ (Fig. III.6C''), in agreement to what was previously published (Lambacher et al., 2016), but inconsistent with the diameter of RPGRIP1L observed in mouse tracheal cells, where the diameter of this protein exceeds 270nm (Shi et al., 2017). Overall, the arrangement of the TZ proteins at the cilia base seem to be quite consistent and well conserved in various organisms, and most of the TZ components form rings of discrete clusters at the cilia base.

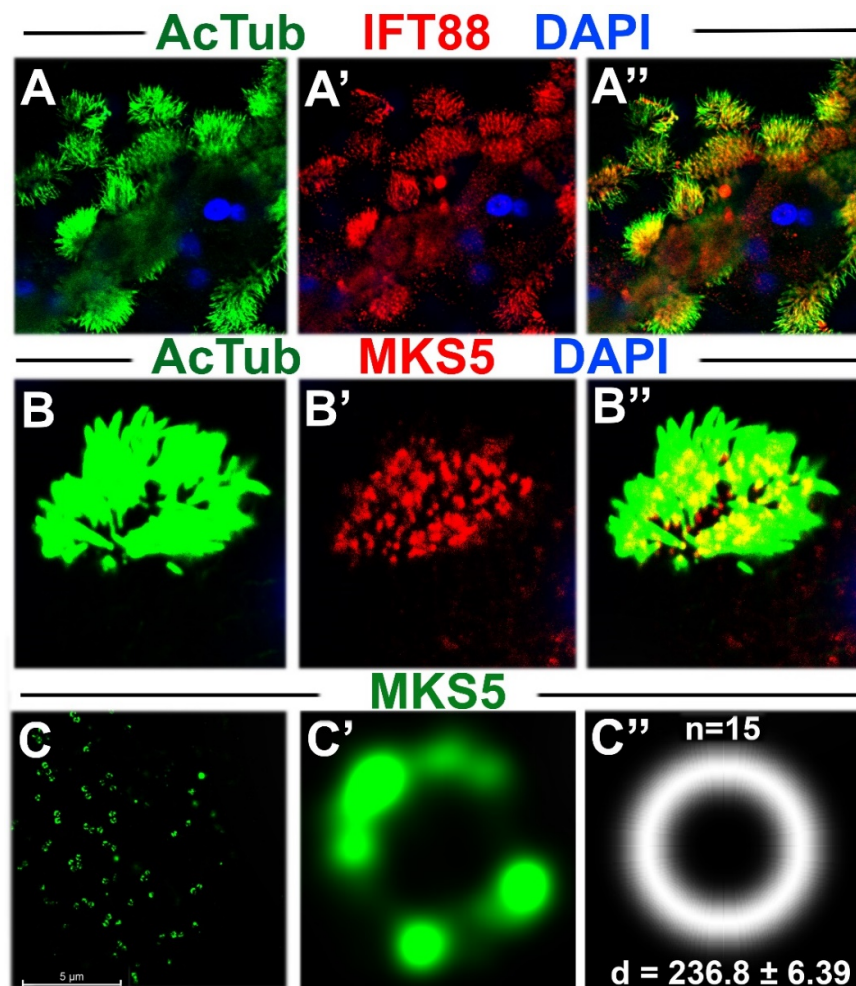


Figure. III.6. TZ proteins form rings in NHBE cells. (A-A'') Confocal images showing motile cilia in primary cultures of nasal epithelial cells stained with anti-acetylated tubulin (green) to mark cilia, anti-IFT88 (red), and counterstained with DAPI to mark the nucleus (blue). Image shows numerous cilia (hundreds) per cell. **(B-B'')** Confocal images of the nasal cells stained with anti-RPGRIP1L to mark the transition zone and anti-acetylated tubulin to mark cilia. **(C-C')** STORM images of primary cultures of normal human bronchial epithelial cells (NHBE) stained with anti- RPGRIP1L followed by secondary antibody conjugated with Alexa fluor647. Images show that RPGRIP1L forms discrete clusters arranged around rings. **(C'')** Averaging 15 rings using codes written in MATLAB shows that RPGRIP1L forms a ring of 236.8 ± 6.39 nm in diameter. Data are mean \pm SD.

III.2.6. Nucleoporins may localise to the cilia base in *T. thermophila*

Nucleoporins have arisen to be strong candidates involved in the gating mechanisms at the cilia base (Kee et al., 2012, Del Viso et al., 2016, Kee and Verhey, 2013, Takao and Verhey, 2016, Takao et al., 2017). Some nucleoporins localise to the cilia base in odora cells (Kee et al., 2012). Others have shown that nucleoporins, such as Nup93 and Nup188, localise at the basal bodies (Del Viso et al., 2016). Possible roles for nucleoporins in ciliogenesis have been reported in several studies. Kif17, a kinesin II motor, entry to cilia was shown to be dependent on Nup62 (Takao et al., 2014), and studies in *xenopus* revealed the importance of Nup188 in cilia formation of the left-right organiser (Del Viso et al., 2016).

For that reason, we investigated the localisation of some nucleoporins at the cilia base in *Tetrahymena thermophila*. To do so, we used two approaches, in the first we used commercially available anti-Nup antibodies that have been tested mainly on human and mouse cells (Table II.3). In the second approach, we generated knock-in lines by epitope tagging at the native locus of the gene in *Tetrahymena thermophila* for some of the nucleoporins, such as Nup96 and

Nup93 as previously described (Gaertig et al., 2013). Using the first approach, some of the antibodies against nucleoporins produced clear signal at the cilia base. For example, anti-mab414, an antibody that recognises FG (Phenylalanine and glycine motif) rich nucleoporins, produced prominent localisation at the cilia base, but not in the nucleus as one would expect (Fig. III.7A). We also used mammalian anti-Nup50 in MKS6 transgenic line. Anti-Nup50 localised proximal to MKS6 at the cilia base (Fig. III.7B-B'), which suggests that it is located near the basal bodies. In some cases, we could also detect a weak signal in the nucleus when we used anti-Nup50 (Fig. III.7B). We also observed a signal at the cilia base when using anti-Nup88 and anti-Nup153, with the latter also showing a clear signal in the nucleus (Fig. III.7C and F, respectively). Anti-Nup93 antibodies did not detect anything in cilia but had an obvious signal in the nucleus (Fig. III.7D). Surprisingly, anti-nup98 stained the ciliary shaft, except for the tips (Fig. III.7E). Finally, using the second approach, neither Nup96 nor Nup93 localise to the cilia base in the knock-in lines using anti-HA antibody. In both lines, the signal was however observed in the nucleus (Fig. III.7G and H).

We next performed STORM imaging using some of the anti-Nup antibodies. Anti-Nup50 in *Tetrahymena* revealed 9-fold symmetrical rings (Fig. III.7I-I'), similar to the arrangement of the TZ components at the cilia base. We then double stained MKS6 transgenic line tagged with triple HA at the C-terminus with two primary antibodies: anti-HA antibody, and anti-Nup153 or Nup50. This step was followed by using secondary antibodies conjugated to Alexa Fluor 647 to detect both primary antibodies, therefore, both proteins are detected in the same channel. Using this double labelling procedure, we could

detect side views, oblique views, and top views of the two proteins. In side views, anti-Nup153 seems to localise as “rod-like” structures at the cilia base, and the top view shows that anti-Nup153 is at the centre of MKS6 ring (Fig. III.7J-J’). Interestingly, MKS6-C terminus and Nup50 both form rings that appear to be in the same register and separated by about 200nm (Fig. III.7K-K’).

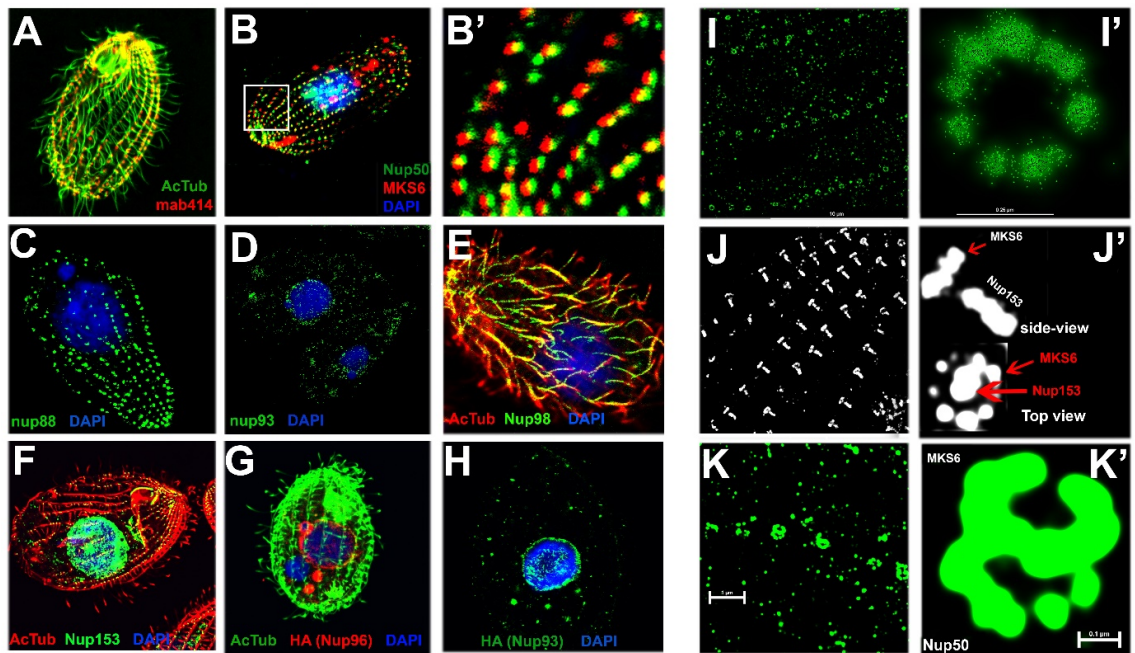


Figure. III.7. Nucleoporins may localise to the cilia base in *Tetrahymena thermophila*. (A) A confocal image of a *Tetrahymena* cell stained with anti-acetylated tubulin (green) and anti-mab414 (red) that marks FG-rich nucleoporins. Anti-mab414 seems to produce a signal at the cilia base in *Tetrahymena thermophila*. (B-B’) Confocal images showing the localisation of MSK6 (TZ-red) using anti-HA antibody and anti-Nup50 (green). B’, inset in B. (C) Confocal image using anti-Nup88 at the cilia base (green) and anti-Nup93 (green) (D). (E) Using anti-Nup98, the protein seems to localise to the ciliary shaft. (F) A confocal image showing a *Tetrahymena* cell stained with anti-acetylated tubulin (red) and anti-Nup153 (green). Anti-Nup153 is detected in cilia base and nucleus. (G and H) Antibody staining against the tag in Nups knock-in lines (Nup96 and Nup93) reveals a clear signal in the nucleus, but not at the cilia base. (I-I’) STORM images of anti-Nup50 in *Tetrahymena thermophila* showing 9-fold symmetrical rings at the cilia base. (J-J’) STORM images produced by double staining with anti-HA (MKS6) and anti-Nup153. Nup153 seems to form “rod-like” structure that extends below the transition zone, J’ shows top and side views of the two proteins as indicated. (K-K’) STORM images of double staining cells with anti-Nup50 and anti-HA (MKS6) showing oblique views of MKS6 and Nup50 in the axial direction. Nup50 seems to localise below the TZ and near the basal body.

In conclusion, our analysis of anti-nucleoporin antibodies in *Tetrahymena thermophila* suggests that the staining patterns may not correspond to nucleoporins. The signals observed at the cilia base are not accompanied with a signal in the nucleus. Moreover, no ciliary localisation was observed in epitope tagged Nup93 or Nup96 transgenic lines. Therefore, our data does not allow us to reliably claim that we localised nucleoporins. However, we took advantage of the fact that anti-Nup50 antibody forms rings below the transition zone and we used it to determine the axial positions of the TZ components relative to Nup50.

III.2.7. Axial positions of TZ proteins

To determine the axial position (along the ciliary axis) of the transition zone proteins, we took advantage of *Tetrahymena thermophila*'s cilia ability to show the side views of the proteins. As mentioned above, anti-Nup50 forms 9-fold symmetrical rings at the cilia base, near the basal body. We used Nup50 as the reference marker relative to which the transition zone proteins were mapped axially. We could localise the axial positions of 10 epitopes in 7 different transition zone proteins. When localising both termini of the same protein, we could determine the way the protein orients at the cilia base.

To measure the distance between Nup50 and transition zone proteins, we first extracted the "molecule list" of side views using the software provided by NIKON: "NIS Elements" (please refer to methods in Chapter III). Side views that only show parallel localisation of both proteins (TZ and Nup50) were selected for MATLAB analysis (Fig. III.8A). The molecule list of the side views

was then run on a code written in MATLAB that measures the distance between the two proteins (Fig. III.8A). Using this approach, we show that Tmem231-C terminus is the furthest from the reference protein: 209.3 ± 2.9 nm (Fig. III.8C-C' and J), followed by MKS6-C terminus: 205.5 ± 4.3 nm (Fig. III.8H-H' and J), MKS1-C terminus: 200.2 ± 3 nm (Fig. III.8F-F' and J), Ahi1-N terminus: 200 ± 2.9 nm (Fig. III.8D-D'' and J), MKS6-N terminus: 199.3 ± 4.4 nm (Fig. III.8I-I' and J), B9d1-C terminus: 198.8 ± 3.7 nm (Fig. III.8G-G' and J), Tmem216-C terminus: 198.4 ± 2.9 nm (Fig. III.8B-B'' and J), and Ahi1-C terminus is the closest to the reference protein with 193.8 ± 5.4 nm (Fig. III.8C-C' and J). In some instances, an oblique orientation of the two proteins is also observed (Fig. III.8B' and D').

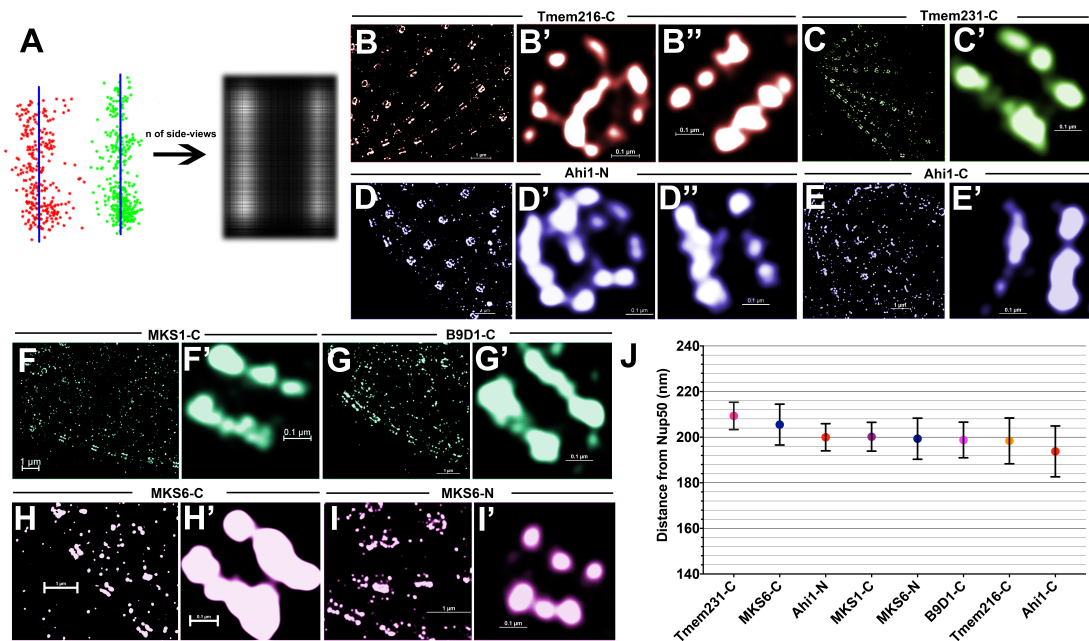


Figure. III.8. Axial positions of TZ proteins. (A) A representation showing parallel localisation between TZ and Nup50 side views. These localisations were used to measure the distance between the TZ protein (red) and Nup50 (green) using codes written in MATLAB. (B-B'') STORM images showing the side views of Tmem216-C terminus and Nup50. B' shows an oblique orientation of the two proteins. B'' shows side-views for the two proteins that can be utilised for measuring the distance between the proteins as shown in A. Tmem216-C terminus is 198.4 ± 2.9 nm; Tmem231-C terminus: 209.3 ± 2.9 nm (C-C'); Ahi1-N terminus: 200 ± 2.9 nm (D-D''); Ahi1-C terminus: 193.8 ± 5.4 nm; (E-E'); MKS1-C terminus: 200.2 ± 3 nm (F-F'); B9d1-C

terminus: $198.8 \pm 3.7\text{nm}$ (**G-G'**); MKS6-C terminus: $205.5 \pm 4.3\text{nm}$ (**H-H'**); and MKS6-N terminus: $199.3 \pm 4.4\text{nm}$ (**I-I'**) away from Nup50. Data are mean \pm SEM. (**J**) Mean distance between transition zone protein and Nup50. Data are mean \pm 95% confidence interval (CI).

On the other hand, NPHP4 manifested different distribution from other TZ proteins in the axial direction. This was expected, since we showed earlier that NPHP4 was the only TZ protein to show 2 layers in the side-views of the protein (Fig. III.4A'' and B''). The analysis of the axial position of NPHP4 relative to Nup50 revealed 2 different conformations. The N-terminus localised at two positions, one at about 201nm and another at 318nm away from Nup50 (Fig. III.9A-A'' and C). The C-terminus also localised at 2 positions as well, with one at about 180nm and another at about 313nm away from Nup50. However, since we used 1-colour STORM imaging, we cannot confirm that both NPHP4 localisations are distal to Nup50 without further analysis with additional antibodies. Therefore, using these immunostaining procedures, we show that the examined TZ proteins are confined to 20-30nm along the ciliary axis (excluding the far axial localisation for NPHP4).

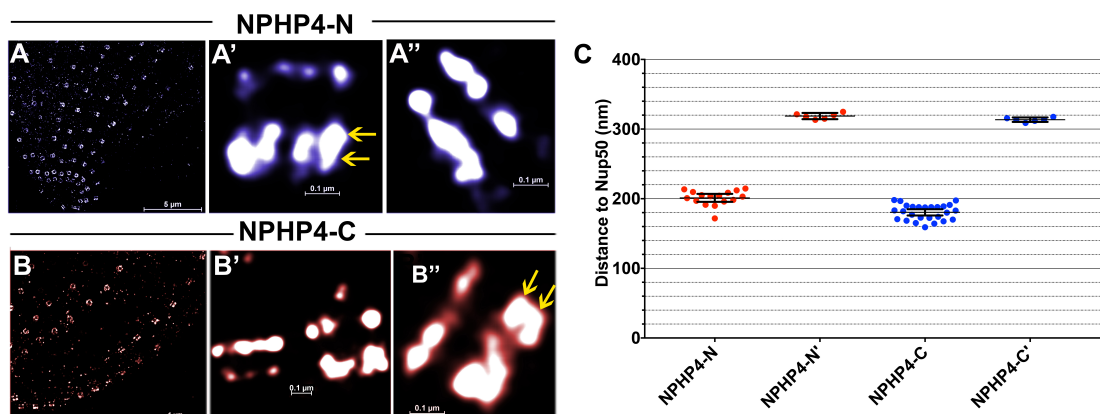


Figure. III.9. Axial positions of NPHP4. (A-A'') STORM images showing the side views of NPHP4-N terminus with respect to Nup50. Arrows show the two layers of NPHP4 in **A'**. (**B-B''**) STORM images showing the side-views of NPHP4-C terminus with respect to Nup50. Arrows

show the two layers of the protein. **(C)** Mean distance between NPHP4 (C- and N- termini) and Nup50. The images are split into 2 groups, the first included all showing distances below 300nm between NPHP4-N or NPHP4-C and the other group included the distances above 300nm (NPHP4-N' and NPHP4-C'). Data are mean \pm 95% CI.

II.3. Discussion

Just a few years ago, imaging biological samples was limited by the resolution of light microscopy, which roughly corresponds to the diameter of the cilium and thus incapable of visualising the fine structure of protein complexes at the base of the cilium (Huang et al., 2010). STED microscopy was utilised to generate super-resolved images and overlapping them with representative electron microscopy images to define the architecture of some proteins at the cilia base (Yang et al., 2015). Albeit being a super-resolution technique, STED microscopy is still limited to a resolution of about 50nm (Sieber et al., 2007). This is not sufficient to detect very subtle differences between localisation of different proteins at the cilia base. Thus, using STORM super-resolution microscopy, which improves the resolution to 20nm in the lateral dimension, one could localise features of cilia roughly equal to 20nm in size (Schermele et al., 2010, Szymborska et al., 2013, Shi et al., 2017). Using 3D-STORM imaging and quantitative analysis, it was shown that some TZ proteins could possibly be structural components of the Y-Links of the TZ (Shi et al., 2017). STORM imaging of RPGRIP1L in hTERT-RPE1 cells showed that this protein is arranged in rings formed of 7, 8, or 9 clusters (Lambacher et al., 2016). Still others have localised several ciliary base proteins, such as Tmem237, Ahi1, Cyb1, and OFD1 using STED imaging and showed that these proteins form

rings at the cilia base (Lau et al., 2012).

To reveal the architecture of transition zone proteins at the cilia base and to show how selected TZ proteins are oriented at the cilia base, we utilised STORM imaging in the ciliate model *Tetrahymena thermophila* of N- and C-tagged transition zone proteins. *Tetrahymena thermophila* is of a great advantage in these studies. Its entire surface is covered with hundreds of cilia (Orias et al., 2011). Many genes, such as those encoding proteins that localise to the basal body and those involved in cilia motility are evolutionarily well conserved with higher vertebrates (Kilburn et al., 2007, Bayless et al., 2015, Gaertig et al., 2013). Consequently, a *Tetrahymena* cell does not have to be positioned in any particular way for imaging, an advantage compared to mammalian cells. Its oval shape also provides an excellent model to look at the proteins from various angles, and thus one can image the top-views, oblique views, and side-views of the same protein. To facilitate imaging the transition zone, *Tetrahymena* cilia can be easily removed by pH shock (Gaertig et al., 2013). *Tetrahymena* are also amenable to genetic analysis. For example, we have added HA-tag at the native locus of at least 7 TZ proteins and 2 nucleoporins. This method of tagging at the native locus of the gene is expected to give the native pattern of expression (Gaertig et al., 2013). Moreover, the fact that one *Tetrahymena* cell possesses numerous cilia is very useful. This makes it possible to collect plenty of data, which is not feasible when using mammalian cell culture. These data can be aligned and averaged using codes written in MATLAB to obtain average diameters (for radial dimensions) and distances (for axial dimension).

We used two different methods to analyse the localisation, architecture

and arrangement of TZ proteins at the cilia base. HA epitope tag was detected by antibody staining using both Alexa Fluor 647-conjugated secondary antibodies (indirect labelling), or directly Alexa Fluor 647-conjugated primary antibody (direct labelling) to evaluate the localisation and determine the radial positions of TZ proteins. Using both immunostaining procedures, we show that transition zone proteins form rings of varying radii relative to the ciliary axis.

Several factors could affect the quality of localisation of the protein when using STORM imaging. These factors include the labelling density, antibody affinity, number of frames collected when acquiring the data, and the choice of software to analyse the data. One important factor is the size of the IgG antibody itself. An IgG antibody is about 12nm long (Lee et al., 2006, Sapphire et al., 2001). Fluorophores are conjugated to lysines on IgGs and lysines are distributed on both light and heavy chains of the IgG molecule (Wang et al., 2005). This makes it difficult to estimate how far the fluorophores are from the epitope.

Moreover, antibodies we used in our study (whether for indirect or direct labelling) had a variable degree of labelling (DOL) that ranged between 3 and 6 (3-6 fluorophores per IgG molecule). This implies that multiple fluorophores can bind to a single IgG molecule. Therefore, to estimate the localisation error in our experiments, we compared measurements based on these two labelling procedures. The comparison of at least 10 epitopes in 7 TZ proteins showed differences that ranged from 0.3nm to 10nm, 4.85nm in average, which provides an estimate of error related to antibody size. This also agrees with previous reports on microtubule antibody staining where the error introduced by using antibody labelling was about 5nm (Pengo, et al., 2015).

Another source of error is the way the antibody binds to the epitope in different TZ lines. Antibodies may bind to their epitopes at different angles relative to the optical axis: parallel, perpendicular, or flexible. Interestingly, our comparison between direct and indirect labelling enabled us to predict the way the antibody binds to its epitope in different TZ proteins. When the difference in the measurement between the direct and indirect labelling is below 5nm, the antibody binds largely parallel to the optical axis. In other cases where the difference between the two labelling procedures is more than 5nm, the angle at which the antibody binds to its epitope is perpendicular or close to perpendicular relative to the optical axis.

Using the immunostaining procedures mentioned above, we show that TZ proteins form rings of varying radii with respect to the ciliary axis. In some cases, we observed doublets when using direct conjugation (Fig. III.3). However, a very accurate quantitative analysis and high sample size is required to confirm that the TZ proteins form rings of 9 doublets. Among the 7 TZ proteins investigated, we show that Tmem216-C terminus is the farthest from the microtubule doublets. NPHP4-C terminus and MKS6-C terminus are the nearest to the microtubule doublets (Fig. III.5.U-V and III.10C).

To evaluate the position of the ciliary membrane, we tagged the C-terminus of Tmem216. Tmem216 was shown to form a complex with a known transmembrane protein, Tmem67 (MKS3) using immunoprecipitation experiments (Valente et al., 2010). STORM localisation of Tmem216-C terminus generated a ring with a radius of 164nm. The analysis of Tmem67 in *Tetrahymena thermophila* using STORM also formed a ring of comparable diameter. The radii of Tmem67-C terminus and Tmem216-C terminus are very

close and are not statistically significant (Fig. III.5U and III.10A). Although there are no reported data on the diameter of the transition zone in *Tetrahymena thermophila*, based on Tmem216 topology, the radial position of Tmem216 suggests its close location to the ciliary membrane (Fig. III.5U and III.10C).

On the other hand, Tmem231, a TZ protein that belongs to the MKS module (Chih et al., 2011, Dowdle et al., 2011, Roberson et al., 2015), was shown using super-resolution imaging that it forms rings adjacent to the ciliary membrane which allowed to speculate that it localises to the membrane (Chih et al., 2011). The antibody used to localise Tmem231 in this study was raised against the last 15 amino acids of the protein (C-terminus) (Chih et al., 2011). This, however, does not agree with our findings about Tmem231. Our analysis shows that the radius of Tmem231-C is about 15nm smaller than that of Tmem216-C terminus, or the membrane (Fig. III.5.U-V and III.10A-C). The radii of Tmem231 and Tmem216-C termini are significantly different (Fig. III.10A), suggesting that Tmem231-C terminus is not near the ciliary membrane.

In addition to that, Tmem231 and B9d1 are known to interact with each other at the cilia base and to function in the transport of ciliary membrane proteins, such as Arl13b and Smoothened (Smo) (Chih et al., 2011, Dowdle et al., 2011). Our analysis shows that B9d1-C terminus is about 5nm away from Tmem231-C terminus and their radii seem to be significantly different (Fig. III.5U and III.10A). The diameters of both Tmem231 and B9d1 were recently investigated using STORM imaging in mouse tracheal cells (Shi et al., 2017). Our radial measurement of B9d1 agrees with that obtained by *Shi et al.*, but our radial measurements of Tmem231-C terminus produced a smaller diameter. *Shi et al.* utilised antibodies against the endogenous proteins, while our studies

relied on using antibodies against the tag at the two termini of the proteins in knock-in lines, which may account for this difference. Moreover, the error introduced by using antibody staining (as explained earlier ~5nm), should be taken into consideration and could account for the difference obtained for the radii of Tmem231 and B9d1. If true, then our analysis agrees with what was previously shown about the measurements of the diameters of B9d1 and Tmem231 (Shi et al., 2017) and also agrees with previous findings that B9d1 and Tmem231 interact at the cilia base (Chih et al., 2011, Dowdle et al., 2011).

Furthermore, B9d1 and MKS1, along with B9d2 proteins form a complex known as the “B9d complex”. This complex is necessary for ciliogenesis (Zhao and Malicki, 2011) and functions as a barrier for transmembrane proteins at the cilia base (Chih et al., 2011, Dowdle et al., 2011). Our STORM analysis shows that B9d1 and MKS1 are almost in the same radial position with a difference of less than 1nm between their radii (Fig. III.5U and III.10A). This is consistent the fact that these two proteins belong to the same complex and physically interact with each other (Chih et al., 2011, Dowdle et al., 2011). However, our data argue against the possibility that both MKS1-C terminus and B9d1-C terminus interact with the ciliary membrane. This is because both proteins localise to the same area of about 20nm away from the transmembrane proteins Tmem216 and Tmem67 (MKS3), or the membrane (Fig. III.5U and III.10A).

Apart from TZ proteins that function in the gating mechanisms, nucleoporins have emerged to possibly be involved in the gating mechanisms at the cilia base (Kee et al., 2012, Diener et al., 2015, Takao and Verhey, 2016). Our analysis of nucleoporins in *Tetrahymena thermophila* is somehow puzzling. We followed two approaches to investigate the localisation of nucleoporins. In

the first, we generated knock-in lines as previously described (Gaertig et al., 2013). We added triple HA tags at the C-terminus of 2 nucleoporins Nup93 and Nup96. In the second approach, we used anti-nucleoporin antibodies commercially available (Table II.3). Using antibody staining against HA in the knock-in lines we could detect nuclear signal, but no observable signal at the cilia base (Fig. II.7.G and H). On the other hand, the analysis of anti-Nup antibodies in *Tetrahymena thermophila* produced signals in several different regions of *Tetrahymena* cilia and ciliary basal bodies. Importantly, some antibodies such as anti-mab414, anti-Nup50, and anti-Nup153 produced signals at the cilia base (Fig. III.7.A, B, and F respectively). Others had either localisation in the nucleus only, such as anti-Nup93 (Fig. III.7D) or inside the ciliary shaft, such as anti-Nup98 (Fig. III.7E).

The staining patterns we observed using anti-nucleoporin antibodies may not correspond to nucleoporins. In most cases, the signal observed at the cilia base was not accompanied by a signal in the nucleus, as it would be expected from nucleoporins. This is supported by the fact that in knock-in lines, Nup93 and Nup96 localised to the nucleus only. In conclusion, our data does not allow us to affirm that we localised nucleoporins. Consequently, this requires further investigation such as immunoprecipitation experiments followed by mass spectrometry to reveal the identity of the proteins recognised by these antibodies in *Tetrahymena thermophila*. Although we cannot confirm that we localised nucleoporins, the analysis of these antibodies was useful. We took advantage of the fact that anti-Nup50 antibody localises to the cilia base. In STORM, anti-Nup50 forms 9-fold symmetrical rings. Therefore, we used this

antibody as a reference protein to determine the axial positions of the TZ components.

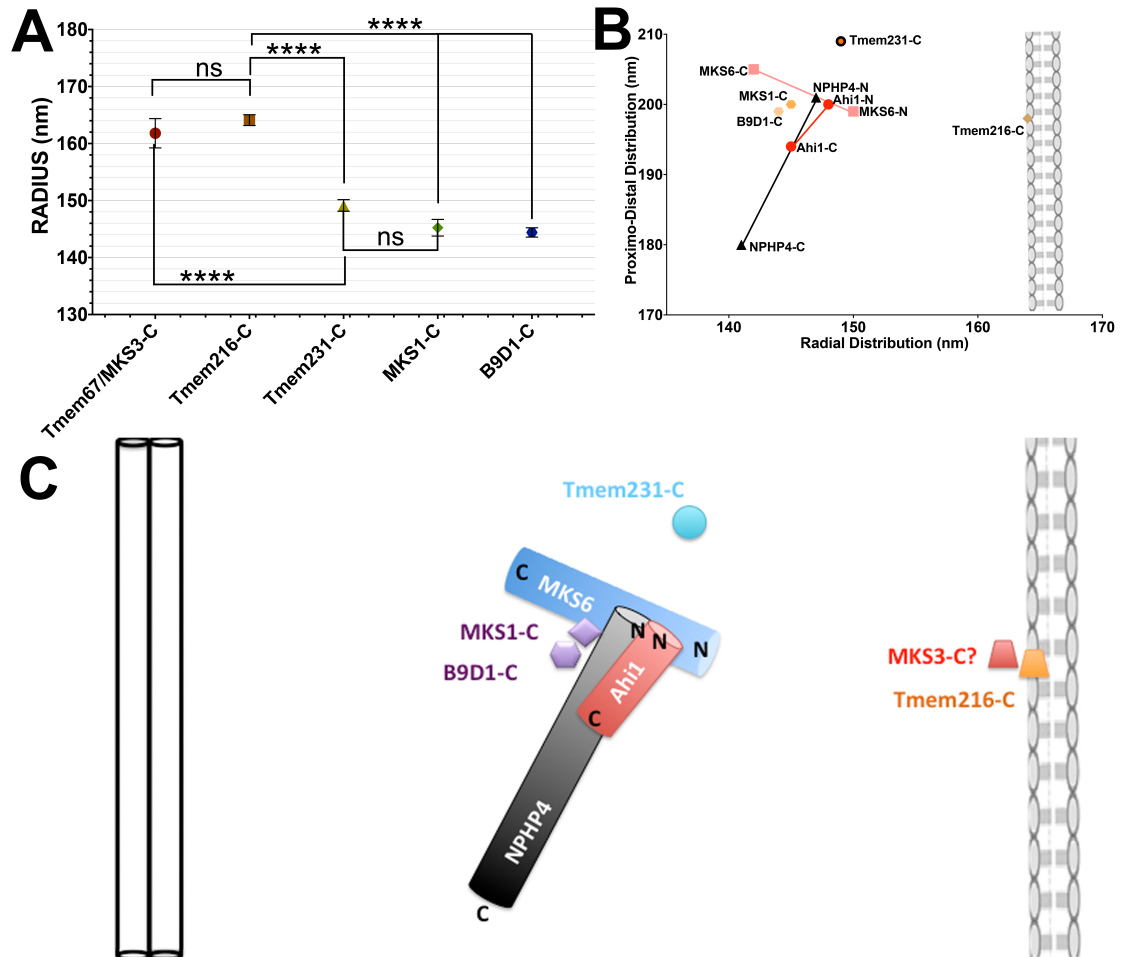


Figure. III.10. Model of the TZ. (A) Mean radii showing the significance of differences between TZ proteins. **(B)** A chart showing the distribution of TZ proteins at the cilia base. The X-axis shows the radial positions and the Y-axis shows the proximo-distal positions of TZ proteins. **(C)** A super-resolved model of TZ proteins showing their orientation and position at the cilia base. The model shows the orientation of MKS6, Ahi1, and NPHP4. It also shows the radial and axial positions for the C-termini of Tmem216, Tmem231, MKS1, B9d1, and MKS3.

Our analysis of the axial positions of TZ components is also of interest. To determine the axial positions of TZ proteins with respect to Nup50, we performed double labelling using anti-HA: to recognise the protein of interest

(TZ in this case), and anti-Nup50 as a reference point. After staining with the primary antibody, the samples were stained with only 1 secondary antibody conjugated to Alexa Fluor 647 that recognises both primary antibodies. Using one secondary antibody is also beneficial, as this does not require 2-colour STORM imaging. If 2-colour STORM imaging is to be used, then other factors must be taken into consideration, such as using a suitable pair of secondary antibodies (Shi et al., 2017) and images should be corrected for chromatic aberration (Erdelyi et al., 2013).

Using the labelling approach mentioned above, we obtained side views of both proteins (TZ and Nup50) in 10 TZ epitopes. Using codes written in MATLAB, we estimated the distance between the transition zone proteins and Nup50. Again in this case, when analysing the 2 termini of the same protein using this strategy, we could determine the way the protein is oriented at the cilia base. For example, the axial position of the C-terminus of MKS6 was somewhat higher than that of the N-terminus, this is also applied to Ahi1, where the N-terminus is higher than its C-terminus. Thus, these proteins seem to be oriented obliquely at the cilia base (Fig. III.10B, C). In conclusion, we present here a super-resolved model showing the radial and axial position of transition zone proteins in unprecedented detail focusing on the orientation of some TZ proteins depending on data collected from the radial and axial positions of the N- and C- termini of the TZ proteins (Fig. III.10B, C).

Chapter IV

“STORM Imaging Unveils the Architecture of the IFT particle in its Docking Site”

IV.1. Introduction

Intraflagellar transport or IFT is a well-conserved system involved in the movement of proteins required to build and maintain cilia in most eukaryotic organisms (reviewed in (Taschner et al., 2016, Scholey and Anderson, 2006, Prevo et al., 2017)). As cilia do not contain protein synthesis machineries, necessary proteins are transported from the cytoplasm to the ciliary compartment by the anterograde IFT, which is powered by kinesin-II motors (Kozminski et al., 1995, Snow et al., 2004). Proteins leave the cilium back to the cytoplasm by the retrograde IFT powered by cytoplasmic dynein-1b/2 motors (Pazour et al., 1999, Hou, 2004 #4962, Yi, 2017 #4963). The anterograde transport is mediated by the IFT-B complex composed of 16 different IFT proteins, while the retrograde transport is accomplished by the IFT-A complex which is composed of 6 different IFT proteins (Cole et al., 1998, Hirano et al., 2017) (Table IV.1).

IFT-B proteins are important for cilia assembly, as mutations in the IFT-B components ceased cilia formation (Taschner et al., 2011, Brazelton et al., 2001, Krock and Perkins, 2008, Tsujikawa and Malicki, 2004). On the other hand, mutations in IFT-A proteins usually lead to the accumulation of ciliary proteins at the cilia tip, and therefore are important for the retrograde transport (Tsao and Gorovsky, 2008, Zhu et al., 2017, Taschner et al., 2011). Still some studies reported roles of IFT-B in the exit of ciliary cargoes (Eguether et al., 2014, Huet et al., 2014), and IFT-A in transporting ciliary membrane proteins (Fu et al., 2016). The IFT particle transports ciliary proteins ranging from tubulin, the most abundant ciliary component (Bhogaraju et al., 2013), structural components such as outer dynein arms (ODAs) to power cilia motility in motile

cilia (Hou et al., 2007, Ahmed and Mitchell, 2005, Chevrette et al., 2000, Taschner et al., 2017), and signalling proteins, such as components of hedgehog (HH) and Wnt (Mourao et al., 2016).

Based on immunoelectron microscopy, *Chlamydomonas* IFT52 was shown to localise at the transition fibres (Deane et al., 2001). Moreover, other IFT proteins, such as IFT57, IFT88, and IFT140, were shown to localise at the region of the basal body too (Sedmak and Wolfrum, 2010, Williams et al., 2011). The docking sites for many IFT proteins and the exact positions where IFT proteins interact with their cargo at the cilia base remained, however, a mystery. Interestingly, the IFT particle with its cargo and motors comprise a megadalton protein complex that must cross the transition zone, a well-organised gate at the cilium base that controls the composition of the cilium depending on several factors including the molecular weight and the structural conformation of the proteins (reviewed in (Reiter et al., 2012)) and (Kee and Verhey, 2013)). Before entering the cilium, the IFT particle, IFT motors, and cargoes are thought to assemble at the cilia base. It is unclear how this megadalton complex crosses the barriers at the cilia base. It is also not known where exactly IFT proteins dock and assemble at the cilia base before they enter the cilium.

Previous attempts to show interactions and ultrastructural details of IFT proteins were based on electron tomographic analysis of IFT trains in *Chlamydomonas reinhardtii* (Pigino et al., 2009) and crystallographic analyses of some IFT proteins (Bhogaraju et al., 2013, Bhogaraju, 2011 #4973, Taschner, 2014 #4974). For instance, using crystallographic studies, the crystal structure of the IFT52/IFT46 C-termini in *Tetrahymena* was resolved at 2.3Å

(Taschner et al., 2014). The ultrastructure of IFT trains in *Chlamydomonas reinhardtii* was analysed using cryo-electron microscopy and electron tomography (Pigino et al., 2009).

Interactions between IFT and their cargoes were also reported. IFT46-N terminus binds with the N-terminus of the adaptor protein ODA16, which is important for the transport of the outer dynein arm complex (ODA) (Ahmed and Mitchell, 2005, Taschner et al., 2017, Hou and Witman, 2017). The transport of tubulin occurs by binding to the N-termini of IFT81/74 (Bhogaraju et al., 2013). Recently, by using STORM imaging, it was shown that IFT88, an IFT-B component, localised to the distal appendages (Shi et al., 2017) and specifically at the gaps between the blades of distal appendages (Yang et. al, 2017). The exact site where other IFT proteins dock at the cilia base remains unclear.

Using STORM imaging combined with quantitative image analysis, we show for the first time the arrangement of several IFT proteins at their “docking sites”. Radially, IFT docking sites span a region between about 140nm and 165nm from the centre of the axoneme. Kif3a, a microtubule-dependant motor, localises more centrally, compared to IFT proteins. Axially, the IFT docking sites localise between the transition zone and the basal body and occupy a region of about 30nm and are at least 50nm proximal to the transition zone. IFT-A complex is located to the outside of IFT-B complex relative to the cilium axis. In the axial dimension, Kif3a, docks slightly distal to IFT proteins suggesting a likely independent docking site for IFT motors. Our STORM analysis also reveals the localisation of the binding sites of cargoes such as tubulin and outer dynein arm (ODA) complex at the cilia base. All these data combined enabled us to present the first super-resolved model of the architecture of the IFT

particles in their docking sites. The model shows the orientation of IFT proteins and their position relative to other proteins at the cilia base.

IV.2. Results

IV.2.1. IFT proteins localise to the cilia base in *T. thermophila*

To determine the localisation of different IFT proteins in *Tetrahymena thermophila*, we used epitope tagging at either the N- or/and C- termini of the coding region of the gene in the macronuclear genome (Gaertig et al., 2013). Tags used in this study included triple HA, single GFP, or triple V5 tags. We first analysed the localisation of IFT proteins using anti-HA, anti-GFP, or anti-V5 antibodies on the Olympus FV1000 confocal microscope. To ensure that tagging was performed correctly, we also assessed the molecular weight of the tagged IFT proteins by western blots.

Surprisingly, all the IFT proteins examined in our study localised to the cilia base (Fig. IV.1). Using antibody staining against the tag at both termini of the proteins (N- and C-), IFT-A complex components IFT40 (Fig. IV.1A-A'), IFT144 (Fig. IV.1B-B'), and IFT122 (Fig. IV.1C-C') localised to the cilia base in *Tetrahymena thermophila*. Similarly, IFT-B complex components IFT46 (Fig. IV.1D-D'), IFT52 (Fig. IV.1E-E'), IFT27 (Fig. IV.1F), IFT54 (Fig. IV.1G-G'), and IFT81 (Fig. IV.1H-H') localised to the cilia base in *Tetrahymena thermophila*. Using western blot analysis, we show that using antibody against the tag revealed the expected sizes of the proteins (Fig. IV.1G). In conclusion, we show that IFT proteins localise to the base of cilia. These studies suggest the

locations where IFT proteins dock at the cilia base before they gain access to enter the cilium.

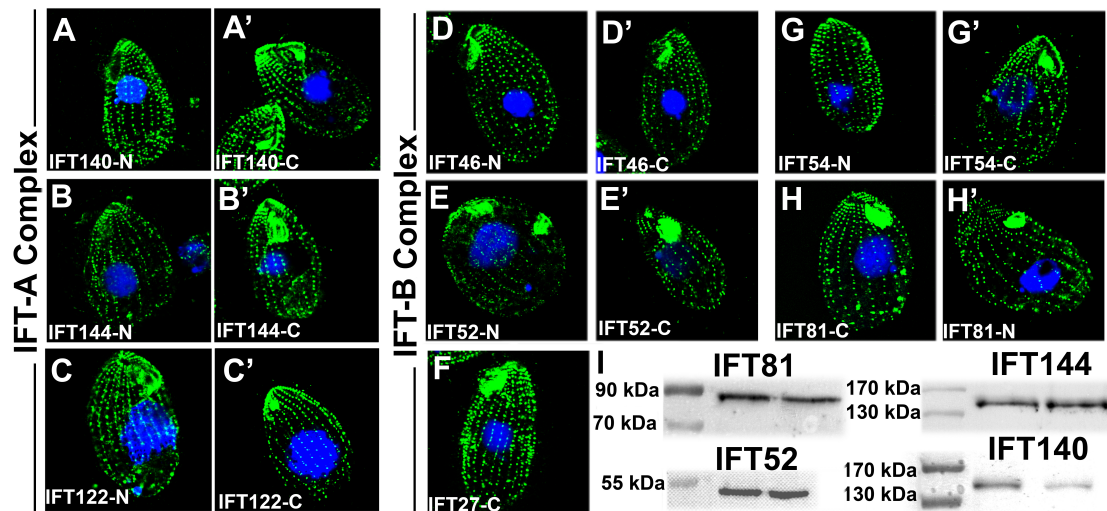


Figure IV.1. IFT proteins localise to the cilia base in *Tetrahymena thermophila*. (A-C') Confocal images showing the localisation of IFT-A proteins at the cilia base using anti-HA antibody (green) to detect the N-terminus or C-terminus of the proteins. IFT140-N terminus (A), IFT140-C terminus (A'), IFT144-N terminus (B), IFT144-C terminus (B'), IFT122-N terminus (C), and IFT122-C terminus (C') all localised to the cilia base. We used anti-HA to recognise all epitopes except for IFT140-C terminus and IFT144-C terminus, where we used anti-GFP antibody (A' and B'). IFT-B complex proteins also localised to the cilia base whether the antibody staining was used against the tag at the C-terminus or the N-terminus of the protein (D-F). The localisation of IFT46 (D-D'), IFT52 (E-E'), IFT27-C terminus only (F), IFT54 (G-G'), and IFT81 (H-H') are shown as indicated. (I) Western blot analysis of IFT81, IFT52 from the IFT-B complex and IFT144 and IFT140 from the IFT-A complex shows the expected size of each protein as indicated. Data in "I" are shown as duplicates.

IV.2.2. STORM imaging of IFT proteins in ciliated and de-ciliated *T.thermophila*

STORM imaging of IFT proteins was recently reported by imaging IFT88, an IFT-B complex component in mammalian cells (Shi et al., 2017) Yang et al., 2017). However, these studies did not reveal the arrangement of different IFT

proteins at the cilia base. Since we showed using confocal imaging that IFT proteins localise to the cilia base in *Tetrahymena thermophila*, it was very enticing to examine these proteins using super-resolution microscopy, such as STORM. Strikingly, STORM imaging of IFT54, for example, showed that IFT proteins form well-defined 9-fold symmetrical rings at the cilia base (Fig. IV.2A-A'). This 9-fold symmetry of IFT proteins was interesting, however, it did not seem consistent with previous studies of the localisation of IFT proteins which showed that IFT particle components localise to the cilia base and the ciliary shaft (Shi et al., 2017, Yang et al., 2015) Yang et al., 2017). The localisation of IFT proteins is likely to change when rapid cilia growth is required. Therefore, we took advantage of the ability to deciliate (decapitate cilia) *Tetrahymena thermophila's* by pH shock (Gaertig et al., 2013) to examine the localisation of IFT proteins. We deciliated the IFT54-C terminus lines and waited for 30-60min to allow cells to rebuild cilia, then fixed and immunostained the cells and imaged them on STORM. Interestingly, IFT localised mainly inside the ciliary shaft of *Tetrahymena* cells (Fig. IV.2B-C). We could also observe that while IFT proteins are re-building cilia again, the IFT localisation at the cilia base in some cases was still observable (Fig. IV.2B, yellow arrows). In other cases, the IFT localisation was only seen inside cilia without observable localisation at the cilia base (Fig. IV.2B, red arrow). This may indicate that IFT proteins in *Tetrahymena* cells dock at the cilia in a “standby mode” until needed for the cilia formation and maintenance.

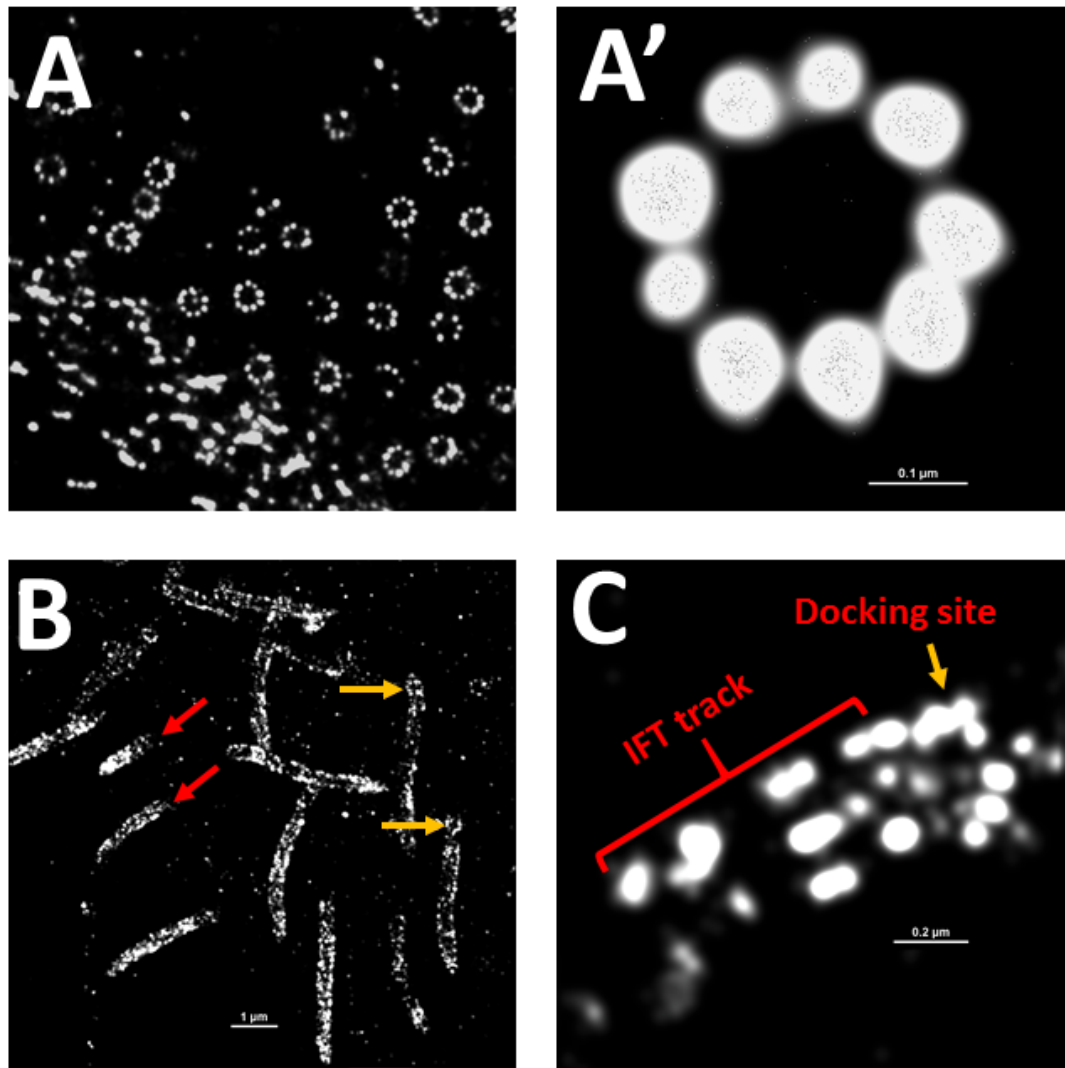


Figure IV.2. IFT proteins are arranged in 9-fold symmetrical rings at the cilia base and move rapidly into cilia following deciliation. (A) STORM image of IFT54-C terminus using anti-HA antibody followed by secondary antibody conjugated to Alexa Fluor 647. STORM images show that IFT54-C form rings of 9-fold symmetry at the cilia base **(A')**. **(B)** *Tetrahymena* cells were deciliated (removed cilia) by pH shock. After 30-60 minutes, cells were fixed and imaged on STORM. STORM images reveal that IFT54-C terminus localises throughout the whole ciliary shaft while regenerating cilia. It noteworthy that the docking sites of IFT-54, even with deformed arrangement, remained in most cilia (yellow arrows). Still, some cilia showed IFT54 inside cilia with no observable docking sites (red arrows). **(C)** Another example of one cilium after 30 minutes of deciliation with the docking site clearly seen at the cilia base (yellow arrow) and the IFT localisation well noticed inside cilia as indicated.

IV.2.3. IFT-B complex proteins form 9-fold symmetrical rings with different radii at the cilia base

To elucidate the radial distribution of IFT-B complex proteins at the cilia base, we utilised STORM image combined with quantitative imaging analysis using codes written in MATLAB to determine the radii of IFT-B proteins with respect to the ciliary axis. Again in this case, we used indirect and direct labelling procedures, as that performed on TZ strains (please refer to methods for more details), using antibodies against the tag at the C- and N- termini of the proteins. Using both labelling procedures, we show that all IFT-B proteins form clear 9-fold symmetrical rings with different radii at the cilia base (Fig. IV.3A-R”).

Using indirect labelling, we show that IFT81-N terminus has the largest radius of 161.9 ± 5 nm (Fig. IV.3O-O”) and IFT52-N terminus having the smallest radius of 140.6 ± 7 nm (Fig. IV.3C-C”). On the other hand, the radius of IFT52-C terminus was much larger from that of the N-terminus with a radius of 158.4 ± 7.3 nm (Fig. IV.3A-A” and S, $p < 0.0001$). The significant difference in the radii between the N- and C- termini of the same protein was also observed in IFT54, IFT46, and IFT81. IFT54-C terminus has a radius of 150.5 ± 6 nm (Fig. IV.3E-E”, S) while its N-terminus was 141 ± 8.6 nm (Fig. IV.3G-G”, S). IFT46-C terminus had a radius of 158.9 ± 5.7 nm (Fig. IV.3I-I”, S) compared to a radius of 143.5 ± 4.8 nm for the N-terminus (Fig. IV.3K-K”, S). IFT81-C terminus was of 157.8 ± 5.4 nm (Fig. IV.3M-M”, S) compared to 161.9 ± 5 nm for the N-terminus of the protein (Fig. IV.3O-O”, S). Finally, IFT27-C terminus had a radius of 157.2 ± 4.2 nm at the cilia base (Fig. IV.3Q-Q”, S). Therefore, using indirect labelling, IFT-B proteins that we analysed thus far span about 20nm in the radial

dimension.

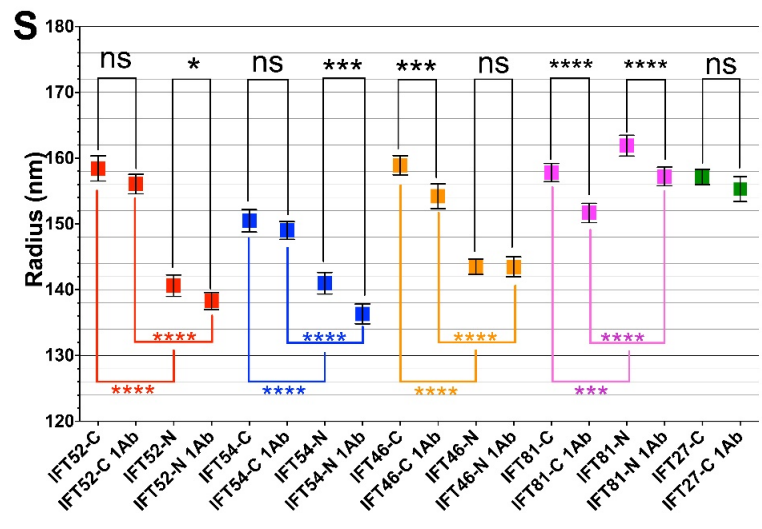
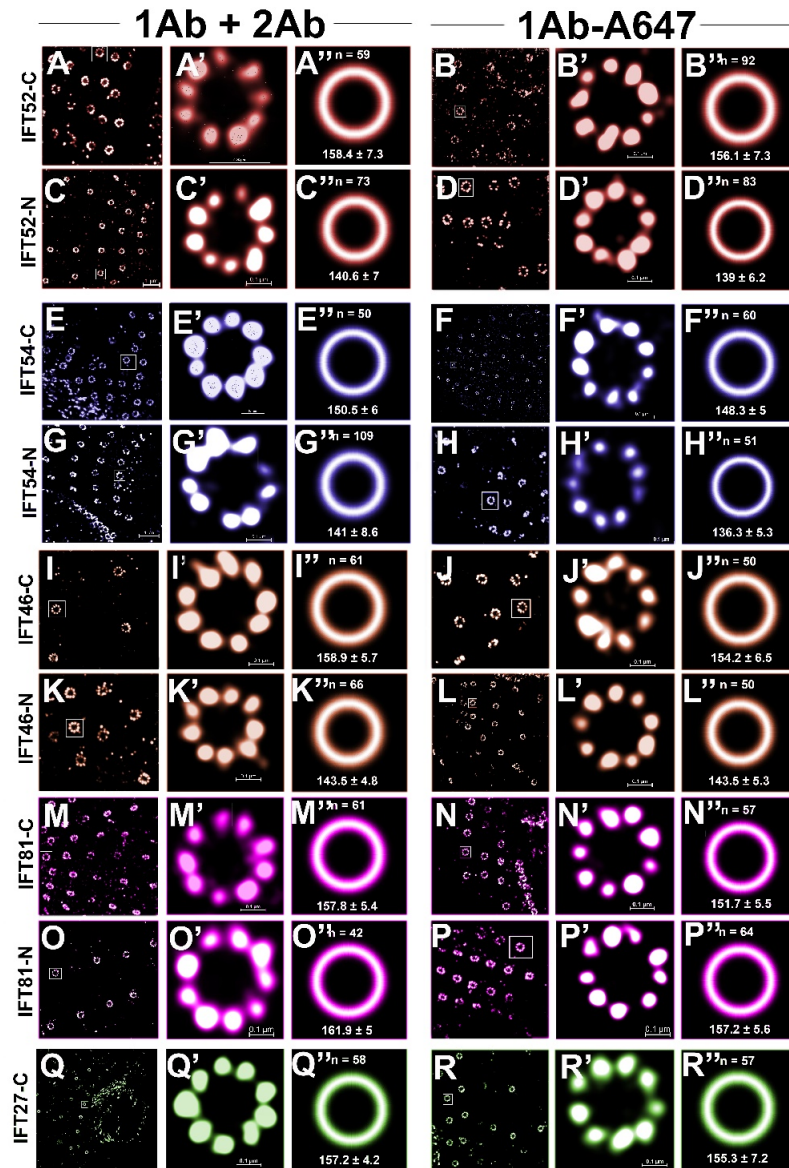


Figure IV.3. IFT-B proteins form 9-fold symmetrical rings with different radii at the cilia base. The radii of different IFT-B proteins using both indirect labelling versus direct labelling procedures are shown as indicated. **(A-B'')** IFT52-C: 158.2 ± 7.3 nm (59 rings) versus 156.1 ± 7.3 nm (92 rings). **(C-D'')** IFT52-N terminus: 140.6 ± 7 nm (73 rings) versus 139 ± 6.2 nm (83 rings). **(E-F'')** IFT54-C terminus: 150.5 ± 6 nm (50 rings) versus 148.3 ± 5 nm (60 rings). **(G-H'')** IFT54-N terminus 141 ± 8.6 nm (109 rings) versus 136.3 ± 5.3 nm (51 rings). **(I-J'')** IFT46-C terminus: 158.9 ± 5.7 nm (61 rings) versus 154.2 ± 6.5 nm (50 rings). **(K-L'')** 143.5 ± 4.8 nm (66 rings) versus 143.5 ± 5.3 nm (50 rings). **(M-N'')** IFT81-C terminus: 157.8 ± 5.4 nm (61 rings) versus 151.7 ± 5.5 nm (64 rings). **(O-P'')** IFT81-N terminus 161.9 ± 5 nm (41 rings) versus 157.2 ± 5.6 nm (64 rings). **(Q-R'')** IFT27-C terminus: 157.2 ± 4.2 nm (58 rings) versus 155.3 ± 7.2 nm (57 rings). Data are means \pm SD. **(S)** The radial distribution of the means \pm 95% Confidence interval (CI) for IFT-B epitopes using indirect versus direct labelling. IFT52-C, IFT54-C, IFT46-N, and IFT27-C did not show significant difference in the measurement of the radii using both immunostaining procedures. IFT52, IFT54, IFT46, and IFT81 showed difference in the measurements of the radii of both termini. **(A'-R')** show insets in **(A-R)**. Based on Student's *t*-tests; * *P*, 0.05, ** *P*, 0.01, *** *P*, 0.001, and **** *P*, 0.0001; not significant, ns. All differences were also significant based on Mann–Whitney test.

Interestingly, 4 out of 9 IFT epitopes had no significant difference in the measurement of the radius when using the two immunostaining procedures (Fig. IV.3S). IFT52-C terminus (Fig. IV.3B-B''), IFT54-C terminus (Fig. IV.3F-F''), IFT46-N terminus (Fig. IV.3L-L''), and IFT27-C terminus (Fig. IV.3R-R'') did not show a significant difference in the measurement of the radius between indirect and direct labelling procedures. A low significant difference was observed for the IFT52-N terminus (Fig. IV.3S and D-D''). IFT54-N terminus (Fig. IV.3H-H''), IFT46-C terminus (Fig. IV.3J-J''), IFT81-C terminus (Fig. IV.3N-N''), and IFT81-N terminus (Fig. IV.3P-P'') all showed a very significant difference in the measurement of the radii between direct and indirect labelling procedures (Fig. IV.3S). When comparing the radii of N- and C- termini of the same protein, we observed a high statistical significance for IFT52, IFT54, IFT46, and IFT81 (Fig. IV.3S). Using direct labelling, IFT-B proteins still span

about 20nm in the radial dimension, very similar to that using indirect labelling. In conclusion, our STORM analysis of IFT-B proteins reveals that they form rings of 9-fold symmetry with different radii at the cilia base. Using both immunostaining procedures, we show that IFT-B proteins investigated in this study span about 20nm in the radial dimension.

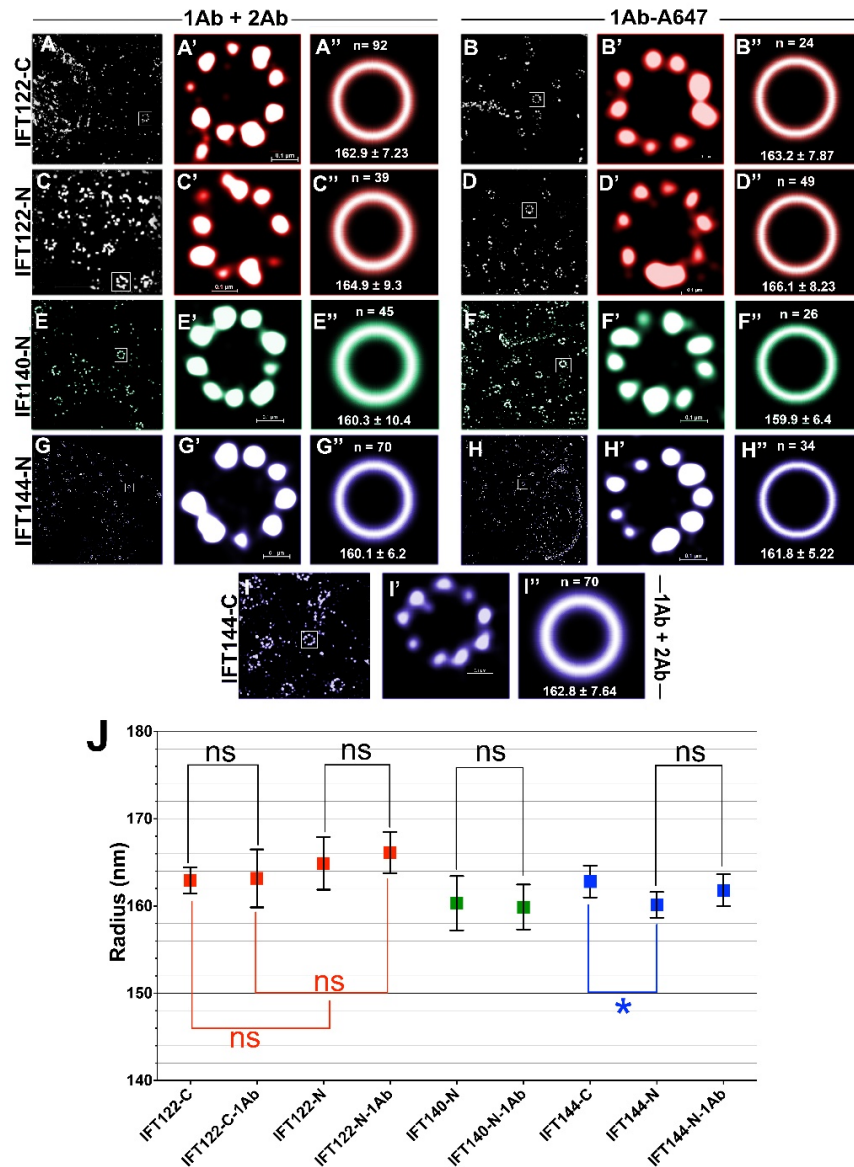


Figure IV.4. IFT-A complex proteins form 9-fold symmetrical rings at the cilia base. Using indirect versus direct labelling, the radii of IFT-A proteins are indicated. (A-B'') IFT122-C terminus: 162.9 ± 7.23 nm (92 rings) versus 163.2 ± 7.87 nm (24 rings). (C-D'') IFT122-N terminus: 164.9 ± 9.3 nm (39 rings) versus 166.1 ± 8.23 nm (49 rings). (E-F'') IFT140-N terminus: 16.3 ± 10.4 nm (45 rings) versus 159.9 ± 6.4 nm (26 rings). (G-H'') IFT144-N

terminus: 160.1 ± 6.2 nm (70 rings) versus 161.8 ± 5.22 nm (34 rings). **(I-I'')** IFT144-C terminus: 162.8 ± 7.64 nm (70 rings). Data are means \pm SD. **(J)** The radial distribution of the means \pm 95% Confidence interval (CI) for all IFT-A epitopes using indirect versus direct labelling. All epitopes examined using indirect versus direct labelling did not show a significant difference in the measurement of the radii. Note that the N- and C-termini of IFT122 did not show a significant difference in the radii, but it was significant for IFT144. Based on Student's *t*-tests; * *P*, 0.05, ** *P*, 0.01, *** *P*, 0.001, and **** *P*, 0.0001; not significant, ns. All differences were also significant based on Mann–Whitney test.

IV.2.4. IFT-A complex localises outside IFT-B complex

We followed the same approach to localise three IFT-A complex proteins: IFT122, IFT140, and IFT144 (Table IV.1). The 3 IFT-A complex proteins display radii that are clearly larger than those in all IFT-B proteins. Using indirect labelling, we show that IFT122-N terminus had the largest radius of 164.9 ± 9.3 nm (Fig. IV.4C-C'', J) followed by the C-terminus of IFT122 with a radius of 162.9 ± 7.23 nm (Fig. IV.4A-A'', J). The radii of C- and N-termini of IFT122 were not significantly different (Fig. IV.4J). IFT144 did not show a significant difference in the measurement of the radii of the C- and N- termini either (Fig. IV.4J). The C-terminus of IFT144 has a radius of 162.8 ± 7.64 nm (Fig. IV.4I-I'') and the N-terminus had a radius of 160.1 ± 6.2 nm (Fig. IV.4G-G''). Finally, we determined the radius of the N-terminus of IFT140 to be 160.3 ± 10.3 nm (Fig. IV.4E-E''), but we could not detect clear rings to be used for measurements for the C-terminus of IFT140. Therefore, IFT-A proteins characterised in this study span only about 5nm in the radial dimension.

Using direct labelling, none of the radii of IFT-A complex proteins showed a significant difference when compared to indirect labelling (Fig. IV.4J). IFT122-C terminus (Fig. IV.4B-B''), IFT122-N terminus (Fig. IV.4D-D''), IFT140-N

terminus (Fig. IV.4F-F''), and IFT-144-N terminus (Fig. IV.4H-H'') all had radii with slight differences compared to those obtained when using indirect labelling but were not statistically significant (Fig. IV.4J). It is worthy to mention that when using direct labelling, all IFT-A complex proteins had radii of about 160nm or higher (Fig. IV.4), while none of IFT-B complex proteins had a radius higher than 160nm, i.e. no overlap in the radii of the two complexes was detected. Thus, we conclude that IFT-A complex proteins form rings of different radii at the cilia base and that IFT-A complex seems to lie outside the IFT-B complex in the radial dimension.

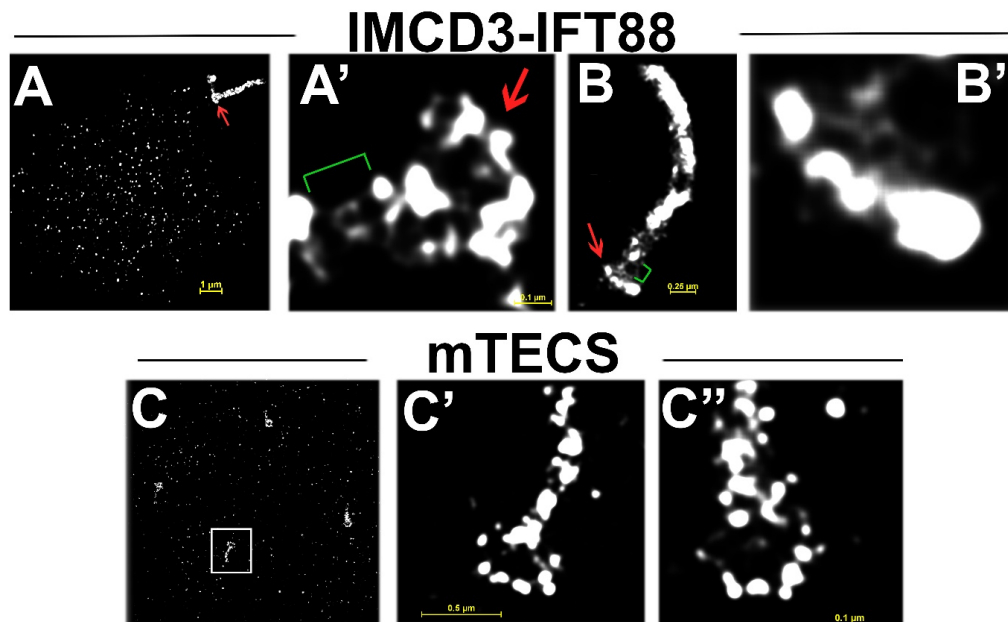


Figure IV.5. STORM images of IFT88 shows rings at the cilia base in mTECs and IMCD3 cells. (A-B') IMCD3 stably expressing IFT88-GFP were stained with anti-GFP antibody followed by a secondary antibody conjugated to Alexa Fluor 647 and imaged on STORM. STORM images show that IFT88 localised to ciliary shaft and shows ring-shaped structures at the cilia base (red arrow). **(A')** shows that IFT88 localises in ring-like structures at the cilia base of the cell shown in **(A)**. Note the gap (green bracket) between the localisations at the cilia base and ciliary shaft. **(B-B')** Another example of IMCD3 cells showing IFT88 localisation in side-views (red arrow, and **B'**). A gap is also seen between the ring-structure and ciliary shaft (green bracket). **(C-C'')** IFT88 also localises to the ciliary shaft and forms a ring-shaped structure at the cilia base using antibody against endogenous IFT88 in primary cultures of mouse tracheal epithelial cells (mTECs). **(C')** inset in **(C)**. **(C'')** shows another example of another cilium in **(C)**.

IV.2.5. IFT88 forms “ring-like structures” in mTECs and IMCD3 cells

IFT88, an IFT-B complex component, was shown to localise to the distal appendages (Shi et al., 2017) by using STORM in mammalian cells, it was shown that IFT88 localised in the gaps between the distal appendages (Yang et al., 2017). We show here by using STORM and quantitative image analysis that IFT88 forms ring-like structures at the cilia base in primary cultures of mouse tracheal epithelial cells (mTECs) (supplied by Dr. Colin Bingle from the Medical School at the University of Sheffield) and in mammalian inner medullary collecting duct cells (IMCD3) cells stably expressing IFT88-GFP (a gift from Hiroaki Ishikawa).

Using antibody staining against GFP followed by secondary antibody conjugated to Alexa Fluor 647 in IMCD3 cell line stably expressing an IFT88-GFP fusion (Ishikawa and Marshall, 2015), we showed using STORM imaging that IFT88 localises to the cilia base and the ciliary shaft (Fig. IV.5A and B). IFT88 appears to form ring-like structures at the cilia base (Fig. IV.5A-A'). We also observed side-views of the protein in some cells which clearly shows discrete clusters (Fig. IV.5B-B'). A gap was also apparent between IFT88 localisation at the cilia base and the ciliary shaft, this gap may correspond to the transition zone (Fig. IV.5A' and B). Moreover, we also used antibody staining against the endogenous IFT88 in primary cultures of mTECs and also showed similar distribution of IFT88 at the cilia base and inside the ciliary shaft (Fig. IV.5C-C'). IFT88 proteins are arranged in ring-like structures at the cilia base in most of the cilia examined. Therefore, we show that in other model systems, such as mouse cells, IFT proteins also form rings at the cilia base, similar to

those seen in *Tetrahymena* cells. These rings may correspond to the site where IFT proteins dock and possibly assemble before they travel into cilia.

IV.2.6. IFT proteins dock between the transition zone and the basal body

IFT moves proteins from the cilia base to the ciliary tip through the anterograde transport and returns proteins to the cilia base through the retrograde transport (Cole et al., 1998, Hirano et al., 2017, Katoh et al., 2016). Limited data are available about the exact localisation of IFT proteins at the cilia base, i.e. the docking sites of the IFT particle. Immuno-EM studies showed that *Chlamydomonas* IFT52 localised near the basal bodies (Deane et al., 2001) and 3D-STORM imaging of IFT88 revealed that this protein is localised about 110nm proximal to the transition zone (Shi et al., 2017). However, the exact location of many IFT proteins and their relative position to the transition zone and basal body in the axial dimension remained obscure.

While the radial positions of IFT proteins revealed that they are arranged in rings with different radii at the cilia base, the determination of the axial positions of IFT proteins is quite important. Both dimensions (radial and axial) can then provide information about the exact locations of IFT proteins in their docking sites at the cilia base. To map IFT proteins axially and reveal IFT particle, we used staining with mammalian anti-Nup50 antibody (please refer to methods and introduction chapter for details) as a reference. To this end, we used antibody staining against tagged protein in parallel with an antibody to Nup50 to mark the basal body followed by secondary antibody conjugated to Alexa Fluor 647 that will recognise both primary antibodies in the same channel

(refer to methods) and then imaged on STORM. This was followed by image analysis using codes written in MATLAB to measure the distances between IFT proteins and Nup50 (similar to the analysis performed on TZ proteins). This enabled us to unveil, for the first time, the axial positions of several IFT proteins at the cilia base. The axial positions combined with radial positions of IFT proteins allowed us to predict the orientation of IFT proteins at the cilia base.

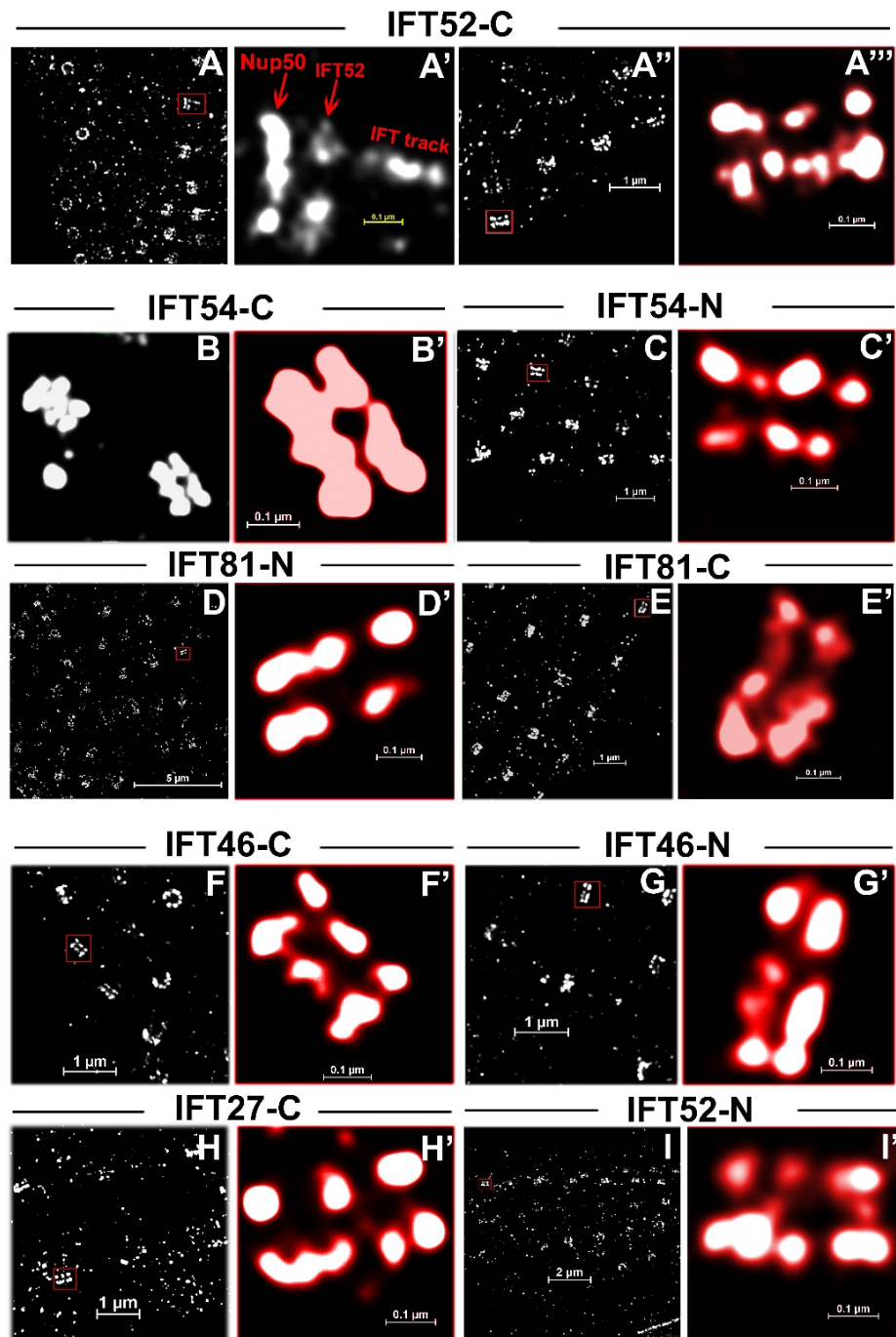


Figure IV.6. Axial positions of IFT-B proteins. Double labelling of IFT-B transgenic lines with anti-HA/GFP to detect IFT proteins, and Nup50 to detect the basal body. **(A-A''')** Side-views of IFT52-C and Nup50 show the position of IFT52-C with respect to Nup50 as indicated by red arrows in **A'**. IFT track is obvious as well (**A'**). **(A'')** shows another example of IFT52-C terminus side-view localisation with respect to Nup50. **(A')** and **(A''')** show insets in **(A)** and **(A'')** respectively. Using quantitative image analysis and codes written in MATLAB, the measurements of the distances between IFT-B proteins and Nup50 are as follows: $116.4 \pm 3.8\text{nm}$ ($n = 11$) for IFT52-C terminus **(A-A''')**, $118.8 \pm 2.8\text{nm}$ ($n = 18$) for IFT52-N terminus **(I-I')**, $103.3 \pm 3\text{nm}$ ($n = 11$) for IFT54-C terminus **(B-B')**, $119.2 \pm 4.2\text{nm}$ ($n = 16$) for IFT54-N terminus **(C-C')**, $130.4 \pm 3.4\text{nm}$ ($n = 18$) for IFT81-N terminus **(D-D')**, $127.1 \pm 4.2\text{nm}$ ($n = 11$) for IFT81-C terminus **(E-E')**, $113.5 \pm 2.5\text{nm}$ ($n = 16$) for IFT46-C terminus **(F-F')**, $107.5 \pm 2.2\text{nm}$ ($n = 18$) for IFT46-N terminus **(G-G')**, and $126 \pm 4\text{nm}$ for IFT27-C terminus ($n = 20$). Data are mean \pm SEM. Based on Student's *t*-tests; * *P*, 0.05, ** *P*, 0.01, *** *P*, 0.001, and **** *P*, 0.0001; not significant, ns. All differences were also significant based on Mann–Whitney test.

Using this double labelling approach, we show that IFT proteins localised distal to Nup50 (Fig. IV.6A-A'). Among IFT-B complex proteins investigated, IFT81 was the farthest from Nup50: its C-terminus is $130.4 \pm 3.4\text{nm}$ (Fig. IV.6D-D' and 7E) and its N-terminus is $127.1 \pm 4.2\text{nm}$ (Fig. IV.6E-E' and 7E) from Nup50. IFT27-C terminus is $126 \pm 4\text{nm}$ away from Nup50 (Fig. IV.6H-H' and 7E). IFT52 N- and C- termini seem to be positioned in the same axial position, with the C-terminus being $116.4 \pm 3.8\text{nm}$ and the N-terminus $118.4 \pm 2.8\text{nm}$ away from Nup50 (Fig. IV.6A-A'', I-I', and 7E). On the other hand, IFT54-N terminus seems to be higher than that of the N-terminus, where the N-terminus is $119.2 \pm 4.3\text{nm}$ (Fig. IV.6C-C' and 7E) and the C-terminus is $103.3 \pm 3\text{nm}$ away from Nup50 (Fig. IV.6B-B' and 7E). The C-terminus of IFT46: $113.5 \pm 3.5\text{nm}$ (Fig. IV.6F-F' and 7E) is higher than that of the N-terminus: $106.5 \pm 5.3\text{nm}$ (Fig. IV.6G-G' and 7E).

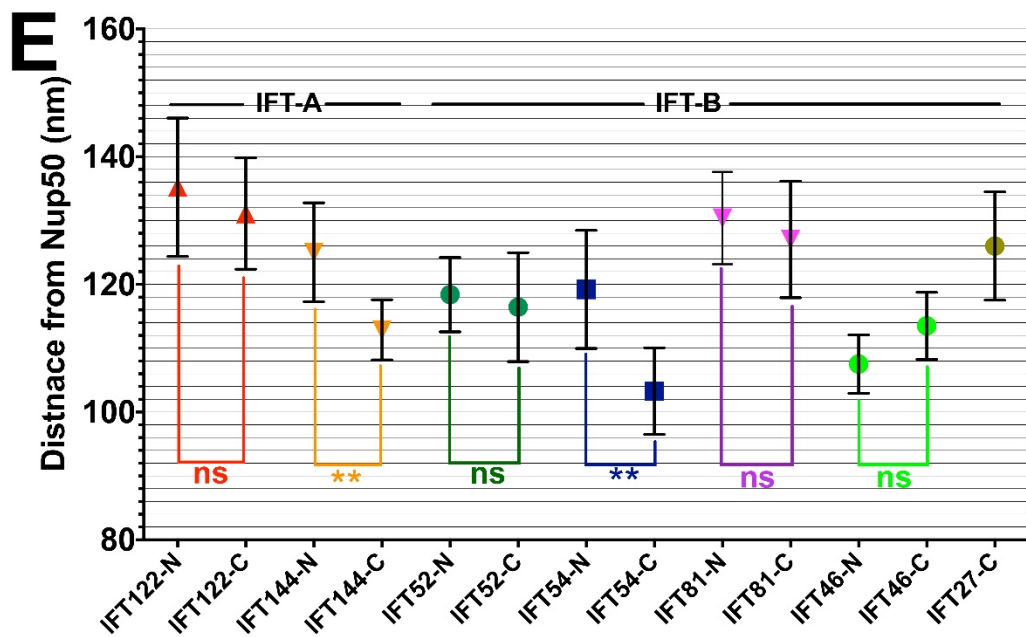
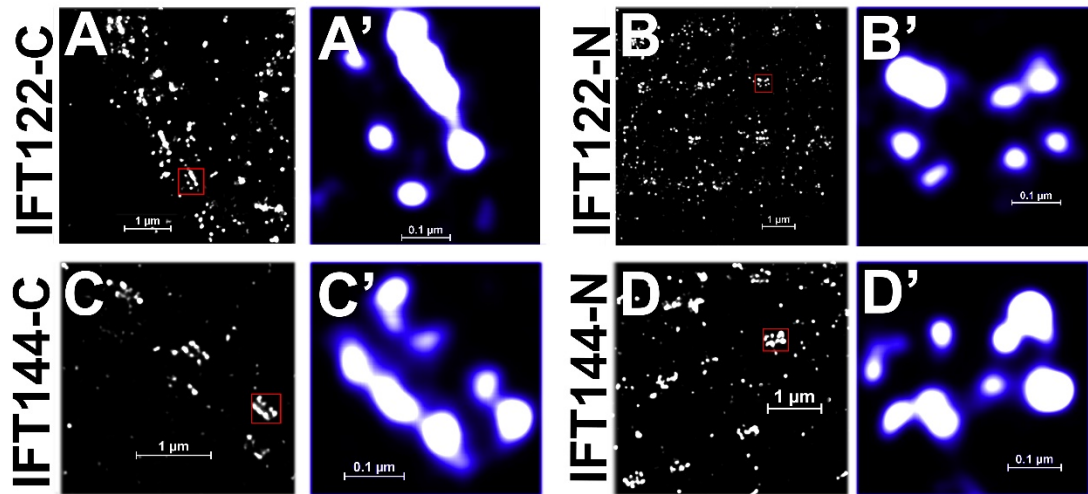


Figure IV.7. Axial positions of IFT-A proteins. (A-A'') IFT122-C terminus is 131.1 ± 3.1 nm ($n = 18$) away from Nup50. (B-B') IFT122-N terminus is 135.2 ± 4.9 nm ($n = 11$). (C-C') IFT144-C terminus is 112.9 ± 2.2 nm ($n = 16$). (D-D') IFT144-N terminus is 125 ± 3.6 nm ($n = 14$) away from Nup50. Data are mean \pm SEM. (E) Mean distance between IFT-A and IFT-B proteins and Nup50 as a reference protein. Data are mean \pm 95% CI. Note that IFT144 and IFT54 had significant difference in the distances between the two termini. Based on Student's *t*-tests; * *P*, 0.05, ** *P*, 0.01, *** *P*, 0.001, and **** *P*, 0.0001; not significant, ns. All differences were also significant based on Mann–Whitney test.

Moreover, we determined the axial positions of two IFT-A complex proteins. IFT122-N terminus is the farthest from Nup50 with a distance of 135.2

$\pm 4.85\text{nm}$ (Fig. IV.7B-B' and E) and its C-terminus is just below the N-terminus with a distance of $131.1 \pm 4.1\text{nm}$ (Fig. IV.7A-A' and E). However, the N-terminus of IFT144 seemed to be much higher compared to the C-terminus, with the former having a distance of $125 \pm 3.6\text{nm}$ (Fig. IV.7D-D' and E) and the latter a distance of $112.9 \pm 2.2\text{nm}$ (Fig. IV.7C-C' and E). In conclusion, we show that IFT proteins dock below the transition zone and distal to the basal body and occupy about 30nm in the axial dimension. With a higher sample size, the significance of the measurements of the radial and axial positions of IFT proteins will most likely improve. However, among IFT proteins examined so far, the C- and N-termini of IFT144 from the IFT-A complex and IFT54 from the IFT-B complex showed significant difference in their axial position revealing their oblique orientation relative to the cilium axis (Fig. IV.7E).

IV.2.7. STORM imaging of the IFT motor Kif3a

Kif3 is a heterotrimeric kinesin-II motor that has important roles in cilia formation in many cells and was also shown to be required for the docking of basal bodies to the apical surface in zebrafish photoreceptors (Zhao et al., 2012, Prevo et al., 2015, Pooranachandran and Malicki, 2015, Scholey, 2013). Kif3a is responsible for powering the anterograde transport (Kozminski et al., 1995, Snow et al., 2004). Thus, it is intriguing to determine where Kif3a would localise with respect to IFT proteins.

As previously, we tagged the N- and C- termini of Kif3a and by using antibody against the tag we show that both termini localise to the cilia base (Fig. IV.8A and E). STORM imaging shows that Kif3a is arranged in 9-fold

symmetrical rings at the cilia base when using N-terminal epitope tags (Fig. IV.8B-B' and C-C') or the C-terminus (Fig. IV.8F-F' and G-G'). The radius of the C-terminus was much larger than the radius of the N-terminus. Kif3a-C terminus has a radius of $130.4 \pm 5.8\text{nm}$ using indirect labelling (Fig. IV.8F-F' and T) and $132.2 \pm 5.4\text{nm}$ using direct labelling (Fig. IV.8G-G' and T). The two measurements were not statistically different (Fig. IV.8T). The radius of Kif3a-N terminus was $121.1 \pm 6.8\text{nm}$ using indirect labelling (Fig. IV.8B-B' and T) and $119.9 \pm 5.2\text{nm}$ using direct labelling (Fig. IV.8C-C' and T). In agreement with kinesin function, using direct or indirect labelling procedures, the radius of Kif3a-N terminus is close to microtubule doublets.

To determine the axial position of Kif3a, we followed the double staining procedures as previously explained in Kif3a transgenic lines. The C-terminus is more than 6nm higher than the N-terminus: the C-terminus is $136.8 \pm 5.6\text{nm}$ (Fig. IV.8H) and the N-terminus is $130.5 \pm 5.3\text{nm}$ away from Nup50 (Fig. IV.8D). Although there is a difference of about 6nm between both the C- and N- termini, this difference is not statistically significant (Fig. IV.8U). Consequently, Kif3a seems to be positioned perpendicular to the microtubule doublets based on data generated so far. Increasing the sample size for both termini could improve the significance and may show an oblique orientation of Kif3a at the cilia base. In all cases, Kif3a is positioned more distal than most IFT-B and IFT-A examined. In conclusion, we show that Kif3a docking sites form 9-fold symmetrical rings just distal to the IFT particle. We also reveal that the N-terminus of Kif3a is very close to the microtubule doublets and the C-terminus is near IFT-B proteins.

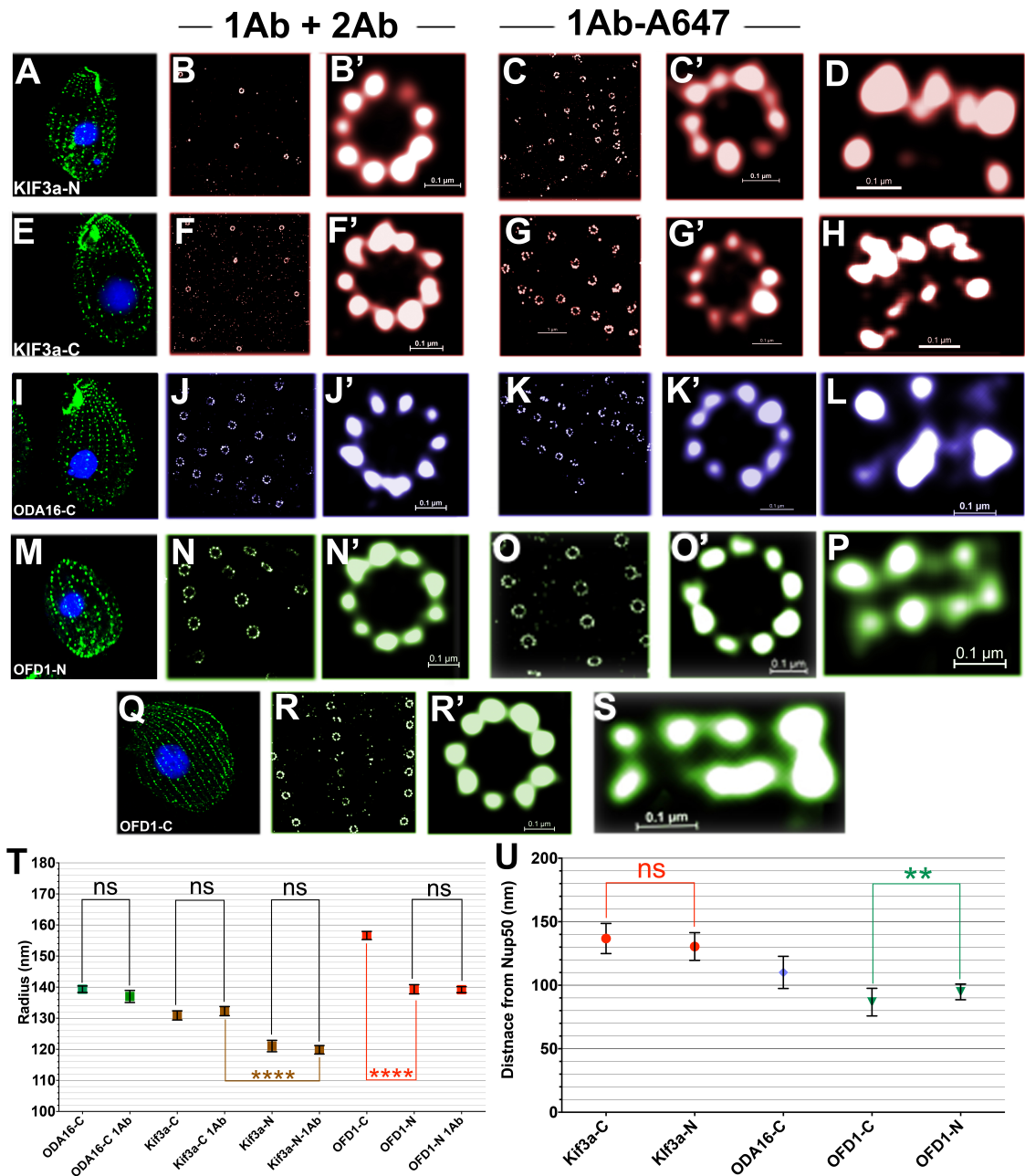


Figure IV.8. STORM analysis of other ciliary proteins. (A-H) Using antibody against the tag in both termini of Kif3a, we show that Kif3a localises to the cilia base. (A and E) Confocal images of Kif3a-N and Kif3a-C terminus respectively showing the localisation of Kif3a (green) at the cilia base and counterstained with DAPI to mark the nuclei. STORM analysis of the radial distribution of Kif3a shows that it forms 9-fold symmetrical rings at both termini, with Kif3a-C terminus having a radius of $130.9 \pm 5.8\text{nm}$ (61 rings) when using indirect labelling (F-F') and $132.3 \pm 5.4\text{nm}$ (54 rings) when using direct labelling (G-G'). Kif3a-N terminus has a much smaller radius with $121.1 \pm 6.9\text{nm}$ (57 rings) when using indirect labelling (B-B') and $119.9 \pm 5.2\text{nm}$ (59 rings) when using direct labelling (C-C'). Data are mean \pm SD. Axial analysis of Kif3a shows that its N-terminus is $130.5 \pm 5.2\text{nm}$ (n = 23) and its C-terminus is $136.8 \pm 5.6\text{nm}$ (n = 19) away from Nup50 (D and H). Data are mean distance \pm SEM. (I-K') Confocal and STORM

imaging of ODA16-C terminus. ODA16-C terminus localises to the cilia base in *Tetrahymena thermophila* (**I**). STORM images show that it forms 9-fold symmetrical rings at the cilia base (**J-K'**), with a radius of $139.3 \pm 5\text{nm}$ (92 rings) when using indirect labelling (**J-J'**) and $137 \pm 6.9\text{nm}$ (51 rings) when using direct labelling (**K-K'**). Axially, ODA16-C is $110.1 \pm 6\text{nm}$ away from Nup50 (**L**). (**M-S**) OFD1 localises at the cilia base as well. Confocal images of OFD1-N terminus (**M**), and OFD1-C terminus (**Q**) using antibody against HA and V5 tags respectively. STORM analysis of OFD1 shows that it forms 9-fold symmetrical rings with a radius of $139.3 \pm 5.1\text{nm}$ (48 rings) (**N-N'**) for the N-terminus when using indirect labelling and $139.2 \pm 4.5\text{nm}$ (89 rings) (**O-O'**) when using direct labelling. However, OFD1-C terminus has a larger radius of $156.6 \pm 4.6\text{nm}$ (50 rings) (**R-R'**). Axially, OFD1-N terminus was $94.75 \pm 3\text{nm}$ (**P**) and its C-terminus was $86.7 \pm 5.2\text{nm}$ (**S**). For radial positions, data are mean \pm SD, while for axial positions, data are mean \pm SEM. (**T**) The radial distribution of the means \pm 95% Confidence interval (CI) for the proteins using indirect versus direct labelling. (**U**) Mean distance of Kif3a, ODA16, and OFD1 proteins with respect to Nup50 as a reference protein. Data are mean \pm 95% CI. Based on Student's *t*-tests; * **P**, 0.05, ** **P**, 0.01, *** **P**, 0.001, and **** **P**, 0.0001; not significant, ns. All differences were also significant based on Mann–Whitney test.

IV.2.8. STORM imaging of other ciliary proteins at the cilia base

Outer dynein arm adaptor 16 (ODA16) is a small adaptor protein that interacts with IFT-B protein IFT46 (Ahmed and Mitchell, 2005, Hou and Witman, 2017, Taschner et al., 2017). The N-terminus of ODA16 interacts with the N-terminus of IFT46, while the C-terminus of ODA16 provides a binding site for dynein arm complex components necessary for the formation and function of motile cilia (Taschner et al., 2017). Its localisation in the IFT particle has not been established. We thus decided to characterise the axial and radial position of ODA16-C terminus and show that ODA16 form nice rows at the cilia base (Fig. IV.8I) and by using STORM imaging we show that ODA16-C terminus forms 9-fold symmetrical rings at the cilia base (Fig. IV.8J-K' and T). It has a radius of $139.3 \pm 5\text{nm}$ using indirect labelling (Fig. IV.8J-J'), and $137 \pm 6.9\text{nm}$ using direct labelling (Fig. IV.8K-K'). There is no significant difference in the radial measurement of ODA16 when using direct versus indirect labelling (Fig.

IV.8T). To determine the axial position of ODA16, we followed the previously described double labelling procedure and show that ODA16-C terminus lies at a distance of $110.1 \pm 6\text{nm}$ distal to Nup50 (Fig. IV.8L and U). The axial position of ODA16-C terminus is likely to indicate the site where ODA complex binds at the cilia base.

Finally, we characterised OFD1, a component of the basal body involved in the determination of centriole lengths and recruits IFT88 to the cilia base (Singla et al., 2010). Using the same approach applied to IFT proteins, we tagged the C-terminus of OFD1 with 3-V5 tag and the N-terminus with 3-HA tag as previously described (Gaertig et al., 2013). We then used antibody against the tag (V5 or HA) and we show that OFD1 localises to the cilia base in *Tetrahymena thermophila* (Fig. IV.8M and Q). STORM imaging of OFD1 revealed 9-fold symmetrical distribution of OFD1 at the cilia base with the radius of the C-terminus: $156.6 \pm 4.6\text{nm}$ (Fig. IV.8R-R' and T) being much larger than that of the N-terminus: indirect labelling of $139.3 \pm 5.1\text{nm}$ (Fig. IV.8N-N' and T) and direct labelling of $139.2 \pm 4.5\text{nm}$ (Fig. IV.8O-O' and T). Axially, the N-terminus of OFD1 is located at $94.8 \pm 3\text{nm}$ (Fig. IV.8P and U), and the C-terminus at $86.7 \pm 5.2\text{nm}$ (Fig. IV.8S and U). Consistent with previous analysis, OFD1 localises proximal to IFT proteins, presumably to the apical side of the basal body. The differences axial positions of the C- and N-termini of OFD1 are statistically significant (Fig. IV.8U) and therefore the orientation of OFD1 is oblique at the cilia base.

IV.3. Discussion

Our data reveal for the first time the architecture of IFT particle in their docking sites at the cilia base. In *Tetrahymena thermophila*, we characterised the radial and axial positions of 3 IFT-A proteins, 5 IFT-B proteins, one IFT-motor, and one cargo adaptor protein. We determined the positions of the N- and C- termini of these proteins and show that IFT proteins dock at least 50nm below the transition zone. We found that IFT-A complex lies to the outside of IFT-B complex in the radial dimension. All the IFT proteins examined localised to clear 9 distinct sites arranged in rings at the cilia base. These distinct sites are most likely the “docking sites” of IFT proteins at the cilia base.

Moreover, we revealed the localisation of the binding sites of tubulin and outer dynein arms at the cilia base. We show the distribution and localisation of the IFT motor Kif3a, the basal body protein OFD1, and the cargo adaptor ODA16. Interestingly, we show that the C-terminus of Kif3a is positioned near IFT-B proteins while the N-terminus is very close to the microtubule doublets. In addition to that, we examined the arrangement and localization of IFT88 in mammalian IMCD3 cells and primary cultures of mouse tracheal epithelial cells (mTECs). IFT88 localises to the cilia base in “ring-like” structures and to the ciliary shaft in the cilia of these cells. We present here the first super-resolved model of the architecture of IFT particles in their docking site, showing the orientation of several IFT proteins and their position relative to transition zone and other basal body proteins at the cilia base.

Previous attempts to reveal the localisation of IFT proteins were based on a combination of transmission electron microscopy and cryo-electron

tomographic analysis of IFT trains in *Chlamydomonas reinhardtii* (Pigino et al., 2009). In addition to that, crystallographic analyses of IFT components and their interactions, such as those between IFT27 and IFT25 (Bhogaraju et al., 2011), IFT81 and IFT74 N-termini interaction with tubulin (Bhogaraju et al., 2013), and the interaction of IFT52-C terminus with that of IFT46-C terminus (Taschner et al., 2014) were reported. Moreover, studies about the interactions between IFT and its cargoes were mainly limited to those between IFT46 and the outer dynein arm complex cargo adaptor (ODA16), which is important for the transport of the outer dynein arm complex (ODA) (Ahmed and Mitchell, 2005, Prevo et al., 2017, Taschner et al., 2017). Recently, using STORM imaging, it was shown that IFT88 localises to the distal appendages (Shi et al., 2017) and specifically at the gaps between the distal appendage blades (Yang et al., 2017).

Our determination of the radial locations of the IFT proteins uncovered the way the IFT proteins are arranged relative to the ciliary axis at the cilia base. Strikingly, depending on the data collected from direct labelling (primary antibody directly conjugated to the fluorophore), IFT-B proteins occupy a space between about 140 and 160nm (Fig. IV.3) relative to the ciliary axis, while IFT-A proteins span a region between about 160 and 165 nm (Fig. IV.4) in the radial dimension. This shows that none of the IFT-B proteins overlap with any of the IFT-A proteins in the radial dimension. This suggests that IFT-A complex lies outside IFT-B complex (Fig. IV.9). These findings prompted us to examine the localisation of the IFT motor, Kif3a, relative to the IFT particle. Our STORM analysis of the radial localisation of Kif3a revealed that the C-terminus is very close to IFT-B proteins (Fig. IV.8 and IV.9) and that the N-terminus is very close

to the microtubule doublets. Moreover, Kif3a forms 9-fold symmetrical rings at the cilia base (Fig. IV.8), very similar to those formed by all IFT proteins. Therefore, our STORM analysis shows that the IFT particle, including Kif3a, spans 40-50nm in the radial dimension at the cilia base.

In the axial dimension, IFT122-N terminus is the farthest from Nup50 (reference protein) (Fig. IV.7B-B' and E), while IFT54-C terminus is the closest to it (Fig. IV.6B-B'). This means that the IFT particle spans about 20-30nm in the axial dimension (Fig. IV.7E and IV.9.B). The distance between the most distal IFT epitope: IFT122-N terminus and the most proximal transition zone epitope: NPHP4-C terminus, is about 50nm. While, the distance between the most proximal IFT epitope: IFT54-C terminus and the most distal transition zone epitope: Tmem231-C is about 110nm. Therefore, the IFT particle is at least 50nm and maximum 110nm away from transition zone (Fig. IV.9.B). The latter distance is consistent with previous conclusion that IFT88 is 110nm proximal to the transition zone (Shi et al., 2017). Kif3a, on the other hand, appears to be more distal compared to the docking sites of the IFT particle (Fig. IV.9B). This is interesting and suggests that Kif3a may dock independently from the IFT particle. The IFT proteins may assemble first before they bind to their motors to power their journey inside the ciliary shaft. It is also probable that the IFT particle is triggered by unknown factor to initiate its movement and only then binds to kinesin motor to gain access to the ciliary shaft.

Furthermore, IFT particles are known to transport cargoes to cilia. For example, tubulin which is the most abundant component of cilia, is transported by binding to the N-termini of IFT74 and IFT81 (Bhogaraju et al., 2013). Our STORM analysis reveals that IFT81-N terminus localises to the external

periphery of the IFT particle (Fig. IV.9), implying that this is where tubulin cargo binds. It was also proposed that the N-terminus of IFT54 also binds tubulin. If this is the case, then our data reveal that this is an entirely different binding site for tubulin, independent of that performed by IFT81-N terminus. On the other hand, outer dynein arms binding site appears to attach to the IFT particle close to the microtubule side as indicated by ODA16-C terminus (Fig. IV.9).

Additionally, crystallographic studies have shown that the interaction between the C-terminus of IFT46 and the C-terminus of IFT52 is only 1.78nm away from each other (Taschner et al., 2014). Our STORM analysis of the radial positions of the C-termini of IFT52 and IFT46 revealed that the two termini are 1.9nm away from each other (Fig. IV.3S and IV.9.B), which strikingly agrees with crystal studies of these proteins (Taschner et al., 2014) and therefore highlights the accuracy and significance of our analysis. In addition to that, the analysis of the radial dimensions of IFT-B proteins revealed that IFT52 extends about 17nm (Fig. IV.3A-D", S and IV.9.B). This in fact is very interesting, as IFT52 is very important for the B-complex and lies at the heart of this complex. It interacts directly with at least four IFT-B proteins: IFT46, IFT70, IFT88, and IFT81 (Taschner et al., 2011). This stretched structure of IFT52 is consistent with its ability to bind to the other proteins within the IFT particle. Finally, cryo-electron microscopy studies estimate radial dimensions of IFT particle to be 25nm (Pigino et al., 2009). Our analysis, however, shows a radial distance of over 40nm between Kif3a-N and IFT81 tubulin binding site. This may indicate that the IFT particle has a different conformation at their docking sites, most likely more open, which may facilitate the binding of cargoes and other proteins before moving into cilia.

We also examined a protein that is known to localise to the basal body of cilia. OFD1 localises to the distal ends of the centrioles and is important for the formation of distal appendages and the recruitment of IFT88 to the base of the cilium, which highlights its importance in ciliogenesis (Singla et al., 2010). Our analysis of the radial position of OFD1 reveals that it is located just proximal to the IFT particles, with its N-terminus being very close to IFT proteins, in agreement with functions of OFD1 in recruiting IFT88 at the cilia base (Singla et al., 2010). The axial positions of the C- and N- termini revealed its oblique orientation at the cilia base and suggests it localises at the apical surface of the basal body.

Our STORM analysis of IFT and other ciliary proteins show that our data are accurate and significant. In fact, we noticed that 8 out of 13 epitopes examined using both direct and indirect labelling procedures did not show a significant difference in the measurement of the radii (Fig. IV.3S, 9T and IV.9A). The maximum difference in the radial measurement for IFT proteins is for IFT81-C terminus: 6.1nm (Fig. IV.3S). This may correspond to the way the antibody binds to the epitope and that when using direct labelling, an error of about 5nm due to the size of the IgG antibody (Ries et al., 2012).

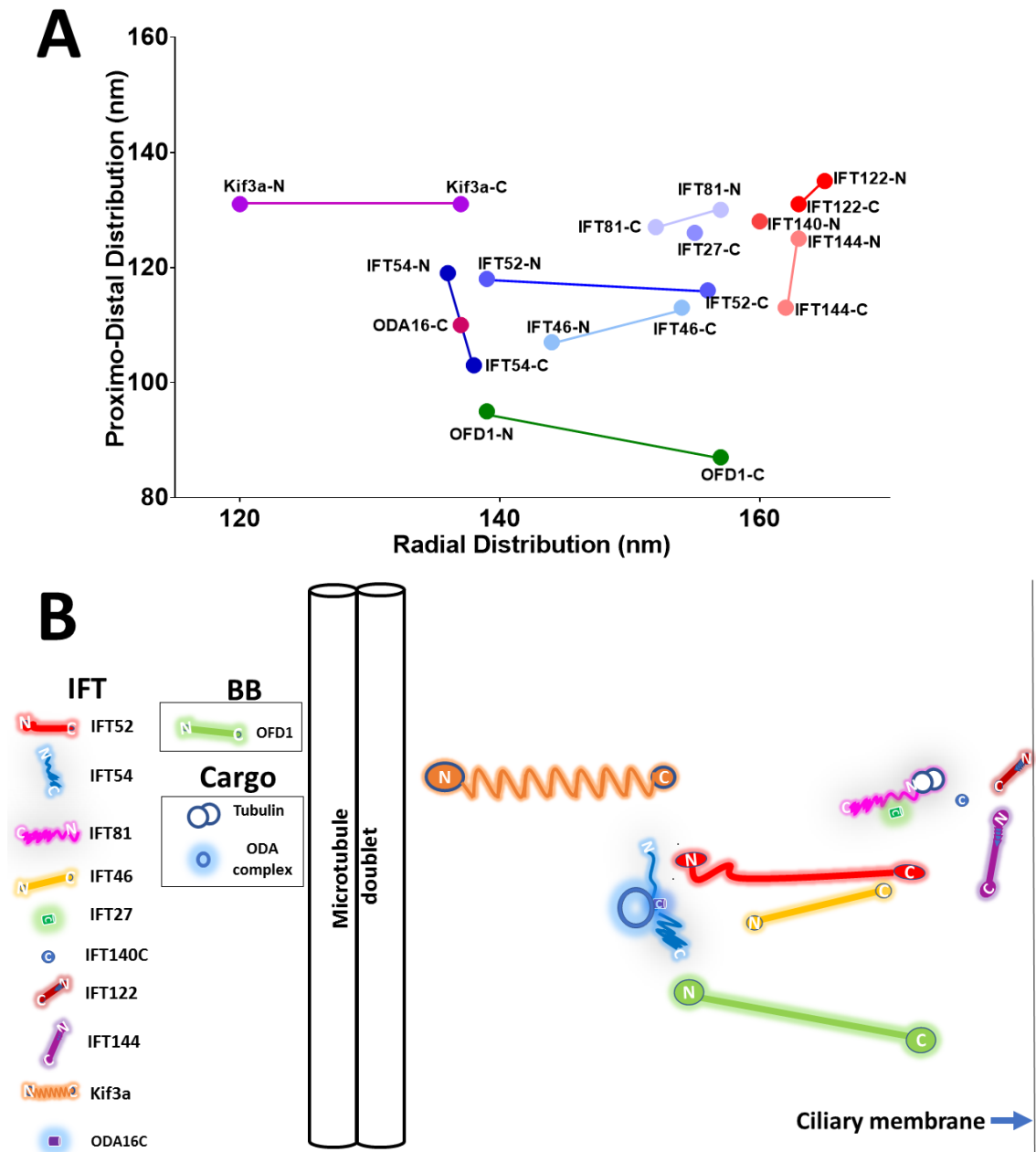


Figure IV.9. Model of the radial and axial distribution of IFT proteins. (A) A graph showing the radial and proximo-distal of IFT-B and IFT-A components showing their orientation in their docking sites at the cilia base. **(B)** A super-resolved model showing the relative position of the IFT particle proteins at the cilia base. IFT-A seems to lie outside IFT-B. The binding sites of tubulin (IFT81-N) and the ODA complex (ODA16-C) are also indicated (not to scale). OFD1 is located proximal to the IFT particle. Kif3a-C terminus is near the IFT-B complex and Kif3a-N terminus is just near the microtubule doublets.

Therefore, by using the data collected for the radial and axial locations of IFT and other ciliary proteins, we demonstrate for the first time the architecture

of IFT proteins in their docking sites at the cilia base. We reveal their position relative to each other and to the IFT motor Kif3a, cargo adaptor ODA16, and the basal body protein OFD1. Importantly, this model unveils the binding sites of tubulin and outer dynein arm and also reveals the way the IFT proteins are oriented in their docking sites at the cilia base (Fig. IV.9B).

	IFT-B Complex		IFT-A Complex
IFT-B1 (Core)	IFT27	Core	IFT122
	IFT22		IFT140
	IFT25		IFT144
	IFT46	Non-core	IFT43
	IFT52		IFT121
	IFT56		IFT139
	IFT70		
	IFT74		
	IFT81		
	IFT88		
IFT-B2 (Peripheral)	IFT20		
	IFT38		
	IFT54		
	IFT57		
	IFT80		
	IFT172		

Table IV.1. The IFT particle. Two complexes comprise the IFT particle: IFT-B and IFT-A complexes. IFT-B complex is subdivided into IFT-B1 (core) which includes 10 proteins and IFT-B2 (peripheral) which includes 6 proteins. IFT-A complex contains 6 proteins subdivided into 3 core and 3 noncore proteins. IFT proteins in purple colour in the table are characterised in this study.

Chapter V

“Apico-basal Polarity Determinants Encoded by *crumbs* Genes Affect Ciliary Shaft Protein Composition, IFT Movement Dynamics, and Cilia Length”

V.1. Introduction

Cilia are finger-like cell surface protrusions that house components of many signal transduction cascades (Schou et al., 2015, Mourao et al., 2016, Malicki and Johnson, 2017). The detection of photons by photoreceptors and chemicals by olfactory sensory neurons is mediated by signal transduction mechanisms inside the ciliary shaft (Jenkins et al., 2009, Kennedy and Malicki, 2009). Vertebrate hedgehog signaling requires cilia and wnt, the platelet-derived growth factor and mTOR pathways are modulated by them (reviewed in (Schou et al., 2015, Mourao et al., 2016, Malicki and Johnson, 2017)). In addition to signaling functions, cilia have a hydrodynamic role: their movement drives the flow of fluid in ducts and vesicles, such as the pronephric duct in zebrafish or the embryonic node in the mouse (Kramer-Zucker et al., 2005, Hirokawa et al., 2012). They also propel cells, such as sperm cells. In cells that display apico-basal polarity, almost without exception, cilia form at the apical surface. Consequently, the ciliary membrane is an apical surface subcompartment, characterized by a unique protein and lipid content (Craigie et al., 2010, Hu et al., 2010, Mukhopadhyay et al., 2010, Chih et al., 2011). Ciliated cells of epithelial sheets thus feature two cell membrane subdivisions: the one that separates the apical and basolateral domains and another one that separates the ciliary membrane from the rest of the apical surface. *crumbs* genes were initially discovered as essential regulators of the apico-basal cell membrane subdivision in fly embryonic epithelia (Jurgens et al., 1984, Tepass and Knust, 1990, Wodarz et al., 1995). They encode transmembrane (TM) proteins that localize to the vicinity of epithelial cell junctions, feature a short cytoplasmic tail and an extracellular domain of varying size (Tepass and Knust,

1990, van den Hurk et al., 2005, Omori and Malicki, 2006). Loss of crumbs function in the fly disrupts the cell junction belt at the boundary of the apical and the baso-lateral surface, and crumbs overexpression expands apical membrane size (Wodarz et al., 1995, Grawe et al., 1996). A similar function of crumbs genes has been observed in vertebrates; mutations in one of the zebrafish crumbs loci, *oko meduzy*, and the locus encoding a related apico-basal polarity determinant, *nagie oko*, a fly *stardust* homolog, cause loss of apical–basal polarity in the eye neuroepithelium and a severe neuronal patterning defect in the retina (Omori and Malicki, 2006, Wei and Malicki, 2002, Malicki and Driever, 1999, Malicki et al., 1996b). A related crumbs function in apico-basal polarity is also evident in fly and zebrafish photoreceptor cells (Hsu et al., 2006, Omori and Malicki, 2006, Pellikka et al., 2002). Finally, while the apico-basal polarity function is mostly mediated by its intracellular tail (Wodarz et al., 1995), Crumbs extracellular domains mediate cell adhesion in the zebrafish photoreceptor cell layer (Zou et al., 2012) and human CRB1 mutations cause severe, early-onset retinal degeneration (den Hollander et al., 1999).

Vertebrate Crumbs and related apico-basal polarity determinants also affect cilia formation. While one *crumbs* gene exists in the fly, the human and zebrafish genomes contains three and five crumbs genes, respectively (Gosens et al., 2008, Omori and Malicki, 2006, van den Hurk et al., 2005). Zebrafish crumbs genes display distinct expression patterns. *crb2b*, for example, is highly enriched in the pronephros and in photoreceptor cells (Hsu et al., 2006, Omori and Malicki, 2006, Zou et al., 2012). *crb3a*, on the other hand, is expressed predominantly in the otic vesicle at stages that were investigated thus far (Omori and Malicki). Consistent with these expression patterns, antisense

morpholino knockdown of zebrafish *crb2b* and *crb3a* reduces cilia size in the pronephros and the ear, respectively (Omori and Malicki). An even stronger crumbs phenotype has been reported in tissue culture; small interfering RNA (siRNA) knockdown of the crumbs 3 gene in Madin Darby canine kidney (MDCK) cells eliminates cilia entirely (Fan et al., 2004). In agreement with crumbs cilia phenotype, downregulation of other apico-basal polarity determinants, aPKC, Par6, and Par3, also leads to cilia loss (Fan et al., 2004, Sfakianos et al., 2007). To explain these observations in mechanistic terms, it has been postulated that Par proteins bridge transmembrane Crumbs 3 with a subunit of the main ciliary kinesin, Kif3a (Sfakianos et al., 2007).

In the kinocilia of the wild type zebrafish hair cells, Crumbs proteins localised to the cilia base (Omori and Malicki), this suggests that Crumbs proteins may be involved in the gating mechanisms that regulate the entry of some ciliary proteins into the ciliary shaft. In addition to that, the Crumbs 3 isoform that ends with the C-terminal sequence CLPI (CRB3-CLPI) was shown to interact with importin β -1 (Fan et al., 2007). Importin β -2 was shown to localise near the basal body and to the proximal region of the ciliary axoneme and was suggested to mediate the entry of Kif17, an IFT kinesin, (Dishinger et al., 2010a). As Crumbs proteins mainly localise to the cilia base in kinocilia of the hair cells in zebrafish (Omori and Malicki) and interact with importins, they may affect the entry or exit of ciliary proteins. In this scenario, Crumbs proteins would facilitate gating functions at the cilia base.

As morpholino knockdown results are frequently difficult to interpret (Kok et al., 2015), we chose to analyze the role of crumbs in ciliogenesis using mutants of several zebrafish crumbs genes. We found that mutant alleles of *oko*

meduzy (*crb2a*), *crb2b*, and *crb3a*, cause changes in cilia length. This is accompanied by a massive accumulation of other Crumbs proteins and intraflagellar transport (IFT) particle components in the ciliary compartment of *ome* and *ome;crb3a* mutants. Such accumulation of IFT proteins inside cilia is mediated by Crumbs proteins and suggest a role of Crumbs proteins in the gating mechanisms at the cilia base. In addition, Crb3 knockdown in mammalian inner medullary collecting duct cells (IMCD3) cells affects the dynamics of IFT particle movement. These studies reveal crumbs-dependent mechanisms that affect the subcellular localization of Crumbs proteins and show that crumbs genes affect ciliary protein composition and modulate intraflagellar transport.

V.2. Results

V.2.1. *crb3a* affects cilia length in vestibular system cristae

Knockdown of the *CRB3* gene in MDCK cells was shown to block cilia formation (Fan et al., 2004). Similar phenotypes were seen following knockdowns of other apico-basal polarity determinants: aPKC, Par6, and Par3 (Fan et al., 2004, Sfakianos et al., 2007). Moreover, morpholino knockdown of *crb3a* in zebrafish was shown to reduce cilia length (Omori and Malicki); however, these ciliary phenotypes have not been investigated in mutants. To address this deficiency, we generated several *crb3a* mutant alleles using TALEN nucleases as previously described (Zu et al., 2013). Two alleles were analyzed in this study, *crb3a*^{sh410} and *crb3a*^{sh346}. The former introduces a

deletion of 13-bp, causing a frameshift between the TM and FERM domains (Fig. V.1A, red arrow and Fig. V.1C'). The latter contains a 1-bp deletion that also causes a frameshift at another site between the TM and FERM domains (Fig. V.1A, blue arrow and Fig. V.1D'). Homozygous carriers of either allele do not display any external abnormalities, survive to adulthood, and are fertile (Fig. V.1.B–D). This is also true for homozygous animals that originate from homozygous mothers and thus did not receive maternal contribution during embryogenesis. However, thorough measurements of cilia length in vestibular system cristae revealed that *crb3a* mutant cilia are somewhat longer compared to those of the wild type (Fig. V.2P). These observations lead to the conclusion that *crb3a* function contributes to cilia length.

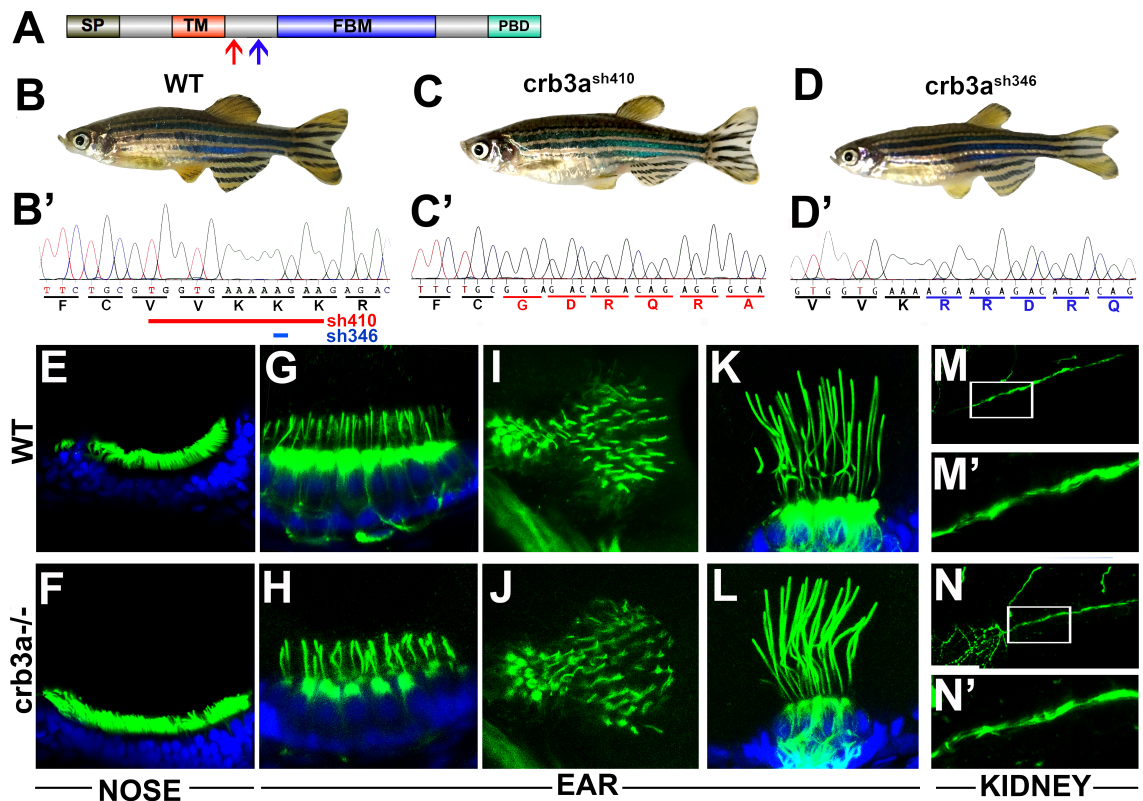


Figure V.1. *crb3a* mutant phenotype. (A) Schematic of Crb3a protein domain structure. Signal peptide (SP); transmembrane domain (TM); FERM-binding motif (FBM); and PDZ-binding domain (PBD) are indicated. Red arrow indicates the start of the frameshift in *crb3a*^{sh410} mutant allele; blue arrow, the start of frameshift in *crb3a*^{sh346} allele. (B–D) External

phenotypes of wild-type (WT) (**B**), *crb3a*^{-/-sh410} homozygous mutant (**C**), and *crb3a*^{-/-sh346} homozygous mutant (**D**) adult zebrafish. (**B'**– **D'**) Sequences of wild-type (**B'**), and two mutant alleles: *crb3a*^{-/-sh410} (**C'**), and *crb3a*^{-/-sh346} (**D'**). Deletions in *crb3a*^{-/-sh410} (red line) and *crb3a*^{-/-sh346} (blue line) mutants are indicated in (**B'**). (**E**–**N'**) Images of wild-type and *crb3a*^{-/-} mutant embryos stained with anti-acetylated tubulin antibody (in green) and counterstained with DAPI (in blue) at 5 days postfertilization: olfactory placode (**E and F**); anterior macula (**G and H**); posterior macula (**I and J**); lateral crista (**K and L**); and pronephros (**M and N**). (**M'** and **N'**) are enlarged images of pronephric cilia shown in (**M and N**).

V.2.2. *oko meduzy (ome)* mutations affect ciliogenesis

ome (*crb2a*) functions in the apico-basal polarity of the eye neuroepithelium and retinal neurogenesis. *ome* mutants are characterized by abnormal body axis curvature, edema, non-uniform eye pigmentation, grossly disorganized retinal neurons, and lethality by 7 dpf (Malicki and Driever, 1999, Malicki et al., 1996a, Omori and Malicki, 2006). Previous studies did not evaluate *ome* function in cilia. To investigate the cilia phenotype, we analyzed vestibular cristae in *ome* mutants and found that cilia are shortened by 30% (Fig. V.2B, quantified in Fig. V.2P). To test functional relationship between *crb3a* and *ome*, we examined cilia of *ome;crb3a* double mutants. This analysis revealed that cilia of double mutants display similar length reduction to *ome* cristae, revealing that *ome* is epistatic to *crb3a*. Similarly, nose cilia are significantly shorter in both *ome* homozygotes and *crb3a;ome* double mutants when compared to those of the wild-type or *crb3a* homozygotes, (Fig. V.2M–O, quantified in Fig. V.2Q). Moreover, olfactory placode cilia of *crb3a;ome* double mutants are significantly shorter than those of *ome* mutants (Fig. V.2Q). Cilia in kidney (Fig. V.2K and L, compare to Fig. V.2J) and maculae (Fig. V.2, E, F, H, and I compare to Fig. V.2, D and G) are not obviously affected in *ome* or double

mutants. These observations reveal that *ome/crb2a* and *crb3a* are necessary for proper cilia formation and control their lengths in a subset of tissues. It appears that *ome* functions downstream or in parallel to *crb3a* in cristae. These two genes also display some functional redundancy in nasal cilia.

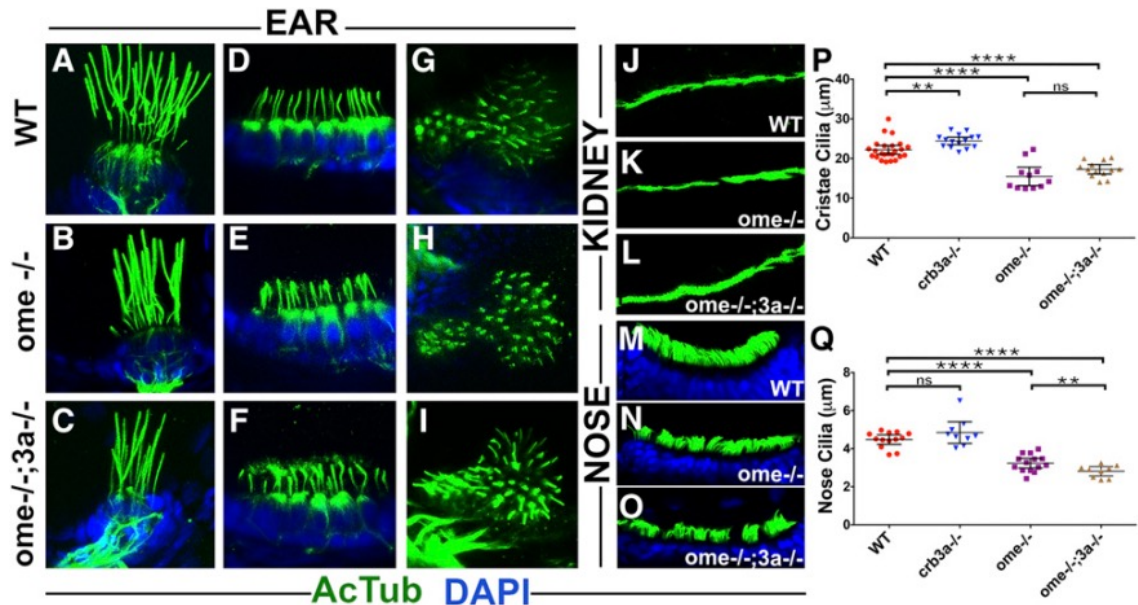


Figure V.2. *oko meduzy* and *crb3a* genes modulate cilia length. (A–O) Whole-mount immunostaining of wild-type (WT), *ome*^{-/-}, and *ome*^{-/-};*3a*^{-/-} double mutant cilia in several tissues at 5 days postfertilization. (A–C) lateral crista, (D–F) anterior macula, (G–I) posterior macula, (J–L) pronephros, and (M–O) nasal pits. Zebrafish larvae were immunostained using anti-acetylated tubulin antibody (in green) and counter-stained with DAPI (in blue) to visualize nuclei. (P) Graph of cilia length in the cristae of WT and crumbs mutants as indicated. Each dot represents the average length of all cilia in one crista. (Q) Graph of cilia length in the olfactory placodes of WT and crumbs mutants as indicated. In (P and Q), data were collected from at least two independent experiments using at least five animals per experiment. The mean and 95% C.I. are indicated. Based on Student's t-tests; ** significant. P , 0.01, *** P , 0.001, and **** P , 0.0001; not significant, ns. All differences were also based on Mann–Whitney test.

V.2.3. Crumbs proteins accumulate in cilia of *oko meduzy* mutants

Crumbs 3 localizes to cilia in mammalian cell culture and is enriched at the base of cilia in zebrafish (Omori and Malicki, 2006, Fan et al., 2004). To investigate how crumbs mutations affect Crumbs protein localization, we

immunostained embryos with anti-acetylated tubulin and anti-Crumbs antibodies. The anti-Crumbs antibody used in these experiments is directed to the cytoplasmic tail and recognizes all zebrafish Crumbs proteins on western blots of Crumbs-GST fusions (Omori and Malicki, 2006, Hsu et al., 2006).

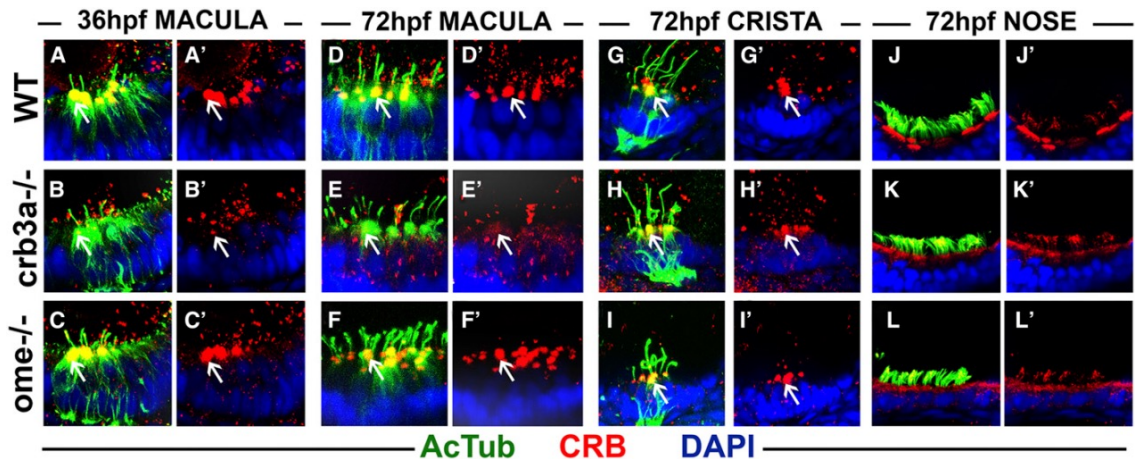


Figure V.3. Crumbs expression in *crb3a* mutants at early stages of development. Confocal images of whole-mount cilia staining with anti-acetylated tubulin (AcTub) (green) and anti-CRB antibody (red). **(A–C’)** Staining of the otic vesicle at 36 h postfertilization (hpf). Crumbs proteins localize to the cilia base in the wild-type (WT) **(A and A’)** and *ome*^{-/-} mutants **(C and C’)**, but are absent in *crb3a*^{-/-} mutant homozygotes **(B and B’)**. At 72 hpf, Crumbs proteins still localize to the cilia base in maculae of WT animals **(D and D’)** and *ome*^{-/-} mutants **(F and F’)**, but very little signal is seen in *crb3a*^{-/-} mutants **(E and E’)**. No obvious differences are found in the localization of Crumbs proteins in the cristae of *ome*^{-/-} **(I and I’)**, *crb3a*^{-/-} **(H and H’)**, and WT individuals **(G and G’)**. The localization patterns of Crumbs proteins in nasal pits of WT **(J and J’)**, *crb3a*^{-/-} mutant **(K and K’)**, and *ome*^{-/-} mutant **(L and L’)** animals do not show any obvious differences either. All samples were counterstained with DAPI to visualize nuclei. Arrows point to Crumbs signal at the apical surface of hair cells.

In the wild-type, Crumbs proteins are found at the base of hair cell kinocilia in ear maculae at 36 and 72 hpf (Fig. V.3, A, A’, D, and D’). This is no longer the case in *crb3a* mutant homozygotes (Fig. V.3, B, B’, E, and E’). However, in contrast to *crb3a* mutants, Crumbs localization in *ome* mutants is not affected (Fig. V.3, C, C’, F, and F’). These observations are in agreement with our previous report that *crb3a*, but not other crumbs genes, is strongly

transcribed in the otic vesicle between 24 and 72 hpf (Omori and Malicki, Hsu et al., 2006). Crumbs proteins are also present at the apical surface of cells in olfactory placodes (Fig. V.3, J and J'). The apical localization is not obviously affected in either *crb3a* or *ome* mutants (Fig. V.3, K-L').

In contrast to ear maculae, hair cells of semicircular canals contain normal levels of Crumbs in *crb3a* and *ome* mutant homozygotes at 3 dpf (Fig. V.3, H-I' compare to Fig. V.3, G and G'). This is also the case for *crb3a* mutants at 5 dpf (Fig. V.4, E-G'', compare to Fig. V.4, A-C''). However, we did observe strong enrichment of Crumbs proteins in olfactory placode cilia of these mutants (Fig. V.4, H-H'', compare to Fig. V.4, D-D'', 10/10 olfactory placodes). Interestingly, in *ome* mutant homozygotes, Crumbs proteins are mislocalized into cilia of both ear cristae and olfactory placodes (Fig. V.4, I-K'', 23/23 cristae and Fig. V.4, L-L'', 11/14 olfactory placodes). These findings reveal that *ome*, and to a lesser extent *crb3a*, strongly affect the subcellular localization of other Crumbs proteins. An enrichment of Crumbs proteins is also found in *ome;crb3a* double mutants both in cristae and olfactory placodes (Fig. V.4, M-O'' 33/33 cristae and Fig. V.4, P-P'' 6/6 olfactory placodes). While Crumbs staining forms puncta in *ome* mutant cilia, *ome;crb3a* double mutants display a uniform Crumbs signal along most of the ciliary axoneme, with the exception of the proximal region (Fig. V.4, I-K'', compare to Fig. V.4, M-O''). These findings reveal regulatory relationships between *crumbs* genes.

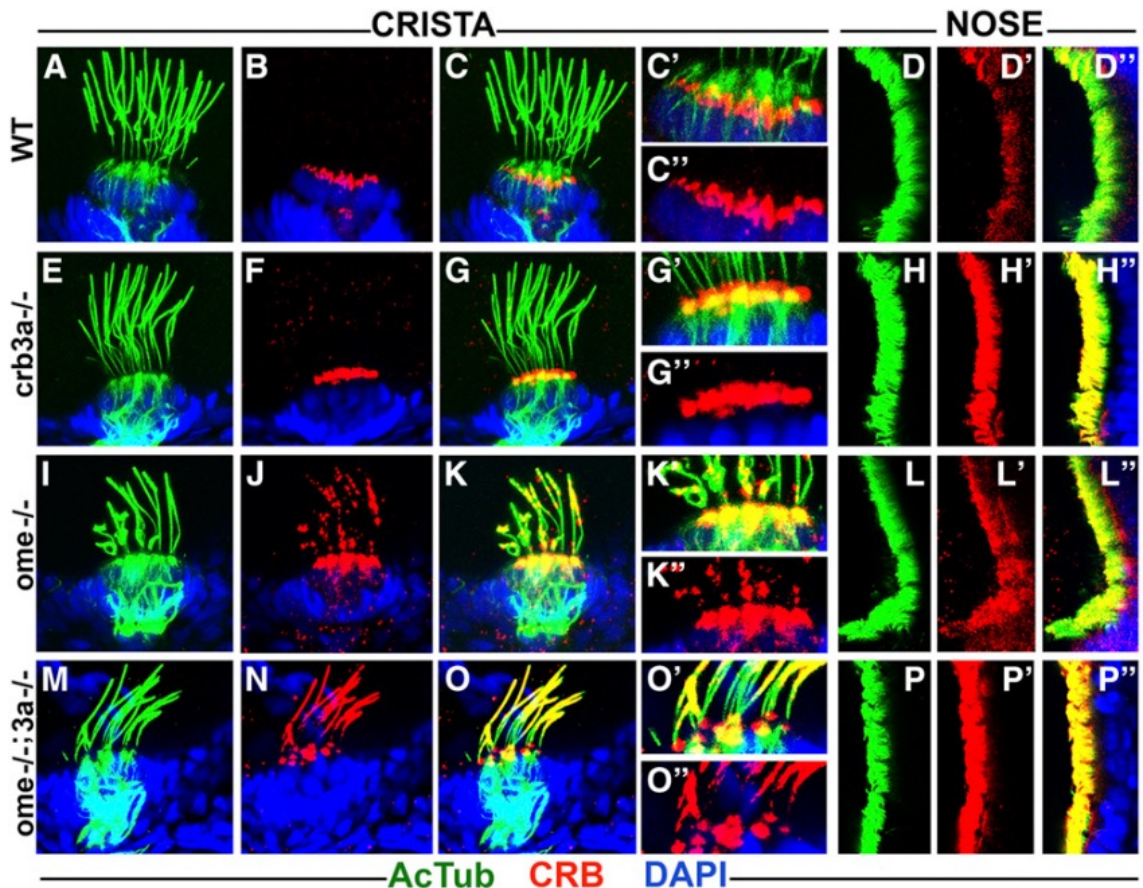


Figure V.4. Crumbs proteins accumulate in cilia of *ome* mutants at 5 days postfertilization (dpf). Confocal images of whole-mount cilia staining with anti-acetylated tubulin antibody (AcTub) (green) and anti-CRB antibody (red) at 5 dpf. Shown are cristae and olfactory placodes of wild-types (WT), *crb3a*^{-/-}, *ome*^{-/-}, and *ome*^{-/-};*crb3a*^{-/-} mutants as indicated. No obvious difference is seen in the localization of Crumbs proteins in cristae cilia of *crb3a*^{-/-} mutants (E–G'') when compared to WT (A–C''). Crumbs proteins are strongly enriched in the cilia of nasal pits in *crb3a*^{-/-} mutants (H–H'') when compared to the WT (D–D''). *ome*^{-/-} and *ome*^{-/-};*crb3a*^{-/-} double mutants show massive accumulation of Crumbs proteins inside cilia of cristae (I–K'' and M–O'') and nasal pits (L–L'' and P–P''). All samples were counterstained with DAPI to visualize nuclei (in blue).

V.2.4. IFT proteins are highly enriched in cilia of *ome*;*crb3a* double mutants

Par3, a key regulator of apico-basal cell polarity, is required for ciliogenesis in cell culture conditions (Sfakianos et al., 2007). Furthermore, the Par3 C-terminal region binds directly to Kif3a, the main anterograde motor of

IFT particles (Nishimura et al., 2004). This led to the hypothesis that the Par3/Par6/aPKC complex bridges Crumbs proteins and Kif3a (Sfakianos et al., 2007) (Fig. 1.7C). If true, Crumbs proteins could affect IFT by competing for the Kif3A motor. To test whether the loss of *ome* and/or *crb3a* function and the accompanying accumulation of Crumbs proteins in cilia affects IFT, we stained *ome* mutants and *ome;crb3a* double mutants with antibodies to IFT particle components: IFT88, IFT52, and Kif17.

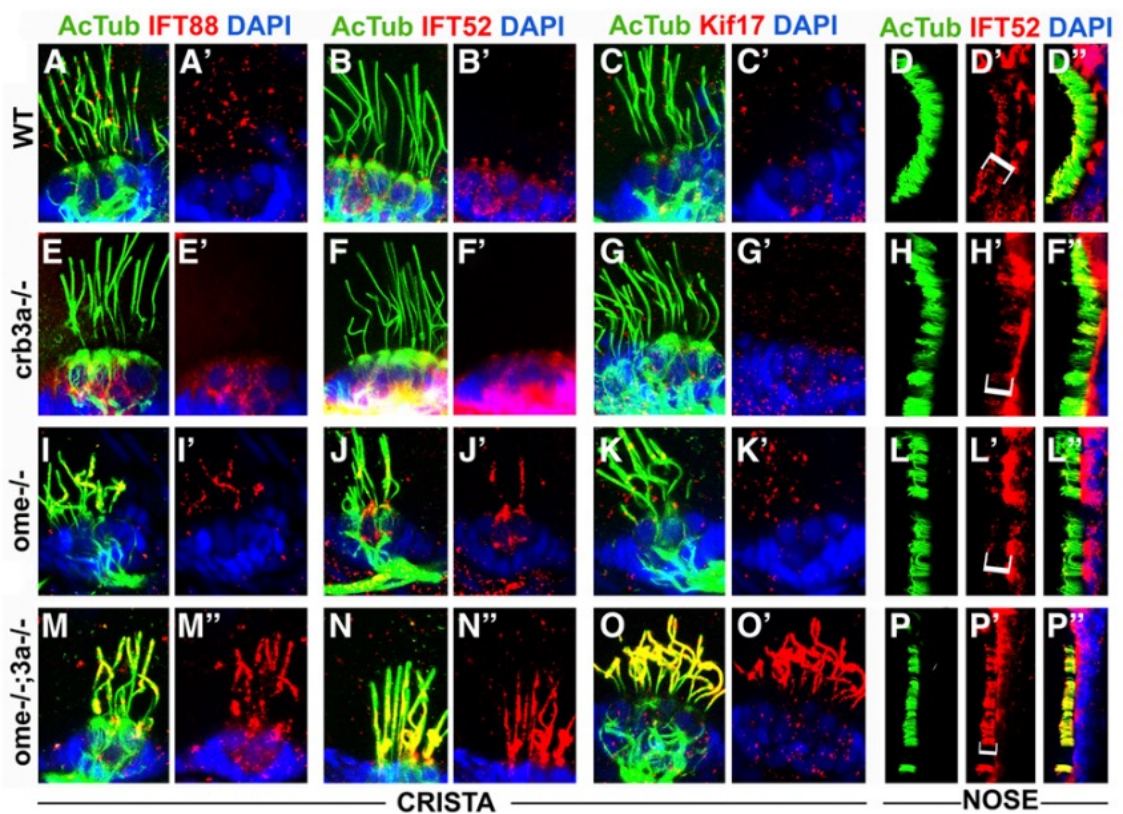


Figure V.5. Intraflagellar transport (IFT) particle components accumulate in the ciliary compartment of *crumbs* mutants. Confocal images of whole-mount cilia staining with antibodies to acetylated tubulin (AcTub) (green), and to IFT proteins (in red): IFT88, IFT52, and Kif17 at 5 days postfertilization. Shown are cristae and olfactory placodes of wild-type (WT), *ome*^{-/-}, *crb3a*^{-/-}, and *ome*^{-/-};*crb3a*^{-/-} double mutants as indicated. IFT proteins are not detected in the ciliary shaft of WT cristae using this staining method (A–C') and a low amount of IFT52 is found in WT olfactory cilia (D–D''). Similarly, in *crb3a*^{-/-} mutants, IFT proteins are not detected in cilia (E–H''). Low levels of some IFT proteins are found in cristae cilia of *ome*^{-/-} mutants (I–K'). Compared to WT, IFT52 localization is not affected in olfactory placode cilia of *ome*^{-/-} mutants (L–L''). In contrast to that, IFT proteins, including Kif17, strongly accumulate in cilia of *ome*^{-/-}

crb3a^{-/-} double mutants (**M–P''**). All samples were counterstained with DAPI to visualize nuclei (in blue). Brackets in (**D'**, **H'**, **L'**, and **P'**) indicate nasal cilia.

In the WT embryos, IFT88 localises slightly to the ciliary axoneme as expected (Fig. V.5, A-A'). IFT52 localised mainly at the cilia base in the cristae mechanosensory cilia (Fig V.5, B-B'). In the olfactory placode, IFT52 is detected at the base and tips of nasal cilia (Fig. V.5, D'-D''). In *crb3a* mutants, IFT protein localization in cilia is largely unchanged when compared to WT embryos (Fig. V.5, E-H'', compare to Fig. V.5, A-D''). However, a prominent accumulation of IFT proteins is observed in cristae cilia of *ome* mutants (Fig. V.5, I-K'). The olfactory cilia in both *crb3a* and *ome* single mutants do not show obvious differences in IFT distribution when compared to the wild type (Fig. V.5, H-H'' and L-L''). Strikingly, in *ome;crb3a* double mutants, IFT proteins massively accumulate inside cilia of ear cristae (Fig. V.5, M-O') and the olfactory placode (Fig. V.5, P-P''). In a control experiment, we have not observed any enrichment of γ -tubulin in *ome;crb3a* double mutants (data not shown). These observations indicate that *ome* and *crb3a* genes function redundantly in the ciliary localization of IFT proteins.

V.2.5. CRB3 affects IFT train dynamics in IMCD3 cells

To further the understanding of the relationship between Crumbs proteins and intraflagellar transport, we decided to test whether IFT train movement is affected by crumbs genes. Imaging of IFT movement is difficult in zebrafish but can be efficiently performed in mammalian cells (Jin et al., 2014, Ishikawa and Marshall, 2015). To this end, we knocked down CRB3 in an

IMCD3 cell line stably expressing an IFT88-GFP fusion (Ishikawa and Marshall). As reported previously, CRB3-knockdown cells display fewer and shorter cilia compared to controls (Fig. V.6, A–D) and the level of CRB3 proteins is reduced (Fig. V.6, C' and D'). Imaging of IFT particle movement using IFT88 fluorescence (Fig. V.6, E and F) revealed that IFT particle speed is somewhat faster in knock-down cells, compared to controls (Fig. V.6G). Moreover, when adjusted for cilia length, IFT tracks are 25% shorter in knockdown cells when compared to control cells (Fig. V.6H). These observations are consistent with the idea that Crumbs affects IFT processivity and speed.

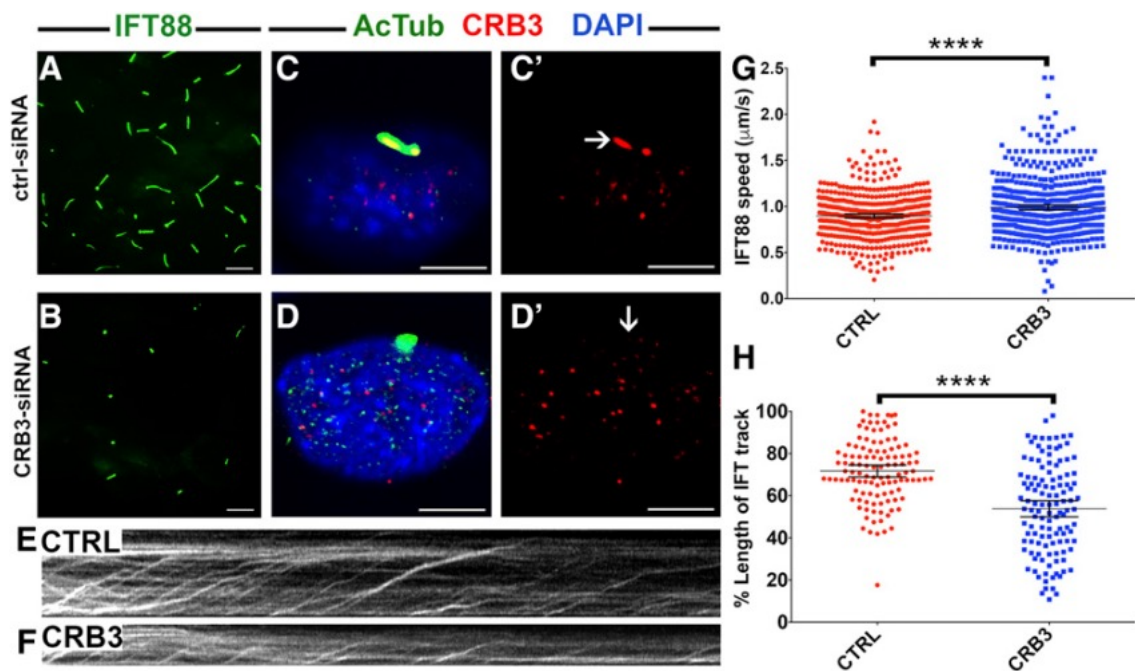


Figure V.6. CRB3 knockdown in mammalian cells affects intraflagellar transport (IFT) dynamics. (A and B) Maximum projections of total internal reflection fluorescence (TIRF) time-lapse recordings of IMCD3 cells grown on transwells and transfected with scrambled CTRL-small interfering RNA (siRNA) (A) or CRB3-siRNA (B). These cells are stably transfected with an IFT88-GFP construct to visualize intraflagellar transport (green signal). (C–D') Confocal images of control (CTRL) siRNA- (C and C') and CRB3 siRNA-treated (D and D') IMCD3 cells. Cilia are stained with antibodies to acetylated tubulin (AcTub) (green) and Crumbs (red).

Samples are counterstained with DAPI to mark nuclei (in blue). **(E and F)** Kymographs of IFT movement in an IMCD3-IFT88 cell line transfected with CTRL or CRB3 siRNA as indicated. **(G)** Graph showing the speed of IFT particle movement in cilia of IFT88-GFP IMCD3 cells. Data collected from three independent experiments. **(H)** Lengths of IFT tracks in CTRL siRNA- and CRB3 siRNA-transfected cells expressed as percentages of total cilia length. Data are collected from two independent experiments. In **(G and H)**, the mean and 95% C.I. are indicated. $P < 10^{-24}$ based on Student's t-tests. Bar, 10 μ m **(A and B)** and 5 μ m **(C–D')**.

V.2.6. *crb2b* mutation increases cilia length in a subset of tissues

Morpholino knockdown studies of *crb2b* revealed that this gene is necessary for the elongation and motility of pronephric cilia (Omori and Malicki). To gain further insight into *crb2b* function in cilia formation, we analysed homozygous carriers of the *crb2b*^{sa18042} allele. The zebrafish *crb2b* gene encodes two polypeptides that share most of the amino acid sequence. The shorter polypeptide does not include 11 N-terminal fibroblast growth factor-like repeats present in the long form and features a separate signal sequence (Zou et al., 2012). The *crb2b*^{sa18042} allele that we chose to use contains a stop codon at amino acid 10 of the long form, and thus is likely to eliminate the function of the long form (red arrow in Fig. V.7, A and B'–C'). A possible use of an alternative initiation codon at position 19 of the open reading frame could lead to protein expression, but it would eliminate most of the signal sequence rendering the long form of Crb2b dysfunctional. *crb2b*^{sa18042} homozygotes have normal external appearance and are fertile (Fig. V.7, B and C). This is also true for the offspring of homozygous mothers.

To analyze cilia morphology in these mutants, we stained them using anti-acetylated tubulin antibody as above. No gross abnormalities were seen in the cilia of most tissues, including the inner ear (Fig. V.7E', compare to 7D'), the

olfactory placode (Fig. V.7G', compare to 7F'), and the lateral line (Fig. V.7I', compare to 7H'). Similarly, contrary to the phenotype observed following morpholino knockdown (Omori and Malicki) (Table V.1), pronephric cilia were not obviously affected in *crb2b* mutants when compared to the wild type (Fig. V.7, K and K', compare to 7J and J'). Staining of mutant homozygotes with anti-CRB antibody did not reveal differences in Crumbs protein localization in cristae (Fig. V.7E, compare to 7D), olfactory placodes (Fig. V.7G, compare to 7F), the lateral line (Fig. V.7I, compare to 7H), and the pronephros (Fig. V.7K'', compare to 7J''). However, a statistically significant difference of cilia length was observed between *crb2b* mutants and the wild-type in cristae and the olfactory placode (Fig. V.7, L and M).

Contrary to cilia shortening seen in *ome* and *ome;crb3a* double mutants, and similar to the *crb3a* cilia phenotype (Fig. V.2P), cilia of *crb2b* mutant homozygotes are longer than those of their wild-type siblings. To test whether IFT protein localization is affected in these mutants, we immunostained homozygous *crb2b* mutant embryos for IFT88 at 5 dpf. No detectable difference was seen in the localization of IFT88 between *crb2b* mutants and the wild-type in inner ear cilia (Fig. V.7O, compare to 7N) and the nose (Fig. V.7Q, compare to 7P). These results further confirm that crumbs genes modulate cilia lengths in several tissues. In contrast to *ome* mutants, *crb2b*^{sa18042} mutant homozygotes do not display crumbs upregulation in cristae cilia.

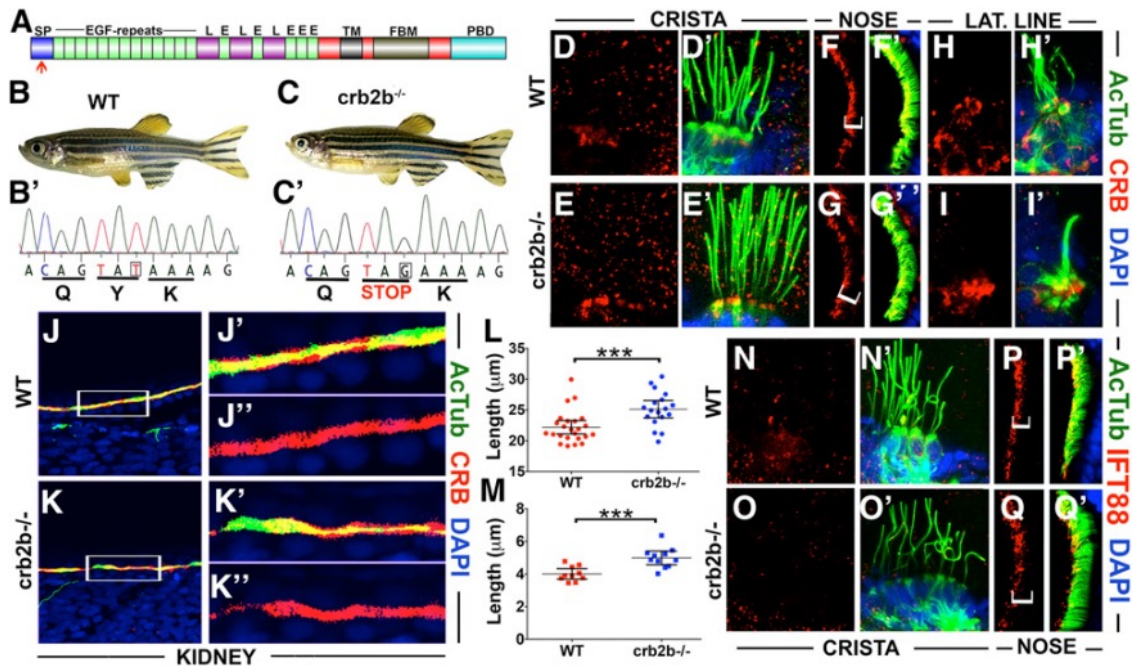


Figure V.7. *crb2b* affects cilia length. (A) Schematic of Crb2b protein domain structure (not to scale). Indicated are the signal peptide (SP), EGF-like repeats (E), Laminin G domains (L), transmembrane domain (TM), FERM-binding motif (FBM), and PDZ-binding do-main (PBD). Red arrow shows the position of mutation in the *crb2b*^{-/-sa18042} mutant allele. (B and C) Phenotypes of wild-type (WT) (B) and *crb2b*^{-/-sa18042} (C) homozygous mutant adult zebrafish. (B' and C') Sequences of WT and *crb2b*^{-/-sa18042} mutant alleles. (D–I') Whole-mount staining of WT and *crb2b*^{-/-sa18042} mutants using anti-acetylated tubulin (AcTub) (green), and anti-CRB (red) antibodies at 5 days postfertilization. Samples were counterstained with DAPI to visualize nuclei (in blue). Crumbs proteins are not detected in the cilia of cristae (D–E') and the lateral (LAT.) line (H–I') of *crb2b*^{-/-sa18042} mutants or their WT siblings. No differences in Crumbs signal are found between WT and mutants in the cilia of olfactory placodes (F–G') and the pronephric duct (J–K''). (L) Graph of cilia length in WT and *crb2b*^{-/-sa18042} mutants. Each dot represents the average length of all cilia in one crista. Data were collected from three independent experiments using at least five animals per experiment. (M) Graph of cilia length in olfactory placodes of WT and *crb2b*^{-/-sa18042} mutants. (N–O') IFT proteins are not detected in the cristae cilia of WT (N and N') and *crb2b*^{-/-sa18042} mutants (O and O'). (P–Q') IFT88 localization is not obviously different in nasal pit cilia of WT (P and P') and *crb2b*^{-/-sa18042} mutant (Q and Q') animals. Brackets in (F, G, P, and Q) indicate nasal cilia. In (L and M), the mean and 95% C.I. are indicated. P, 0.001 based on Student's t-test and Mann–Whitney test.

V.3. Discussion

Our studies reveal that *crumbs* genes function in three inter-connected aspects of ciliogenesis: the regulation of protein composition in the ciliary shaft, IFT movement dynamics, and cilia length determination (summarized in Table V.1). The absence of some *crumbs* genes, either singly and/or in double mutants, results in a massive accumulation of other Crumbs proteins and IFT particle components inside the ciliary shaft in some tissues. In a subset of cilia, the increase in ciliary Crumbs localization correlates with a decrease of cilia length. Interestingly, IFT dynamics is affected following *Crb3* knock-down in mammalian cells; IFT trains are somewhat faster and IFT tracks are markedly shorter. As discussed below, this may be related to a global role of Crumbs proteins in the morphogenesis of the apical surface of the cell.

crb3a^{sh410} mutant allele investigated in this study was generated using TALEN nucleases (Zu et al., 2013) and introduces a deletion of 13-bp, causing a frameshift between the TM and FERM domains (Fig. V.1A, red arrow and Fig. V.1C'). The homozygote animals survived to adulthood (Fig. V.1.B–D). *crb2b*^{sa18042} (obtained from SANGER) homozygotes also manifest normal external appearance and are fertile (Fig. V.7, B and C). *crb2b*^{sa18042} allele contains a stop codon at amino acid 10 of the long form, and thus is likely to eliminate the function of the long form (red arrow in Fig. V.7, A and B'–C'). Our sequencing data of *crb3a* reveals a frameshift mutation between the TM and FERM domains and the sequencing data of *crb2b* allele shows a stop codon at amino acid number 10 (Fig. V.1C' and Fig. V.7C'). These sequencing results indicate that *crb3a* and *crb2b* are most likely dysfunctional.

To further investigate whether these mutant alleles are dysfunctional, we performed western blots using anti-CRB antibody on embryos at different developmental stages (3 dpf, 4dpf, and 5dpf). Our results show that western blotting with anti-Crumbs antibodies is difficult. *Hsu et al.* reported that their antibody recognized a band of 150 kDa as expected (Hsu et al., 2006). *Zou et al.* observed much higher molecular weight band that did not correspond to predicted protein sizes. They suggested that this is due to posttranslational modifications (Zou et al., 2012). Our attempts at western blotting produced results similar to these of Zou et al.; the antibody that we use detects bands that have different molecular weights from predicted ones and we do not see consistent differences between wild-type and mutant strains.

An increase in ciliary Crumbs content in *ome* mutants is counterintuitive and reveals that crumbs genes or their protein products may negatively regulate each other. Such regulation could occur at the level of transcript or protein expression. It could also be mediated by protein degradation pathways. Previous studies suggested that crumbs expression may be regulated post-transcriptionally. The zebrafish *Crb3a* protein is enriched in mechanosensory hair cells while its transcript is uniformly expressed throughout the otic vesicle, suggesting a regulatory mechanism that affects translation or protein stability (Omori and Malicki). Since mouse studies of the retina did not detect changes in the transcriptome of the *Crb2* mutant during development, cross talk between crumbs genes on the level of transcriptional regulation appears less likely (Alves et al., 2013). Consistent with the above, zebrafish studies did not reveal compensatory Crumbs protein upregulation in *ome* mutants and similarly did not detect transcriptional upregulation of *Crb2b* in the same mutants (Hsu et al.,

2006). Alternatively, as discussed below, changes in Crumbs protein level in cilia may reflect the function of this group of genes in gating mechanisms at the cilia base.

Equally unexpected is the enrichment of IFT proteins in the cilia of crumbs mutants. It could be partially explained by the trapping of the heterotrimeric IFT kinesin by the mislocalized Crumbs in the ciliary shaft (see below). In addition, the regulation of IFT protein content by Crumbs could occur at the level of gating mechanisms that regulate trafficking into the ciliary compartment. This is suggested by observations that a Crumbs 3 isoform interacts with Importin β -1 in a RAN-regulated manner (Fan et al., 2007). A related importin, importin β -2 localizes to the proximal region of the ciliary axoneme and was proposed to mediate the ciliary entry of kif17, one of the two IFT kinesins, also in a RAN-regulated fashion (Dishinger et al., 2010b). It is thus possible that Crumbs mutations affect RAN–Importin-mediated gating mechanisms at the cilia base that regulate IFT entry into the ciliary compartment. This possibility is also supported by observations that Crumbs is enriched at the base hair cell kinocilia, where it could function in regulating cilia-directed traffic (Omori and Malicki).

crumbs mutants display cilia abnormalities only in some organs. One possible reason is that crumbs genes, *crb2b* and *crb3a* in particular, are expressed in a subset of tissues. Another and perhaps more intriguing possibility is that the crumbs cilia phenotype varies across tissues due to intrinsic differences in cilia assembly mechanisms. Cristae cilia in particular are genetically different from most other cilia. The most striking indication of their unique genetic characteristics is that they are unaffected in mutants of *kif3b*, a

subunit of the major ciliary kinesin, while most other cilia, including kinocilia of ear maculae, are absent in *kif3b* mutants (Zhao et al., 2012). Similarly, the *kif3a* mutant phenotype of cristae cilia differs from that of other cilia. Short-cristae cilia form in the absence of *kif3a* function and, in contrast to maculae for example, IFT88 protein persists at the base of these cilia in *kif3a* mutants (Pooranachandran and Malicki, 2016). Although morphological abnormalities of cilia in *crumbs* mutants are fairly subtle, the accumulation of Crumbs and IFT proteins in the ciliary shaft may have profound functional consequences, such as malfunction of cilia-mediated signal transduction cascades. This may account for the severity of the *oko meduzy* phenotype in many organs including the central nervous system, the cardiovascular system, and the pronephros (Malicki and Driever, Omori and Malicki).

What mechanism could account for the role of Crumbs in cilia elongation? It was previously reported that the C-terminus of Par3, a key regulator of apico-basal polarity, binds directly to the C-terminal coiled coil region of Kif3a, the main anterograde motor of IFT particles (Nishimura et al., 2004). This, combined with observations that Crb3 and Par3 function in ciliogenesis, led to the idea that the Par3/ Par6/aPKC complex bridges Crumbs proteins to Kif3a (Fan et al., 2004, Sfakianos et al., 2007) (Fig. 1.7C). A genetic interaction between *crumbs* and kinesin-1 was also reported in the fly eye (League and Nam, 2011). It is then tempting to hypothesize that Crumbs proteins compete for the Kif3a motor and, as a consequence, slow down IFT. In this model, cilia shortening in *ome* mutants is explained by the accumulation of other Crumbs proteins in cilia.

The results of crumbs function analysis in tissue culture are difficult to reconcile with cilia elongation in the zebrafish model. In contrast to fish phenotypes, RNAi knockdown in tissue culture has the opposite effect and causes cilia loss. This could be due to a global role of crumbs in cell polarity. Although cell junctions are largely intact in *Crb3* siRNA knockdown cells and in *Crb3* mutant mice, analysis of epithelia in *Crb3* mouse mutants reveals substantial abnormalities, such as the appearance of prominent blebs on the apical surface of lung cells and a shortening and fusion of apical villi in the intestine (Fan et al., 2004, Whiteman et al., 2014). These defects reveal a role of *Crb3* in apical surface morphogenesis, which could account for cilia loss in tissue culture studies. Nonetheless, the *Crb3* mouse mutant phenotype is inconsistent with tissue culture studies as it does not affect cilia morphology (Whiteman et al., 2014).

crb3 mutant phenotypes also differ between fish and mice; the mouse knockout phenotype is lethal whereas the zebrafish *crb3a* phenotype is not (Whiteman et al., 2014). This is most likely due to the duplication of the *crb3* gene in the zebrafish genome. It has been argued for quite a while now that gene duplication frequently leads to a subfunctionalization of duplicates relative to the ancestral gene (Force et al., 1999, Braasch et al., 2016). This is likely to have happened in the case of *crb3* genes: zebrafish *crb3a* is mainly expressed in the otic vesicle and only weakly in the digestive system, while the *crb3b* transcript is found strongly expressed in the digestive system and not at all in the ear (Omori and Malicki). It is thus likely that zebrafish *crb3a* mutants are viable because, in contrast to mouse *Crb3* mutants, they do not affect essential digestive organ functions.

Differences between the outcome of tissue culture studies and genetic analysis in animal models are not uncommon and are frequently difficult to explain. Although HDAC6 and Rab8 appear to function as potent regulators of ciliogenesis in tissue culture studies (Nachury et al., 2007, Pugacheva et al., 2007), mice mutant for these genes do not display cilia defects (Zhang et al., 2008, Sato et al., 2014, Ying et al., 2016). Similarly, substantial differences are frequently seen between morphant and mutant phenotypes in zebrafish (Kok et al., 2015). In our study of *crumbs* mutants, we also found phenotypic differences in comparison to morpholino knock-downs performed previously (Omori and Malicki) (summarized in Table V.1). Such differences could be explained by compensatory mechanisms that become active in mutants, such as the upregulation of paralogous genes. Increased presence of Crumbs proteins in the cilia of *crumbs* mutants may represent such a compensatory mechanism. Such mechanisms may account for some of the differences seen between tissue culture, morphant, and mutant analyses. Taken together, our data show that some *crumbs* genes affect the subcellular localization of protein products expressed by other *crumbs* genes, either through direct regulatory relationships or indirectly by affecting the function of gating mechanisms at the cilia base. *crumbs* genes function in multiple interrelated aspects of ciliogenesis, including intraflagellar transport, the determination of cilia length, and the protein composition of the ciliary shaft.

Table V.1. Summary of mutant and morphant crumbs phenotypes in cilia

Genotype	Tissue Examined	Cilia Length Phenotype	Crumbs Localisation (3dpf)	Crumbs Localisation (5dpf)	IFT in Cilia (5 dpf)
Wild-type	Ear macula	—	Cilia base	Cilia base	n.d.
	Ear cristae	—	Cilia base	Cilia base	None
	Nasal placode	—	Cilia base	Weak in ciliary shaft	?
	Kidney	—	Cilia base/apical surface (36 hpf)	n.d.	n.d.
crb3a^{-/-}	Ear macula	n.d.	Absent	Cilia base	n.d.
	Ear cristae	Longer	Cilia base	Cilia base	None
	Nasal placode	No change	Cilia base	Strong ciliary shaft	?
crb3a^{MO}	Ear macula	Shorter ^a	Reduced (2 dpf) ^a	n.d.	n.d.
Ome^{-/-}	Ear macula	n.d.	Cilia base	Cilia base	n.d.
	Ear cristae	Shorter	Cilia base	Cilia base, puncta in ciliary shaft	Weak
	Nasal placode	Shorter	Cilia base	Ciliary shaft	Cilia base
crb3a^{-/-}; ome^{-/-}	Ear cristae	Shorter	n.d.	Cilia base, ciliary shaft, weaker proximally	Strong
	Nasal placode	Shorter	n.d.	Strong ciliary shaft	Ciliary shaft
crb2b^{-/-}	Ear cristae	Longer	n.d.	Cilia base	None
	Nasal placode	Longer	n.d.	Weak in ciliary shaft	?
	Kidney	No obvious change	cilia base/apical surface	n.d.	n.d.
crb2b^{MO}	Kidney	Shorter and disorganized ^a	reduced (1 dpf) ^a	n.d.	n.d.

dpf, days postfertilization

IFT, intraflagellar transport

n.d., not determined

?, weak signal comparable to background

hpf, hours postfertilization;

MO, morpholino;

^aOmori and Malicki (2006)

Chapter VI

“Conclusions and Future Directions”

The aim of my main PhD project was to reveal the architecture of gating mechanism, focusing mainly on transition zone and IFT proteins using a combination of STORM imaging and quantitative image analysis. Furthermore, I investigated the relationship of the apico-basal polarity determinants, *crumbs* genes, to ciliary gating. For this purpose, I used several model systems including *Tetrahymena thermophila*, *Danio rerio* (zebrafish), mammalian cell lines, and primary cultures of human and mouse cells. I used a broad range of molecular biology, genetics, and imaging techniques such as confocal microscopy, “TIRF imaging, and “Stochastic Optical Reconstruction Microscopy” (STORM). This was followed by a thorough quantitative image analysis. In this chapter, I discuss the main findings and comment on the significance of my work in the future.

VI.1. Conclusions

VI.1.1. STORM analysis reveals the IFT docking sites and the architecture of TZ proteins at the cilia base

Our STORM analysis of many ciliary proteins revealed their orientation and relative position to each other at the cilia base. We show that transition zone proteins, IFT proteins, and other ciliary proteins are arranged in rings with different radial and axial positions at the cilia base (Fig. VI.1 and Table VI.1). Our STORM analysis of the ciliary proteins led to important findings:

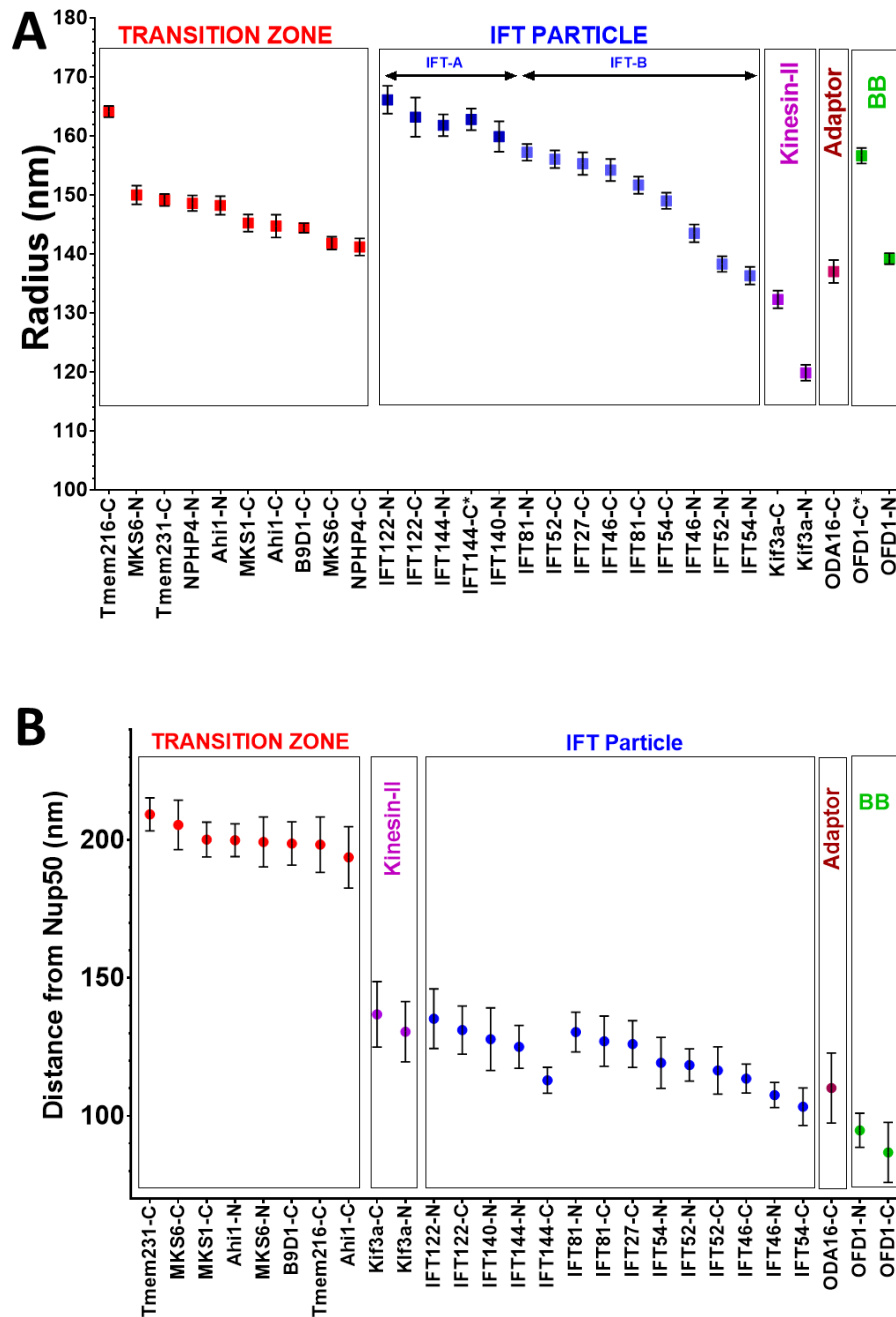


Figure VI.1. Radial and Axial Positions of the proteins characterised in this study. (A) Radial distribution of the mean \pm 95% confidence interval (CI) of the proteins examined this study. All data shown in this graph are obtained by direct labelling except for IFT144-C terminus and OFD1-C terminus, which were characterised using indirect labelling (denoted by *). **(B)** The axial positions were determined by mapping all the proteins with respect to Nup50 that seems to localise to the basal bodies in *Tetrahymena thermophila*. TZ proteins are the farthest from Nup50 and OFD1, is the closest to Nup50. Note that IFT docking sites are just distal to OFD1 and are at least 50 nm below the TZ proteins. TZ: transition zone; IFT: Intra-flagellar transport; BB: basal body.

1. We reveal for the first time the architecture of IFT proteins in their docking

sites at the cilia base.

2. IFT-A complex is located outside IFT-B complex in the radial dimension (Fig. VI.1.A).
3. Kif3a-C terminus is close to IFT-B proteins and Kif3a-N terminus to very close to the microtubule doublets (Fig. VI.1.A).
4. The transition zone proteins localise about 50nm distal to the IFT particle (Fig. VI.1B and Table VI.1).
5. We reveal the locations of the binding site of tubulin and the outer dynein arm at the cilia base (Fig. VI.2 and 3D).

All these data combined enabled us to generate a detailed super-resolved model showing the orientation of several IFT proteins and their relative position with respect to TZ and basal body proteins (Fig. VI.2 and 3).

VI.1.2. *crumbs* genes affect ciliogenesis and may be part of the ciliary gating structures at the cilia base

Our analysis of *crumbs* genes showed that they affect ciliogenesis in a subset of tissues in zebrafish. Surprisingly, when some *crumbs* were depleted, other crumbs accumulated massively inside the ciliary compartment. This was also accompanied by accumulation of IFT proteins inside the ciliary shaft of these mutants. This finding is of interest as it may indicate roles of Crumbs proteins in the modulation of IFT proteins and therefore, Crumbs proteins may be involved in the gating mechanisms at the cilia base (Fig. VI.4). The absence of *Crb3* in IMCD3 cells produced relatively shorter cilia with reduced IFT track lengths, and IFT trains were somewhat faster in the cilia of knocked-down

cells, indicating a possible role of Crumbs proteins in IFT movement into cilia.

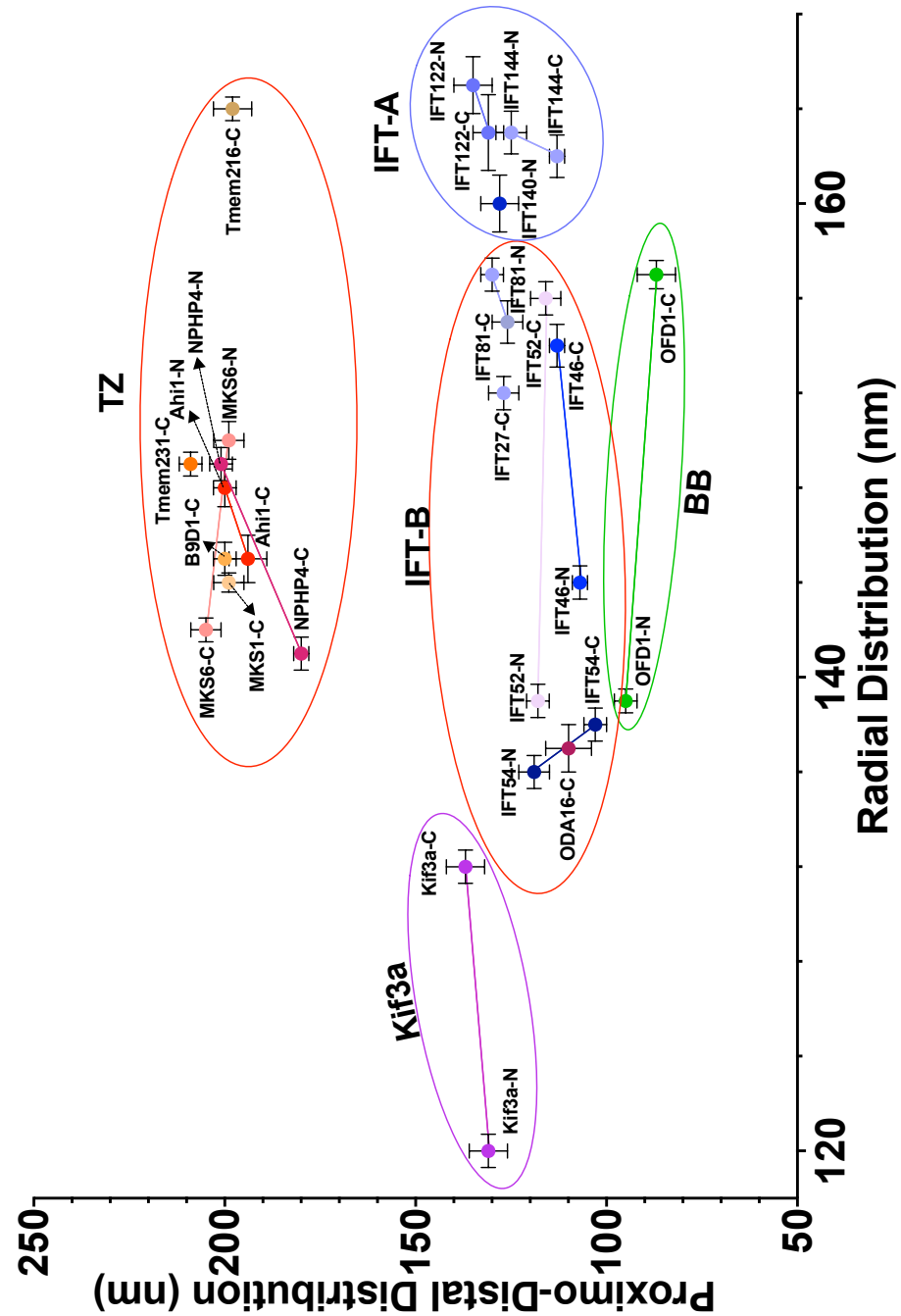


Figure VI.2. The orientation of the proteins examined in this study. A graph showing the radial and proximo-distal positions of the proteins investigated in this study. The X-axis represents the radial position and the Y-axis shows the proximo-distal, or axial, position of each protein. Data are mean \pm SEM.

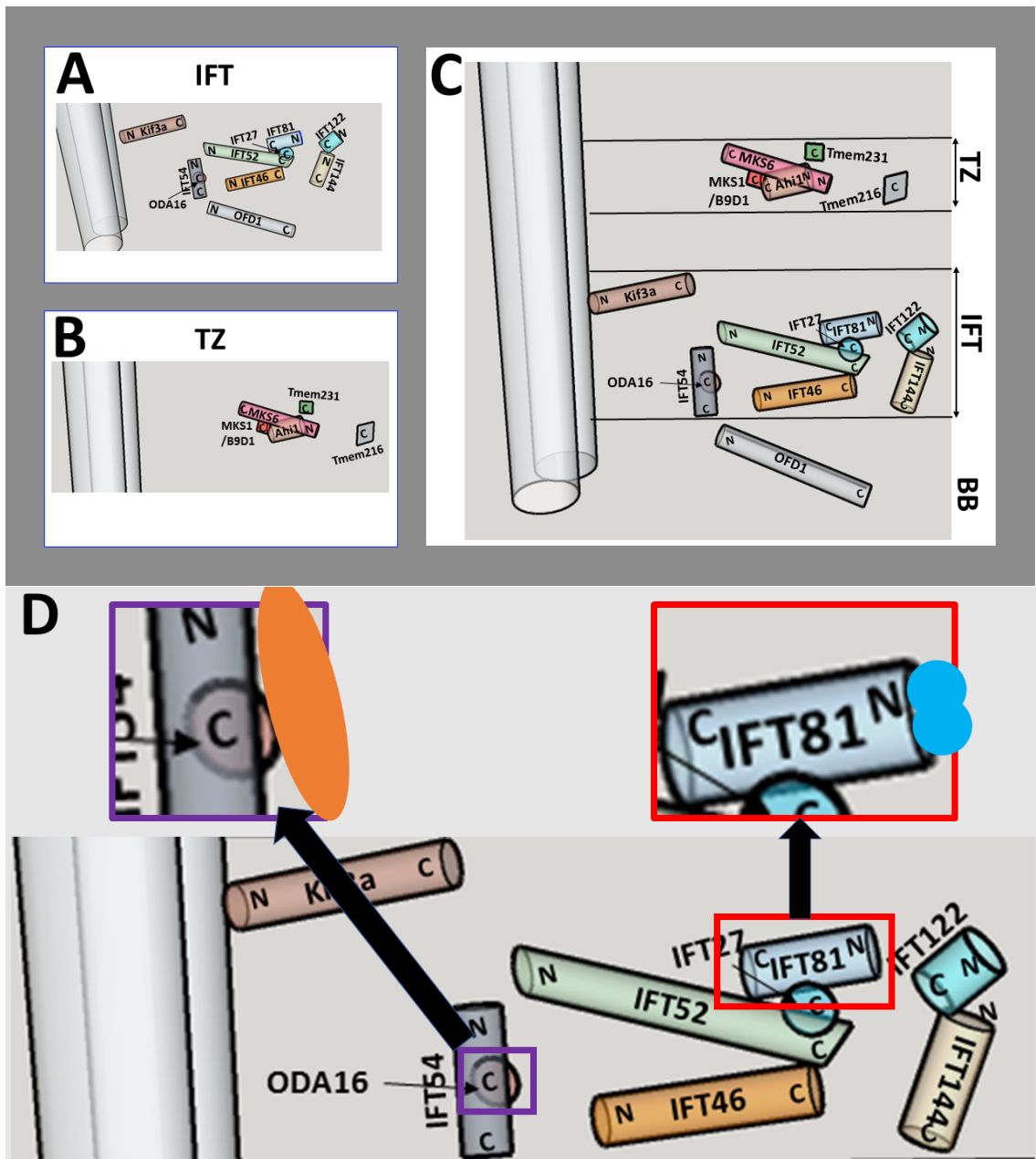


Figure VI.3. 3D model of the cilia base. (A) Super-resolved model of the IFT particle. (B) Super-resolved model of the TZ. (C) Super-resolved model of the proteins analysed in this study showing the relative position of TZ, IFT, and BB proteins at the cilia base. (D) A zoomed image of the IFT particle focusing on the positions where tubulin binds to the N-terminus of IFT81 (blue) and the outer dynein arm complex (ODA) binds to the C-terminus of the adaptor ODA16 (orange).

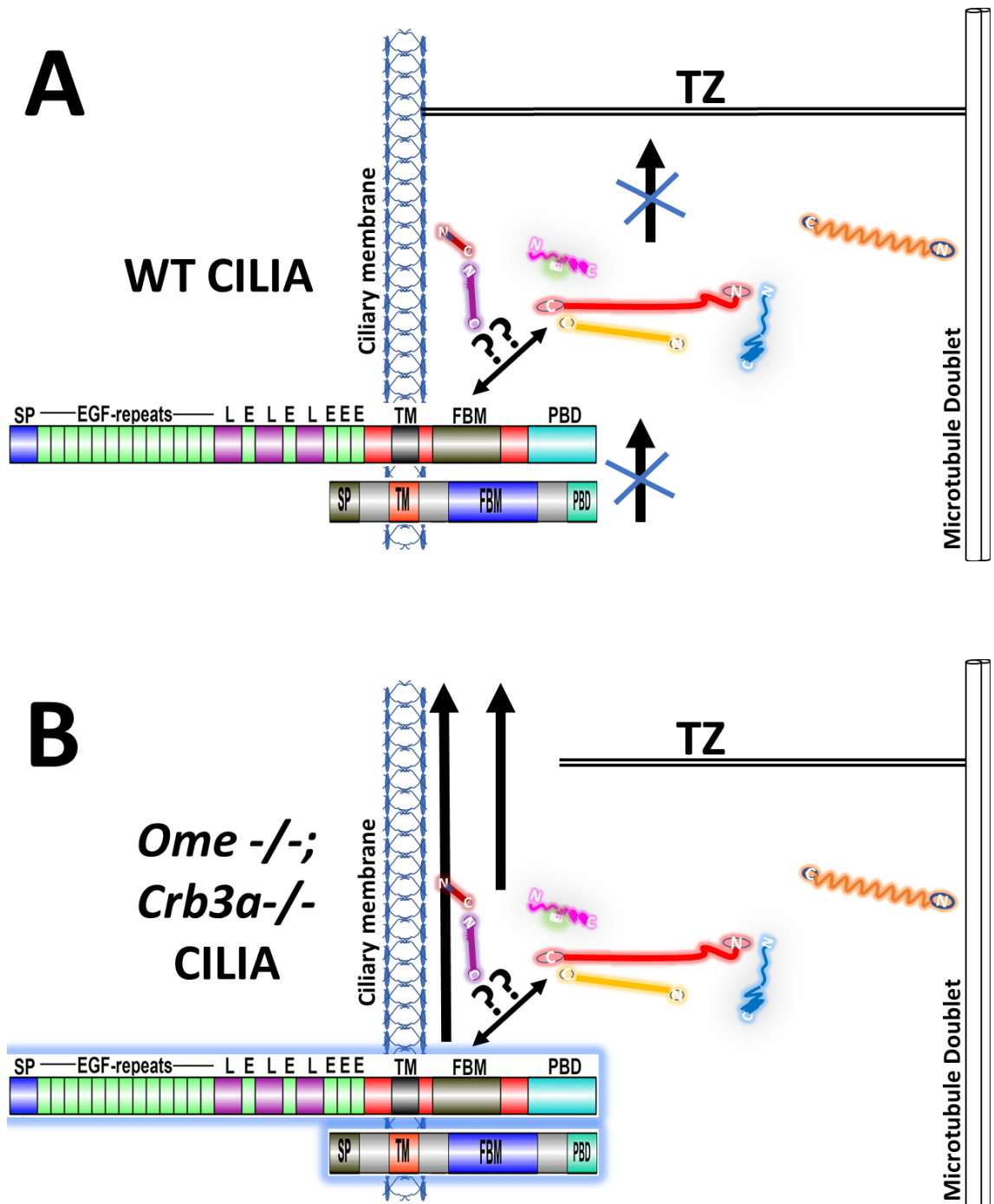


Figure VI.4. Crumbs proteins affect ciliogenesis and may contribute to gating mechanisms at the cilia base. (A) Crumbs proteins are localised to the cilia base in wild-type cilia. **(B)** In the absence of *crb3a* and *crb2a* (*ome*), cilia are shorter and other Crumbs proteins entered the cilium (See also Figure V.4). Surprisingly, IFT protein were highly enriched inside the ciliary shaft of these mutants suggesting a possible role of Crumbs proteins in gating IFT entry into cilia.

VI.2. Future Directions

Our analysis of architecture of ciliary proteins at the cilia base in addition to revealing for the first time the docking sites of IFT proteins provides a foundation for a plethora of experiments in the future. Our imaging approaches can be applied to localise many other ciliary proteins and address many more questions. In addition, our analysis of *crumbs* genes uncovered possible roles of these genes in the gating mechanisms at the cilia base. I outline here some approaches that can be used in the future to extend studies presented in this thesis.

VI.2.1. Nanobodies and photoactivatable fluorescent proteins

Our analysis of many ciliary proteins whether using indirect or direct labelling procedures depended on using antibodies. Antibodies mainly rely on conventional IgG molecules, which are about 12nm long (Lee et al., 2006, Sapphire et al., 2001). Although we could detect statistical differences in measurements of the radii when using indirect versus direct immunostaining, other staining procedures could probably reduce the error introduced by using antibody staining. For example, nanobodies are only 2.5 x 4 nm antigen-binding fragments obtained from camelid antibodies that lack light chains (Pleiner et al., 2015, Yan et al., 2015). Since nanobodies are only 2.5 by 4nm, it is expected that using them in STORM imaging will introduce smaller error when compared to using conventional antibody staining.

On the other hand, genetically encoded photoconvertible fluorescent

proteins such as mEos and Dronpa, which have been developed and tested to be compatible for STORM imaging (Habuchi et al., 2005, Wiedenmann et al., 2004, McKinney et al., 2009), can be also used to localise TZ and IFT proteins with high precision. In this case, there will be no need to use antibodies and therefore, this procedure is expected to localise the epitopes with the least error possible. Imaging proteins fused to photoconvertible fluorescent proteins can be performed using “PhotoActivatable Light Microscopy or PALM” (Betzig et al., 2006, Hess et al., 2006). However, it is worthy to mention that photoconvertible fluorescent proteins are not as bright as organic dyes and therefore, this would affect the localisation precision as well (Huang et al, 2011).

VI.2.2. Analysis of double transgenic lines and mutants

Our STORM analysis of protein architecture at the cilia base has proven to be very useful and produced remarkable set of data that enabled us to generate a super-resolved model of the cilia base (Fig. VI.3). Many important questions arise from our findings and here I list some of them.

1. How many IFT protein complexes are in one docking site? To tackle this, generation of double transgenic lines by tagging 2 different IFT proteins, such as IFT52 and IFT54, with different tags: IFT52-HA and IFT54-GFP, could be utilised to detect the number of IFT proteins in one docking site.
2. How would missing one IFT protein affect the localization of other IFT proteins and the stability of the whole IFT particle? For example, it would be interesting to know what happens to IFT-B proteins in the absence of IFT-A proteins or vice versa. These experiments, of course, are demanding, as

they require the generation of transgenic lines in mutant backgrounds, which might be technically difficult. This could be also applied for TZ proteins to determine the hierarchy of localisation of different transition zone proteins at the cilia base.

3. How stable are IFT proteins in their docking sites? One way to test the stability of IFT proteins at their docking sites is to perform FRAP experiments on IFT strains tagged with GFP for example. The determination of the time required for IFT proteins to return to their docking sites by measuring the duration required to recover fluorescence is an indication of their stability. In addition, IFT strains can be deciliated followed by FRAP imaging at different time points. In this case, it would be possible to examine how IFT proteins behave in their docking sites when cilia are regenerated following deciliation.

VI.2.3. STORM imaging of other proteins

Our imaging analysis could be applied to determine the orientation and location of other important ciliary proteins. For example, BBS proteins are thought to be necessary for the turnover of proteins at the cilia tip to initiate the retrograde transport (Jin et al., 2010, Wei et al., 2012). BBS7 has been shown to be required to stabilise the IFT particle (Ou et al., 2005) and the BBS regulator LZTFL1 was shown to mediate interaction of IFT particle to the BBSome (Eguether et al., 2014). IFT27, an IFT-B protein, is thought to mediate the exit of the BBSome from the cilium (Liew et al., 2014). Since we showed that IFT27 forms 9-fold symmetrical rings at the cilia base and localised its

radial and axial distribution too, it would be interesting to determine how BBS proteins fit in our current model.

We've characterised in this study the radial and axial position of Kif3a, the kinesin-II motor that powers anterograde IFT. On the other hand, it would be very interesting to investigate where cytoplasmic dynein 2, motors of retrograde transport, localise to the cilia base using STORM imaging. Dyneins form very large protein complexes composed of many subunits and therefore it may be challenging to localise all components of this complex (Pazour et al., 1999).

VI.2.4. Immuno-electron Microscopy and correlation of STORM with EM

Electron microscopy (EM) has always been widely used to reveal ultrastructural details of several organelles, including cilia and flagella (Rogowski et al., 2013). EM alone does not reveal details about specific proteins and their subcellular localisation. However, immuno-electron microscopy can detect and localise specific proteins in biological samples using primary antibodies conjugated with gold particles (Berryman and Rodewald, 1990). Immuno-EM has been widely used to pinpoint specific localisation of many ciliary proteins in several model systems. For example, *Chlamydomonas* IFT52, was shown to localise to the distal appendages of the basal bodies (Deane et al., 2001). Many other IFT proteins were also localised using Immuno-EM in retinal cells (Sedmak and Wolfrum, 2010). Transition zone proteins Cep290/NPHP6 (Craigie et al., 2010) and NPHP4 (Awata et al., 2014) were also localised using Immuno-EM. Therefore, Immuno-EM could be used in the future on the lines we generated in *Tetrahymena thermophila* to reinforce

our findings obtained by STORM imaging. Finally, several protocols have been developed to correlate STORM with EM images to better understand protein complexes as described in (Kim et al., 2015).

VI.2.5. Analysis of Crumbs proteins in Knock-in lines followed by STORM imaging

Our analysis of *crumbs* genes suggested a role in the trafficking of some ciliary proteins at the cilia base, so more investigation about the exact location of crumbs proteins is required. It has been postulated that Crb3 indirectly interacts with Kif3a through Par3/Par6/aPKC (Sfakianos et al., 2007). Future experiments would focus on determining possible interactions between Crumbs and other ciliary proteins at the cilia base. This could be achieved by performing immunoprecipitation and co-localisation experiments. In addition to that, super-resolution microscopy can be used to localise the exact position of Crumbs proteins in mammalian cells or thin sections/cryo-sections of zebrafish ciliated tissues. Crumbs localisation can be analysed using knock-in lines in zebrafish by epitope tagging of endogenous Crumbs proteins as previously described (Hoshijima et al., 2016). These lines, if successful, can be excellent tools to reveal how Crumbs proteins behave at the cilia base and inside the ciliary shaft. These lines could be also used to prepare sections to be imaged on STORM microscopy.

Table VI.1. Ciliary proteins analysed for the STORM study

Line (Terminus)	Radial dimension + SD (nm)		Axial dimension + SEM (nm)
	Indirect	Direct	
TRANSITION ZONE (TZ)			
MKS6-C	145 ± 8	142 ± 6	205.5 ± 4.3
MKS6-N	157 ± 10	150 ± 7	199.3 ± 4.4
Ahi1-C	148 ± 9	145 ± 7	193.8 ± 5.4
Ahi1-N	158 ± 5	148 ± 6	200 ± 2.9
NPHP4-C	147 ± 6	141 ± 6	313 ± 1 & 180 ± 2
NPHP4-N	148 ± 5	149 ± 5	319 ± 2 & 201 ± 3
MKS1-C	151 ± 9	145 ± 6	200.2 ± 3
B9d1-C	151 ± 9	144 ± 5	198.8 ± 3.7
Tmem216-C	159 ± 6	164 ± 6	198.4 ± 2.9
Tmem231-C	154 ± 6	149 ± 5	209.3 ± 2.9
INTRAFLAGELLAR TRANSPORT (IFT)			
IFT52-C	158 ± 7	156 ± 7	116 ± 4
IFT52-N	141 ± 7	139 ± 6	118 ± 3
IFT54-C	150 ± 6	148 ± 5	103 ± 3
IFT54-N	141 ± 9	136 ± 5	119 ± 4
IFT81-C	158 ± 5	152 ± 5	130 ± 3
IFT81-N	162 ± 5	157 ± 6	127 ± 4
IFT46-C	159 ± 6	154 ± 6	113 ± 3
IFT46-N	143 ± 5	143 ± 5	106 ± 5
IFT27-C	157 ± 4	155 ± 7	126 ± 4
IFT122-C	163 ± 7	163 ± 8	131 ± 4
IFT122-N	165 ± 9	166 ± 8	135 ± 5
IFT144-C	163 ± 8	162 ± 8	113 ± 2
IFT144-N	160 ± 6	162 ± 5	125 ± 4
IFT140-N	160 ± 10	160 ± 6	NA
Kif3a-C	130 ± 6	132 ± 5	137 ± 6
Kif3a-N	121 ± 7	120 ± 5	130 ± 5
ODA16-C	139 ± 5	137 ± 7	110 ± 6
BB			
OFD1-C	157 ± 5	NA	87 ± 5
OFD1-N	139 ± 5	139 ± 4	95 ± 3

References

- AHMED, N. T., GAO, C., LUCKER, B. F., COLE, D. G. & MITCHELL, D. R. 2008. ODA16 aids axonemal outer row dynein assembly through an interaction with the intraflagellar transport machinery. *J Cell Biol*, 183, 313-22.
- AHMED, N. T. & MITCHELL, D. R. 2005. ODA16p, a Chlamydomonas flagellar protein needed for dynein assembly. *Mol Biol Cell*, 16, 5004-12.
- ALLSHIRE, R. C., GOSDEN, J. R., CROSS, S. H., CRANSTON, G., ROUT, D., SUGAWARA, N., SZOSTAK, J. W., FANTES, P. A. & HASTIE, N. D. 1988. Telomeric repeat from *T. thermophila* cross hybridizes with human telomeres. *Nature*, 332, 656-9.
- ALVES, C. H., SANZ, A. S., PARK, B., PELLISSIER, L. P., TANIMOTO, N., BECK, S. C., HUBER, G., MURTAZA, M., RICHARD, F., SRIDEVI GURUBARAN, I., GARCIA GARRIDO, M., LEVELT, C. N., RASHBASS, P., LE BIVIC, A., SEELIGER, M. W. & WIJNHOLDS, J. 2013. Loss of CRB2 in the mouse retina mimics human retinitis pigmentosa due to mutations in the CRB1 gene. *Human Molecular Genetics*, 22, 35-50.
- ARTS, H. H., DOHERTY, D., VAN BEERSUM, S. E., PARISI, M. A., LETTEBOER, S. J., GORDEN, N. T., PETERS, T. A., MARKER, T., VOESENEK, K., KARTONO, A., OZYUREK, H., FARIN, F. M., KROES, H. Y., WOLFRUM, U., BRUNNER, H. G., CREMERS, F. P., GLASS, I. A., KNOERS, N. V. & ROEPMAN, R. 2007. Mutations in the gene encoding the basal body protein RPGRIP1L, a nephrocystin-4 interactor, cause Joubert syndrome. *Nat Genet*, 39, 882-8.
- AWATA, J., TAKADA, S., STANDLEY, C., LECHTRECK, K. F., BELLVE, K. D., PAZOUR, G. J., FOGARTY, K. E. & WITMAN, G. B. 2014. NPHP4 controls ciliary trafficking of membrane proteins and large soluble proteins at the transition zone. *J Cell Sci*, 127, 4714-27.
- BACHMANN, A., SCHNEIDER, M., THEILENBERG, E., GRAWE, F. & KNUST, E. 2001. Drosophila Stardust is a partner of Crumbs in the control of epithelial cell polarity. *Nature*, 414, 638-643.
- BAYLESS, B. A., GALATI, D. F. & PEARSON, C. G. 2015. Tetrahymena basal bodies. *Cilia*, 5, 1.
- BERBARI, N. F., LEWIS, J. S., BISHOP, G. A., ASKWITH, C. C. & MYKYTYN, K. 2008. Bardet-Biedl syndrome proteins are required for the localization of G protein-coupled receptors to primary cilia. *PNAS*, 105, 4242-4246.
- BERRYMAN, M. A. & RODEWALD, R. D. 1990. An enhanced method for post-embedding immunocytochemical staining which preserves cell membranes. *J Histochem Cytochem*, 38, 159-70.
- BESHARSE, J. C., FORESTNER, D. M. & DEFOE, D. M. 1985. Membrane assembly in retinal photoreceptors. III. Distinct membrane domains of the connecting cilium of developing rods. *The Journal of neuroscience : the official journal of the Society for Neuroscience*, 5, 1035-48.
- BESHARSE, J. C. & HORST, C. J. 1990. The photoreceptor connecting cilium A model for the transition zone. *Ciliary and flagellar membranes*. Springer.
- BETZIG, E., PATTERSON, G. H., SOUGRAT, R., LINDWASSER, O. W., OLENYCH, S., BONIFACINO, J. S., DAVIDSON, M. W., LIPPINCOTT-SCHWARTZ, J. & HESS, H. F. 2006. Imaging intracellular fluorescent proteins at nanometer resolution. *Science*, 313, 1642-5.
- BHOGARAJU, S., CAJANEK, L., FORT, C., BLISNICK, T., WEBER, K., TASCHNER, M., MIZUNO, N., LAMLA, S., BASTIN, P., NIGG, E. A. & LORENTZEN, E. 2013. Molecular basis of tubulin transport within the cilium by IFT74 and IFT81. *Science (New York, N.Y.)*, 341, 1009-1012.
- BHOGARAJU, S., TASCHNER, M., MORAWETZ, M., BASQUIN, C. & LORENTZEN, E. 2011. Crystal structure of the intraflagellar transport complex 25/27. *EMBO J*, 30, 1907-18.
- BILDER, D., SCHOBER, M. & PERRIMON, N. 2003. Integrated activity of PDZ protein complexes regulates epithelial polarity. *Nat Cell Biol*, 5, 53-8.

- BLACQUE, O. E., CEVIK, S. & KAPLAN, O. I. 2008. Intraflagellar transport: from molecular characterisation to mechanism. *Front Biosci*, 13, 2633-52.
- BRAASCH, I., GEHRKE, A. R., SMITH, J. J., KAWASAKI, K., MANOUSAKI, T., PASQUIER, J., AMORES, A., DESVIGNES, T., BATZEL, P., CATCHEN, J., BERLIN, A. M., CAMPBELL, M. S., BARRELL, D., MARTIN, K. J., MULLEY, J. F., RAVI, V., LEE, A. P., NAKAMURA, T., CHALOPIN, D., FAN, S., WCISEL, D., CANESTRO, C., SYDES, J., BEAUDRY, F. E., SUN, Y., HERTEL, J., BEAM, M. J., FASOLD, M., ISHIYAMA, M., JOHNSON, J., KEHR, S., LARA, M., LETAW, J. H., LITMAN, G. W., LITMAN, R. T., MIKAMI, M., OTA, T., SAHA, N. R., WILLIAMS, L., STADLER, P. F., WANG, H., TAYLOR, J. S., FONTENOT, Q., FERRARA, A., SEARLE, S. M., AKEN, B., YANDELL, M., SCHNEIDER, I., YODER, J. A., VOLFF, J. N., MEYER, A., AMEMIYA, C. T., VENKATESH, B., HOLLAND, P. W., GUIGUEN, Y., BOBE, J., SHUBIN, N. H., DI PALMA, F., ALFOLDI, J., LINDBLAD-TOH, K. & POSTLETHWAIT, J. H. 2016. The spotted gar genome illuminates vertebrate evolution and facilitates human-teleost comparisons. *Nat Genet*, 48, 427-37.
- BRAZELTON, W. J., AMUNDSEN, C. D., SILFLOW, C. D. & LEFEBVRE, P. A. 2001. The bld1 mutation identifies the Chlamydomonas osm-6 homolog as a gene required for flagellar assembly. *Current biology : CB*, 11, 1591-1594.
- BRESLOW, D. K., KOSLOVER, E. F., SEYDEL, F., SPAKOWITZ, A. J. & NACHURY, M. V. 2013. An in vitro assay for entry into cilia reveals unique properties of the soluble diffusion barrier. *J Cell Biol*, 203, 129-47.
- BROWN, J. M., COCHRAN, D. A., CRAIGE, B., KUBO, T. & WITMAN, G. B. 2015. Assembly of IFT trains at the ciliary base depends on IFT74. *Curr Biol*, 25, 1583-93.
- BRYAN, T. M., SPERGER, J. M., CHAPMAN, K. B. & CECH, T. R. 1998. Telomerase reverse transcriptase genes identified in Tetrahymena thermophila and Oxytricha trifallax. *Proc Natl Acad Sci U S A*, 95, 8479-84.
- BUISSON, J., CHENOUEARD, N., LAGACHE, T., BLISNICK, T., OLIVO-MARIN, J. C. & BASTIN, P. 2012. Intraflagellar transport proteins cycle between the flagellum and its base. *Journal of cell science*.
- CASSIDY-HANLEY, D. M. 2012. Tetrahymena in the laboratory: strain resources, methods for culture, maintenance, and storage. *Methods Cell Biol*, 109, 237-76.
- CHALKER, D. L. 2012. Transformation and strain engineering of Tetrahymena. *Methods Cell Biol*, 109, 327-45.
- CHEVRETTE, M., JOLY, L., TELLIS, P., KNAPIK, E. W., MILES, J., FISHMAN, M. & EKKER, M. 2000. Characterization of a Zebrafish/Mouse somatic cell hybrid panel. *Genomics*, 64, 119-26.
- CHIH, B., LIU, P., CHINN, Y., CHALOUNI, C., KOMUVES, L. G., HASS, P. E., SANDOVAL, W. & PETERSON, A. S. 2011. A ciliopathy complex at the transition zone protects the cilia as a privileged membrane domain. *Nature cell biology*, 14, 61-72.
- CHISHTI, A. H., KIM, A. C., MARFATIA, S. M., LUTCHMAN, M., HANSPAL, M., JINDAL, H., LIU, S. C., LOW, P. S., ROULEAU, G. A., MOHANDAS, N., CHASIS, J. A., CONBOY, J. G., GASCARD, P., TAKAKUWA, Y., HUANG, S. C., BENZ, E. J., JR., BRETSCHER, A., FEHON, R. G., GUSELLA, J. F., RAMESH, V., SOLOMON, F., MARCHESI, V. T., TSUKITA, S., HOOVER, K. B. & ET AL. 1998. The FERM domain: a unique module involved in the linkage of cytoplasmic proteins to the membrane. *Trends Biochem Sci*, 23, 281-2.
- CHOZINSKI, T. J., GAGNON, L. A. & VAUGHAN, J. C. 2014. Twinkle, twinkle little star: photoswitchable fluorophores for super-resolution imaging. *FEBS Lett*, 588, 3603-12.
- COLE, D. G. 2003. The intraflagellar transport machinery of Chlamydomonas reinhardtii. *Traffic*, 4, 435-42.
- COLE, D. G., DIENER, D. R., HIMELBLAU, A. L., BEECH, P. L., FUSTER, J. C. & ROSENBAUM, J. L. 1998. Chlamydomonas kinesin-II-dependent intraflagellar transport (IFT): IFT particles

- contain proteins required for ciliary assembly in *Caenorhabditis elegans* sensory neurons. *J Cell Biol*, 141, 993-1008.
- COLLINS, K. & GOROVSKY, M. A. 2005. *Tetrahymena thermophila*. *Curr Biol*, 15, R317-8.
- CRAIGE, B., TSAO, C. C., DIENER, D. R., HOU, Y., LECHTRECK, K. F., ROSENBAUM, J. L. & WITMAN, G. B. 2010. CEP290 tethers flagellar transition zone microtubules to the membrane and regulates flagellar protein content. *The Journal of cell biology*, 190, 927-40.
- CZARNECKI, P. G. & SHAH, J. V. 2012. The ciliary transition zone: from morphology and molecules to medicine. *Trends Cell Biol*, 22, 201-10.
- DAVE, D., WLOGA, D. & GAERTIG, J. 2009. Manipulating ciliary protein-encoding genes in *Tetrahymena thermophila*. *Methods Cell Biol*, 93, 1-20.
- DAVIS, E. E. & KATSANIS, N. 2012. The ciliopathies: a transitional model into systems biology of human genetic disease. *Curr Opin Genet Dev*, 22, 290-303.
- DAWE, H. R., SMITH, U. M., CULLINANE, A. R., GERRELLI, D., COX, P., BADANO, J. L., BLAIR-REID, S., SRIRAM, N., KATSANIS, N., ATTIE-BITACH, T., AFFORD, S. C., COPP, A. J., KELLY, D. A., GULL, K. & JOHNSON, C. A. 2007. The Meckel-Gruber Syndrome proteins MKS1 and meckelin interact and are required for primary cilium formation. *Hum Mol Genet*, 16, 173-86.
- DEANE, J. A., COLE, D. G., SEELEY, E. S., DIENER, D. R. & ROSENBAUM, J. L. 2001. Localization of intraflagellar transport protein IFT52 identifies basal body transitional fibers as the docking site for IFT particles. *Curr Biol*, 11, 1586-90.
- DEL VISO, F., HUANG, F., MYERS, J., CHALFANT, M., ZHANG, Y., REZA, N., BEWERSDORF, J., LUSK, C. P. & KHOKHA, M. K. 2016. Congenital Heart Disease Genetics Uncovers Context-Dependent Organization and Function of Nucleoporins at Cilia. *Dev Cell*, 38, 478-92.
- DEMPSEY, G. T., BATES, M., KOWTONIUK, W. E., LIU, D. R., TSIEN, R. Y. & ZHUANG, X. 2009. Photoswitching mechanism of cyanine dyes. *J Am Chem Soc*, 131, 18192-3.
- DEMPSEY, G. T., VAUGHAN, J. C., CHEN, K. H., BATES, M. & ZHUANG, X. 2011. Evaluation of fluorophores for optimal performance in localization-based super-resolution imaging. *Nature methods*, 8, 1027-1036.
- DEN HOLLANDER, A. I., HECKENLIVELY, J. R., VAN DEN BORN, L. I., DE KOK, Y. J., VAN DER VELDE-VISSER, S. D., KELLNER, U., JURKLIES, B., VAN SCHOONEVELD, M. J., BLANKENAGEL, A., ROHRSCHEIDER, K., WISSINGER, B., CRUYBERG, J. R., DEUTMAN, A. F., BRUNNER, H. G., APFELSTEDT-SYLLA, E., HOYNG, C. B. & CREMERS, F. P. 2001. Leber congenital amaurosis and retinitis pigmentosa with Coats-like exudative vasculopathy are associated with mutations in the crumbs homologue 1 (CRB1) gene. *Am J Hum Genet*, 69, 198-203.
- DEN HOLLANDER, A. I., TEN BRINK, J. B., DE KOK, Y. J., VAN SOEST, S., VAN DEN BORN, L. I., VAN DRIEL, M. A., VAN DE POL, D. J., PAYNE, A. M., BHATTACHARYA, S. S., KELLNER, U., HOYNG, C. B., WESTERVELD, A., BRUNNER, H. G., BLEEKER-WAGEMAKERS, E. M., DEUTMAN, A. F., HECKENLIVELY, J. R., CREMERS, F. P. & BERGEN, A. A. 1999. Mutations in a human homologue of *Drosophila* crumbs cause retinitis pigmentosa (RP12). *Nat Genet*, 23, 217-21.
- DIENER, D. R., LUPETTI, P. & ROSENBAUM, J. L. 2015. Proteomic analysis of isolated ciliary transition zones reveals the presence of ESCRT proteins. *Curr Biol*, 25, 379-84.
- DISHINGER, J. F., KEE, H. L., JENKINS, P. M., FAN, S., HURD, T. W., HAMMOND, J. W., TRUONG, Y. N., MARGOLIS, B., MARTENS, J. R. & VERHEY, K. J. 2010a. Ciliary entry of the kinesin-2 motor KIF17 is regulated by importin-beta2 and RanGTP. *Nat Cell Biol*, 12, 703-10.
- DISHINGER, J. F., KEE, H. L., JENKINS, P. M., FAN, S., HURD, T. W., HAMMOND, J. W., TRUONG, Y. N.-T., MARGOLIS, B., MARTENS, J. R. & VERHEY, K. J. 2010b. Ciliary entry of the

- kinesin-2 motor KIF17 is regulated by importin- β 2 and RanGTP. *Nature cell biology*, 12, 703-710.
- DOWDLE, W. E., ROBINSON, J. F., KNEIST, A., SIREROL-PIQUER, M. S., FRINTS, S. G., CORBIT, K. C., ZAGHLOUL, N. A., VAN LIJNSCHOTEN, G., MULDER, L., VERVER, D. E., ZERRES, K., REED, R. R., ATTIE-BITACH, T., JOHNSON, C. A., GARCIA-VERDUGO, J. M., KATSANIS, N., BERGMANN, C. & REITER, J. F. 2011. Disruption of a ciliary B9 protein complex causes Meckel syndrome. *American journal of human genetics*, 89, 94-110.
- EGUETHER, T., SAN AGUSTIN, J. T., KEADY, B. T., JONASSEN, J. A., LIANG, Y., FRANCIS, R., TOBITA, K., JOHNSON, C. A., ABDELHAMED, Z. A., LO, C. W. & PAZOUR, G. J. 2014. IFT27 links the BBSome to IFT for maintenance of the ciliary signaling compartment. *Developmental cell*, 31, 279-290.
- EISEN, J. A., COYNE, R. S., WU, M., WU, D., THIAGARAJAN, M., WORTMAN, J. R., BADGER, J. H., REN, Q., AMEDEO, P., JONES, K. M., TALLON, L. J., DELCHER, A. L., SALZBERG, S. L., SILVA, J. C., HAAS, B. J., MAJOROS, W. H., FARZAD, M., CARLTON, J. M., SMITH, R. K., JR., GARG, J., PEARLMAN, R. E., KARRER, K. M., SUN, L., MANNING, G., ELDE, N. C., TURKEWITZ, A. P., ASAI, D. J., WILKES, D. E., WANG, Y., CAI, H., COLLINS, K., STEWART, B. A., LEE, S. R., WILAMOWSKA, K., WEINBERG, Z., RUZZO, W. L., WLOGA, D., GAERTIG, J., FRANKEL, J., TSAO, C. C., GOROVSKY, M. A., KEELING, P. J., WALLER, R. F., PATRON, N. J., CHERRY, J. M., STOVER, N. A., KRIEGER, C. J., DEL TORO, C., RYDER, H. F., WILLIAMSON, S. C., BARBEAU, R. A., HAMILTON, E. P. & ORIAS, E. 2006. Macronuclear genome sequence of the ciliate *Tetrahymena thermophila*, a model eukaryote. *PLoS Biol*, 4, e286.
- ERDELYI, M., REES, E., METCALF, D., SCHIERLE, G. S., DUDAS, L., SINKO, J., KNIGHT, A. E. & KAMINSKI, C. F. 2013. Correcting chromatic offset in multicolor super-resolution localization microscopy. *Opt Express*, 21, 10978-88.
- FAILLER, M., GEE, H. Y., KRUG, P., JOO, K., HALBRITTER, J., BELKACEM, L., FILHOL, E., PORATH, J. D., BRAUN, D. A., SCHUELER, M., FRIGO, A., ALIBEU, O., MASSON, C., BROCHARD, K., HURAUULT DE LIGNY, B., NOVO, R., PIETREMENT, C., KAYSERILI, H., SALOMON, R., GUBLER, M. C., OTTO, E. A., ANTIGNAC, C., KIM, J., BENMERAH, A., HILDEBRANDT, F. & SAUNIER, S. 2014. Mutations of CEP83 cause infantile nephronophthisis and intellectual disability. *Am J Hum Genet*, 94, 905-14.
- FAN, S., FOGG, V., WANG, Q., CHEN, X. W., LIU, C. J. & MARGOLIS, B. 2007. A novel Crumbs3 isoform regulates cell division and ciliogenesis via importin beta interactions. *J Cell Biol*, 178, 387-98.
- FAN, S., HURD, T. W., LIU, C. J., STRAIGHT, S. W., WEIMBS, T., HURD, E. A., DOMINO, S. E. & MARGOLIS, B. 2004. Polarity proteins control ciliogenesis via kinesin motor interactions. *Curr Biol*, 14, 1451-61.
- FAN, Z. C., BEHAL, R. H., GEIMER, S., WANG, Z., WILLIAMSON, S. M., ZHANG, H., COLE, D. G. & QIN, H. 2010. Chlamydomonas IFT70/CrDYF-1 is a core component of IFT particle complex B and is required for flagellar assembly. *Mol Biol Cell*, 21, 2696-706.
- FILGES, I., NOSOVA, E., BRUDER, E., TERCANLI, S., TOWNSEND, K., GIBSON, W. T., ROTHLSBERGER, B., HEINIMANN, K., HALL, J. G., GREGORY-EVANS, C. Y., WASSERMAN, W. W., MINY, P. & FRIEDMAN, J. M. 2014. Exome sequencing identifies mutations in KIF14 as a novel cause of an autosomal recessive lethal fetal ciliopathy phenotype. *Clin Genet*, 86, 220-8.
- FISCH, C. & DUPUIS-WILLIAMS, P. 2011. Ultrastructure of cilia and flagella - back to the future! *Biol Cell*, 103, 249-70.
- FLIEGAUF, M., BENZING, T. & OMRAN, H. 2007. When cilia go bad: cilia defects and ciliopathies. *Nat Rev Mol Cell Biol*, 8, 880-93.

- FORCE, A., LYNCH, M., PICKETT, F. B., AMORES, A., YAN, Y. L. & POSTLETHWAIT, J. 1999. Preservation of duplicate genes by complementary, degenerative mutations. *Genetics*, 151, 1531-45.
- FU, W., WANG, L., KIM, S., LI, J. & DYNLACHT, B. D. 2016. Role for the IFT-A Complex in Selective Transport to the Primary Cilium. *Cell Rep*, 17, 1505-1517.
- GAERTIG, J., WLOGA, D., VASUDEVAN, K. K., GUHA, M. & DENTLER, W. 2013. Discovery and functional evaluation of ciliary proteins in *Tetrahymena thermophila*. *Methods Enzymol*, 525, 265-84.
- GARCIA-GONZALO, F. R., CORBIT, K. C., SIREROL-PIQUER, M. S., RAMASWAMI, G., OTTO, E. A., NORIEGA, T. R., SEOL, A. D., ROBINSON, J. F., BENNETT, C. L., JOSIFOVA, D. J., GARCÍA-VERDUGO, J. M., KATSANIS, N., HILDEBRANDT, F. & REITER, J. F. 2011. A transition zone complex regulates mammalian ciliogenesis and ciliary membrane composition. *Nature genetics*, 43, 776-784.
- GARCIA-GONZALO, F. R. & REITER, J. F. 2012. Scoring a backstage pass: mechanisms of ciliogenesis and ciliary access. *The Journal of cell biology*, 197, 697-709.
- GARCIA-GONZALO, F. R. & REITER, J. F. 2017. Open Sesame: How Transition Fibers and the Transition Zone Control Ciliary Composition. *Cold Spring Harb Perspect Biol*, 9.
- GILULA, N. B. & SATIR, P. 1972. The ciliary necklace. A ciliary membrane specialization. *J Cell Biol*, 53, 494-509.
- GOETZ, S. C. & ANDERSON, K. V. 2010. The primary cilium: a signalling centre during vertebrate development. *Nat. Rev. Genetics*, 11, 331-344.
- GOSENS, I., DEN HOLLANDER, A. I., CREMERS, F. P. & ROEPMAN, R. 2008. Composition and function of the Crumbs protein complex in the mammalian retina. *Exp Eye Res*, 86, 713-26.
- GRAWE, F., WODARZ, A., LEE, B., KNUST, E. & SKAER, H. 1996. The *Drosophila* genes crumbs and stardust are involved in the biogenesis of adherens junctions. *Development*, 122, 951-9.
- GUSTAFSSON, M. G., SHAO, L., CARLTON, P. M., WANG, C. J., GOLUBOVSKAYA, I. N., CANDE, W. Z., AGARD, D. A. & SEDAT, J. W. 2008. Three-dimensional resolution doubling in wide-field fluorescence microscopy by structured illumination. *Biophys J*, 94, 4957-70.
- HABUCHI, S., ANDO, R., DEDECKER, P., VERHEIJEN, W., MIZUNO, H., MIYAWAKI, A. & HOFKENS, J. 2005. Reversible single-molecule photoswitching in the GFP-like fluorescent protein Dronpa. *Proc Natl Acad Sci U S A*, 102, 9511-6.
- HAZIME, K. & MALICKI, J. J. 2017. Apico-basal Polarity Determinants Encoded by crumbs Genes Affect Ciliary Shaft Protein Composition, IFT Movement Dynamics, and Cilia Length. *Genetics*.
- HERSCHLAG, D. & CECH, T. R. 1990. Catalysis of RNA cleavage by the *Tetrahymena thermophila* ribozyme. 1. Kinetic description of the reaction of an RNA substrate complementary to the active site. *Biochemistry*, 29, 10159-71.
- HESS, S. T., GIRIRAJAN, T. P. & MASON, M. D. 2006. Ultra-high resolution imaging by fluorescence photoactivation localization microscopy. *Biophys J*, 91, 4258-72.
- HIRANO, T., KATOH, Y. & NAKAYAMA, K. 2017. Intraflagellar transport-A complex mediates ciliary entry and retrograde trafficking of ciliary G protein-coupled receptors. *Mol Biol Cell*, 28, 429-439.
- HIROKAWA, N., TANAKA, Y. & OKADA, Y. 2012. Cilia, KIF3 molecular motor and nodal flow. *Current opinion in cell biology*, 1-9.
- HOSHIJIMA, K., JURYNEC, M. J. & GRUNWALD, D. J. 2016. Precise Editing of the Zebrafish Genome Made Simple and Efficient. *Dev Cell*, 36, 654-67.
- HOU, Y., QIN, H., FOLLIT, J. A., PAZOUR, G. J., ROSENBAUM, J. L. & WITMAN, G. B. 2007. Functional analysis of an individual IFT protein: IFT46 is required for transport of outer dynein arms into flagella. *J Cell Biol*, 176, 653-65.

- HOU, Y. & WITMAN, G. B. 2017. The N-terminus of IFT46 mediates intraflagellar transport of outer arm dynein and its cargo-adaptor ODA16. *Mol Biol Cell*, 28, 2420-2433.
- HSU, Y. C., WILLOUGHBY, J. J., CHRISTENSEN, A. K. & JENSEN, A. M. 2006. Mosaic Eyes is a novel component of the Crumbs complex and negatively regulates photoreceptor apical size. *Development*, 133, 4849-59.
- HU, Q., MILENKOVIC, L., JIN, H., SCOTT, M. P., NACHURY, M. V., SPILIOTIS, E. T. & NELSON, W. J. 2010. A septin diffusion barrier at the base of the primary cilium maintains ciliary membrane protein distribution. *Science (New York, N.Y.)*, 329, 436-439.
- HUANG, B., BABCOCK, H. & ZHUANG, X. 2010. Breaking the diffraction barrier: super-resolution imaging of cells. *Cell*, 143, 1047-58.
- HUANG, B., WANG, W., BATES, M. & ZHUANG, X. 2008. Three-dimensional super-resolution imaging by stochastic optical reconstruction microscopy. *Science*, 319, 810-3.
- HUANG, L., SZYMANSKA, K., JENSEN, V. L., JANECKE, A. R., INNES, A. M., DAVIS, E. E., FROSK, P., LI, C., WILLER, J. R., CHODIRKER, B. N., GREENBERG, C. R., MCLEOD, D. R., BERNIER, F. P., CHUDLEY, A. E., MÜLLER, T., SHBOUL, M., LOGAN, C. V., LOUCKS, C. M., BEAULIEU, C. L., BOWIE, R. V., BELL, S. M., ADKINS, J., ZUNIGA, F. I., ROSS, K. D., WANG, J., BAN, M. R., BECKER, C., NÜRNBERG, P., DOUGLAS, S., CRAFT, C. M., AKIMENKO, M.-A., HEGELE, R. A., OBER, C., UTERMANN, G., BOLZ, H. J., BULMAN, D. E., KATSANIS, N., BLACQUE, O. E., DOHERTY, D., PARBOOSINGH, J. S., LEROUX, M. R., JOHNSON, C. A. & BOYCOTT, K. M. 2011. TMEM237 is mutated in individuals with a Joubert syndrome related disorder and expands the role of the TMEM family at the ciliary transition zone. *American journal of human genetics*, 89, 713-730.
- HUET, D., BLISNICK, T., PERROT, S. & BASTIN, P. 2014. The GTPase IFT27 is involved in both anterograde and retrograde intraflagellar transport. *Elife*, 3, e02419.
- HUPPKE, P., WEGENER, E., BOHRER-RABEL, H., BOLZ, H. J., ZOLL, B., GARTNER, J. & BERGMANN, C. 2015. Tectonic gene mutations in patients with Joubert syndrome. *Eur J Hum Genet*, 23, 616-20.
- HURD, T. W., GAO, L., ROH, M. H., MACARA, I. G. & MARGOLIS, B. 2003. Direct interaction of two polarity complexes implicated in epithelial tight junction assembly. *Nat Cell Biol*, 5, 137-42.
- ISHIKAWA, H., IDE, T., YAGI, T., JIANG, X., HIRONO, M., SASAKI, H., YANAGISAWA, H., WEMMER, K. A., STAINIER, D. Y., QIN, H., KAMIYA, R. & MARSHALL, W. F. 2014. Correction: TTC26/DYF13 is an intraflagellar transport protein required for transport of motility-related proteins into flagella. *Elife*, 3, e02897.
- ISHIKAWA, H. & MARSHALL, W. F. 2011. Ciliogenesis: building the cell's antenna. *Nature Reviews Molecular Cell Biology*, 12, 222-234.
- ISHIKAWA, H. & MARSHALL, W. F. 2015. Efficient live fluorescence imaging of intraflagellar transport in mammalian primary cilia. *Methods in Cilia & Flagella*, 127, 189-201.
- JENKINS, P. M., MCEWEN, D. P. & MARTENS, J. R. 2009. Olfactory cilia: linking sensory cilia function and human disease. *Chem Senses*, 34, 451-64.
- JENSEN, V. L., LI, C., BOWIE, R. V., CLARKE, L., MOHAN, S., BLACQUE, O. E. & LEROUX, M. R. 2015. Formation of the transition zone by Mks5/Rpgrip1L establishes a ciliary zone of exclusion (CIZE) that compartmentalises ciliary signalling proteins and controls PIP2 ciliary abundance. *EMBO J*, 34, 2537-56.
- JIANG, S. T., CHIOU, Y. Y., WANG, E., CHIEN, Y. L., HO, H. H., TSAI, F. J., LIN, C. Y., TSAI, S. P. & LI, H. 2009. Essential role of nephrocystin in photoreceptor intraflagellar transport in mouse. *Hum Mol Genet*, 18, 1566-77.
- JIANG, S. T., CHIOU, Y. Y., WANG, E., LIN, H. K., LEE, S. P., LU, H. Y., WANG, C. K., TANG, M. J. & LI, H. 2008. Targeted disruption of Nphp1 causes male infertility due to defects in the later steps of sperm morphogenesis in mice. *Hum Mol Genet*, 17, 3368-79.

- JIN, D., NI, T. T., SUN, J., WAN, H., AMACK, J. D., YU, G., FLEMING, J., CHIANG, C., LI, W., PAPIERNIAK, A., CHEEPALA, S., CONSEIL, G., COLE, S. P. C., ZHOU, B., DRUMMOND, I. A., SCHUETZ, J. D., MALICKI, J. & ZHONG, T. P. 2014. Prostaglandin signalling regulates ciliogenesis by modulating intraflagellar transport. *Nature Cell Biology*, 16, 841-851.
- JIN, H. & NACHURY, M. V. 2009. The BBSome. *Curr Biol*, 19, R472-3.
- JIN, H., WHITE, S. R., SHIDA, T., SCHULZ, S., AGUIAR, M., GYGI, S. P., BAZAN, J. F. & NACHURY, M. V. 2010. The conserved Bardet-Biedl syndrome proteins assemble a coat that traffics membrane proteins to cilia. *Cell*, 141, 1208-19.
- JURGENS, G., WIESCHAUS, E., NUSSLEIN-VOLHARD, C. & KLUDING, C. 1984. Mutations affecting the pattern of the larval cuticle in *Drosophila melanogaster*. *Roux Archiv. of Dev. Bio.*, 193, 283-295.
- KATOH, Y., TERADA, M., NISHIJIMA, Y., TAKEI, R., NOZAKI, S., HAMADA, H. & NAKAYAMA, K. 2016. Overall Architecture of the Intraflagellar Transport (IFT)-B Complex Containing Cluap1/IFT38 as an Essential Component of the IFT-B Peripheral Subcomplex. *J Biol Chem*, 291, 10962-75.
- KEADY, B. T., SAMTANI, R., TOBITA, K., TSUCHYA, M., SAN AGUSTIN, J. T., FOLLIT, J. A., JONASSEN, J. A., SUBRAMANIAN, R., LO, C. W. & PAZOUR, G. J. 2012. IFT25 links the signal-dependent movement of Hedgehog components to intraflagellar transport. *Dev Cell*, 22, 940-51.
- KEE, H. L., DISHINGER, J. F., BLASIUS, T. L., LIU, C. J., MARGOLIS, B. & VERHEY, K. J. 2012. A size-exclusion permeability barrier and nucleoporins characterize a ciliary pore complex that regulates transport into cilia. *Nature cell biology*, 14, 431-437.
- KEE, H. L. & VERHEY, K. J. 2013. Molecular connections between nuclear and ciliary import processes. *Cilia*, 2, 11.
- KENNEDY, B. & MALICKI, J. 2009. What drives cell morphogenesis: a look inside the vertebrate photoreceptor. *Dev Dyn*, 238, 2115-38.
- KENNEDY, M. B. 1995. Origin of PDZ (DHR, GLGF) domains. *Trends Biochem Sci*, 20, 350.
- KILBURN, C. L., PEARSON, C. G., ROMIJN, E. P., MEEHL, J. B., GIDDINGS, T. H., CULVER, B. P., YATES, J. R. & WINEY, M. 2007. New *Tetrahymena* basal body protein components identify basal body domain structure. *The Journal of cell biology*, 178, 905-912.
- KLIONSKY, D. J., ABDALLA, F. C., ABELIOVICH, H., ABRAHAM, R. T., ACEVEDO-AROZENA, A., ADELI, K., AGHOLME, L., AGNELLO, M., AGOSTINIS, P., AGUIRRE-GHISO, J. A., AHN, H. J., AIT-MOHAMED, O., AIT-SI-ALI, S., AKEMATSU, T., AKIRA, S., AL-YOUNES, H. M., AL-ZEER, M. A., ALBERT, M. L., ALBIN, R. L., ALEGRE-ABARRATEGUI, J., ALEO, M. F., ALIREZAEI, M., ALMASAN, A., ALMONTE-BECERRIL, M., AMANO, A., AMARAVADI, R., AMARNATH, S., AMER, A. O., ANDRIEU-ABADIE, N., ANANTHARAM, V., ANN, D. K., ANOOPKUMAR-DUKIE, S., AOKI, H., APOSTOLOVA, N., ARANCIA, G., ARIS, J. P., ASANUMA, K., ASARE, N. Y. O., ASHIDA, H., ASKANAS, V., ASKEW, D. S., AUBERGER, P., BABA, M., BACKUES, S. K., BAEHRECKE, E. H., BAHR, B. A., BAI, X.-Y., BAILLY, Y., BAIOCCHI, R., BALDINI, G., BALDUINI, W., BALLABIO, A., BAMBER, B. A., BAMPTON, E. T. W., BÁNHEGYI, G., BARTHOLOMEW, C. R., BASSHAM, D. C., BAST, R. C., BATOKO, H., BAY, B.-H., BEAU, I., BÉCHET, D. M., BEGLEY, T. J., BEHL, C., BEHREND, C., BEKRI, S., BELLAIRE, B., BENDALL, L. J., BENETTI, L., BERLIOCCI, L., BERNARDI, H., BERNASSOLA, F., BESTEIRO, S., BHATIA-KISSOVA, I., BI, X., BIARD-PIECHACZYK, M., BLUM, J. S., BOISE, L. H., BONALDO, P., BOONE, D. L., BORNHAUSER, B. C., BORTOLUCI, K. R., BOSSIS, I., BOST, F., BOURQUIN, J.-P., BOYA, P., BOYER-GUITTAUT, M., BOZHKO, P. V., BRADY, N. R., BRANCOLINI, C., BRECH, A.,

- BRENMAN, J. E., BRENNAND, A., BRESNICK, E. H., BREST, P., BRIDGES, D., BRISTOL, M. L., BROOKES, P. S., BROWN, E. J., BRUMELL, J. H., et al. 2012. Guidelines for the use and interpretation of assays for monitoring autophagy. *Autophagy*, 8, 445-544.
- KOK, F. O., SHIN, M., NI, C.-W., GUPTA, A., GROSSE, A. S., VAN IMPEL, A., KIRCHMAIER, B. C., PETERSON-MADURO, J., KOURKOULIS, G., MALE, I., DESANTIS, D. F., SHEPPARD-TINDELL, S., EBARASI, L., BETSHOLTZ, C., SCHULTE-MERKER, S., WOLFE, S. A. & LAWSON, N. D. 2015. Reverse genetic screening reveals poor correlation between morpholino-induced and mutant phenotypes in zebrafish. *Developmental cell*, 32, 97-108.
- KOZMINSKI, K. G., BEECH, P. L. & ROSENBAUM, J. L. 1995. The Chlamydomonas kinesin-like protein FLA10 is involved in motility associated with the flagellar membrane. *J Cell Biol*, 131, 1517-27.
- KRAMER-ZUCKER, A. G., OLALE, F., HAYCRAFT, C. J., YODER, B. K., SCHIER, A. F. & DRUMMOND, I. A. 2005. Cilia-driven fluid flow in the zebrafish pronephros, brain and Kupffer's vesicle is required for normal organogenesis. *Development*, 132, 1907-21.
- KROCK, B. L. & PERKINS, B. D. 2008. The intraflagellar transport protein IFT57 is required for cilia maintenance and regulates IFT-particle-kinesin-II dissociation in vertebrate photoreceptors. *J Cell Sci*, 121, 1907-15.
- LAMBACHER, N. J., BRUEL, A. L., VAN DAM, T. J., SZYMANSKA, K., SLAATS, G. G., KUHN, S., MCMANUS, G. J., KENNEDY, J. E., GAFF, K., WU, K. M., VAN DER LEE, R., BURGLIN, L., DOUMMAR, D., RIVIERE, J. B., FAIVRE, L., ATTIE-BITACH, T., SAUNIER, S., CURD, A., PECKHAM, M., GILES, R. H., JOHNSON, C. A., HUYNEN, M. A., THAUVIN-ROBINET, C. & BLACQUE, O. E. 2016. TMEM107 recruits ciliopathy proteins to subdomains of the ciliary transition zone and causes Joubert syndrome. *Nat Cell Biol*, 18, 122-31.
- LAU, L., LEE, Y. L., SAHL, S. J., STEARNS, T. & MOERNER, W. E. 2012. STED microscopy with optimized labeling density reveals 9-fold arrangement of a centriole protein. *Biophys J*, 102, 2926-35.
- LEAGUE, G. P. & NAM, S. C. 2011. Role of kinesin heavy chain in Crumbs localization along the rhabdomere elongation in Drosophila photoreceptor. *PLoS One*, 6, e21218.
- LECHTRECK, K. F., LURO, S., AWATA, J. & WITMAN, G. B. 2009. HA-tagging of putative flagellar proteins in Chlamydomonas reinhardtii identifies a novel protein of intraflagellar transport complex B. *Cell Motil Cytoskeleton*, 66, 469-82.
- LEE, E., HART, K., BURGESS, G., HALVERSON, G. R. & REID, M. E. 2006. Efficacy of murine monoclonal antibodies in RBC phenotyping of DAT-positive samples. *Immunohematology*, 22, 161-5.
- LEVENTEA, E., HAZIME, K., ZHAO, C. & MALICKI, J. 2016. Analysis of cilia structure and function in zebrafish. *Methods Cell Biol*, 133, 179-227.
- LIEW, G. M., YE, F., NAGER, A. R., MURPHY, J. P., LEE, J. S., AGUIAR, M., BRESLOW, D. K., GYGI, S. P. & NACHURY, M. V. 2014. The intraflagellar transport protein IFT27 promotes BBSome exit from cilia through the GTPase ARL6/BBS3. *Developmental cell*, 31, 265-278.
- LIM, R. Y. & FAHRENKROG, B. 2006. The nuclear pore complex up close. *Curr Opin Cell Biol*, 18, 342-7.
- LIN, Y. C., NIEWIADOMSKI, P., LIN, B., NAKAMURA, H., PHUA, S. C., JIAO, J., LEVCHENKO, A., INOUE, T., ROHATGI, R. & INOUE, T. 2013. Chemically inducible diffusion trap at cilia reveals molecular sieve-like barrier. *Nat Chem Biol*, 9, 437-43.
- LINDEMANN, C. B. & LESICH, K. A. 2010. Flagellar and ciliary beating: the proven and the possible. *Journal of cell science*, 123, 519-28.

- LOKTEV, A. V., ZHANG, Q., BECK, J. S., SEARBY, C. C., SCHEETZ, T. E., BAZAN, J. F., SLUSARSKI, D. C., SHEFFIELD, V. C., JACKSON, P. K. & NACHURY, M. V. 2008. A BBSome subunit links ciliogenesis, microtubule stability, and acetylation. *Developmental Cell*, 15, 854-65.
- LUCAS, J. S., BURGESS, A., MITCHISON, H. M., MOYA, E., WILLIAMSON, M., HOGG, C. & NATIONAL PCD SERVICE, U. K. 2014. Diagnosis and management of primary ciliary dyskinesia. *Arch Dis Child*, 99, 850-6.
- MAKAROVA, O., ROH, M. H., LIU, C. J., LAURINEC, S. & MARGOLIS, B. 2003. Mammalian Crumbs3 is a small transmembrane protein linked to protein associated with Lin-7 (Pals1). *Gene*, 302, 21-9.
- MALICKI, J. & DRIEVER, W. 1999. *oko meduzy* mutations affect neuronal patterning in the zebrafish retina and reveal cell-cell interactions of the retinal neuroepithelial sheet. *Development*, 126, 1235-1246.
- MALICKI, J., NEUHAUSS, S. C., SCHIER, A. F., SOLNICA-KREZEL, L., STEMPLE, D. L., STAINIER, D. Y., ABDELILAH, S., ZWARTKRUIS, F., RANGINI, Z. & DRIEVER, W. 1996a. Mutations affecting development of the zebrafish retina. *Development*, 123, 263-273.
- MALICKI, J., SCHIER, A. F., SOLNICA-KREZEL, L., STEMPLE, D. L., NEUHAUSS, S. C., STAINIER, D. Y., ABDELILAH, S., RANGINI, Z., ZWARTKRUIS, F. & DRIEVER, W. 1996b. Mutations affecting development of the zebrafish ear. *Development*, 123, 275-283.
- MALICKI, J. J. & JOHNSON, C. A. 2017. The Cilium: Cellular Antenna and Central Processing Unit. *Trends Cell Biol*, 27, 126-140.
- MCINTYRE, J. C., WILLIAMS, C. L. & MARTENS, J. R. 2013. Smelling the roses and seeing the light: gene therapy for ciliopathies. *Trends Biotechnol*, 31, 355-63.
- MCKINNEY, S. A., MURPHY, C. S., HAZELWOOD, K. L., DAVIDSON, M. W. & LOOGER, L. L. 2009. A bright and photostable photoconvertible fluorescent protein. *Nat Methods*, 6, 131-3.
- MENNELLA, V., KESZTHELYI, B., MCDONALD, K. L., CHHUN, B., KAN, F., ROGERS, G. C., HUANG, B. & AGARD, D. A. 2012. Subdiffraction-resolution fluorescence microscopy reveals a domain of the centrosome critical for pericentriolar material organization. *Nat Cell Biol*, 14, 1159-68.
- MERRIAM, E. V. & BRUNS, P. J. 1988. Phenotypic assortment in *Tetrahymena thermophila*: assortment kinetics of antibiotic-resistance markers, *tsA*, death, and the highly amplified rDNA locus. *Genetics*, 120, 389-95.
- MITCHISON, H. M. & VALENTE, E. M. 2017. Motile and non-motile cilia in human pathology: from function to phenotypes. *J Pathol*, 241, 294-309.
- MOLLET, G., SILBERMANN, F., DELOUS, M., SALOMON, R., ANTIGNAC, C. & SAUNIER, S. 2005. Characterization of the nephrocystin/nephrocystin-4 complex and subcellular localization of nephrocystin-4 to primary cilia and centrosomes. *Hum Mol Genet*, 14, 645-56.
- MOURAO, A., CHRISTENSEN, S. T. & LORENTZEN, E. 2016. The intraflagellar transport machinery in ciliary signaling. *Curr Opin Struct Biol*, 41, 98-108.
- MUKHOPADHYAY, S., WEN, X., CHIH, B., NELSON, C. D., LANE, W. S., SCALES, S. J. & JACKSON, P. K. 2010. TULP3 bridges the IFT-A complex and membrane phosphoinositides to promote trafficking of G protein-coupled receptors into primary cilia. *Genes Dev*, 24, 2180-93.
- NACHURY, M. V., LOKTEV, A. V., ZHANG, Q., WESTLAKE, C. J., PERANEN, J., MERDES, A., SLUSARSKI, D. C., SCHELLER, R. H., BAZAN, J. F., SHEFFIELD, V. C. & JACKSON, P. K. 2007. A core complex of BBS proteins cooperates with the GTPase Rab8 to promote ciliary membrane biogenesis. *Cell*, 129, 1201-13.
- NACHURY, M. V., SEELEY, E. S. & JIN, H. 2010. Trafficking to the Ciliary Membrane: How to Get Across the Periciliary Diffusion Barrier? *Annual review of cell and developmental biology*, 26, 59-87.

- NAHIDIAZAR, L., AGRONSKAIA, A. V., BROERTJES, J., VAN DEN BROEK, B. & JALINK, K. 2016. Optimizing Imaging Conditions for Demanding Multi-Color Super Resolution Localization Microscopy. *PLoS One*, 11, e0158884.
- NAJAFI, M. & CALVERT, P. D. 2012. Transport and localization of signaling proteins in ciliated cells. *Vision research*, 75, 11-18.
- NISHIMURA, T., KATO, K., YAMAGUCHI, T., FUKATA, Y., OHNO, S. & KAIBUCHI, K. 2004. Role of the PAR-3-KIF3 complex in the establishment of neuronal polarity. *Nature cell biology*, 6, 328-334.
- NOVARINO, G., AKIZU, N. & GLEESON, J. G. 2011. Modeling human disease in humans: the ciliopathies. *Cell*, 147, 70-9.
- OLIVIER, N., KELLER, D., RAJAN, V. S., GONCZY, P. & MANLEY, S. 2013. Simple buffers for 3D STORM microscopy. *Biomed Opt Express*, 4, 885-99.
- OMORI, Y. & MALICKI, J. 2006. *oko meduzy* and Related crumbs Genes Are Determinants of Apical Cell Features in the Vertebrate Embryo. *Current Biology*, 16, 945-57.
- ORIAS, E., CERVANTES, M. D. & HAMILTON, E. P. 2011. *Tetrahymena thermophila*, a unicellular eukaryote with separate germline and somatic genomes. *Res Microbiol*, 162, 578-86.
- OTT, C. & LIPPINCOTT-SCHWARTZ, J. 2012. Visualization of live primary cilia dynamics using fluorescence microscopy. *Curr Protoc Cell Biol*, Chapter 4, Unit 4 26.
- OU, G., BLACQUE, O. E., SNOW, J. J., LEROUX, M. R. & SCHOLEY, J. M. 2005. Functional coordination of intraflagellar transport motors. *Nature*, 436, 583-7.
- PAZOUR, G. J., AGRIN, N., LESZYK, J. & WITMAN, G. B. 2005. Proteomic analysis of a eukaryotic cilium. *J Cell Biol*, 170, 103-13.
- PAZOUR, G. J., DICKERT, B. L. & WITMAN, G. B. 1999. The DHC1b (DHC2) isoform of cytoplasmic dynein is required for flagellar assembly. *J Cell Biol*, 144, 473-81.
- PEDERSEN, L. B. & ROSENBAUM, J. L. 2008. Chapter Two Intraflagellar Transport (IFT) Role in Ciliary Assembly, Resorption and Signalling. *Curr Top Dev Biol*, 85, 23-61.
- PELLIKKA, M., TANENTZAPF, G., PINTO, M., SMITH, C., MCGLADE, C. J., READY, D. F. & TEPASS, U. 2002. Crumbs, the *Drosophila* homologue of human CRB1/RP12, is essential for photoreceptor morphogenesis. *Nature*, 416, 143-9.
- PFEFFER, U., FERRARI, N., TOSETTI, F. & VIDALI, G. 1989. Histone acetylation in conjugating *Tetrahymena thermophila*. *J Cell Biol*, 109, 1007-14.
- PIGINO, G., GEIMER, S., LANZAVECCHIA, S., PACCAGNINI, E., CANTELE, F., DIENER, D. R., ROSENBAUM, J. L. & LUPETTI, P. 2009. Electron-tomographic analysis of intraflagellar transport particle trains in situ. *J Cell Biol*, 187, 135-48.
- PLEINER, T., BATES, M., TRAKHANOV, S., LEE, C. T., SCHLIEP, J. E., CHUG, H., BOHNING, M., STARK, H., URLAUB, H. & GORLICH, D. 2015. Nanobodies: site-specific labeling for super-resolution imaging, rapid epitope-mapping and native protein complex isolation. *Elife*, 4, e11349.
- POORANACHANDRAN, N. & MALICKI, J. 2015. Genetic analysis of ciliary kinesins in vertebrate sensory neurons. *Genetics*.
- POORANACHANDRAN, N. & MALICKI, J. J. 2016. Unexpected Roles for Ciliary Kinesins and Intraflagellar Transport Proteins. *Genetics*, 203, 771-85.
- PREVO, B., MANGEOL, P., OSWALD, F., SCHOLEY, J. M. & PETERMAN, E. J. G. 2015. Functional differentiation of cooperating kinesin-2 motors orchestrates cargo import and transport in *C. elegans* cilia. *Nature cell biology*, 17, 1536-1545.
- PREVO, B., SCHOLEY, J. M. & PETERMAN, E. J. G. 2017. Intraflagellar transport: mechanisms of motor action, cooperation, and cargo delivery. *FEBS J*, 284, 2905-2931.
- PUGACHEVA, E. N., JABLONSKI, S. A., HARTMAN, T. R., HENSKE, E. P. & GOLEMIS, E. A. 2007. HEF1-dependent Aurora A activation induces disassembly of the primary cilium. *Cell*, 129, 1351-63.

- QIN, H., DIENER, D. R., GEIMER, S., COLE, D. G. & ROSENBAUM, J. L. 2004. Intraflagellar transport (IFT) cargo: IFT transports flagellar precursors to the tip and turnover products to the cell body. *J Cell Biol*, 164, 255-66.
- REITER, J. F., BLACQUE, O. E. & LEROUX, M. R. 2012. The base of the cilium: roles for transition fibres and the transition zone in ciliary formation, maintenance and compartmentalization. *EMBO Rep*, 13, 608-18.
- RIES, J., KAPLAN, C., PLATONOVA, E., EGHLIDI, H. & EWERS, H. 2012. A simple, versatile method for GFP-based super-resolution microscopy via nanobodies. *Nat Methods*, 9, 582-4.
- RINGO, D. L. 1967. Flagellar motion and fine structure of the flagellar apparatus in *Chlamydomonas*. *The Journal of cell biology*, 33, 543-571.
- ROBERSON, E. C., DOWDLE, W. E., OZANTURK, A., GARCIA-GONZALO, F. R., LI, C., HALBRITTER, J., ELKHARTOUFI, N., PORATH, J. D., COPE, H., ASHLEY-KOCH, A., GREGORY, S., THOMAS, S., SAYER, J. A., SAUNIER, S., OTTO, E. A., KATSANIS, N., DAVIS, E. E., ATTIE-BITACH, T., HILDEBRANDT, F., LEROUX, M. R. & REITER, J. F. 2015. TMEM231, mutated in orofacioidigital and Meckel syndromes, organizes the ciliary transition zone. *J Cell Biol*, 209, 129-42.
- ROGOWSKI, M., SCHOLZ, D. & GEIMER, S. 2013. Electron microscopy of flagella, primary cilia, and intraflagellar transport in flat-embedded cells. *Methods Enzymol*, 524, 243-63.
- ROSENBAUM, J. L. & CARLSON, K. 1969. Cilia regeneration in *Tetrahymena* and its inhibition by colchicine. *J Cell Biol*, 40, 415-25.
- RUST, M. J., BATES, M. & ZHUANG, X. 2006. Sub-diffraction-limit imaging by stochastic optical reconstruction microscopy (STORM). *Nat Methods*, 3, 793-5.
- SANG, L., MILLER, J. J., CORBIT, K. C., GILES, R. H., BRAUER, M. J., OTTO, E. A., BAYE, L. M., WEN, X., SCALES, S. J., KWONG, M., HUNTZICKER, E. G., SFAKIANOS, M. K., SANDOVAL, W., BAZAN, J. F., KULKARNI, P., GARCIA-GONZALO, F. R., SEOL, A. D., O'TOOLE, J. F., HELD, S., REUTTER, H. M., LANE, W. S., RAFIQ, M. A., NOOR, A., ANSAR, M., DEVI, A. R., SHEFFIELD, V. C., SLUSARSKI, D. C., VINCENT, J. B., DOHERTY, D. A., HILDEBRANDT, F., REITER, J. F. & JACKSON, P. K. 2011. Mapping the NPHP-JBTS-MKS protein network reveals ciliopathy disease genes and pathways. *Cell*, 145, 513-28.
- SAPHIRE, E. O., PARREN, P. W., PANTOPHLET, R., ZWICK, M. B., MORRIS, G. M., RUDD, P. M., DWEK, R. A., STANFIELD, R. L., BURTON, D. R. & WILSON, I. A. 2001. Crystal structure of a neutralizing human IGG against HIV-1: a template for vaccine design. *Science*, 293, 1155-9.
- SATO, T., IWANO, T., KUNII, M., MATSUDA, S., MIZUGUCHI, R., JUNG, Y., HAGIWARA, H., YOSHIHARA, Y., YUZAKI, M., HARADA, R. & HARADA, A. 2014. Rab8a and Rab8b are essential for several apical transport pathways but insufficient for ciliogenesis. *Journal of Cell Science*, 127, 422-431.
- SCHERMELLEH, L., HEINTZMANN, R. & LEONHARDT, H. 2010. A guide to super-resolution fluorescence microscopy. *J Cell Biol*, 190, 165-75.
- SCHMIDT, K. N., KUHNS, S., NEUNER, A., HUB, B., ZENTGRAF, H. & PEREIRA, G. 2012. Cep164 mediates vesicular docking to the mother centriole during early steps of ciliogenesis. *The Journal of cell biology*, 199, 1083-1101.
- SCHOLEY, J. M. 2003. Intraflagellar transport. *Annu Rev Cell Dev Biol*, 19, 423-43.
- SCHOLEY, J. M. 2013. Kinesin-2: A Family of Heterotrimeric and Homodimeric Motors with Diverse Intracellular Transport Functions. *Annual review of cell and developmental biology*.
- SCHOLEY, J. M. & ANDERSON, K. V. 2006. Intraflagellar transport and cilium-based signaling. *Cell*, 125, 439-42.
- SCHOU, K. B., PEDERSEN, L. B. & CHRISTENSEN, S. T. 2015. Ins and outs of GPCR signaling in primary cilia. *EMBO reports*.

- SEDMAK, T. & WOLFRUM, U. 2010. Intraflagellar transport molecules in ciliary and nonciliary cells of the retina. *The Journal of cell biology*, 189, 171-186.
- SERWAS, D., SU, T. Y., ROESSLER, M., WANG, S. & DAMMERMANN, A. 2017. Centrioles initiate cilia assembly but are dispensable for maturation and maintenance in *C. elegans*. *J Cell Biol*, 216, 1659-1671.
- SFAKIANOS, J., TOGAWA, A., MADAY, S., HULL, M., PYPAERT, M., CANTLEY, L., TOOMRE, D. & MELLMAN, I. 2007. Par3 functions in the biogenesis of the primary cilium in polarized epithelial cells. *The Journal of cell biology*, 179, 1133-1140.
- SHAHEEN, R., ANSARI, S., MARDAWI, E. A., ALSHAMMARI, M. J. & ALKURAYA, F. S. 2013. Mutations in TMEM231 cause Meckel-Gruber syndrome. *J Med Genet*, 50, 160-2.
- SHAHEEN, R., SCHMIDTS, M., FAQEIH, E., HASHEM, A., LAUSCH, E., HOLDER, I., SUPERTI-FURGA, A., CONSORTIUM, U. K., MITCHISON, H. M., ALMOISHEER, A., ALAMRO, R., ALSHIDDI, T., ALZAHIRANI, F., BEALES, P. L. & ALKURAYA, F. S. 2015. A founder CEP120 mutation in Jeune asphyxiating thoracic dystrophy expands the role of centriolar proteins in skeletal ciliopathies. *Hum Mol Genet*, 24, 1410-9.
- SHI, X., GARCIA, G., 3RD, VAN DE WEGHE, J. C., MCGORTY, R., PAZOUR, G. J., DOHERTY, D., HUANG, B. & REITER, J. F. 2017. Super-resolution microscopy reveals that disruption of ciliary transition-zone architecture causes Joubert syndrome. *Nat Cell Biol*, 19, 1178-1188.
- SIEBER, J. J., WILLIG, K. I., KUTZNER, C., GERDING-REIMERS, C., HARKE, B., DONNERT, G., RAMMNER, B., EGGELING, C., HELL, S. W., GRUBMULLER, H. & LANG, T. 2007. Anatomy and dynamics of a supramolecular membrane protein cluster. *Science*, 317, 1072-6.
- SILVERMAN, M. A. & LEROUX, M. R. 2009. Intraflagellar transport and the generation of dynamic, structurally and functionally diverse cilia. *Trends Cell Biol*, 19, 306-16.
- SINGLA, V., ROMAGUERA-ROS, M., GARCIA-VERDUGO, J. M. & REITER, J. F. 2010. *Odf1*, a human disease gene, regulates the length and distal structure of centrioles. *Dev Cell*, 18, 410-24.
- SLAATS, G. G., GHOSH, A. K., FALKE, L. L., LE CORRE, S., SHALTIEL, I. A., VAN DE HOEK, G., KLASSON, T. D., STOKMAN, M. F., LOGISTER, I., VERHAAR, M. C., GOLDSCHMEDING, R., NGUYEN, T. Q., DRUMMOND, I. A., HILDEBRANDT, F. & GILES, R. H. 2014. Nephronophthisis-associated CEP164 regulates cell cycle progression, apoptosis and epithelial-to-mesenchymal transition. *PLoS Genet*, 10, e1004594.
- SNOW, J. J., OU, G., GUNNARSON, A. L., WALKER, M. R., ZHOU, H. M., BRUST-MASCHER, I. & SCHOLEY, J. M. 2004. Two anterograde intraflagellar transport motors cooperate to build sensory cilia on *C. elegans* neurons. *Nat Cell Biol*, 6, 1109-13.
- SOROKIN, S. 1962. Centrioles and the formation of rudimentary cilia by fibroblasts and smooth muscle cells. *The Journal of cell biology*, 15, 363-77.
- STEPANEK, L. & PIGINO, G. 2016. Microtubule doublets are double-track railways for intraflagellar transport trains. *Science*, 352, 721-4.
- SZYMANIAK, A. D., MAHONEY, J. E., CARDOSO, W. V. & VARELAS, X. 2015. Crumbs3-Mediated Polarity Directs Airway Epithelial Cell Fate through the Hippo Pathway Effector Yap. *Dev Cell*, 34, 283-96.
- SZYMANSKA, K. & JOHNSON, C. A. 2012. The transition zone: an essential functional compartment of cilia. *Cilia*, 1, 10.
- SZYMBORSKA, A., DE MARCO, A., DAIGLE, N., CORDES, V. C., BRIGGS, J. A. G. & ELLENBERG, J. 2013. Nuclear pore scaffold structure analyzed by super-resolution microscopy and particle averaging. *Science (New York, N.Y.)*, 341, 655-658.
- TAKAO, D., DISHINGER, J. F., KEE, H. L., PINSKEY, J. M., ALLEN, B. L. & VERHEY, K. J. 2014. An Assay for Clogging the Ciliary Pore Complex Distinguishes Mechanisms of Cytosolic and Membrane Protein Entry. *Current Biology*, 24, 2288-2294.

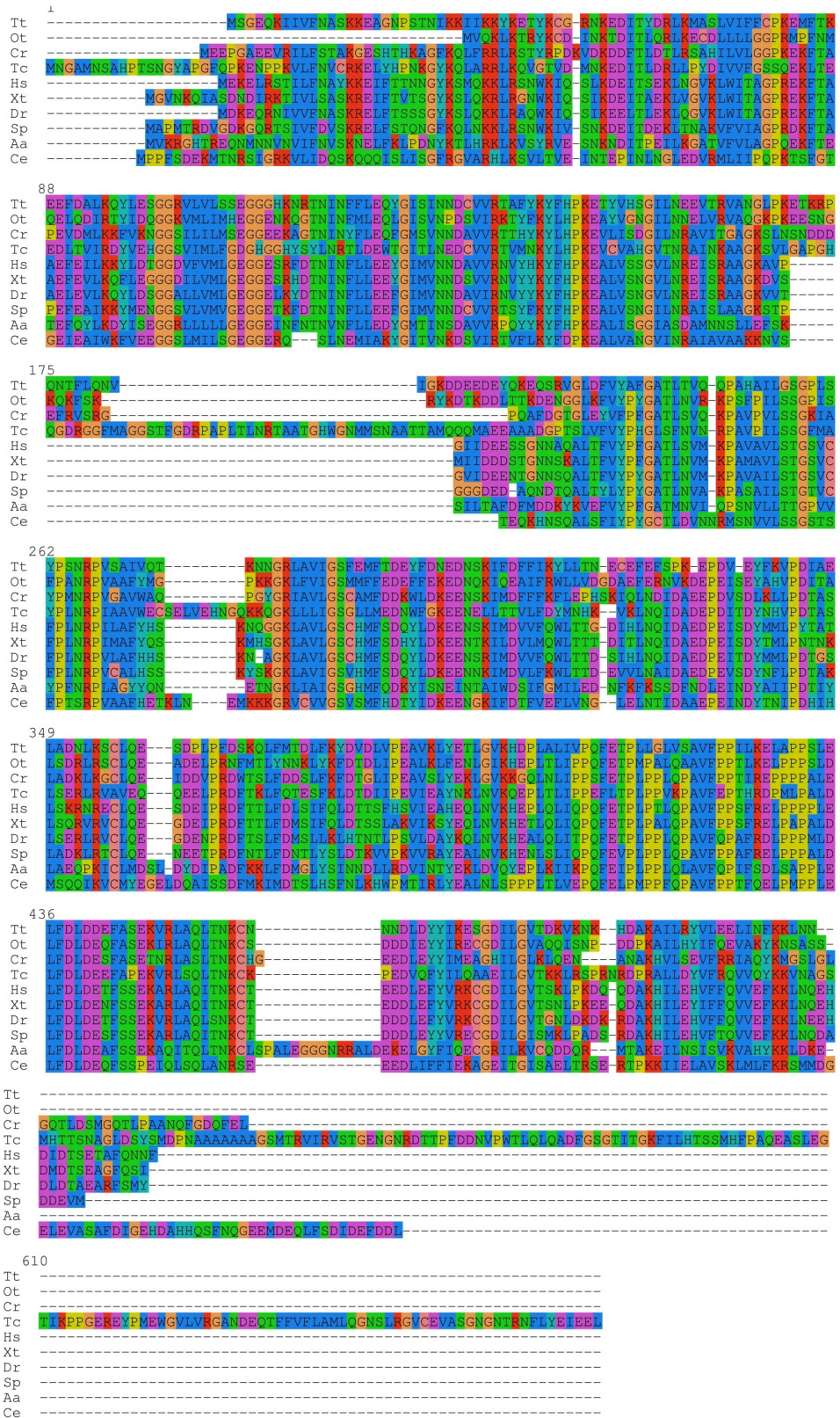
- TAKAO, D. & VERHEY, K. J. 2016. Gated entry into the ciliary compartment. *Cell Mol Life Sci*, 73, 119-27.
- TAKAO, D., WANG, L., BOSS, A. & VERHEY, K. J. 2017. Protein Interaction Analysis Provides a Map of the Spatial and Temporal Organization of the Ciliary Gating Zone. *Curr Biol*, 27, 2296-2306 e3.
- TANENTZAPF, G. & TEPASS, U. 2003. Interactions between the crumbs, lethal giant larvae and bazooka pathways in epithelial polarization. *Nat Cell Biol*, 5, 46-52.
- TANOS, B. E., YANG, H. J., SONI, R., WANG, W. J., MACALUSO, F. P., ASARA, J. M. & TSOU, M. F. 2013. Centriole distal appendages promote membrane docking, leading to cilia initiation. *Genes Dev*, 27, 163-8.
- TASCHNER, M., BHOGARAJU, S., VETTER, M., MORAWETZ, M. & LORENTZEN, E. 2011. Biochemical Mapping of Interactions within the Intraflagellar Transport (IFT) B Core Complex: IFT52 BINDS DIRECTLY TO FOUR OTHER IFT-B SUBUNITS. *The Journal of Biological Chemistry*, 286, 26344-26352.
- TASCHNER, M., KOTSIS, F., BRAEUER, P., KUEHN, E. W. & LORENTZEN, E. 2014. Crystal structures of IFT70/52 and IFT52/46 provide insight into intraflagellar transport B core complex assembly. *J Cell Biol*, 207, 269-82.
- TASCHNER, M., MOURAO, A., AWASTHI, M., BASQUIN, J. & LORENTZEN, E. 2017. Structural basis of outer dynein arm intraflagellar transport by the transport adaptor protein ODA16 and the intraflagellar transport protein IFT46. *J Biol Chem*, 292, 7462-7473.
- TASCHNER, M., WEBER, K., MOURAO, A., VETTER, M., AWASTHI, M., STIEGLER, M., BHOGARAJU, S. & LORENTZEN, E. 2016. Intraflagellar transport proteins 172, 80, 57, 54, 38, and 20 form a stable tubulin-binding IFT-B2 complex. *EMBO J*, 35, 773-90.
- TEPASS, U. & KNUST, E. 1990. Phenotypic and developmental analysis of mutations at the crumbs locus, a gene required for the development of epithelia in *Drosophila melanogaster*. *Roux Arch Dev Biol*, 199, 189-206.
- THAUVIN-ROBINET, C., LEE, J. S., LOPEZ, E., HERRANZ-PEREZ, V., SHIDA, T., FRANCO, B., JEGO, L., YE, F., PASQUIER, L., LOGET, P., GIGOT, N., ARAL, B., LOPES, C. A., ST-ONGE, J., BRUEL, A. L., THEVENON, J., GONZALEZ-GRANERO, S., ALBY, C., MUNNICH, A., VEKEMANS, M., HUET, F., FRY, A. M., SAUNIER, S., RIVIERE, J. B., ATTIE-BITACH, T., GARCIA-VERDUGO, J. M., FAIVRE, L., MEGARBANE, A. & NACHURY, M. V. 2014. The oral-facial-digital syndrome gene C2CD3 encodes a positive regulator of centriole elongation. *Nat Genet*, 46, 905-11.
- THOMPSON, R. E., LARSON, D. R. & WEBB, W. W. 2002. Precise nanometer localization analysis for individual fluorescent probes. *Biophys J*, 82, 2775-83.
- TSAO, C.-C. & GOROVSKY, M. A. 2008. Different effects of Tetrahymena IFT172 domains on anterograde and retrograde intraflagellar transport. *Molecular biology of the cell*, 19, 1450-1461.
- TSUJIKAWA, M. & MALICKI, J. 2004. Intraflagellar transport genes are essential for differentiation and survival of vertebrate sensory neurons. *Neuron*, 42, 703-16.
- VALENTE, E. M., LOGAN, C. V., MOUGOU-ZERELLI, S., LEE, J. H., SILHAVY, J. L., BRANCATI, F., IANNICELLI, M., TRAVAGLINI, L., ROMANI, S., ILLI, B., ADAMS, M., SZYMANSKA, K., MAZZOTTA, A., LEE, J. E., TOLENTINO, J. C., SWISTUN, D., SALPIETRO, C. D., FEDE, C., GABRIEL, S., RUSS, C., CIBULSKIS, K., SOUGNEZ, C., HILDEBRANDT, F., OTTO, E. A., HELD, S., DIPLAS, B. H., DAVIS, E. E., MIKULA, M., STROM, C. M., BEN-ZEEV, B., LEV, D., SAGIE, T. L., MICHELSON, M., YARON, Y., KRAUSE, A., BOLTSHAUSER, E., ELKHARTOUFI, N., ROUME, J., SHALEV, S., MUNNICH, A., SAUNIER, S., INGLEHEARN, C., SAAD, A., ALKINDY, A., THOMAS, S., VEKEMANS, M., DALLAPICCOLA, B., KATSANIS, N., JOHNSON, C. A., ATTIE-BITACH, T. & GLEESON, J. G. 2010. Mutations in TMEM216 perturb ciliogenesis and cause Joubert, Meckel and related syndromes. *Nat Genet*.

- VALENTE, E. M., ROSTI, R. O., GIBBS, E. & GLEESON, J. G. 2014. Primary cilia in neurodevelopmental disorders. *Nat Rev Neurol*, 10, 27-36.
- VAN DEN HURK, J. A., RASHBASS, P., ROEPMAN, R., DAVIS, J., VOESENEK, K. E., ARENDS, M. L., ZONNEVELD, M. N., VAN ROEKEL, M. H., CAMERON, K., ROHRSCHEIDER, K., HECKENLIVELY, J. R., KOENENKOP, R. K., HOYNG, C. B., CREMERS, F. P. & DEN HOLLANDER, A. I. 2005. Characterization of the Crumbs homolog 2 (CRB2) gene and analysis of its role in retinitis pigmentosa and Leber congenital amaurosis. *Mol Vis*, 11, 263-73.
- VONDERFECHT, T., STEMM-WOLF, A. J., HENDERSHOTT, M., GIDDINGS, T. H., JR., MEEHL, J. B. & WINEY, M. 2011. The two domains of centrin have distinct basal body functions in Tetrahymena. *Mol Biol Cell*, 22, 2221-34.
- WANG, L., AMPHLETT, G., BLATTLER, W. A., LAMBERT, J. M. & ZHANG, W. 2005. Structural characterization of the maytansinoid-monoclonal antibody immunoconjugate, huN901-DM1, by mass spectrometry. *Protein Sci*, 14, 2436-46.
- WANG, Z., FAN, Z. C., WILLIAMSON, S. M. & QIN, H. 2009. Intraflagellar transport (IFT) protein IFT25 is a phosphoprotein component of IFT complex B and physically interacts with IFT27 in Chlamydomonas. *PLoS One*, 4, e5384.
- WANNER, A., SALATHE, M. & O'RIORDAN, T. G. 1996. Mucociliary clearance in the airways. *Am J Respir Crit Care Med*, 154, 1868-902.
- WEATHERBEE, S. D., NISWANDER, L. A. & ANDERSON, K. V. 2009. A mouse model for Meckel syndrome reveals Mks1 is required for ciliogenesis and Hedgehog signaling. *Hum Mol Genet*, 18, 4565-75.
- WEI, Q., XU, Q., ZHANG, Y., LI, Y., ZHANG, Q., HU, Z., HARRIS, P. C., TORRES, V. E., LING, K. & HU, J. 2013. Transition fibre protein FBF1 is required for the ciliary entry of assembled intraflagellar transport complexes. *Nature communications*, 4, 2750.
- WEI, Q., ZHANG, Y., LI, Y., ZHANG, Q., LING, K. & HU, J. 2012. The BBSome controls IFT assembly and turnaround in cilia. *Nature cell biology*, 14, 950-7.
- WEI, X. & MALICKI, J. 2002. *nagie oko*, encoding a MAGUK-family protein, is essential for cellular patterning of the retina. *Nature Genetics*, 31, 150-157.
- WHITEMAN, E. L., FAN, S., HARDER, J. L., WALTON, K. D., LIU, C. J., SOOFI, A., FOGG, V. C., HERSHENSON, M. B., DRESSLER, G. R., DEUTSCH, G. H., GUMUCIO, D. L. & MARGOLIS, B. 2014. Crumbs3 is essential for proper epithelial development and viability. *Mol Cell Biol*, 34, 43-56.
- WIEDENMANN, J., IVANCHENKO, S., OSWALD, F., SCHMITT, F., RÖCKER, C., SALIH, A., SPINDLER, K.-D. & NIENHAUS, G. U. 2004. EosFP, a fluorescent marker protein with UV-inducible green-to-red fluorescence conversion. *PNAS*, 101, 15905-15910.
- WILLIAMS, C. L., LI, C., KIDA, K., INGLIS, P. N., MOHAN, S., SEMENEC, L., BIALAS, N. J., STUPAY, R. M., CHEN, N., BLACQUE, O. E., YODER, B. K. & LEROUX, M. R. 2011. MKS and NPHP modules cooperate to establish basal body/transition zone membrane associations and ciliary gate function during ciliogenesis. *The Journal of cell biology*, 192, 1023-41.
- WILLIAMS, C. L., WINKELBAUER, M. E., SCHAFER, J. C., MICHAUD, E. J. & YODER, B. K. 2008. Functional Redundancy of the B9 Proteins and Nephrocystins in *Caenorhabditis elegans* Ciliogenesis. *Mol Biol Cell*, 19, 2154-2168.
- WODARZ, A., HINZ, U., ENGELBERT, M. & KNUST, E. 1995. Expression of crumbs confers apical character on plasma membrane domains of ectodermal epithelia of *Drosophila*. *Cell*, 82, 67-76.
- WON, J., MARÍN DE EVSIKOVA, C., SMITH, R. S., HICKS, W. L., EDWARDS, M. M., LONGO-GUESS, C., LI, T., NAGGERT, J. K. & NISHINA, P. M. 2011. NPHP4 is necessary for normal photoreceptor ribbon synapse maintenance and outer segment formation, and for sperm development. *Human Molecular Genetics*, 20, 482-496.

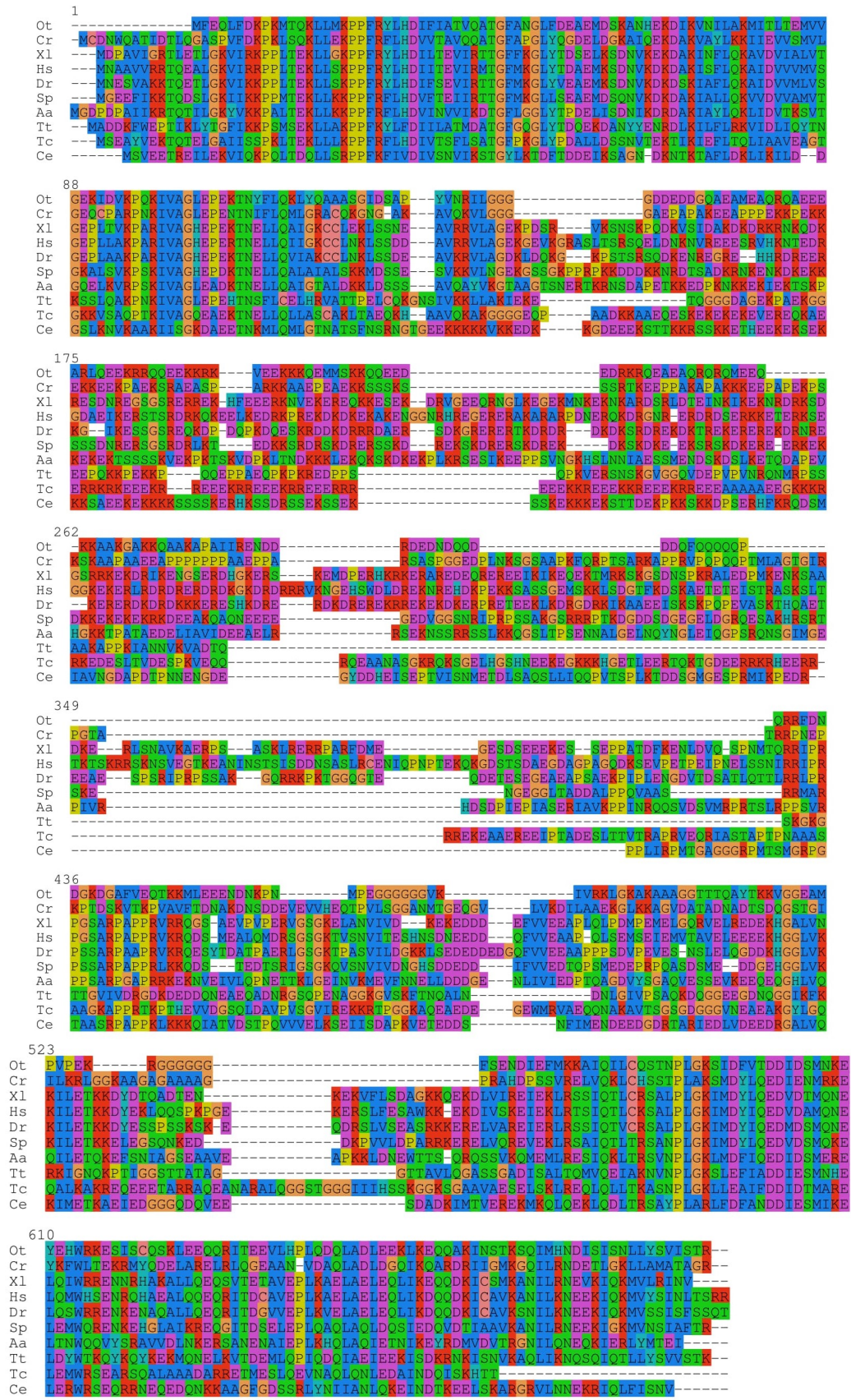
- YAN, J., WANG, P., ZHU, M., LI, G., ROMAO, E., XIONG, S. & WAN, Y. 2015. Characterization and applications of Nanobodies against human procalcitonin selected from a novel naive Nanobody phage display library. *J Nanobiotechnology*, 13, 33.
- YANG, T. T., CHING, W., WANG, W., MAZO, G., TANOS, B., CHEN, Z., THI TRAN, M., CHEN, Y., WENG, R., HUANG, C., JANE, W., TSOU, M., & LIAO, J. Architecture of mammalian centriole distal appendages accommodates distinct blade and matrix functional elements. *BioRxiv*. doi: <https://doi.org/10.1101/193474>.
- YANG, T. T., SU, J., WANG, W. J., CRAIGE, B., WITMAN, G. B., TSOU, M. F. & LIAO, J. C. 2015. Superresolution Pattern Recognition Reveals the Architectural Map of the Ciliary Transition Zone. *Sci Rep*, 5, 14096.
- YE, X., ZENG, H., NING, G., REITER, J. F. & LIU, A. 2014. C2cd3 is critical for centriolar distal appendage assembly and ciliary vesicle docking in mammals. *Proceedings of the National Academy of Sciences*, 111, 2164-2169.
- YEE, L. E., GARCIA-GONZALO, F. R., BOWIE, R. V., LI, C., KENNEDY, J. K., ASHRAFI, K., BLACQUE, O. E., LEROUX, M. R. & REITER, J. F. 2015. Conserved Genetic Interactions between Ciliopathy Complexes Cooperatively Support Ciliogenesis and Ciliary Signaling. *PLoS Genet*, 11, e1005627.
- YING, G., GERSTNER, C. D., FREDERICK, J. M., BOYE, S. L., HAUSWIRTH, W. W. & BAEHR, W. 2016. Small GTPases Rab8a and Rab11a Are Dispensable for Rhodopsin Transport in Mouse Photoreceptors. *PLoS One*, 11, e0161236.
- ZAGHLOUL, N. A. & KATSANIS, N. 2009. Mechanistic insights into Bardet-Biedl syndrome, a model ciliopathy. *J Clin Invest*, 119, 428-37.
- ZHANG, Y., KWON, S., YAMAGUCHI, T., CUBIZOLLES, F., ROUSSEAU, S., KNEISSEL, M., CAO, C., LI, N., CHENG, H. L., CHUA, K., LOMBARD, D., MIZERACKI, A., MATTHIAS, G., ALT, F. W., KHOCHBIN, S. & MATTHIAS, P. 2008. Mice Lacking Histone Deacetylase 6 Have Hyperacetylated Tubulin but Are Viable and Develop Normally. *Molecular and cellular biology*, 28, 1688-1701.
- ZHAO, C. & MALICKI, J. 2011. Nephrocystins and MKS proteins interact with IFT particle and facilitate transport of selected ciliary cargos. *EMBO J*, 30, 2532-44.
- ZHAO, C., OMORI, Y., BRODOWSKA, K., KOVACH, P. & MALICKI, J. 2012. Kinesin-2 family in vertebrate ciliogenesis. *PNAS*, 109, 2388-93.
- ZHU, B., ZHU, X., WANG, L., LIANG, Y., FENG, Q. & PAN, J. 2017. Functional exploration of the IFT-A complex in intraflagellar transport and ciliogenesis. *PLoS Genet*, 13, e1006627.
- ZOU, J., WANG, X. & WEI, X. 2012. Crb apical polarity proteins maintain zebrafish retinal cone mosaics via intercellular binding of their extracellular domains. *Developmental Cell*, 22, 1261-74.
- ZU, Y., TONG, X., WANG, Z., LIU, D., PAN, R., LI, Z., HU, Y., LUO, Z., HUANG, P., WU, Q., ZHU, Z., ZHANG, B. & LIN, S. 2013. TALEN-mediated precise genome modification by homologous recombination in zebrafish. *Nature methods*.

APPENDIX – Examples of alignments for some proteins using serial cloner

Alignment for IFT52



Alignment for IFT54



Alignment for IFT144

1	
Hs	-----MKRIFSLLEKTTWIGAPITQFAWKKT-----GGNYLAVTGADYIVKIFDRHGQKRS
Xl	-----MKRVFSLTEKSLIGYPHYAWORN-----LGNVIYAVTGDVHTVKIYDRHGQKDD
Dr	-----MKRVFTLSEKSWSGSCLQYKWKKT-----VGNYLAVAGPDNLVKIFDRHGQKVN
Sp	-----MKRVFQLTDKTHGPGPLRFECWQTT-----LGNYLATYGSDDNVHVIYDRHGERRD
Aa	-----MSGDKVLYRNEEPHGQGDVYFLWQTGGSAQLMASTGSDGTAVAVFNRQGLLVE
Tt	-----MASSKKVFEFKDLDLNGSGKVLFSWSQD-----CSYIYAVCGQSKVYVYVLDKRGRKLE
Ot	-----MISSEKAKNIFTYTEPDLGYGTVCSAWSQD-----GNFIVAVGENRVIIRILDROKRGIL
Tc	MLVAIVLFFSSLSLSCLIPKFFLIRLCLIVVCFKMGVQKKFELSTKELGGVILFSWSSS-----GTQLAVYSANGKLOILSPDGKLLN
Cr	-----MKKLFQVGPDLIGDGKVLFEWSPK-----GNFLAAAGSKRKNVIFDRNGRLYD
Ce	MSLKVIPCTLTKNQEVFKCVSAQLQYRRGEEEHGSGPLIHRWFPN-----GHTVAVACANNTVIYYDKKGNVID
88	
Hs	EINLPG-----NCVAMDWDKGDVLAIVAEKSSCIYLWDANTNKTSQLDNG-----MRDQMSFLLWSKVGSLFVAVGTVXGNLL
Xl	EINLPG-----VCFALDWDKDGNALAMVADRSSSIYMWDPNCTKTSQLDSSG-----MRDQMSFLLWSKAGSLLAVGTSTKGSLL
Dr	ELILPG-----NCVSLDWDKGDILAVIAEKSSSVYLWDANVNKTSQLDSSG-----MRDQMSFLLWSKTPGLLAVGTSTKGNLL
Sp	EINLPG-----SCTGIGWDKGDILALICDKSSVYVFLWDANVHRKTSQVDSG-----FKDILTLYLLWSKSGPQLAIGTVKGNLL
Aa	RIVLQG-----LCAGFAWDKGDVLAITQSSPOLIVWDSNSQKQHVHDIG-----LRDPPSCIITWSTRNLLAVATSRGNLS
Tt	ETVLKS-----KKNVIGLEWDDKDEFLAILQENSTCFLWNVFNONSFEQDLE-----EKSQKSFPIKWSKTHPVLVIGTEKGILY
Ot	FFPSSC-----QPRIEALGWDKDNDSLAILTG-----TNVVISIWSMGLKKFYEVLELP-----NKDKASFICWSGHYPVLCIGSEKGSIV
Tc	TSSFFPG-----VVRIAWDYSSDTLALIQKNSNVLTOSTCKQSSDSIDSG-----LHELCLFLAWSRRGSHLAVGSTKGTFFV
Cr	EVHFPPAEYPPNDGRACAAAQMWDPAGEQLAILPAGNTHVFILWLAGNKEVOKIESEF-----KIQEFSQMAWSRNGMYLGVAVTVKGNVM
Ce	ALNPTG-----KLIDIAWDKEGDVLAIAVANITGTIYLWDVNSRNTDTVESGATSSKELPTCLAWSPTPTLVLVIGNNAAGNIV
175	
Hs	IYNHOTSRRKIPVLGKHTKRITCGCWNAE-----NLLALGGEDKMITVSNQEGDTIRO-----TQVRSEPSNMQFFLMKMDDRITSA
Xl	IYNLQTSRRKIPVLGKHTKRITCGCWSSO-----NLLALGGEDKMITVSNQEGDTIRO-----TSVRMDPSDIIQFVSMKTDERASAG
Dr	IYNQOTSRRKIPVLGKHTKKITCGCWSSO-----NLLALGSEDRSITISNHEGDTIRO-----TSVRADPADVQFVSMKTDERSSPG
Sp	IYNHOTSRRKIPVLGKHTKKIICGAWSAQ-----NLLALGSEDRITVSNQDGDITAT-----TGVRLDPSDIIQFSEMKVDERTSSG
Aa	IYNHATTKRIPVLGKHTKRITCGAWGFANWSSNVGMVHIALGSEDKTISLNSNEEGDTLRS-----VQLRDNPSDMHFAEMKTDERLIPG
Tt	FYNKKTQKKIPVLMGKHSKKITGDNWDE-----GLLITGSEEKVLTVSSHNSDSKGESITVQHEPNSLQWAROKTDDRDSO
Ot	FYHRKSQRKIPCLSKHGKVTGHDWHAEE-----GLLITCSGDKLLTISNQQGDTVQDSFIVKAEPQIKWCPK-----DINK
Tc	VINSETLKKLPVVGHTHKAIVDGKWSVD-----NTLVMVGEDNVLSVSEEDGVLRRQ-----VSLKMLP LSVTLVLDLQGGGKSP
Cr	MYNARERKKTPLVGHKHTKIVAAAANKD-----NIMALAGQDKTITLTDGVTGDTIKTFHLLKVPMDLCSVDRKEDGYRRRE
Ce	VYNHRTSRRIAVMGKHORSVTOITVTPPE-----DYVISCSDDNTLSVTTLEGTTVST-----TTTNGEPTNMDYGSVN-----GKGGSS
262	
Hs	ESMISVVLGKKT-----LFFLNLEPDPNPADLEFOODFGNIVCYNWYGDGRIMIGFSCGHFVVISHTHGEIGOEIFQARNHKD-----NLTSIAV
Xl	ESTVSVVGRKT-----LFLFNLDPPDNPIELAFQPRYGTIVSHKWYGDGYIMIGFSGHFFVVISHTHREIIGOELFQAHNHKD-----SLTSIAI
Dr	OSTVSVVALGKKT-----LFLFNLDPPDNPIELAFQQRYGNIISYRWYGDGYIMIGFSGHYFVVISHTHREIIGOELFQAHNHKD-----SLTSIAI
Sp	ESTISVIVGKKT-----LFLYNLDDRDNPIELAFQQRYSVVAYTWYGDGYIMIGFSGNGYFIVISHTHREIIGOELFQARDHKD-----SLTGIAI
Aa	ENTISMLGKRT-----LFLYHLPEPDSPTTELGFOORYGSLLOHWFGDGYVLLGFSLGHVVAISTHPREVGOELWQVKNHRD-----SLNSIAV
Tt	RTITAILSNKS-----ILMYDLNKKQLELVYEPYKGYVDYQLEGGYIVTGFTEGYVAHVSSHLYELRDEIQSKRIEQS-----SLDALCT
Ot	KFAAIIIGOKO-----MILVDTPTFKQSYIVSFSANYGKVLTYQWYGENHLLIVGFANGIVALISVPSDSMAEKNINIVGPTGIDICIV
Tc	IATAALINFGK-----TLEHFNLETFKAQPPVFESKLGITVTCDFISGGLVGVGFSSGAVALVNASVKGVMCGVVRSFHDITVNALACCO
Cr	ENTYSLNINRKTLYIMQCTAEGDRPLELAFLDYTPIMKHSWFGDGYITLGYKNGYVAVVSSHRSREISEEVHSGKYLDLITDVTYCA
Ce	VTMVSVVIIGKKT-----LMLAHYNALDEPVNLOFOEKYGNHISYWFNDGYILIGEDRGYIISISAHNNEIGSELVSFLEYRGG-----YLASIAV
349	
Hs	SQTLNKVATCGDNCIKIQDLVDLXDMY-----VILNLDEENKGLGTLTSDDDGOLLALSTQRGSLHVFLLKLPILIGDACSTRIAYLTSLLE
Xl	SQSLGKAASCGDNCIKIHDLTELKEMY-----AIINLDDEETKGLDTLTSDDDGOLLAVSTQRGSLNVFLTKLPVLIGDTCGTKIAYLTSLLE
Dr	SQSLNKAASCGDNCIKIHDLTDLKEMY-----AIVTLDEETKGLDQMCWTDGOLLAVSSOQGLHVFLLKLPILIGDSSGTRIAAYLTSLLE
Sp	SLSLNKAASCGDNCIKIHDLSDLKELY-----AIVNLEEETKGLTEIEWEDGOLLAIGTORGFMHVYLLKLPILIGDSHGTRLAYLTSLLE
Aa	CKDLELIASCGDNNIKIHSMSNLQETV-----KILTLHDOA-----ALKNIEWSSDQOLLGVTTSQGAICVFTVTKLHSLYAVSPPRIALLSSLAE
Tt	NDLIYKLAVAGENQIHLYNIGTWEEVKSQRIEPLKAAAGNVTKMOWANNQOLLVVATANGHLYGLTISIPFLTSTYGSIVSVLSSFTE
Ot	NADLOKIAVAQMTIKFYSLEDWTEQIGERLEITKSAGKITDLHWTKDGSILTITGNGYFFGFLTIVIPSICAAASDTYALLSSLTE
Tc	NFSMCAAVGENALKPFRADGSIVENAMERVELEGGAYGTLRGVWESKDGSNVLTSTEQCOLISYKLNVSAVSTTKGFTIYFLSSSRV
Cr	SLGRVAMAGAN-----CVRVLDANADYNEIKGDAVDLD-----ANQAIEKVGWTKDGOVLTIVGTHNGYMHSLASLPMVYDFHGTIRVLYLTSLLE
Ce	STSFNKLLITIGDNMVKVRDLDELTTVT-----MLTEIE-----TEKNLSEIEVTEEDGQLVAVSSQSGVLSIFVTKMPTLAASYNNSICYLNLNLO
436	
Hs	VTVANPVEGEL-----PITVSVDEPNFVAVGLYHLAVGMNNAWFYVLGEN-----AVKKLKDMEYLGTV
Xl	VTVANNVDGEL-----PITVSVVEPNFVAVGQYHLAVGMNNAWFYALTPN-----GVEKLMDEYLGSAV
Dr	VTVANPVEGES-----PVPVAVEVEPSFIAVGPYHVAVGMNNAWFYALGDS-----GVERVKDTEYLGTV
Sp	VTVNVPIEQEP-----AVPIATEVEPTFVALGPYHLAAGMNNNAWFYILSDK-----DYYSIQITMOAGWPEKLDREYLGTVIN
Aa	VATHHYAPDKIKSAPTMIALEIEPSFLAVGPYHMACGMNNHWFFYDLGRT-----LITDSPLLLGDREYMSKIK
Tt	VSIVDTSRINQIQNVSSINLETEPGFLSLGLYHLAAGLNNNVWYVYLWLDQ-----KRNKGIKGGEMIKRDRYLGTVK
Ot	VSVVDCSKNNMI-----VAKANLDIEPTFLNLGANHFGVGLNNSIWYFKWRTP-----GMEGOMQVVELVCKREYFGTIK
Tc	VTKSLQDDRIT-----TYNANVDIDPAITAAARGILAVCAGHNVLFYITTEGN-----EFSLLRRADFP SAIS
Cr	MTLLDVSRROT-----VARIENEPAFCCGLGPSHAAVGMNNAWFYSLGK-----VGKVVQRREYLGTVIT
Ce	VTVVAEVEKKG-----SSTLELNIEPTVMGLGPLNLAVANNNTVFFDYHTPAQMQAAQLOSTQSAAEKPTIVAAEFINRVEYLGTVIT

523
Hs **STCLHS**DYAAALF**EGK**VQLHLIESEIL--**DAQEERE**TRLPFAVD--**DKCRIL**CHALTSDFLIYGTDT**IGVVOYFY**IEDWQFVNDYR--
Xl **NMCLNS**DYAAALF**EGK**VQLHVIENKDE--**DAQEERE**TRLPFASD--**DKCRIL**CHALTGDFLIYATNTGLIKFFYLEDWQYVNEYR--
Dr **SMCLNC**DYAAALF**EGK**LQLHVIDGDEC--**VVQEDR**OTKLPFEPD--**QKYLIL**SHALTSDFLIYGTDT**IGLIGL**QCFYEDWQSVYEYR--
Sp **SMCLNAD**YAAVS**FENK**VQLHLIQIETEG**VDN**EERE**TRLP**FPD**KE**--**SN**GKITCHTLTADFLIYGT**HN**GMLHYFFIEDWQVNEFR--
Aa **EVALSSEY**CAVL**CGG**QIMLHP**IES**TNE--**ARMN**REP**KIP**FD**EV**RGMS**ES**VIT**CL**TL**TN**DF**LC**FATD**IG**N**IV**MF**S**LER**W**ST**V**VO**FR**--
Tt **DIRL**NEFWAAVL**TDG**K**CI**L**HT**I**OP**NNN--**VK**DK**Q**FP**Q**TE--**TD**KAT**IS**GG**IT**ND**FL**IM**L**D**SS**G**K**I**RY**Y**H**LED**Q**Q**F**V**VE**Y**KE**--
Ot **QVVM**NEEW**TAV**L**SEG**K**VT**L**HQ**I**ED**TK--**SN**DR**RF**P**Q**TD--**QD**K**P**IT**Y**I**AL**T**D**S**FL**LM**V**DT**Q**G**K**L**Y**Y**L**IED**NT**MI**SE**HR--
Tc **ALKV**SS**RI**AA**V**CD**GK**I**EL**NE**IR**SGE--**NS**T**TF**P**ENG**--**TAN**IS--**LD**MT**EV**LL**F**Y**AT**TE**K**IC**V**V**N**L**ID**F**Q**CV**VE**HT--
Cr **AI**KL**NE**T**QA**AV**L**T**G**GH**V**V**V**HP**IS**VEA--**GH**AP**DE**L**D**V**V**IP**GP**G--**Q**PAN**IT**CV**AL**TP**F**V**IT**GS**RT**IG**L**SY**YL**SP**VD**TP**V**NE**FR**H--
Ce **NI**OL**NY**MA**AV**N**F**GS**R**L**RL**HR**IR**NS--**ED**NV**S**IE**FP**EA**N**--**R**NAT**LY**S**Y**AL**T**EN**FL**IF**TT**S**NN**Y**IV**Y**F**S**L**SE**WA**IV**SE**Y**R**--

610
Hs **HPV**SV**K**K**IF**PP**DP**NG**TR**LV**F**IDE**K**SD**G**F**V**Y**CP**V**N**D**A**Y**E**IP**DF**SP**TI**K**G**--**VL**W**EN**W**P**M**D**K**GV**F**I**AY**DD**D**K**V**Y**Y**F**V**F**H**K**D**T**I**Q**G--
Xl **HSV**S**I**R**K**I**F**PP**DA**T**GT**TL**V**L**I**DE**K**TE**G**F**V**Y**CP**L**N**D**N**L**Y**E**IP**DF**SP**TI**K**G--**IL**W**EN**W**R**M**D**R**S**V**F**V**A**Y**DD**D**K**L**Y**Y**F**V**F**H**K**D**T**I**Q**G--
Dr **HTV**G**R**K**V**FP**DP**NG**TR**LV**F**IDE**K**SD**G**F**Y**CP**V**ND**S**VE**IP**DF**SP**AI**K**G--**VL**W**EN**W**IS**S**K**GV**F**V**A**Y**ED**D**K**V**Y**T**A**F**H**K**D**T**I**Q**G**--
Sp **HVV**G**R**IR**F**SD**PS**GT**RL**V**F**IDE**K**SD**G**F**V**Y**PN**D**Q**LE**IP**DF**SP**TI**K**N--**VL**W**EN**G**Y**N**K**GV**F**V**A**Y**DD**E**K**V**Y**Y**F**V**S**R**E**TV**NG**--
Aa **HQV**G**K**IT**L**H**AD**L**D**GT**RL**V**F**IDE**K**SD**G**F**V**Y**IS**A**TE**ES**IR**IP**DF**FP**H**AV**G**--**VL**W**D**--**F**SH**ST**V**I**AF**D**R**SS**CV**Y**Y**AL**R**AS**V**H**G--
Tt **ADC**Q**L**V**K**I**Y**PN**F**SG**TR**V**V**CF**D**N**K**GS**AY**LE**FA**Q**E**Q**F**Y**PL**EH**F**PO**RA**E**K**--**VL**W**D**--**Q**K**D**PN**L**F**AV**L**Q**N**D**L**T**IF**I**N**K**NN**I**NG**L**T**I**Q--
Ot **SON**PI**V**K**V**FP**N**K**R**GT**K**CV**ID**NT**G**NG**Y**IF**CP**V**DD**SM**H**FP**N**FS**A**GT**ES**--**IL**W**D**--**A**DD**PN**I**F**V**T**V**D**K**E**M**O**T**Y**L**I**PL**S**LE**G**L**T**I**V**--
Tc **PS**IG**I**K**R**AV**P**NT**S**CT**R**VAL**I**G**K**ND**A**L**Y**FN**P**V**L**TL**L**IQ**TE**GF**E**A**EH**KN--**IL**W**D**--**Q**D**Y**GL**V**S**Y**D**S**K**T**M**V**F**V**Y**SP**H**S**R**Y**G--
Cr **DD**GG**I**V**RL**FP**Q**A**I**GA**R**L**VE**ED**D**K**G**AL**H**LE**N**P**V**ND**H**V**V**AV**P**--**Y**T**G**RA**E**T--**V**M**W**D--**T**S**D**T**N**V**M**V**I**G**D**T**AL**HS**F**L**V**VP**S**L**T**G--
Ce **H**V**V**P**V**RS**I**FP**HP**T**N**V**V**CCC**F**DD**R**LE**A**MI**Y**SA**V**DD**EV**RL**P**SV**G**SS**A**HY**K**GA**I**W**E**TF**I**D**K**NT**F**AV**F**D**SON**I**V**F**L**L**S**K**O**H**I**Q**G**--

697
Hs -----**AK**V**I**L**A**G**S**T**K**V**P**F**A**H**K**P**L**L**L**Y**N**G**E**L**T**C**O**T**O**S**G**K**V**N**N**I**Y**L**S**T**H**G**F**L**S**N**L**K--**D**T**G**P**D**EL**R**P**M**L**A**Q**N**L**M**L**K**R**F**S**D**A**W**E--
Xl -----**SK**V**I**F**A**G**G**T**K**L**P**F**S**H**K**P**V**L**L**H**N**G**D**L**T**C**O**T**O**S**G**K**L**N**N**I**N**L**S**T**H**S**F**I**G**S**T**G--**D**A**G**A**T**E**L**K**Q**M**L**T**Q**A**M**L**R**R**F**S**D**A**W**D--
Dr -----**SK**V**I**L**V**G**G**T**K**L**P**F**S**H**K**P**L**L**L**H**N**G**E**L**T**C**O**T**O**S**G**K**I**N**S**V**L**N**T**H**A**F**L**N**N**O**H**S--**E**SS**K**D**K**L**Q**S**F**L**Q**A**V**M**L**K**R**F**S**D**A**W**S**--
Sp -----**P**A**V**I**L**V**G**T**T**K**L**P**Y**A**Q**Q**P**L**M**L**H**N**G**E**L**V**C**O**T**O**S**G**K**T**S**V**H**L**S**T**Y**N**F**L**E**R**P**Q--**D**I**P**H**P**E**V**R**S**A**L**O**K**S**I**L**L**H**O**Y**K**E**A**W**M**--
Aa -----**K**R**I**E**K**V**G**V**T**S**L**I**S**D**Q**M**P**L**M**L**Y**D**G**E**L**C**L**H**S**G**G**L**T**N**I**V**L**D**T**H**A**N**K**-----**P**G**R**D**V**K**E**Q**L**R**A**V**L**M**R**K**Y**N**E**A**W**E--
Tt **P**V**K**E**L**L**A**I**E**D**I**K**N**P**G**P**P**V**O**T**I**L**D**R**G**V**K**P**L**T**L**S**N**L**L**K**C**F**P**S**G**S**I**NG**O**N**L**T**S**H**S**Y**L**G**S**Y**K**R**D**D**I**D**O**G**H**Y**R**E**L**L**Q**L**H**K**Y**N**N**C**L**I--
Ot **H**L**P**E**Y**L**K**L**E**E**V**E**K**N**K**P**G**V**I**T**F**V**D**K**L**K**P**I**L**K**G**G**F**V**Y**S**H**A**R**T**D**G**T**R**G**O**F**L**T**H**S**Y**I**N**S**W**R**G**P**O**E**T**D**E**G**H**L**R**Y**F**L**O**C**L**A**I**O**R**Y**S**S**C**M**D--
Tc -----**P**T**S**E**S**V**V**I**K**D**T**N**T**E**N**L**V**T**P**I**P**V**G**Y**T**P**V**A**L**F**K**G**V**I**T**O**T**S**S**G**S**L**D**F**V**H**L**K**S**H**N**Q**A**M**T**R**V**NP**E**A**F**Y**T**N**F**S**L**N**H**L**R**W**A**S**O**N**I**S**T**S**O**E--
Cr -----**P**O**V**O**D**L**G**K**Q**A**V**P**A**I**H**T**P**L**T**V**C**NG**V**V**G**CR**L**K**S**G**A**M**D**N**V**L**E**S**H**K**M**L**Q**P**G**D--**A**V**A**R**A**A**P**A**K**R**F**A**A**L**K**L**Y**K**L**D**A**V**E**--
Ce -----**E**S**V**I**Y**V**S**A**T**R**L**P**H**A**Y**V**P**L**S**L**N**K**G**I**V**T**C**L**M**S**N**G**L**S**S**V**L**L**D**S**H**K**T**E**S**V**I**S--**D**K**S**E**T**V**I**D**D**L**L**R**S**L**L**M**H**R**W**S**T**A**W**K--

784
Hs **M**C**R**--**I**L**N**D**E**A**A**W**N**E**L**A**R**A**C**L**H**H**M**E**V**E**F**A**I**R**V**Y**R**I**G**N**V**G**I**V**M**S**L**E**O**I**K**G**I**E**D**Y**N**L**L**A**G**H**L**A**M**F**T**N--**D**Y**N**L**A**Q**D**L**Y**L**A**S**S**C**P**I**A**A**L**E--
Xl **L**C**K**--**I**L**N**D**Q**L**G**W**N**E**L**A**R**A**C**L**H**H**M**E**V**E**F**A**I**R**V**Y**R**T**I**G**N**V**G**M**V**M**S**L**E**O**I**K**G**I**E**D**H**N**L**L**A**G**H**L**A**M**F**A**G**--**D**F**N**L**A**Q**D**L**Y**L**A**S**G**S**P**A**A**L**E**--
Dr **I**C**K**--**A**L**N**S**S**E**A**W**G**E**L**G**R**A**C**L**H**H**M**E**V**E**L**A**I**R**V**Y**R**M**G**N**V**M**S**L**E**D**I**K**G**I**E**D**O**N**L**L**A**G**H**L**A**M**C**N--**D**Y**N**R**A**Q**D**L**Y**L**T**S**S**Y**P**A**A**L**E**--
Sp **L**C**O**--**L**L**N**S**K**E**A**W**L**D**L**A**K**D**A**T**H**A**D**I**E**F**A**L**R**V**Y**R**H**I**G**E**A**G**M**V**L**S**L**O**K**I**T**G**I**D**D**R**N**L**L**S**G**H**L**A**M**Y**O**E--**D**F**N**L**A**Q**D**L**F**L**A**S**S**R**P**I**T**A**L**E--
Aa **L**C**N**--**L**L**N**D**V**E**E**W**K**E**L**G**R**S**S**I**A**D**L**N**V**S**P**A**K**V**Y**R**I**G**D**V**A**M**V**Y**A**L**E**I**V**O**I**E**D**L**N**T**L**A**G**H**C**H**A**L**L**N--**K**I**D**E**A**K**T**L**F**A**K**S**G**N**P**O**E**A**L**E--
Tt **A**A**O**--**F**L**H**NA**V**L**Y**K**E**L**G**R**K**A**L**E**F**V**D**L**D**V**A**L**K**S**Y**Q**L**A**G**S**L**S**M**V**M**T**I**Q**S**F**O**H**I**N**E**K**N**I**Y**G**N**I**A**M**I**L**G**--**Q**Y**D**L**A**Q**E**L**F**L**K**S**S**O**P**I**L**A**L**E--
Ot **A**A**R**A**C**F**R**Y**S**Q**V**F**F**E**A**L**G**K**Q**C**L**K**Y**L**D**L**D**T**A**E**A**A**F**Q**M**C**K**N**G**M**V**Y**S**I**T**S**I**K**H**E**S**E**K**N**I**L**M**G**H**V**A**S**I**L**E**--**K**H**D**V**A**Q**E**Y**F**L**K**S**K**P**E**L**A**L**E**--
Tc **A**E**D**--**L**A**V**K**A**L**H**V**L**D**V**E**L**A**I**R**L**Y**R**O**L**S**O**P**S**L**V**L**C**L**E**N**I**K**H**I**N**E**K**N**L**L**I**G**H**I**S**M**I**M**G**--**F**F**K**D**A**O**S**F**F**L**R**S**S**O**P**I**C**A**L**O--
Cr **C**A**K**--**O**L**R**O**V**E**S**W**R**T**L**A**L**A**A**L**D**V**L**I**D**I**T**A**I**N**A**Y**R**E**I**G**D**A**S**M**V**L**S**L**E**R**V**R**O**H**E**D**R**N**L**L**S**A**H**I**M**V**L**L**E**K**D**Y**G**O**A**O**E**L**F**L**R**S**S**V**P**R**A**A**L**E--
Ce **I**C**I**H--**S**N**D**G**S**H**W**N**O**F**A**M**A**A**L**L**D**S**D**V**G**M**A**K**I**F**R**E**I**T**G**D**A**A**M**V**T**A**L**E**L**I**E**T**I**E**E**K**N**L**L**H**A**Q**I**Y**I**L**S**--**R**Y**D**D**A**E**O**L**Y**L**E**S**S**R**P**M**E**A**L**N--

871
Hs **M**R**R**D**L**Q**H**W**D**S**A**L**Q**L**A**K**H**L**A**P**D**O**T**P**F**I**S**K**E**Y**A**I**O**L**E**F**A**G**D**Y**V**N**A**L**A**H**Y**E**K**-----**G**I**T**G**D**N--**K**E**H**D**E**A**C**L**A**G**V**A**O**M**S**I**R**--
Xl **M**R**R**D**L**Q**H**W**D**S**A**L**Q**L**A**K**R**L**A**P**D**O**T**P**F**I**S**K**E**Y**A**M**O**L**E**F**T**G**D**Y**V**N**A**L**A**H**Y**E**K**-----**G**I**T**G**D**N**K**F**O**H**D**E**T**C**L**A**G**V**A**R**M**S**I**R--
Dr **M**R**R**D**L**Q**H**W**D**S**A**L**Q**L**A**K**R**L**D**P**D**E**I**P**F**I**S**K**E**Y**A**I**O**L**E**F**V**G**D**Y**V**N**A**L**A**H**Y**E**K**-----**G**I**T**G**N**K**F**O**D**H**D**E**S**C**L**A**G**V**A**R**M**S**I**R--
Sp **M**R**R**D**L**L**H**W**D**Q**A**L**K**L**A**K**T**L**A**P**G**O**I**P**Y**I**S**K**E**Y**A**Q**O**L**E**F**T**G**D**Y**P**N**A**L**T**H**Y**E**K**-----**G**I**T**T**E**Q**E**R**D**H**D**E**I**C**A**T**G**V**A**R**M**S**I**R--
Aa **I**C**R**D**L**L**O**W**E**Q**A**M**A**L**A**S**L**A**P**E**Q**L**P**F**L**A**R**E**Y**A**Q**O**L**E**F**T**G**S**Y**A**E**A**L**M**N**F**E**R**G**L**K**S**D**I**L**P--**S**S**D**G**V**I**E**O**D**V**L**N**O**H**L**S**I**C**K**A**G**I**A**R**T**S**I**X--
Tt **M**R**S**D**I**O**D**Y**L**T**A**L**N**L**A**K**S**I**A**P**O**E**E**P**I**C**R**R**L**A**F**O**I**E**N**O**G**N**N**O**E**A**R**K**L**Y**E**R**A**V**L**N--**K**D**D**R**P**S**D**R**S**K**I**D**N**H**N**O**L**C**F**A**G**I**S**R**T**S**I**X--
Ot **M**R**M**D**L**Q**D**W**F**O**A**L**K**L**C**K**O**I**A**P**E**K**E**Q**F**I**C**R**L**A**S**O**V**E**N**O**G**N**T**I**E**A**Q**K**L**Y**E**K**A**L**L**N--**F**N**E**O**T**D**E**K**I**N**V**E**O**H**N**T**O**C**Y**G**G**I**A**R**T**A**I**R--
Tt **M**R**H**D**L**Q**W**E**S**A**L**A**L**A**R**Q**M**A**P**E**R**V**F**I**L**S**K**E**Y**A**Q**O**L**E**Y**R**G**E**Y**A**K**A**L**E**M**Y**R**A**G**E**R**A**M**P**K**G**H**A**S**T**O**L**T**A**A**O**E**V**K**S**H**N**A**V**C**S**G**A**A**R**C**L**L**R--
Cr **M**R**M**D**L**K**H**W**T**D**A**L**K**L**A**E**O**L**D**P**D**A**I**A**T**I**C**K**E**H**G**A**M**L**E**M**T**G**E**Y**S**N**A**K**S**H**Y**O**Q**A**L**-----**D**A**L**A**V**S**V**G**P**A**O**P**D**L**E**A**C**K**A**G**I**A**R**T**T**L**O**--
Ce **M**R**R**D**L**L**E**W**P**K**A**L**V**L**A**E**M**N**P**R**E**I**P**Y**L**S**K**E**Y**A**O**E**L**L**I**G**D**H**A**N**S**L**A**N**Y**E**K**G-----**V**M**E**N**P**O**N**L**F**E**L**O**E**H**N**E**I**C**O**S**G**I**A**R**M**A**I**K--

958
Hs **M**G**D**I**R**R**G**V**N**Q**A**L**K**H**P**S**R**V**L**K**R**D**C**G**A**I**L**E**N**M**K**O**F**S**E**A**O**L**Y**E**K**G**L**Y**D**K**A**A**S**V**Y**I**R**S**K**N--**W**A**K**V**G**D**L**L**P**H**V**S**S**P**K**I**H**L**O**Y**A**K**A**K**E**A**D**G--
Xl **M**G**D**I**R**R**G**V**N**Q**A**L**K**H**P**S**R**L**K**K**D**C**G**A**I**L**E**S**M**K**O**L**T**E**A**A**O**L**Y**E**K**G**O**Y**F**D**K**A**A**S**V**Y**I**R**C**K**N**--**W**A**K**V**G**E**L**L**P**H**V**S**S**P**K**I**H**L**O**Y**A**K**A**K**E**A**D**G--
Dr **M**G**D**I**R**R**G**A**N**Q**A**I**R**H**P**S**K**A**L**K**K**D**C**G**A**I**L**E**S**M**K**O**Y**S**E**A**O**L**Y**E**K**G**O**Y**D**K**A**A**S**V**Y**I**R**C**K**N--**W**A**K**V**G**E**L**L**P**N**V**T**S**P**K**I**H**L**O**Y**A**K**A**K**E**A**D**G--
Sp **I**G**D**I**R**R**G**V**S**M**A**M**M**N**N**R**A**V**K**R**D**C**A**S**I**L**E**S**M**K**O**Y**S**E**A**O**L**Y**E**R**G**G**Y**P**D**K**A**A**S**V**Y**I**R**C**K**N--**W**A**K**V**G**E**L**L**P**O**I**T**S**P**K**I**H**T**O**Y**A**K**A**K**E**A**D**G--
Aa **C**G**D**Y**R**R**G**V**Q**L**A**L**E**L**N**D**K**E**L**F**N**E**C**G**E**A**L**M**T**N**G**N**L**N**E**A**A**L**L**E**K**G**E**N**W**D**C**C**E**L**Y**I**N**L**K**O--**W**K**K**I**D**R**I**L**P**N**V**T**S**L**K**L**H**A**A**Y**A**K**A**K**E**M**E**G--
Tt **I**G**D**I**O**R**G**V**T**I**A**K**E**L**I**D**N**N**V**I**E**I**A**V**V**C**E**N**M**K**O**Y**L**E**A**A**L**Y**O**K**S**G**M**L**E**K**A**A**S**L**Y**E**S**K**D**--**F**K**K**A**P**L**I**S**M**I**K**S**P**N**L**L**K**O**Y**A**K**A**K**E**S**E**G**--
Ot **M**G**D**I**O**R**G**F**N**I**A**N**E**L**N**D**K**T**L**V**I**E**I**A**G**V**S**E**S**M**K**O**W**T**E**A**A**K**L**Y**O**R**G**O**L**V**E**K**A**A**S**I**Y**O**I**G**M**--**F**A**A**A**P**L**L**N--**K**O**I**T**S**P**S**I**L**L**M**V**A**K**A**K**E**G**E**K--
Tc **I**G**S**I**R**E**G**V**L**A**L**D**S**N**D**E**A**L**I**M**D**C**A**E**I**L**E**S**T**R**O**F**E**D**A**A**H**L**Y**E**K**A**S**E**F**F**H**A**A**T**L**Y**I**L**E**A**K**N**L**K**A**A**S**R**V**I**P**K**I**T**S**R**N**I**I**G**M**F**A**K**A**K**E**S**E**G--
Cr **I**G**D**L**R**O**G**R**O**L**A**M**O**L**N**S**Q**L**F**E**C**A**L**I**L**E**G**L**Q**L**T**E**A**E**M**Y**E**R**A**G**O**F**E**R**A**A**S**I**Y**O**I**T**K**N--**F**A**A**A**P**L**M**A**R**I**S**S**S**K**L**O**L**O**F**A**K**A**K**E**A**E**G**--
Ce **I**G**D**L**R**R**G**V**Q**L**A**K**O**L**E**G**R**V**V**K**R**D**C**A**I**L**E**O**M**K**O**Y**T**E**A**A**O**L**Y**E**V**G**L**F**D**R**A**A**V**C**L**K**A**N**A**--**W**A**K**V**G**E**L**L**D**H**V**K**S**P**K**I**H**I**O**Y**G**K**I**M**E**K**E**K--

1045

Hs **RYKEAVVAYENAKQWQSVIRIYLDHLNNEPEKAVNIVR**---ETQSLDGAKMVARFFLQLGDYGSATQFLVMSKCNNEAFTLAQQHNMKEI
Xl **KYKEAVFAYENAKDWDNVIRISLDHLNNEPEKAVSIVR**---ETQSLGAKMVARFFLRLGDYGSATQFLVLSKCNDEAFQLAQQHNMKEI
Dr **KYKEAAMAYESARDWDNVIRILLEHLNNEPEEAVRIVR**---ETHSIEGAKMVARFFLRLSDYGSATQFLVLSKCNDEAFQLAQQHNMKEI
Sp **KYKDAALAYQNAKDWDNVIRIQLDYLKNEPEEAVRVVK**---ESGSVEGAKMVARFFLRLSDYGSATQFLVMSKCNNDQAFQLAQQHNMKEI
Aa **HYADAINSYHLAGDLDVVRITYLEYLSDPHSASEILL**---ETRSVEGSKLLSKYFEQHDYGSATQFLVLSGSIQSDAFATAQKONKIRY
Tt **AYNEAEOTYEOAESWEDVVRINLNDKLDNLRKATAVLR**TKCDTSTVCLMVANVCEKQNGYGEVLFLLKAGKKEEAFQKAQQYNVMDA
Ot **NYREAEEKAYERANDYENIRLNLDLHDNPEKAKHIFRT**TKSQLPQCALMIAQYCETRGFKKEAIEFLVLGGKREEAFILAQSHOVMDA
Tc **AFKAEALAYTQEDWDNVIRIKVEKLNLDLYGAYVVVR**---QTSRAAAAIVANMCKKRGEGFSAVEFVFLAKSFEAFGLAKKNCMST
Cr **FWQEAAYAYEAGDMADVRLCLERLSQPRAYATVR**---KTQSVAAANQLSRFCQSDQDFGGAVFLLMAGQMDQAFDIAMGHNEMDT
Ce **KYKVAVKCYETGRDYDNOVRLLLDPLNDPDEAVRVVR**---ESRSIEGAKLVAKFFVKLGDYNSATQFLVMSQCVQEAFAELAEKKNNAVRE

1132

Hs **YADITGSEDTT**-----**NEDYOSIALYFEFEKRYLOAGKFFLLCGOYSRALKHFLKCPSS**---EDNVAIEMAIETVGOAKDELLET
Xl **YADITGSENTS**-----**NEDYOSIALYFEFEKHFQAGKFFLLCGOYQALQHFHKCPIT**---EDNLAIEMAIETVGRAKDDLLET
Dr **YADITGSEAT**-----**IEDYOSIALYFEFEKNNHLOAGKFFQKCGOYSRALKHFLKCPSS**---DDSVAIEMAIETAVGEAKDESLT
Sp **YADITGODAS**-----**HEDYOSIALYFEFEKNNHLLAGKFFLLCEQYQALQHFHKCPNT**---DDSQAIEMAIETVGGKCRDDQLA
Aa **YGEVLEQSSNAK**-----**PSDYLVLAATHFENEKYTELLAGKYFFLGKEYSKALKHLLKASSFSN**---ENTALS LAIDCVASANDEKLS
Tt **YSDNMKDFIT**-----**LEERLRIAQYYENOGIWWKAAKHFEOAKNPTKSLKLYLKAGDOY**---IDDMIDLVCRNKQOESIQ
Ot **YAKIILQIDENK**-----**SDEHLRIAQYYEKGKQWGAAKHFEKSEQYNKALKLYIAEGEKM**---IPDMIDMVAKVR---TEALT
Tc **LEGALLNQACLIDGIAPASNOAEFAMIAQYYEQNGKPGOAGLFYHIAGNFPALARNYLDAGESE**---DIEKAIQVVGKSRSDALT
Cr **FARIVAASAK**-----**PVDYQRIAQYYESRGEYDKAADMWSKCDQAPRAVQLYLKVGITN**---ALEKAVQVVEQTRSHOLG
Ce **YAKAIEQHGK**-----**TSQALELAEYYNRVNDMFMAAKIFYTQAGQYNNAINLLFRKNGDDB**---NCVALAVDCGIRKSKDRTLN

1219

Hs **NQLIDHLIGENDGMPKDAKYLFRLYMALQYREAAQT**TAIIAREEQSAGNYRNAHDVLFVSMYAEIKSQIKIPSEMATNLMILHSYI
Xl **TQLIDFLMGEKDGMPKDAKYLFRLYMALQYREAAQT**TAIIAREEQSAGNYRNAHDVLFVSMYTELKAQIKIPSEMATNLMILHSYI
Dr **NQLIDHLMGESDGMKDAKYLFRLYMALQYREAAQT**TAIIAREEQSAGNYRNAHDVLFVSMYAEIQTQIKIPSEMATNLMILHSYI
Sp **HQLIDYLMGETDGIKDAKYLFRLYMALQYREAAQT**TAIIAREEQIAGNYRNAHDVLFVSMYTELKAQIKIPSEMANNLMILHSYI
Aa **NQLIEYLLIGETDGVKDPKLLFRLYMALQYREAAQT**TAIIAREEQTAGNYRNAHDVLFVSMYQELKRNNTIADSMKASLILLHRYT
Tt **QTLIDYLLIE**---**GEKPKDPIYLLKLYDKIGNIQSLVKIAT**IASDEHDQGNKYIAHERLFEYQKVKENVAIPFDLEOKLMIHSYI
Ot **HELVDYLLIGOTDNPKEPQWTFKLYRAIGNVQAVKI**AVNIAQOQOELGNYKYAHDILLDFKDIRMSNNKIPFDLNRMLLHSFT
Tc **NRLIDYLMGETDGEKPEPSYIFKLYMALKSYEKA**AKTSVLSTKQEMGNLYTAHKTLVDAYRILRDKKMHVNDLRRSLMLLHSYV
Cr **VLVIDYVNEEKDGTTRD**---**EFRRKLNIAIAGQFAEAARDALEMAR**FEQEEGNYRVAHDKLFGLVQKLEALNKKPPGELLRALMLLHSYI
Ce **NKLVKFLIGE**---**DGNVKKDPAQLFRLYVGLGR**TKDAAQTAVVVAQIHOAKGNRYIARDLLFQMHQOLREKMMRIPLDMNKSLMAIHSYI

1306

Hs **LVKIHVKNGDHMK**---**GARMLIRVANNISKFP**SHIVP**ILTSTVIECHRAGL**KNSAF**SFAAMLMRP**---EYRSKIDAKYKKKIEGMVRR
Xl **LVKIHVKRGDHLK**---**GARMLIRVANNISKFP**SHIVP**ILTSTVIECHRAGL**KNSAF**SFAAMLMRP**---EYRNKIDIKYKKKIEAMVRR
Dr **LVKIHVKRGDHLK**---**GARMLIRVANNISKFP**SHIVP**ILTSTVIECHRAGL**KNSAF**SFAAMLMRP**---EYRNKIDIKYKKKIEAMVRR
Sp **LVKIHVKKGDHKK**---**GARMLIRVANNISKFP**SHIVP**ILTSTVIECHRAGL**KNSAF**SFAAMLMRP**---EYRNSIDLKYYKKKIEAIVRK
Aa **LVRTHVKKGNHLO**---**AARLLLOVAKNISQFP**SHVVP**ILTSTVIECHRAGL**KNSAF**SFAAMLMRP**---EYRNSIDLKYYKKKIEAIVRK
Tt **LARKYLAYKEEDKEIE**LAAWLLNRVCKNISQFP**THAVN**ILTSVIAAMKSKNRP**LAYKWSVELVRP**---EYRSHINEKYKTRINIARK
Ot **LAKRLVKMNDHVG**---**GARMLIRVANNISKFP**SHIVP**ILTSTVIECHRAGL**KNSAF**SFAAMLMRP**---EYRNSIDLKYYKKKIEAIVRK
Tc **IAPKPLMKIMKDDDE**---**TASRMLLRVVRNTHKPK**HISVIYTSALQCLKSGFRKSAFDNACLIIONGKYGTLEDEKTRKKIEGIVRR
Cr **LVKSLIANNDHTT**---**AARMLVRVANNISKFP**SHIVP**ILTSTVIECHRAGL**KNSAF**SFAAMLMRP**---EYRNSIDLKYYKKKIEAIVRK
Ce **LVKALINRRETLL**---**AARLLIRTCGEIQRF**THVVP**ILTSSVVICIQANL**KKSAH**KFAAQLMTP**---EYRPKIHEKYKKKIEDIVRK

1393

Hs **EDISEIEEA**---**TTPCPFCFKFLIPECELLCPGCKNSIPYCIAT**GRHMLKDDWTVC**PHCDFP**ALYSELK**IMLN**---TESTCPMCSERLN
Xl **HDSTEIEEE**---**NTPCPFCFSFLIPECELLCPGCKNNLPYCIAT**GRHMVKENWCVC**AHCGFS**ALHSEFIS**LLLE**---TETTCPMCSEPLS
Dr **PDTSEVEEE**---**SSPCPYCGFSLP**DCELLCPGCKNNLPYCIATGRHMVKEDWCV**PCDF**PALHSQF**TOLLE**---TESVCPMCSEALN
Sp **PKTEEDEEP**---**TKPCPNCKYELEETE**LSCPDCKNTTPYCIITGRHMV**QDWA**VC**KCDF**PALYSEL**SFLE**---SEDTCPMCSENIK
Aa **APRGQLEDEGAYESS**PCPVCDANL**SMDF**ICGQCKT**ILP**CIAT**GOHIV**KDDVAAC**PECDF**PAMK**VEMMKILE**STENOCT**MGEEID**
Tt **PLK**---**EEPEVE**---**NKTECPFCKEYVGEFQ**LVCE**SCQNV**IPFCIAS**GT**HV**ADQL**CF**CP**SR**FPAN**IN**YFI**Y**AESE**EG**KCP**CS**VOIN**
Ot **AVKTE**---**EDETE**---**PVSPCPFC**K**FEI**PE**TR**LE**CP**SK**NN**IP**FC**V**AS**G**KHMT**L**KEWS**NC**PN**CK**L**PA**IY**S**DF**K**RL**LE**ADP**---TCPMCETNVT
Tc **RGKEEMDDPPE**---**KTSPCPFC**DA**QV**PE**TE**LD**CG**ACK**N**LP**FC**IV**T**G**KHMV**K**ENY**SE**CP**IC**Q**FP**ALY**SS**F**VI**LL**RS**Q**---TCPMCESI**ID**
Cr **PEKDE**---**EELEE**---**PLADCPFC**N**MP**EP**TE**LO**CI**SC**ON**IL**PP**DL**AT**EK**RM**VL**SD**WA**EC**PG**CK**FP**AS**AS**Q**FR**II**SA**EG**---RCPMCND**PVD**
Ce **GGNQKDLVEEN**---**TPCPICDD**L**MP**AY**AM**SC**DN**CK**SL**VP**Y**CI**L**IG**R**H**IV**AS**DF**SR**CP**H**CE**MP**GF**Y**SEF**---KLS**IL**LN**EN**C**YM**CG**GD**L**K**

1480

Hs **AAQLKKISDCTOYLRT**EEEL-----
Xl **ANQLKRVEDCTEYLKQ**EEEB-----
Dr **VSEVKKVLECSKY**LOO**QLEA**-----
Sp **AGOVTKISDPSSY**LOA**QGE**EE-----
Aa **ASRLVDIDDIPY**IDGA**AT**-----
Tt **-LNEVKVENPEQAAS**IL**KOL**R**AT**ROS**SEOKKK**-----
Ot **FISLQLCSDPDTE**F**KOL**IN**LM**K**ES**GP**A**EE**EA**NG**DDDD**G**DDMD**-----
Tc **VNKVOKQSDPD**L**KAYLA**-----
Cr **LAHVKKVQDPLTK**IQ**OOA**Q**OTNA**SG**GGAS**-----
Ce **GAIPEDAKAYLE**K**MEQDYK**-----

Alignment for Tmem231

	1		
Hs		MALYELFSHPVERSSYRAG--LCSKAALFLLAAALTYIPLLVAFRSH--GFWLKRSSYEEOPTVRFQHQVLLVALLGP-----	
Xt		MALYEVYSHPALLRYS--ICSKATLFILIVLRLTYIPLLVAFRSY--GFWLKFTSYEEOPNVRFOYDVLIALLSST---	
Dr		MAFYDVYAHPALIRYRTC-VCTRATLFVGVVLCITYISPLLVAYSQ--GFWLKRSSYEEOPTVRFQHQVLLVALLGP-----	
Sp		MAVLELFSSTPIRTRYNAS-YCTKATVFAILAFVTVIPFLIAYRSE--GFWIKFAFYREOQDVVKFKHQIILLVLTDS---	
Cr		--MVQVYTEPLCRRYGSG-VIGEAAALFFAYLSAIVLALVAFATG--GFWVKLTPDNVQATVSYTQDAILIFEGAE---	
Ot		-----MGK--WTSASALICYFFIIVAFVLPILLVTRTH--NFWVRRSTIYEEOPNINHLNEALVIFOTTGTFOYA	
Tt*-49		--MVRVSEDFCNFYAE--FCSRASIVCILLMCLTFLAPFYLSFTTD--NFWLNIKLNQEOPTQIYQAYLLQOGSIT---	
Tt-20		--MVYLIAEQLOQFYKCKRFWSTTMCFTGLLYLFIILVVPFLAFVVD--DFWLGHKVSFEEOPTQIYQAYLLQOGSIT---	
Aa		MQLFNLHRKSIYVLYQNR--LCSLSTLAIALVLLSLILPYCVISFINPGALWDRYRRLVYEQPKVHFYQYFLAEIDR---	
Ce		MPHVDIFTEPVRYTYRSS--ECSWSAFYIKLVNVRFYFLPILIFITD--GLWKKTNTPREVPIVSTGDFIAYAYGHDR---	
Tt-80		-MAYOLYSSPFORFYCAS--PISPAALVCFCTYFMVAIIPFLVASTQ--NLWOTQVITGMEQVDMNFQNDNNFHSVLIKRADS	
84			
Hs		ESDGFRAWSTFPAFNRLOGDRLRVPLVSTREEDRNODGKTDML--HFKLELPLOSTEHVIGVQLILTFYSYLRHRMA	
Xt		---TGN--YLAWSTYPGFNNLVGDKLRIPHISAREEDRNODGKMDLL--NFQLELPLOPNDNIYGVQLILTFYQLSKMS---	
Dr		---TGN--YLAWSTFENFNRLIGDNLRIPEISAQEEDKNDGKSDVL--LLOISVPLKPAEQMFSVQLLLTFYQLSRMS---	
Sp		---QIG--YVFWSTYLNFNLLQANLRIPLIKRSREEDSNRDKNDKF--LFSIEVPVLDTEKVLGAQVIFIFDYRLYRES---	
Cr		---TGOVAFWSTSPVLNAEFSNLYTAASVQSSMDVNDGKADLI--TFQASVANDFPVHSVAKALLQLHYSLTGHL---	
Ot		SVNKKIIDLITSNAASSSFVILQYILNYLQVQN--FDQNDGLTDRI--MLRVEINIDPST--IRSIMIICQFSYQISTKI---	
Tt*-49		---DTLQINPVWKKKIKGQLNIEKVDEY-----EVSFTVTFNFGS--LMEIILEMDYMLSDVS---	
Tt-20		---QEYISTSIEMLDKMGITSLDQKNLIFMFVTRVDNNSDGLYEEFNIFTOIQFTNVADTTIKAMECSIYFFTTVSLRDKV---	
Aa		---PDDNRLITCSSFOSYNELTDHSQECNAIKVMADDGNMDGKTDKLS--ASVAFNLPDESTG--MAFYTFYFFLDAEVKSNQ---	
Ce		---SITSSSYVLSNAASSQOLSTSQLLHFFSDVSEENKQNFNNQNSLQ--TLNIEFOMSTON--LSINTLLIYAFSLRMLRDI---	
Tt-80		---TLSTYTI SNLLYQNP LNNDGTLVSLQGLTHOSYDYNDDGKVDHL--EINLQLITLQGTIVVDADIVIFMGNFKKYT---	
167			
Hs		TLVMQSMALFQSSFPVPGSQ---LYVNGDLRLQO---KOPLSGGLDARYNISVINGTSPFAYDYDLTHIVAAYQERNVTT	
Xt		TFIMQSMALIQYSSIPGSG---LYMNGDLKLOO---ROPLNHRGLDITYNVSVINRSSPFASTYALTNIISSYQERNVTT	
Dr		TLVVMQTLAFIQHSSPVPGSG---LFCGDLRLNQ---RTPLPHRGLHSTYNSVIDGSSPFASTYDLTNIIRLYQORNLT	
Sp		DVRMESMAYVSHTSAMPAGE---LNVDGDLRL---KOPLAHQYDTRYNDPIIDSTSVFADYFSFKIFSSYQORNIST	
Cr		QLDMYSFAYLAQSSPAPGAA---LYTDGELLSS---TNQLDRNYSRYNPMLNNSSTPSYSTAVQPSVALEMQSLSSY	
Ot		EADIKLTFNLIQTPLGASQ---INALGTELNQ---RNIFAFGLKRLINLYTDNLHSQLQEK--SILEFYQIYNQKNVTL	
Tt*-49		QLKSRQIMFLSFSASYNFDN---VQFYGVNFDO---QSPLYYNGENKLOYKQPLYNSDIOFHNYMRANLI--YKNOTSSL	
Tt-20		SIQMQAPLHIRLSRSTNNQK---THIVGDIQFVQ---KNPLQASQIIRNNYNYTVPILPPNQDYMGLTDFLKDIONRNETL	
Aa		HFTIPAMISLSKOTPTPTFTSGRISHLGHLRASOSVALQCPFFMRNIKTHFNHNYRPNENYTSVEEFLPESILHRIEHSNAA	
Ce		HSIVDTELEFLTDIQLTSPIAQ---IQTIARLSMDQ---SNPFETKEHIRIIRRRRQDVEHYQHSVLKRTITGAPIALKMERK	
Tt-80		KIQSYGMRLRFKTNNSQSNLIGS---VVFVIGYVPLRT---NOPLPRSKYKTLQIYENPFITGWMLLDIQIYQKYYORDFRIDAE	
250			
Hs		VLNDPNPILWVGRAAD---APFVINAIIRYP---VEVISYQPGFWEVMKFAWVQYVSILLIFLWVFERIKI--FVFQNOV	
Xt		VLNAPNPILWVGRAAS---DPFVIKAVIRYP---VESISYVPGFWEMLKYAWIQYVSILLIFLWVFERIKI--FVFQNOV	
Dr		HLSGVTPVWTVGRAAN---APFOISAQIHYE---VEMIDYQPGFWEIKFAWIQYVSILLIFLWVFOHIOT--FIFQNOV	
Sp		RFECDYEVWLTGRGTG---CPFIKGTIYYE---EETIVYVPGFQWIKFQWIKYLSVLFVLFVLMERVKTI--FVFENQI	
Cr		LSRNFTTYSNFPVWVGGTIGTSFNLQMRIRIPP---NOVIFYRPAIEMKKGWIQWLATFIVLWYLLQWAEW--FVFYVRL	
Ot		DYQVENLDIIPGSGSS---TLISMDLRIPS---LQOIVMVPVSVLESKNAWIQYLALLIPCLWAIYHLILGFARFNRV	
Tt*-49		KYEYFTQMLKVSAAA---RTVQVNGRIHIPK---YONILYIPSIETLKFQWAAVYFSIFIVMLYLFRMVLK--OMYRHSV	
Tt-20		RANYIQTYGPDNTNTDTDIIPNQLTANIFLKVVP---LTPILYVPTLRENKLVFQYVVFLEIPYIWLISIIIS--FSLKNNI	
Aa		YFAFEHRTQWSREGS---GDVEIQVQLLIGGEDGQKTALLYNASLWQKVAQFWAQYFVSVLIVLWMDAKLD--WMFDSYW	
Ce		STLLLSAPSSP---OSLSISLAVP---EMEFYKTCFWELLKWFVIQYLASFTIYVYVTSCTS--YMFNRV	
Tt-80		YQTHVTOCIQPSQT---YQSIYVNFKILLDLNK---QEEVLYKPSFLQIRNAWVQYFGLLEPSIYFGRFFLQ--FIYKYKE	
333			
Hs		VTTIPVTVI---PRGDLCKEHLG---	
Xt		LTTVPGPILPS--LYKSHQS---	
Dr		LPITITIP---PFKQHRG---	
Sp		VNTIVHHPVPTQYKNHFT---	
Cr		VETRVVSVDLC--PROQRF---	
Ot		LPAQIKSNIP--EIKAIKGF---	
Tt*-49		FPVSVMDNLP--QKAFRQFGKYKQD---	
Tt-20		FKNTISNNLP--LKEQNELA---	
Aa		IRAMRVVP---WKEKVV---	
Ce		FYVNDVVE---	
Tt-80		ESTYIVDNL---PKQEKLN---	

Alignment for Tmem216

1		
Tt	-----MSSSQIRDSVQPLSSPFLQSMIYFDQIYTVLYFFLEGCIFFYKGFGLYYP	
Cr	-----MNPQPVDMPQALAPAPVGTGQPGQPGVAQQQKPRRRVLTSLGFQIFIFGGWWDVIYYILNILVFVYKGLQLPYP	
Vc	-----MNTAQPVSGAPAPQTPAPAGSVPGQQPPQKPRRRVLTSLGFQIFIFGGWWDVAYIILNILVFVYKGLQLPYP	
Hs	-----MIPRGLKMAPRGKRLSSSTPEILFFLNGWYNATYFLLLELFIFLYKGVLLPYP	
Xl	-----MAPKGRR---RG-VLSSSTPEVLFFLNGWYCASFYLETLLFIYKGLILPYP	
Dr	-----MAAHGRQ---PVLSSSTPLQILFHLNGWYFAAFFVAEILMFIYKGVILPYP	
Sp	-----MANGEGTSSAPATSAAPRRG---TIAVLSSSLPQILFYLNGWYFAFLWICEALMYIYKGSVLPYP	
Ot	-----MNTGLNAQQPPKAQLNAQANKNVPOSQQQYPLVQPLONYTSNTKPPPEPNSLLQLSLLYFDTYFTWILVLTFCFFFLKLYALPYP	
Ph	-----MGSSSLGFILLYLNSYFICIFIIAETICIGIFKIINLPYP	
Ce	-----MISNVRSSLVYQILLSLQKTLISIVYFLVIFILYFYKGAIIYPYP	
Tc	-----MNVGTFPTAGGPSLSFOLLLYGSAGWSGIWFVVTLGLLIYKGSMLHFP	
88		
Tt	SSTIEQDIVLLVAFGICEITRLQMGSVGNKTESTSHVWFLVNIIPAIAGYFYFLLLOTYSLM--TELIMATIGLIFILEELIWFAS	
Cr	NONFAMEFSFSWLWILIEIPRLFLASKGNKTERSTPIILSFILALPLLGMYIYFVAFQTYVLR--IDLFLNGAALA-----	
Vc	GRNFAMEFSFSWLWILIEAPRLFLASKGNKTESVGP IIFSCILAMP LLAMYVYFVAFQTYVLR--IDQLLNGIATAFVALQVVFAIL	
Hs	TANLVLDVVMMLLYLGEIVIRLFFGTGKGLCQRKMLSSISVALTFPSAMMASYYLLLOTYVLR--LEAIMNGILLFFCGSELLLEVL	
Xl	TSNLILESFLFLYLGIEVSRFLGCRGNLCERKPLLVVSLGLTVPAGLLALYFLLLOTYALR---DVLNLCILLFFYGLEAILSCV	
Dr	QDNLILDVLLLLFSGLETLRLFYGWKGNLCORSLALFVSVAILVPCAVLSVYYLLLOTYVLR--LEFVLNAVLLCFYGFELVLGVM	
Sp	TENLAGEWVLIPLLVAIEYVRLFLGKKNLTKVHVHLAVSLASMATLFGALYLILWQTYVLR--AELILNAVLLCFGLLELVFSII	
Ot	QGWEMETIFLITYSELOYARILSGIKGNRIEWSIESIMFMIFLTAESIFANGFFIGLOTYVLM--LEVVLHGAICFAGLETLLCII	
Ph	TGVLMSSESLIMIFLSCETETIRIFMGHKGNLTKOSLGLVLSILLTIPSVLGLLYFLLWQTYVLR--IESILCGIQLSLOGIEFCFAII	
Ce	RYVRVMEFFVITPFIPIEYLRINWGSRGNLESTAFALSTVLSIP I I I I I L V Y L E F F O N Y V L R -- I E E I F T Y V M G F F V I E T L L S L V	
Tc	PAALPMEIVSALLLLVIDFAALSIGTRGNLAEEVGTSCLAIGLLLVAAVGAIYYMWLQTYVMM--LDLAFSAIILGLNVLAVLAGVY	
175		
Tt	ALTSFKNFEKQOY-----	
Cr	-----	
Vc	TTVRFILATRF-----	
Hs	TLAAFSSMDRI-----	
Xl	ALITLCREPTY-----	
Dr	TISIFSRANIY-----	
Sp	AVISFGRANQTVR-----	
Ot	CIILFVRTDOOPQQQORTP-----	
Ph	CLLRECKAGVY-----	
Ce	LTITFSSSGQPSG-----	
Tc	AVQGVIRAKHSPPRRFAPQPHGLPSFMRDKVKRHKED	

Alignment for OFD1

```

1
Ot MNSOQNFYSSQDQKENISDDSNQ--QENELKRRLYENMKKAGILDGLKSNMRGRLYEQQLKLNKDGSLNIDKDS-----NRLSFKLA
Sl MNSQQHIIQSFSQDKENYSDESNGNYQESLKRRLYENMKKAGILDGLKSNMRGRLYEQQLKLNKDKAGINLKDQI-----NRLNFKLA
Im -----MNNQNDSEIDNYKEKLFQSFKNITGVLDQVKTQLRHHKMEKLVOSQKQONLOIQQLD-----NOKQLRKRLL
Tt -----MEQGEDNNDQYKELFLHFSDTIGMLNSVKAOMRHKMIKLVKSQKVOOVQOKIHDEKNOHKALLMRIM-----SEMLLKRVL
Pt -----MDOSFNDLKFQLOEQELOKEGMVENMKTOLRYKLLERLQMOOKKIPSSDKVSE-----SEMLLKRVL
Xt -----MSSADFKSLSQEDLRKRLYQTFKNGVLDLSLKTQLRNQLIHLLKYPITFNGEPEVCYLEALE-----SDSLLHRAS
Hs -----MMAQSNMFTVADVLSQDELKRLKLYQTFKDRGILDTLKTQLRNQLIHELMHPVLSGELQPRSIIVE-----GSSLLIGAS
Dr -----MSASKEESLSPDEMROKLYQTFKSRGLLDTLKTQLRNQLIQEIQAPVRRGESASRRSADH-----TDSVLVSAC
Cr -----MSEPTDAQEG--LDQAAFNKKMLTHMQSSGVVG-----QVKLLTQLOKGOIVOLGPPPGDE-----PGLKRHAL
Vc -----MSEPGDAREGHLDQAEFKKKMLSQLQTAGVVGQSG--LRAQLLSALKKGQVVOLGPPPGDK-----PGLKRHAL
Sk -----MLSPQEEELSAEELKSLFHSFREAGVLDLSLKSQLRNQLITELSHGGITGKIPRHVSVKD-----ESLMLRAS

88
Ot ISIIADLMQKCDMAYALSVFLPECGIQ--EILSKPEILEVLKLDKDENYLSNGTSSKQSKETPPLLIDLMDILKONGSVKPNMSSCY
Sl VSMVADLQKCDMPYALSVFLPECGLO--EVLKSAEILEVMKLDKDEHYINSAES--RESTPLLLDLVQIILKONGSVRPNMTSCY
Im -----EHADAVFNLEQRLNSVDNQFKEKVKETSCYTOGDMEERLQYKRFETRMKAEMNTEIVRIREFEISQIRMEEQKNNKVMQD
Tt ASIVSEYFDKNDYSYNSIFQPESGYAN--KILQRFEILDIMNCKN-----IDNPKISILETMVETYLNNVKNVPTNCATQT-----
Pt ASAVADYLRARMYDLSLVFVPEITFGA--ALLNKEELKILKIDN-----LQG--SILSQMPSDILLKPKPELKSNAATQT-----
Xt NSMVADHLRCKGYEYLSLVFYPECGLEKEMFTVHDFLHLLKINPNSQLYKSLTSSAHSASAKGFLFOLLMELTDYHVHREG--RAD
Hs NSLVADHLRCGYEYLSLVFPEGLAKEKVFTHQDILLQILKINPTSSLYKSLVSGSKENOKGFLMHPFKELAEYHQAKES--CNME
Dr NSVVVDHLRSAGYEYLSLVFQPEGLSKDKVLSRDVLIQIMKISPHMPLKSLVSNIOG--QSGFLKSLMELTDHVSYRDC--SDNS
Cr NSMIADYMBAYQYNSLVFKEESGVESEPLLEDELDVLIKIDRETFFQSYMKSKAHGGSDACVLMNLVSAISEAAAAAG--KE
Vc NSMIADYLAAYQYNSLVFKEESGIEARPLLEDELDVLIKIDRETFFQSYMKSKAHAGPGSCVILNLLSAISEAAAAAG--KE
Sk NSILADHLRRCYDYTLVSVFLPESGTGDQKLFIVRDLLOLLOINPQSKLFDLSSSITTFNENESFLWQLLTQLASRYGGGCH--DKS

175
Ot IOTEAGEEESLSDOKLRKIDNMYMEKODIERLMPFKALEERMLKYKQECDDLOYKMDLENEVRRLEFESSKIRMDEAQRYRLKLOE
Sl IOTEAGEEESMTLDOKLRKIDYNFMEKAEIERMMPFKALEERMLKYKQECDDMOYKMDLESEIRRLKEFELSKLRMDEAQRYRQKLOE
Im -----EHADAVFNLEQRLNSVDNQFKEKVKETSCYTOGDMEERLQYKRFETRMKAEMNTEIVRIREFEISQIRMEEQKNNKVMQD
Tt -----EHADAVFNLEQRLNTVDHKYREKVOEINTPAH--EIERLQRFLKREFENRIKAEEMNAEVVRIREFEEMAAVMEEQEKYKRLMSE
Pt -----FYGDAVINLEOKLSMVDNMYKSKIELELKPQYDMEERLKMKREYQRLKTEIATETRIRIREFEAOHIRLEADKYRQKLOE
Xt TQTVTTSYKDSVVEKLFIDEQFEDIYKRR--KFFESLESKISDYRREMEEOIRTEMAOKLQHFQDVEIATIKLEEITEKSOQREMSD
Hs TQTSST--FNRLSLAEKQLQLIDDFADAYPOR--TKFESLEIKLNEYKREIEEQLRAEMCOKLFKFDTEIATIKMEAKKKYKELITM
Dr TQTTLSIAAHKESLVEKMQLIDEEYEVLRHRG--DRWASVEAKLAEYRKEIQEQAQIELNAKLOHFMQDVEIATIKVQEEKERSKEILE
Cr SFTQTIIGDRYQLEVRMKOLEDEYQSRLRNARLSPNAGIEERLALYRQETEEQAAAEVAROVERVREMEVAAARLDEASKARRALEA
Vc SFTQTIIGDRYQLEVRMQLLENEYQSRLRNARLSPNAGIEERLALYRQETEEQAAAEVAROVERVREMEVAAARLDEASKARRAMEA
Sk LQTEGPPVCFSTSLDDKLDCEQAYSNKLDNN--ELGSSLEERLMSHRRQIEAQARTDVNAEILRFKENDLARVKLEERREKARKEIEIQ

262
Ot YRDDLEKLOQDKLKEKIRENEAWERIKNKERDLDKISFEYRQKLRDEEVMRSRESEVKKITIELEQLMRLNERDHLNKTSDYELK
Sl YRDDLEKLOQDKIKELKLVRENEAWDRINKNERDLDKISFEYRQKLRDEEVMRSRENEIKKITIELEOOLMRLNERDLLSKTQDYELK
Im YREDLEKNYMELAKLDRDKDIFEKCNQMKETESLNHGHRQKILKDFELIRLREBQIEKQKALNEESEKLGKAKINLEKELKEK
Tt YREELEKGYMDRLTKLREREKDTLEKCTNKKMETIESINHHRORILKDFELLRMRDEFDIKORILNDETILKIQKQKLENLEQELKEK
Pt YREELEKNFOEKLNVLRERENETLMAAOKTKELESINYQYRQILKEHEITKKEQIEKQRIANEEELKFORAKLDVMERDLSKK
Xt FRRELEKTYQTKLEGLVSRKNAIERLQROEIEAKEIYSOROSLLKDDIVRARESDLRORMEAFERTOKLEAKNRSIDEFLLRKR
Hs FONDFEKCAQAKSEALVLRKSTLERIHKHQEIEETKEIYAQRQLLKDMDLLRGREAEKORVEAFELNOKLOEKKHSITAEALRRQ
Dr LRRDMKTYELKSEALISREKNAIERLQKHQIEEKDIYAQRAVLRLEISVRSREMEELRORMEAFDQKSCALHEEKVKTMDLRRR
Cr ERLELDRLHGERLAKLROREEMMDKLRROORDVENVAYEYRQIRLREERLRNHKTEIQOQODSROEQIKQLERSLELREAVGAR
Vc ERLELDRLHGERLTKLROREEMMDKLRROORDVENVAYEYRQIRLREEMRNOKTEMOQOLDAROEOLKQLERSLELREAVAAAR
Sk SRKEMERTYOIKSDALGEREHSLSERLQKEREIMEKETFIQROKVLLEELDSLVRREATVRRREADLNAAKAVKIEEDRRRAIEDNLRKR

349
Ot LKEIDVLRKAKLDHLESTENFKSEFORKFQDQDFENHRRKLOIEEDEOKIKLEKERMA-----MIENKNVKLIKDFE
Sl LKEIEVHRIKLOKDNLESVENFKSEFORKFQDQDFYHRRKLOIEEDEOKIKLEKDRIS-----IVENRNVKIKDFE
Im IKKAEDSOLIEKKYNDIAYSKLEAHRLEVEKLELLEKKILDEDLKIKQMKVFFLN-----OFTENKKLAEADNR
Tt IKKAESALIEKKYQNDLAYTKLEAHRDLEAEKLEIEKKRILDEDMYKIKQVKETAA-----QLTDQTKKLTENR
Pt LADANGNEDVIRRYEAOIHAAKASAEFYEEREQIRNKLKOLEGDLRNMENLKSTIK-----LLORENEQMVVEENK
Xt ELEVNKIEDTFDOKLKNELLHQIHELNEEYIKRTKKVSEDEERRNKVEASKLREEAVVIN-----MKKHESE
Hs EQNKSFEETYDRKLNELLKYOLELKDYYIIRTNRLIEDERKNEKAVHLOEELIATN-----SKKEELN
Dr ELSVKTMEDSFEQKLSSELLKYOLELKEENMKRTEKLTENEERIRAEATRLOKEAAVIE-----AKTQDYE
Cr EAAAEEKIAEATEAAAQAAVEARQDVEREYMEKSSLAQQRMQIEMDRSRIELRSEATAETAGARAKEERLRALETARAEAEARAA
Vc EAAAEKLLAEATEVVAEAQVAARQDVEREYELKNGVACQRLQLEMDRARMQELRSEAMADLAAARAKDDRLRALETARAEAEARAA
Sk EAAVARIETIEYHQLTEKMASYDLEOKSKYITRLOSLEISEARNKEETRLLAERARVN-----LAREDLK

```


958

Ot ATIDN--VQSKKPSPIKEEEKYQ
Sl MSHKNTTHQOHOPSSILSPVKNT
Im YKQSE---DLOQQINTIDVQEG
Tt SKQTLNQISGLQDNPISLEQHKY
Pt ---OSNIIEEYSEL
Xt SERQSI LAEDHEDSIVSSSQOSP
Hs LESEMYLEGLGRSHIASPSPCPD
Dr RADEEHDEHSLNTECVKVSNTD
Cr QRPPQYLT SQHQHEDHDQQAEPF IASHRGGAGHDSAAADDETPDPHAAQRHNSGGGGSVPHPTPODVP TPOHDSTPGOTHAAAPDRG
Vc SGP TSHSSSTIQPV SQPPQQQQQ
Sk PPRSVLKKDRSAPSLSPSHSKPAG

1045

Ot ---PSVNLVGYNGAS---STTTNKNLASAFDSKONSATKPAANTQONT
Sl ---QEEKYSSYNA---SKTPAODNKFGTTANNNNQATEQASIQKQ
Im ---KND---VFSNK---NLLEIPDIYQKQKIKINIS
Tt ---KKEDSOSLSKDK---AMLSIPOTFTQQAEEKHSLKDSPLDTKKQT
Pt ---M
Xt ---KORLSPIPKNEHVSSINCVDVPDIPVDAEKDYSYKQDVSCHEVSNHAEPOKLY
Hs ---RMP LPSPTESRHLSLTP---PVSSPPEOKVGLYRRQTELODKSEFSVDVCKLA
Dr ---R PALMFER---LTSPTPAEELSSSISPSSPVMKSTTRHTOSPA
Cr SAHVVSFDPPATQVQYPLRDMQAFGRSSLEFPYSAAEPTAPTAVVTSAPAVAAPAGLVLTNSLGTTPPAQAVEDEEEOEDEPPPPP
Vc QPHVP---AEPLAPPPPPPPAPGMC---SPLPLALPADPAPLAPLAS---PALVAPPGLVFTSDLGT---RAPASPAEAHPAAEP
Sk ---SVTIIVEDGOVKCKIVTSPTEKSSSTSPILPSL

1132

Ot TITPSTTTNNALSSKPTFKPSTNPFAPKRPSSSGSNSGATGNNNNSDNNTQNYNNP TSYGGYGNKQEENK---OSTSIFPDPFAKP
Sl TSN---TKPTFKPSTNPFAPK---TNTITANVGTITNNEFGAPITNTLNNANTFSPSPNPPATNNYGGWQPSGFOTNLEGS
Im ---IKIFIMILLK---IKIRLIIVIIIMIKIKANHC---IMKKRKKMI
Tt TLQPLIDLTKK---DQKSSNLNYLPPPIIQKQPOQSDFNLYLDDFDDLDLDFSDKKNKKSQCPQLKDDKDLWLSLPKDSDLNKKSVSNP
Pt ---M
Xt FDDLNSTNSSLKDQEDITPEQLASDLSPSGDVVHDNNVIANVPAVATSE---LDSLSSHHTENTIKHEKAEVGERKGEEC---VREI
Hs FQDNEEFESSESAGNMPRQLEMGGLSAGDMSHVDAAAAAPLSYQHPVSDQKQIEEKEEKEIREQQVKERRQREERRQSNLOEV
Dr KLQEILLSSSSQESSPOPEKITLHDLTEP---IOMVSAQPCCLQDC---EPLOQDHPDVOISSSSSSSSSSQREEEC---OREI
Cr PKPTIPGLVMVSGFTRPGSAAGAAAPSPAPAAPOLPPPPAVADLPPPPPQDVESVMOAKMRMLQERERALAAC---VPPIR
Vc RKPTIPGLVIVSGFAPRSSPEPPPPPPPEGRSEELDS---HSEPLDLANVMOAKMRMLQERERALAACRQOQQQQHPPPLE
Sk SXPLEVEPIILSVSSPRRPIPKTGGYHSPVSKKDNNDLLITGDAWKSSSIPHDVVEDEKQEEQIEFSSAKSSPRLKKEKTSYDDWES

1219

Ot SSNTGTYSNNTAKDSIF-----NRNNSLKKAKEKERTONSDIISDHLVDDYEDDFVEESVRNPPPASKNDFNKSPTTTGG
Sl NKNNNNSANNPSSNLYGSSLPALNNNSNNAI NRNNSLRRS-ADKSDAISDNIVDDYDEDFIEESNRQPSK---KKEQP KOQPASS--
Im FRQKK---K KKKKNGRK---KK---TDEKKMIFKLLKMFKKKN
Tt FSKKKEDPFSSKNEDIYKKKFDPPGKKDDKFGSKDDPFSSKKNDFSLPSTONKQKFEQKPAAPYKQDKSITDNKEDDKTISEEIEEI
Pt ---M
Xt SEEGKDLYEDSVVKIKTFNE---KRDNTEGSPGICDLEEAASSSVKS---SANPLDKYMKMILQNRACQEVSEKIDKESLDDVSVVEKV
Hs LERERRELEKLYQERKMI EESLKI KIKKELEMENELEMSNOEIKKSAHSENPLEKYMKIIQOEQOQESADKSSKMMVOEGSLVDLTL
Dr HTLQOQPHEEOTQEQRDDAG---GHVTSAAASPTGGAEAN---PLORYMOMLMDQKQOQSPNKE---SSGSHEENL
Cr RLOSQKSVSSRASTAGGTGPFYFAGRSTSGSEPTPSSPGADATAMSSGGPPPRREDSNSELIAREAQDTVAEELSTITTRALLRPTS
Vc RRLSRNHSSSRYSGEVRFLGTTGGVGGMSMEASSPPGAGASG---GLAAHVEDSTSDIVAGEEYDTVAPELSTLH---RRGRSHEG
Sk SKSERSEHQQPVVSLDAAWKHEVTSLDTIEWKQVKSEQELEK---EREDEKRWEEKKKK

1306

Ot NVFGQPF TAAQTNNNNAYGNDTEEASEAFEEDDLVDDYF
Sl ---IFSKPVATNVIG---TEEESSNAYEED-FVDDYF
Im ---M
Tt VDYNEEIVEDLEYF
Pt ---M
Xt SN---ESITALSHGEDDENFW
Hs QSSDKVESLTFGSHEELDDSW
Dr QSENHEHSAGVISHDEADDFW
Cr LEGGPRSTISSVNRRELKSGVSVRSEASGFSTGIEAPGPGSEHLHCGOSMRSMGLMGLTDDIPSSLGDADYQLPGLGDDDD-GVEAPE
Vc GIGHLSROSSVSRRELVRGFTSIARSEASALS---MEVPG---LGGPSMRALSTVLTLDNLSL---EGFEVRLGDDDDDDGVEGPF
Sk ---M

1393

Ot -----
Sl -----
Im -----
Tt -----
Pt -----
Xt -----
Hs -----
Dr -----
Cr EILGGYGNFAAEFSAGSVF
Vc SEG-VGAFAAEFSAANSVF
Sk -----